LOW REYNOLDS NUMBER EXPERIMENTS IN AN AXIAL FLOW TURBOMACHINE

Thesis by

Joseph Neustein

In Partial Fulfillment of the Requirements

For the Degree of

Doctor of Philosophy

California Institute of Technology

Pasadena, California

1957

TO RON

AND THOSE WHO HELPED HIM

ACKNOWLEDGEMENTS

I wish to express my sincere thanks to Dr. W. D. Rannie for his guidance and contributions during the course of this investigation. Beyond this I am deeply grateful for his encouragement and kindness which made it possible for me to carry on with this work.

Many members of the Hydrodynamics Laboratory Staff aided me in various ways. Most particularly I wish to thank Drs. A. Acosta, V. Vanoni, and B. Parkin, and Messrs. J. Kingan, C. Eastvedt, S. Wheeler, E. Daly, and R. Lohrman.

I am grateful to the members of the Institute's faculty who granted me the privilege and aid to become a graduate member of the Institute. Professor F. E. Marble was particularly helpful with his encouragement and advice in many matters.

I also wish to acknowledge financial assistance from an Aire-search Fellowship. Funds from the United States Navy, Office of Naval Research were used to purchase the glycerine needed for the turbomachine investigation. The wind tunnel used in this investigation is the property of the United States Air Force. The water and turbo-machinery tunnels are the property of the United States Navy, Bureau of Ordnance.

The contents herein were typed by Miss R. Winkel and Mrs. E. Fox, and the final figures were prepared by Mrs. A. Tingley.

ABSTRACT

The performance of a single stage, axial flow turbomachine was studied experimentally at very low Reynolds numbers. The investigation had two primary objectives: first, a quantitative evaluation of overall performance as a function of Reynolds number, and second, a study of the flow within the blade rows.

The investigation established that sudden or critical changes in performance do not occur in the type of machine tested between a Reynolds number (based on rotor tip speed and rotor chord) of 150,000 and 20,000. The deterioration of performance is explained in terms of viscous flow phenomena within the blade rows.

TABLE OF CONTENTS

TABLE OF CONTENTS (Cont'd)

TABLE OF CONTENTS (Cont'd)

TABLE OF CONTENTS (Cont'd)

TABLE OF CONTENTS (Cont'd)

TABLE OF CONTENTS (Cont'd)

SUMMARY

Real fluid effects in an axial flow turbomachine involve many complex fluid mechanical phenomena, the details of which are not accounted for in practical applications of turbomachines. Nevertheless, for high Reynolds number operation, turbomachine designs are relatively successful. This fortunate circumstance stems from the fact that at high Reynolds numbers the total losses are usually relatively small with the result that the input power and pressure rise depend for the most part on non-viscous flow processes. The losses, moreover, are known from experience to be similar in a given type of turbomachine (i.e., axial or centrifugal). For this reason, satisfactory design estimates of losses can be made from existing experimental loss data.

As a general result of these considerations, turbomachine design procedures need not include details of the viscous flow processes. Instead, viscous flow considerations are used to establish limits on design parameters, while for the actual design, the viscous effects are collected into correction quantities such as efficiency, deviation angles, and area-contraction ratios.

With a reduction in Reynolds number, the viscous losses in a turbomachine necessarily take on added importance. The usual design rules will become inadequate at sufficiently low Reynolds numbers. Furthermore, a strong likelihood exists that the losses may differ significantly from one design to another.

Low Reynolds number operation of turbomachines is of considerable interest, for there exists a number of important applications where such operation is necessary. Some examples are: compressors

in jet engines for high altitude aircraft, fans and compressors for high altitude wind tunnels, compressors in small gas turbines used in aircraft cooling systems at high altitude, and pumps for use with oil and other fluids of very high viscosity. There is a practical necessity, therefore, to extend theoretical and experimental knowledge of viscous flow effects in turbomachines.

Many attempts have been made to isolate and study, both theoretically and experimentally, particular viscous flow problems which seem to be important in turbomachines. In this category can be listed, for example, blade profile losses, secondary flows in wall boundary layers, radial flows in the boundary layers of rotating blades, interaction between blade-surface and wall boundary layers, flow in corners, interference due to viscous wakes, three dimensional boundary layer growth on rotating cylinders, etc. Progress in each of these areas has been made. Unfortunately, all of the problems mentioned occur to some degree in a turbomachine; and even though each problem be solved individually, there still remains the task of understanding their combined interactions.

The foregoing considerations emphasize the need for experimental studies at low Reynolds numbers with a complete axial flow turbomachine in order to obtain some insight in regard to the combined actions of the important viscous flow patterns.

Although some overall performance data for turbomachines operated at low Reynolds numbers have been reported, no accompanying experimental information is supplied to help clarify the viscous flow processes within these machines. Clearly, the determination of detailed

viscosity effects in a turbomachine is difficult. However, it seems reasonable that at sufficiently low Reynolds numbers, the more important viscous flow features, particularly the movements of boundary layers, should become so pronounced that they can be observed by some experimental means. In anticipation of this possibility, the present investigation was undertaken.

It should be emphasized that this study was not formulated with the intention of solving any of the viscous flow problems in turbomachinery. The results, rather, were expected to be more in the nature of explorations to help clarify, from an engineering point of view, how viscous effects, such as boundary layer movements, actually occur in a practical machine, and at what point these effects become sufficiently large to materially modify overall performance. Thus, a low Reynolds number experimental study with an axial flow turbomachine was initiated with two primary objectives in mind: first, a quantitative evaluation of the overall performance of a single stage as a function of Reynolds number, and second, a quantitative and qualitative study of individual blade row characteristics with a view to describing some of the more important viscous flow features which prevail in guide vanes, rotor blades, and stator blades.

The study was made with an existing axial flow turbomachine which had been modeled from a larger jet-engine-type of axial flow compressor. Since the machine was part of a closed-circuit tunnel, low Reynolds numbers could be obtained by using a mixture of glycerine and water as the working fluid. In this way the attainment of low Reynolds numbers could be realized, and yet at the same time,

dynamic pressures could be maintained high enough to permit reasonably accurate flow measurements. A glycerine-water mixture also has the desirable features of being Newtonian and transparent. The former property allows the results to be applied directly to water, air, and many oil applications. The latter property makes possible the visualization of flow patterns within the machine. During the tests small Reynolds number changes were accomplished by changing the turbomachine rotative speed, while large Reynolds number changes were brought about by changing the glycerine-water mixture ratio.

The overall performance was determined over a range of Reynolds numbers, R_T, (based on rotor tip speed and rotor chord) from 2000 to 150,000. The flow rate at each Reynolds number was varied from near shut-off to the maximum permitted by the turbomachine-tunnel system. The range of R_T covered includes the region of practical interest for low Reynolds number applications of axial flow turbomachines.

Blade row characteristics were studied by means of quantitative flow surveys before and after each blade row, and by means of extensive flow visualization experiments within each blade row. The visualization involved the use of tufts attached to both rotating and stationary surfaces. In addition, injection of colored tracer fluid was used in the stator row to verify the results deduced from the tufts, and to provide further information in regions where the use of tufts was not feasible.

The results, which comprise the main element of this paper, are presented in some detail, inasmuch as similar information is not

known to be available elsewhere. The order of the contents follow the objectives, i.e., the overall performance is presented first, followed by a description of results for each blade row. A large number of photographs which describe boundary layer movements within the machine are included. A partial summary of results is presented last.

In general, the investigation established that sudden or critical changes in performance do not occur in the type of machine tested, between R_T (v.s.) of 150,000 and 20,000. Below 20,000 the performance deteriorated more rapidly. A critical Reynolds number might be interpreted as occurring between R_T of 20,000 and 10,000.

The losses were found to vary with R_T in the following manner: (loss = 1 - efficiency = $1 - \eta$)

$$(1 - \eta) \propto R_T^{-0.22} \quad (1.5 \times 10^5 > R_T > 2 \times 10^4)$$

$$(1 - \eta) \propto R_T^{-0.37} \quad (R_T < 2 \times 10^4)$$

The results also clarified many of the viscous flow details in each blade row which are associated with the deterioration of performance. These include the radial flow of blade-surface and wall boundary layers, the separation of chord-wise-moving flow and of flow in corners, the secondary flow along stationary and rotating walls within a blade row, and certain elements of blade row interactions. These effects were very pronounced at R_T of 4000 and below. Consequently, a considerable part of the paper is concerned with results obtained at these lower Reynolds numbers.

Visualization studies of the relative flow over the rotor blade surfaces verified the observation (ref. (35)) that laminar separation

and reattachment can exist at very low Reynolds numbers, even for blade shapes designed for high Reynolds-number operation. In the present machine this result was attributed to the turbulence and non-steady flow effects arising from thick guide-vane wakes.

From the point of view of a designer, information is presented in regard to overall performance, guide vane turning, and guide vane and stator total pressure losses, all as functions of Reynolds number. These are expected to be indicative of performance in turbomachines similar to the one tested here (cf. Concluding Remarks).

Other details are concerned with problems such as wall boundary layers, flow reversal at low flow coefficients, tip clearance flow, flow patterns near shut-off, and flow comparisons in stators with rotating and stationary hubs. In the case of certain isolated problems, e.g., cross flow in wall boundary layers, the experimental data are interpreted in the light of existing theoretical results.

LIST OF SYMBOLS

C_D	Discharge coefficient
C_P	Total pressure tube Reynolds number correction (cf. p. 23)
C_T	Torque coefficient, $\frac{T}{\frac{\pi}{2} \rho r_t^3 (1 - \zeta_h^2) u_t^2}$
i	Incidence angle
P	Pressure
P_T	Total pressure
P_S	Static pressure
ΔP	Pressure difference
r	Radius
r_h	Hub radius
r_t	Tip radius
R	Reynolds number
R_D	Reynolds number based on rotor tip diameter and rotor tip speed
R_i	Total pressure tube Reynolds number based on inside radius of tube and free stream velocity computed from measured total pressure
R_P	Reynolds number based on pipe diameter and average velocity at nozzle discharge
R_S	Reynolds number based on mean-radius chord and velocity entering stator at mean radius
R_T	Reynolds number based on rotor chord and rotor tip speed
$R_\phi \sim R_{GV}$	Reynolds number based on rotor chord (rotor chord = 1.897", guide vane chord = 1.956") and average axial velocity
T	Torque
u_t	Rotor tip speed
V	Velocity
V_a	Axial velocity (used on photos)
V_δ	Velocity at outer edge of boundary layer

α Angle of attack

β Flow angle measured from machine axis

δ Boundary layer thickness

ζ Radius ratio, r/r_t

ζ_h Hub-tip ratio

η Efficiency, $(\phi\psi)/C_T$

θ Air turning angle

λ Dimensionless absolute tangential velocity, tangential velocity/rotor tip speed; (usually referred to as whirl or tangential velocity)

ρ Density

ϕ Average flow coefficient

ϕ_L Dimensionless axial velocity, axial velocity/rotor tip speed; (usually referred to as axial velocity)

ψ Head coefficient

ψ_S Static head coefficient

ψ_T Total head coefficient

(Note: In most cases, head coefficients are referred to the maximum total pressure at the nozzle discharge)

ω Angular velocity

$\curvearrowleft$ Average total head loss across stator, $\frac{\Delta P_T \cos^2\beta}{\frac{1}{2}\rho u_t^2 \phi^2}$ ($\zeta = 0.80$ rotor exit)

1, 2, --, 12, x Stations along turbomachine casing (cf. fig. 5)

4', 6' Circumferential stations spaced 8° apart

Subscripts:

GV Guide vanes

R Rotor

S Stator

(2-1), etc. Difference in quantities at stations 2 and 1, etc.

Turbomachine configuration:

CS Compact stage: guide vanes, rotor and stator in first stage

ES Expanded stator: guide vanes, rotor in first stage, stator in third stage

ERS Expanded rotor and stator: guide vanes, rotor in second stage, stator in third stage

Other symbols are defined where used.

I. INTRODUCTION

The data obtained in the airfoil investigation of reference (45) demonstrated that isolated airfoils can be made to sustain relatively high lift at R values below 10,000 and possibly as low as 5,000. The extension of these results to two-dimensional cascades and finally to three-dimensional cascades and axial turbomachines would appear to be the logical sequence for further investigations. In the two-dimensional case, however, if the wall effects can be disregarded, (if they cannot, the cascade is not strictly two-dimensional) results similar to the isolated airfoil case are to be expected. Quantitatively, of course, information related to losses and flow deviation angles as influenced by R would be obtained; but the essential character of the viscous flow can be expected to remain about the same as for the isolated airfoil. This is borne out, for example, by the fact that laminar bubbles have been observed in cascade tests.[1] Furthermore, these bubbles can be removed, at sufficiently high R, simply by roughening the blade surface upstream of the transition point, an effect which implies that turbulence and sharp leading edges can be expected to produce similar results for both isolated wings and two-dimensional cascades even at low R.

On the other hand, in three-dimensional cascades, i.e., where the radius is now part of the cascade geometry, the radial pressure gradient constitutes a new variable which can modify the blade boundary layer flow by causing it to move radially. At high values of R, however, this boundary layer movement is not of major importance, and reasonable flow predictions neglecting this condition can be made. For such cases, then, the isolated airfoil results in regard to R and turbulence

effects again are expected to be qualitatively applicable. Thus, for example, in reference (2) where the influence of R ($5\times10^4 < R < 25\times10^4$) on the performance of a three-dimensional stator cascade was studied, laminar bubbles with subsequently attached flow occurred at a Reynolds number of 55,000. No critical Reynolds number effects were observed. Chemical traces, however, indicated radial motions in the blade surface boundary layers.

As the R is decreased below about 75,000 the importance of the radial movement of the boundary layer in three-dimensional cascades will increase due to the additional quantity of fluid involved in the boundary layer.

In a rotating blade row the boundary layer is unstable in a radially outward direction. In addition the viscous pumping action of the rotating hub, i.e., the addition of energy through formation of a cross-flow boundary layer, an unimportant effect at very high R, serves to complicate the flow picture as the R decreases. Other wall effects which may differ significantly between an actual machine and a stationary cascade are involved. These include factors such as secondary flows initiated by wall boundary layers entering a blade row; clearance flows between the rotor blades and casing, and between the rotating hub and stator blades; and scraping flows associated with relative rotational motion between a blade and a wall boundary layer.

Clearly, the general situation is quite complicated. Nevertheless, the foregoing considerations suggest that the determination of the important low R problems and effects in turbomachines requires a

direct study within an actual turbomachine. Admittedly, such an investigation might reveal complex flow patterns whose detailed character could not be described very satisfactorily. On the other hand the more important gross phenomena are likely to become clear. The present investigation was undertaken with the latter point of view in mind.

Many of the features related to the movements of boundary layers in axial turbomachines have been treated in the literature. For convenience and clarity the published results which will be discussed here may be classified by their relation to rotating or to stationary elements of the turbomachine.

ROTATING ELEMENTS

Problems related to rotors are treated in references (3), (4), (5), (6), and (7). Experimental observations are very meager because of the difficulty of following boundary layer motions in a rotating machine, particularly when gas is used as the working fluid. In reference (3) Ruden found that the boundary layer on the rotor blade suction surface of an axial flow fan moved toward the rotor tip, the greatest deviation from the chordwise direction being near the hub. He interprets the flow process near the hub to be caused by the combined action of centrifugal force and secondary flow in the hub boundary layer between blades. The resulting removal of the boundary layer from the hub region extended the stalling limit at the hub while reducing it at the tip. Ruden also anticipates that the deflection of the boundary layer flow should become stronger with increasing boundary layer thickness,

and that a minimum thickness is the basis for deflection. The boundary layer movement along the rotor blade pressure surface appeared to be negligible.

Rotor results similar to Ruden's are reported by Weske[4] who notes further that radial displacements occur in wakes and that such motion is important in regard to efficiency and operating characteristics.

The outer wall boundary layer characteristics behind rotors of axial flow compressors have been described by Rannie et al.[5],[6] and by Mager et al.[7] Mager established that the important parameters concerning the secondary flow in the boundary layer are the turning of the flow outside the boundary layer and the product of the curvature of the streamline outside the boundary layer and the boundary layer thickness. Rannie found that at high flow rates the growth of the casing and hub boundary layer was no greater than would be expected in an annular duct without blading. At lower flow rates he observed a pronounced, progressive decrease of axial velocity near the inner boundary layer across the rotor and subsequent blade rows.

Several theoretical studies of rotor boundary layer flow problems have been carried out, notably by Fogarty,[8] Graham,[9] and Mager.[10], [11], [12] Fogarty studied the movement of a laminar boundary layer on an infinite-span, thin, rotating blade. He demonstrated that the chordwise velocity is independent of the spanwise velocity due to rotation, and hence that the separation line is unaffected by rotation. For two particular examples, the spanwise velocities in the

boundary layers were found to be small compared with the chordwise velocities.

By applying momentum integral methods, Graham was able to extend the work of Fogarty to infinite cylinders of arbitrary section set at zero lift. For a circular cylinder and for a laminar flow airfoil, the spanwise flow was found to be small. Graham also refers to a paper by Smith[13] who used Falkner - Skan separation profiles and obtained larger spanwise velocities than for non-separation profiles.

Mager's studies concern a number of different aspects related to rotor boundary layers. Although his analyses are based on small perturbation methods and consequently are limited in their quantitative application, the qualitative results are nevertheless important. Detailed use of these results will be made in connection with the experimental data obtained in the present investigation. It is to be noted here, however, that Mager's analysis of the three-dimensional, laminar boundary layer flow over a plane provides a partial basis for understanding the deflection in the wall boundary layer between both moving and stationary blades. He also treats the case of laminar flow in a corner* with continuous curvature, and thus demonstrates that in the presence of blade-to-blade pressure gradients, the chordwise flow in the corner (e.g. between the hub and the suction surface of a rotor blade) may experience complete separation, the resulting flow remaining attached to the corner but proceeding normal to the chord direction.

---

* The corner is stationary.

In addition to the foregoing, Mager has also analyzed the flow of a thick laminar boundary layer under sudden lateral perturbation.[12] Of particular interest in this paper is his solution for the boundary layer growth downstream of the leading edge of a moving wall onto which has moved a previously formed boundary layer. This situation is analogous to the boundary layer flow at the beginning of a rotating shroud.

STATIONARY ELEMENTS

In one of the early NACA investigations on turbine nozzles, Goldstein[14] noted the occurrence of radial boundary layer movements from the inner and outer shroud walls. Goldstein explains this motion in terms of the stability (cf. infra) characteristics of the wall boundary layers. This stability phenomena, may have a significant influence in the wall boundary layer growth in an axial flow machine. According to Goldstein (ibid.), if one considers simply the balance between the radial pressure gradient and the centrifugal force and assumes the angular momentum of a fluid particle to be conserved, then consideration of the behavior of a fluid particle which is removed from a wall boundary layer, leads to the following stability classification:

Unstable Wall Boundary Layers	Stable Wall Boundary Layers
Rotating Hub	Stationary Hub
Stationary Outer Shroud	Rotating Outer Shroud

A particle in a stable wall boundary layer, if moved to a new radial position, will tend to return to its original radial location. In the unstable case the particle will tend to move in a direction away from its

original radial location.

Goldstein concludes that the minimum wall boundary layer growth should occur when the inner and outer shroud boundary layers are unstable, i.e., in cases where the inner shroud rotates and the outer shroud is stationary.

More recently other NACA investigators[15] thru [22] have made extensive flow-visualization studies of boundary layer movements in both two- and three-dimensional stationary blade configurations. Some of the more important findings which are related to the present study are given in the following list which has been divided, for the most part, into two- and three-dimensional results:*

Two-Dimensional

1. The end wall boundary layer deflection depends primarily upon the amount of turning in the mainstream.

2. A passage vortex formation is the principal secondary-flow phenomenon in rectangular bends and in cascades.

3. Cascade parameters, such as aspect ratio and stagger,** which do not alter the main stream turning, had no apparent influence on the secondary flow.

---

* Two- and three-dimensions refer only to the geometry of the ducting or blading system and not to the secondary flow process which is always three-dimensional.

** Clearly, these two variables, for some conditions, must influence the secondary flow. For example, with extremely low aspect ratios, the hub and casing boundary layers will interact and modify the spanwise flow. In regard to stagger, pressure rise cascades, in contrast to pressure drop cascades, may exhibit flow reversal near the walls with a resulting modification of the wall boundary layer deflection.

4. In the case of relative motion between the blade and an end wall (the pressure surface leading as in a compressor) the scraping flow on the pressure surface replaces the secondary flow and tip clearance vortices by a less well defined roll-up near the pressure surface. In addition the scraping prevents flow from the pressure surface into the clearance region. As a result of turbine experiments, however, the scraping effect was found to be reduced for high blade stagger.*

Fluid near the blade end of the suction surface moved down onto the moving wall and was carried over to the pressure surface of the adjacent blade.

5. For stationary end walls, flow moved from the pressure surface down to the end wall and thence over to the suction surface.

6. The plane, laminar cross flow theory of Mager's,[10] which was modified by Hansen and Herzig[22] so as to remove the restriction on the magnitude of the free stream cross flow, was found to predict quite accurately the deflection of the boundary layer at the wall of bends.

Both the theory and experiments showed that the deflection increased with increasing boundary layer thickness.

Three-Dimensional

The following results were obtained with high-turning turbine nozzles:

---

* Increasing blade stagger corresponds to rotating the chord leading edge away from the direction of the machine axis.

1. Deflection of the wall boundary layers was always large. The process was similar to that which occurred in the two-dimensional cascade studies.

2. Strong radial inflow was observed to occur along the suction surface for supersonic outlet Mach numbers. The region of inflow extended upstream to the position of a large pressure rise which resulted from the existence of a shock. Without the shock, radial inflow occurred near the trailing edge and downstream in the wakes. Thus, part of the casing boundary layer was displaced to lower radii downstream. Moreover, part of the suction surface boundary layer became part of the hub boundary layer. Large loss regions were found near the hub.

3. The radial inflow at the trailing edge was modified by the presence of a second blade row. When the second row was in motion, the radial inflow was reduced.

4. A blade surface fence located at midspan reduced the measured wake loss near the hub.

5. Smoke studies made at Reynolds numbers (based on blade chord and inlet velocity) of about 5,000 - 15,000* showed boundary layer movements similar to those at higher Reynolds number and Mach number (subsonic).

6. At subsonic outlet Mach numbers, flow near the hub passed around the trailing edge from pressure to suction surface.

---

* In these cases the turning of the mainstream presumably remained high due to the large pressure drop across the cascade and to the high solidity (approximately 1.5 at both hub and tip).

Based on the foregoing results, one can postulate, for a complete compressor stage, (i.e., guide vanes, rotor, and stator) a partial picture of boundary layer movements which may occur as the Reynolds number is reduced.

First, because boundary layer thicknesses will increase everywhere in the machine, deflections of boundary layer fluid should increase. In the guide vanes, which produce much less turning than the nozzles of reference (20), radial inflow may occur near or downstream of the trailing edge. The extent of this effect, however, should be materially less than observed in reference (20) because of lower design turning.

In the rotor, deflection in the hub boundary layer should increase. This in turn should be coupled with an increase in the deflection in the corner flow. These two effects should then amplify the radial outflow along the rotor blade suction surface. At sufficiently low Reynolds numbers the cross flow may move into a separated corner. The radial outflow will then become severe, and the chordwise flow will be forced to separate from the blade surface. When this condition prevails, the rotor losses should become very large. Downstream of the rotor, part of the casing boundary layer will have originated at the hub. Radial inflow in the wakes behind the rotor may also occur.

In the stator, with a moving hub, secondary flow in the casing boundary layer should increase. Then, as for the rotor hub, at sufficiently low Reynolds numbers the cross flow at the casing coupled

with separation of the corner flow should cause strong radial inflow along the suction surface. If sufficiently strong, the radial inflow may extend to the hub and cross over to the pressure surface. The radial inflow will cause separation of the chordwise flow with consequent large losses.

Very little boundary layer movement on the pressure surfaces of any blade row is to be expected.

A general pattern of radial motion through the stage (and subsequent stages) may result, i.e., boundary layer fluid may move inward in the guide vanes, outward in the rotor, and inward again in the stator.

Other factors such as blade row interactions, and vortex formation and transport cannot be foreseen. Furthermore, it is not clear at what magnitude of Reynolds number the boundary layer growth and motions become sufficiently severe to reduce the overall performance radically.

Up to the time of completion of the present study, only one published paper, reference (23), presented any detailed performance of an axial flow turbomachine at very low R_T (8500). A number of important features of that investigation are to be noted. The variation of R_T was accomplished in part by changes in blade aspect ratio; the results show effects apparently attributable to these changes. For example, the head coefficient and efficiency are materially less for the higher of two aspect ratio tests made at the same value of R_T.

Further, the stage configuration contained a rotor and stator

without guide vanes. The importance of this feature will become clear in the later discussion of present results.

The data presented in reference (23) also show a rather sharp change in efficiency at R_T of about 80,000. This implies presumably, some form of critical R effect. Further, between R_T of 850,000 and 8,500, the flow coefficient at peak efficiency changed from about 0.47 to 0.20, while the peak efficiency changed from about 94 °/o to 10 °/o, the peak head coefficient dropping from a value greater than 1.0 to about 0.23 at the same time.

The causes for this change in performance cannot be gleaned from performance maps alone, however, and more detailed information was not given in the reference. As a consequence, further studies which provide information in regard to flow details within the compressor are needed.

A more recent publication regarding low Reynolds number flow in axial turbomachines is that of Sohn.*(24) No numerical performance data were presented so that a comparison with Eckert's results(23) cannot be made. However, Sohn discusses the concept of a critical Reynolds number and relates its occurrence to the laminar bubble phenomena (cf. Part I of present paper). By empirical means based on some two-dimensional cascade data he formulates a procedure for determining the Reynolds number for which reattachment fails to occur. This he specifies to be the critical Reynolds number.

---

* This paper appeared in the literature after both parts of the present paper had been completed.

The laminar bubble is undoubtedly a factor of importance in a turbomachine, and, because of this possibility, of course, Part I of the present study was carried out at low Reynolds numbers. However, other viscous effects, such as those described earlier in the present section, may be equally as or more important than the bubble phenomena. It seems, in fact, that a critical Reynolds number in a turbomachine is more likely to stem from a combination of interacting viscous effects rather than from a single cause.

Finally, as a concluding remark regarding other investigations, it is to be noted that the low Reynolds number performance of radial flow machines has been studied, e.g., by Ippen.[25] In addition, recent detailed experiments involving extensive flow visualization in radial flow machines at low Reynolds number were completed by Acosta at the California Institute of Technology. A discussion of the radial flow machine problems is not appropriate to the present paper and is therefore omitted.

In the present investigation the variation of R_T was accomplished with a single set of turbomachine blading by using glycerine-water mixtures as the working fluid in the axial turbomachine described in reference (26). A glycerine-water mixture has a number of features which make it valuable as a working fluid. The mixture is Newtonian; it is transparent; and the viscosity can be reduced simply by the addition of water. Although the viscosity of pure glycerine is very sensitive to temperature, if the concentration by volume is less than 85 $^{o}/o$ glycerine, the temperature effect is not

severe. The specific gravity of an 80 °/o mixture is about 1.2 which makes available for measurement considerable dynamic pressure even at very low flow rates. The high specific gravity also makes more practical the use of tufts for purposes of flow visualization. In order to minimize the quantity of glycerine to be used (initially, about 1000 gallons were introduced into the tunnel), it was necessary that the mixture for the maximum desired viscosity be used first and then diluted with water to give lower viscosities. Consequently, tests at the lowest values of R_T had to be made first, and these tests could not be repeated once the mixture was changed.

The investigation was carried out on an axial flow turbomachine designed for high R_T operation, but used in the present case at considerably lower values of R_T. Specifically, the free-vortex stage described in reference (5) was studied over a range of R_T from 2000 to 150,000, the lower value corresponding to that encountered, for example, in oil pumping applications, the upper value corresponding to the lower range encountered in usual jet-engine applications.* The stage configuration and blade shapes, however, were more typical of gas turbine compressors in contrast to liquid pump designs.

The study included the determination of over-all performance of the single stage and the measurement of flow details before and after each blade row. Considerable use was made of tufts and injection of colored tracer fluid to visualize the flow patterns and to

---

* For extremely high altitude operation of jet engines, the value of R_T at the compressor inlet should be lower than 150,000.

provide photographic information from which many qualitative features of the flow processes within both the stationary and moving blade rows were clarified.

II. EQUIPMENT

2:1 Description of Turbomachine and Tunnel System

The turbomachine and tunnel system used for the present investigation is described in detail in references (26) and (27). In general the system consists of a closed circuit tunnel, figure 1, containing an axial flow pump, figure 2, which serves both as the pumping unit for the tunnel and as the test unit. In the present study only a single stage of blading was used, i.e., the guide vane row, one rotor row, and one stator row.

The design of the turbomachine is described in reference (27). Essentially the machine is a scaled version of the axial flow air compressor discussed in reference (5). Thus, although the working fluid used was liquid, the turbomachine investigated herein corresponded to an axial flow air compressor rather than to an axial flow liquid pump. The blading was designed to produce a free-vortex flow at a flow coefficient of 0.45 and with a work coefficient of 0.40. The experiments of reference (27) showed that the design work coefficient was obtained at a flow coefficient of 0.41, the difference from design being attributed to hub and casing boundary layer effects.

Details of the blading are given in references (5), (26), and (27). The information has been reproduced in Table I and in figure 3.

2.2 Instrumentation

Operating control of the turbomachine was accomplished with a hand-operated throttle valve (figure 1) and an automatic speed

controller designed to hold a fixed speed within 0.01 °/o for speeds greater than 150 rpm. Torque load measurements were made directly with weights and an electrical null device. Torque sensitivity was approximately 1 °/o of the measured values.

Flow measurements were obtained with the probes shown in figure 4. Calibrations of the yaw and static pressure probes were made in an air jet. The probe holder permitted radial positioning within 0.01 inches and angular orientations within 0.1 degree. Pressure lines were connected to a series of O-ring valves, and all measurements were made with Statham differential pressure gages calibrated and used with a Baldwin-Southwark strain gage bridge. Two types of pressure gages were used, one having a full-scale range of 1 PSI, the range of the other being 0.3 PSI.

These pressure gages were also used as null indicators for the measurement of flow direction. In this regard it is worth noting that manometers or any device requiring the flow of fluid through connecting tubes could not be used due to the extremely low Reynolds number within the pressure lines and the resulting excessively long response times.

During the course of a test frequent checks of the zeros of the pressure gages could be made without shutting down the turbomachine. In this manner corrections were made for drift in the gage zeros.

Static pressure holes were located, figure 5, along the casing before and after each blade row.

The measurement of fluid temperature was made with a mercury thermometer located in a jacket above the throttle valve. The fluid viscosity was measured before and after each test with a Brookfield Viscosimeter, this being a concentric, rotating cylinder device. The viscosity determination at a given temperature was reproducible within about 2 percent. Specific gravity was measured with a hydrometer.

Considerable use was made of flow visualization to provide qualitative information regarding the flow processes within both the rotating and stationary blade passages as well as along the casing and hub between blade rows. For the most part tufts, (.009" and .013" dia. threads) glued to surfaces and to thin rods, were used and were photographed with a camera coupled with a lighting system which was synchronized to the rotation of the machine. A remotely controlled, adjustable contactor on the dynamometer shaft, wired in turn to a stroboscopic contactor, permitted the synchronization of the lighting system and any desired part of the rotor. This feature made it possible to distribute a large number of tufts over several rotor blade passages, and thereby to obtain in some detail the tuft behavior over localized parts of the blade surface as well as within the blade passage.

In regard to the rotor, the use of tufts had to be considered with care. In the present case the tufts were lighter than the working fluid and hence centrifugal effects would tend to force the tufts radially inward. However, because of low Reynolds numbers (based on the tuft diameter) and low rotative speeds, the viscous forces predominated in determining the direction taken by a tuft. Some difficulties were

encountered with tufts attached to rotating rods. Further discussion of this problem will be presented later. At this point, however, it is useful to consider further some general features of tuft behavior.

A tuft constitutes a thin flexible rod constrained at one end and unable to support a pressure gradient. As mentioned above, in the present application the inertial forces acting on the tuft situated in a rotating system can be neglected. (This would not be the case, for example, if air were the working fluid.) Thus, the shear forces alone determine the orientation of a tuft in both the rotating and stationary systems. A tuft of sufficiently small diameter placed along a solid surface lies in a region of shear flow. If the tuft is assumed to have essentially a solid surface, consideration of the shear force acting on the tuft shows that the tuft will assume a direction somewhere between that taken by the outermost and innermost parts of the boundary layer. Therefore, in cases where strong changes in direction occur within the boundary layer, the direction described by a tuft will be representative of some average state. Where strong gradients in flow direction occur along the length of a tuft, the choice of length becomes important, although the tuft is actually capable of assuming very distorted shapes. In cases of separated flow the direction taken by a tuft will be affected by its length. If the tuft is too long, it may become oriented in the direction of the flow outside the separated region and thus not indicate the direction of motion of the separating fluid. Even in such a situation, however, the tuft still reflects the existence of a separated state.

In the case of the stator blades the validity of flow directions obtained from tufts was verified by means of colored fluid injected at various parts of the stator passage. This technique was also used to provide a picture of the clearance and scraping flows associated with the stator blades. In the experiments with fluid injection, the specific gravity of the tunnel fluid was about 1.2. For coloring, $KMnO_4$ was first combined with the glycerine-water mixture. The specific gravity was maintained at 1.2. However, because of rapid oxidation, the color disappeared quickly. Improved coloring was obtained by combining the $KMnO_4$ with water only. The effect of the difference in specific gravity was examined and was found not to be of major importance in the particular experiments to be described herein (cf. 5:2.3.1.2.).

In general the tufts were found to be sensitive indicators of flow direction, even in the case of non-steady phenomena such as in the passage of a rotating stall region.

III. METHODS AND TESTS

3:1 Control of Viscosity

The range of R_T covered in the present study was accomplished with two different glycerine-water mixtures and with water alone as the working fluid. Tests at R_T of 4000 and below were made with a viscosity of approximately 85 cps. Following these experiments the mixture was changed to give a viscosity of about 14 cps, the corresponding range of R_T being from 12,000 to 22,000. During a series of tests the value of R_T was allowed to vary due to the change in viscosity with temperature. Although constant values of R_T could have been realized by adjustment of the rotor speed, this procedure was not used because of subsequent corrections which would then have to be made to all pressure data. Consequently, most of the data involve a small, but certainly not important, range of R_T. The two glycerine-water mixture ratios which were used (approximately 82 $^o/_o$ and 62 $^o/_o$ glycerine by volume) remained constant during their period of use. Therefore, temperature was the only factor influencing viscosity once the mixture was fixed.

3:2 Flow Rate Determination

Measurement of flow rates was accomplished by calibrating the nozzle located upstream of the turbomachine (figure 1) as a function of Reynolds number. A typical velocity distribution across one diameter at the nozzle discharge (only one diameter was used for calibration purposes) is shown in figure 6. The experimental

discharge coefficients are given in figure 7 for the range of pipe Reynolds numbers included in the present study. Comparison of these results with the results of reference (28) indicate reasonable agreement, although an exact comparison cannot be made because of differences in conditions at the nozzle inlet. (In the reference cited, the nozzle inlet was open to a plenum chamber).

Flow rates were also obtained from surveys made within various parts of the turbomachine. A comparison of these various flow rate measurements is given in Table II. The flow coefficients based on the nozzle calibration are seen to be consistently low relative to other measurements. Based on averages of these data it is possible to improve the accuracy of the nozzle calibration shown in figure 7. However, for the results to be described herein, all flow coefficients were based only on figure 7.

3:3 Reynolds Number Corrections for Total Pressure Measurements

The effect of Reynolds number on the measurement of total pressure with an impact tube immersed in an incompressible fluid is such as to cause the stagnation pressure at the tube to exceed the sum of the static and dynamic pressures of the free stream. A theoretical evaluation of this effect is possible in certain cases. For example in reference (29), the stagnation pressure at the nose of a body of revolution in uniform, incompressible flow is shown to be given by

$P_{T_W} = P_{T_\infty} - \mu \left(\frac{\partial v}{\partial y}\right)_\delta$ * where the symbols are explained in the following sketch:

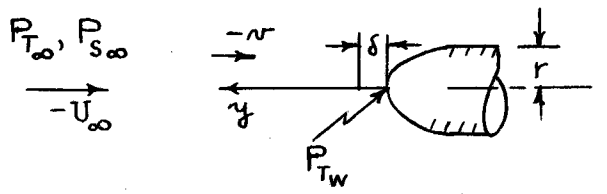

Note: $\left(\frac{\partial v}{\partial y}\right)_\delta < 0$

For the particular case of a source-shaped tube, the total pressure at the wall becomes (ibid)

$$P_{T_W} = P_{T_\infty} + \frac{2}{1 + \frac{0.394}{\sqrt{R}}} \frac{U_\infty}{r} \quad \text{where} \quad R = \frac{\rho U r}{\mu} .$$

For arbitrary nose shapes

$$\frac{P_{T_W} - P_{S_\infty}}{\frac{1}{2} \rho U_\infty^2} \doteq C_p = 1 + \frac{4C_1}{R + C_2 \sqrt{R}}$$ **

---

* This equation can also be derived from the solution[41] of the boundary layer flow near the stagnation point of a plane surface at right angles to the direction of the incident stream.

** For $R < 1$, reference (30) gives the relation

$$C_p = \frac{\text{const}}{R} .$$

where C_1 and C_2 are constants which depend on the nose shape.

In practice the relation for C_p is complicated by the finite hole size.* Furthermore, if the response time is to be minimized, the hole size should be relatively large.[31] Consequently, an empirical determination of C_p (R) is usually necessary.

In reference (32) experimental values of C_p are presented for several different nose shapes. For present purposes, therefore, a particular end shape (that used by Macmillan, ibid., cf. figure 8) was selected for which a reasonable calibration was available. All total pressures, and hence velocities, were corrected by means of this calibration. Figure 8 shows the calibration curve used herein. This curve, taken from reference (32), was modified to give the correction in terms of measured rather than true tube Reynolds number. In addition the curve was extrapolated to lower Reynolds numbers than given in reference (32). Such extrapolation was based on the observation that for all of the tubes described in the reference, (ibid.) the calibration curves for tube Reynolds numbers below 10 were essentially parallel.

For the data presented herein, the tube Reynolds number correction was necessary only for the data obtained at R_T of 2,000 and 4,000.

---

* It is to be noted that if low Reynolds number is attained by reduction in density, the relation for C_p may be further complicated by the phenomenon of slip (ibid). The magnitude of C_p increases with increasing slip (ibid).

3:4 Flow Survey Procedure

The procedure for making flow surveys was dictated by the turbomachine design. In particular a measuring sequence was used whereby flow angle data were recorded first and were then used to set the angular orientations of the total and static pressure tubes.

IV. TEST PROGRAM

The test program comprised two main features; namely, first, the determination of the single stage performance as a function of R_T; and second the study of flow processes associated with each blade row.

For tests at high values of R_T, performance maps, at least in the high flow coefficient range, can be obtained simply by use of fixed total pressure rakes. At low values of R_T, however, large variations of flow angle occurred from hub to tip, the variations, moreover, changing measurably with ϕ and with R_T. Detailed pressure surveys were therefore required. On the other hand primary interest lay in comparative performance as a function of R_T. Such comparisons were readily realized by basing the performance map on static pressures measured along the casing. In this manner performance maps were obtained over the full range permitted by the pump and tunnel system.

The performance of each blade row was studied photographically and by detailed flow surveys upstream and downstream of the blade row. All of the survey data were obtained at either 171 or 291 rpm. This range of rpm permitted a change in R_T by a factor of 1.7 for each glycerine-water mixture. Higher rpm were not used in order to avoid blade bending, particularly for those blades which were mounted on plastic segments for photographic studies. Lower rpm were undesirable because of speed control difficulties and torque measurement inaccuracies.

Data were obtained at R_T values of approximately 2000, 4000, 12,000, 22,000, and 150,000. The large interval between 22,000 and

150,000 was not studied, since, as will be shown later, very little change in over-all performance and only minor alterations in the flow details were observed between these limits.

V. EXPERIMENTAL RESULTS AND DISCUSSION

5:1 Overall Single Stage Performance

The overall single stage performance was obtained for the entire flow-rate range permitted by the turbomachine and tunnel system. The results are presented in the usual form for incompressible fluids; namely, head coefficient and efficiency are plotted as functions of average flow coefficient for each constant value of R_T . As explained previously, the output of the turbomachine is given in terms of static pressure changes along the casing wall. This procedure served to reduce the experimental labor without sacrificing the essential Reynolds number comparisons which were being sought. Where detailed flow surveys were made, the weighted total head coefficients and corresponding efficiencies are included in the overall performance maps.

5:1.1 Head Coefficient Characteristics

The head coefficient was determined from the difference between the maximum casing static pressure measured downstream of the stator (Station 5,* cf. figure 5) and either the static pressure upstream (Station 1) or downstream (Station 2) of the guide vanes. Both differences are presented, since for the high flow coefficient range the use of Station 2 gives results more nearly comparable to the total head coefficient, (in fact for no losses, at design conditions the static head rise based on Station 2 would be exactly equal to the total head rise) while at low flow coefficients, because Station 2 strongly reflects flow reversal from the rotor, (cf. 6:2.2.4) Station 1 gives the more

---

* Station 8 was also used; cf. infra.

appropriate results.

The static head coefficients are shown in figures 9a and 9b. It is immediately clear that major changes in the performance map occur only below R_T of 12,000, in spite of the fact that changes in flow details, to be discussed later, were observed between R_T of 12,000 and 150,000. For the two lowest values of R_T, the high ϕ range could not be obtained because of the limitation imposed by losses in the tunnel system. Nevertheless, the peak values were attained, and these show that at R_T of 2000, the value of $\psi_{(5-2)}$ is about 0.25 which compares to 0.39 at R_T of 150,000. For R_T of 3500, and higher, (the following remark probably applies to R_T of 2000 also) the characteristics in the high ϕ range are essentially parallel, a condition which is also in evidence in the results of reference (23). This result implies, from a practical point of view, that the essential effect of R_T is to change the magnitudes and positions of the high ϕ part of the performance map but that the variation of ψ with ϕ in this range is reasonably the same at all values of R_T down to as low as 2000. The following is suggested as an explanation for this result: at high R_T the rotor relative leaving angle is essentially constant in the high ϕ range. Thus, in the absence of radial equilibrium effects, the rotor output depends only on the entering flow direction, hence on the flow coefficient. At low R_T, separation of the chordwise-moving fluid occurs at practically all ϕ (cf. 5:2.2.1.1.3). In the high ϕ range, however, the relative flow direction followed by the separated fluid

probably remains fairly constant. Thus again, in the absence of radial equilibrium effects, the rotor output would vary directly with ϕ .

For ϕ values below 0.2, the pressure coefficient, $\psi_{(5-1)}$, figure 9a, attains an essentially constant value of about 0.19 for all R_T . In other words the performance in the very low ϕ range is essentially independent of R_T . This condition leads to the deduction that the limiting low R_T characteristic is effectively flat between ϕ of about 0.1 and 0.2 and has a ψ value corresponding to the low ϕ leveling point of the high R_T characteristic. For the present machine, therefore, the performance characteristics for R_T less than 2000, figure 9a, probably fall between that shown for R_T of 2000 and the line $\psi_{(5-1)}$ equal to 0.19, with a rapid drop to zero head occurring at ϕ of about 0.2. However, very near to complete shut-off (a condition not attained in these experiments because of the nature of the throttle valve design) the pressure coefficient will again increase.

It is to be noted again that the foregoing remarks are based on static pressure, not total pressure, changes. The flagged data points shown in figure 9b give the mass-weighted total pressure coefficients for the complete stage, and it is seen that these values correspond reasonably closely to the $\psi_{(5-2)}$ curves except for the two lowest R_T . At these values of R_T the total head coefficient, corrected for nozzle losses, is lower than $\psi_{(5-2)}$. The differences are due primarily to the additional losses incurred between Station 5, where the static pressure was measured, and Station 7, where the total pressures were measured. At higher R_T the additional losses are

small. For the lower R_T closer agreement with the total pressure result is achieved by using the static pressure at Station 8. The head coefficient $\psi_{(8-2)}$ and efficiency $\eta_{(8-2)}$ are shown in figures 9b and 10b. The magnitudes differ from $\psi_{(5-2)}$ and $\eta_{(5-2)}$ but otherwise no essential changes are involved.

On the low ϕ side, for R_T of 2000 and 4000, the detailed surveys to be shown later indicate that the $\psi_{(5-1)}$ values are considerably lower than the total head coefficients measured behind the rotor. (Stator surveys were not made at these low values of ϕ). Still further details, however, will show that little of the kinetic energy is likely to be recovered with the existing stator design. Consequently, the $\psi_{(5-1)}$ data at low values of ϕ and R_T are probably a reasonable measure of usable energy for the stage design tested.

5:1.2 Efficiency Characteristics

The efficiency was determined from the values of $\psi_{(5-2)}$, $\psi_{(8-2)}$, $\psi_{(5-1)}$, the measured torque, and values of ϕ determined from the nozzle calibration. For R_T below 12,000 the values of ϕ are probably low by the order of 5 °/o. Furthermore, the output head includes the contribution from the low efficiency, viscous pumping action of the rotating hub. In the same sense the input torque includes that amount of torque required to produce this viscous pumping, the entire three-stage length of hub being involved.

A rough estimate of the latter effect can be obtained from the theoretical results of Schlichting[33] for a spinning, infinite, half body

in straight axial, laminar flow. The hub torque coefficient (cf. Symbols)

$$C_{T_h} = \frac{1}{\pi} \frac{\phi}{\sqrt{R_\phi}} \sqrt{\frac{c}{r_h}} \left(\zeta_h\right)^4 \frac{1}{1 - \left(\zeta_h\right)^2} C_M$$

where

$$\zeta_h = \frac{r_h}{r_t}$$

C_M = Torque coefficient given in reference (33) as a function of $\frac{L}{r_h}$

L = Half-body length

For $\frac{L}{r_h} = 3$, $R_\phi = 700$, $\phi = 0.3$, the value of C_M (33) is 11, and $C_{T_h} \sim .006$. For these conditions the experimental value of C_T is approximately 0.22. Since the correction is relatively small and is, moreover, compensated somewhat by the energy addition to the cross-flow boundary layer, it was omitted in the data to be presented herein.

As a result of these considerations, the efficiencies to be reported are considered to be conservative measures of the single stage performance, particularly at R_T below 12,000.

Figures 10a and 10b contain the data for $\eta_{(5-1)}$ (based on $\Psi_{(5-1)}$) and $\eta_{(5-2)}$ (based on $\Psi_{(5-2)}$).* The results show that

---

* Values of $\eta_{(8-2)}$ are also included for the lower R_T.

the peak value of $\eta_{(5-2)}$ at R_T of 12,000 is 62 °/o while the peak total pressure-rise efficiency has about the same value. Even at R_T of 3500 the peak value of $\eta_{(5-2)}$ is about 46 °/o. For comparison it is to be recalled that in reference (23) the peak efficiency (the specific measurements upon which this efficiency is based were not stated in the reference) at R_T of 8500 was about 10 °/o.

Between R_T of 150,000 and 20,000 there occurs, of course, a significant reduction in the peak value of $\eta_{(5-2)}$ (or $\eta_{(5-1)}$). Yet in view of the large change in R_T, the measured reduction in $\eta_{(5-2)}$ is much smaller than might have been anticipated. Certainly the reduction is sufficiently small to warrant the interpretation that between R_T of 150,000 and 20,000, a very pronounced and hence critical Reynolds number effect does not occur.

5:1.3 Torque Coefficient Characteristics

The torque coefficient data include bearing losses and the torque associated with the rotating hub (cf. p. 32). The region between the pump drive shaft and the inside surface of the hub also contained the working fluid. The rotation of this fluid was expected to be approximately that of a solid body and should therefore have only a small influence on torque.

The torque coefficients presented in figure 11 contain several features. For all R_T, in the region of maximum C_T, which corresponds essentially to maximum η , the relation between C_T and ϕ is approximately parabolic which implies a linear variation between ψ and ϕ in this range. Except for the high ϕ data at R_T of 3500, a

consistent increase in C_T occurs with decreasing R_T, the most pronounced increase occurring below R_T of 4000. A correspondingly large increase in rate of change of fluid angular momentum occurs, of course. Some insight into this change will be found in the later description of flow survey and photographic details.

A further feature of interest occurs at the lowest value of ϕ where each torque curve becomes essentially flat. Changes in C_T between shut-off and the minimum ϕ values at which data were obtained are unlikely to be drastic, which would lead to the conclusion that for this type of machine the level of the starting torque, sometimes important for pumping applications, should not exceed the peak-operating torque for a given R_T .

5:1.4 Critical Reynolds Number Range

The overall performance data provide information in regard to what might be termed a "critical" Reynolds number range. A number of criteria may be used, and four of these are shown in figure 12 where the variations of $\eta_{(5-2)_{max}}$, $\Psi_{(5-2)_{max}}$, $\phi_{[@(5-2)]_{max}}$ and $C_{T_{max}}$ are given as functions of R_T . The range of R_T in which very rapid changes begin to occur lies between 20,000 and 10,000.

A further indication of the critical range is given by the variation of $\eta_{(5-2)_{max}} \Big/ \left[1 - \eta_{(5-2)_{max}}\right]$ (i.e. output/losses) with R_T as shown in figure 13. The data suggest the following functional relations:

$$\frac{\eta}{1-\eta} \propto R_T^{0.18} \qquad 150,000 > R_T > 20,000$$

$$\frac{\eta}{1-\eta} \propto R_T^{0.65} \qquad R_T < 20,000$$

These may be useful guides for the estimation of changes in peak efficiency due to Reynolds number effects in single stage, axial turbomachines similar to the one tested here.

At this point it is also of interest to compare the present results to the data compiled by Davis et al.[34] From a survey of data from many turbomachines, Davis shows, very roughly, that for peak efficiency

$$(1-\eta) \propto (R_D)^{-\gamma'} \qquad (D = \text{tip diameter})^*$$

From his data for axial flow compressors, the values of γ' for R_D between 2×10^5 and 10^6 vary between 0.6 and 0.18. For the present results, the values of γ' as shown in figure 14 are

$$\gamma' = 0.22^{**} \qquad 1.5 \times 10^5 > R_T > 2 \times 10^4;\ 10^6 > R_D > 1.4 \times 10^5$$

$$\gamma' = 0.37 \qquad R_T < 2 \times 10^4; \qquad R_D < 1.4 \times 10^5$$

Thus, in the present case the loss variation for $R_T > 20,000$ corresponds approximately to the lowest value shown by Davis.

---

* For the present machine, $R_D = 7\ R_T$

** It is interesting to note that flat plate drag laws based on plate Reynolds number give exponents of 0.20 for turbulent flow and 0.50 for laminar flow.

5:1.5 Static Pressure Variation Along Casing

As a further indication of overall performance the static pressures were measured along the casing of the machine from a position in front of the guide vanes (Station 1, figure 5) to a position far downstream of the stage (Station 12). These pressures, referred to the pressure at Station 1 and converted to coefficient form, are presented in figure 14 for three values of ϕ at each value of R_T. The ϕ values correspond to η_{max}, $\psi_{T_{max}}$, and ϕ_{min}.* A number of features, some of which will be amplified further by the more detailed experiments, are apparent from the static pressures.

First, the similarity of the curves for $R_T > 12,000$ provides an additional basis for the conclusion that no radical or "critical" Reynolds number effects occur at higher values of R_T.

Second, the pressure change (including values at flow rates other than those shown in figure 15) across the guide vanes gives a measure of the total pressure loss across the guide vanes, and provides in addition a basis for stipulating the initiation of flow reversal from the rotor tip region back into the guide vanes. (Cf. 5:2.1.4)

Third, the occurrence of a large pressure drop across the stator followed by a pressure rise** immediately downstream where no blade

---

* The value ϕ_{min} corresponds to the lowest flow rate attainable at each R_T.

** The downstream pressure rise also appears in the high R_T data. In these cases, however, the rise results only from the fact that the static pressure hole location is near the suction surface of a stator blade, and consequently produces a static pressure measurement which is lower than the pitchwise average.

rows exist reflects the occurrence of strong separation at the casing end of the stator blades. The existence of this condition will be demonstrated later. (cf. 5:2.3.1.2)

Fourth, at all R_T and ϕ values, except near shut-off where flow reversal downstream of the stage occurs along the hub (cf. 5:3.3) the pressure drop along the casing becomes steeper between Stations 8 and 12. Since the downstream end of the rotating hub is approximately at Station 7, the higher pressure drop is attributed to the termination of energy addition to the cross-flow boundary layer along the rotating hub, and to the subsequent retardation of the cross-flow along the stationary hub.

Fifth, the high static pressure coefficients behind the rotor at near shut-off conditions are indicative of high energy input from the rotor to the fluid. The fact that the net output far downstream is low (cf. figure 10) points to the existence of flow patterns (cf. figure 59), which involve high losses.

5:1.6 Throttle Setting Dependence on Reynolds Number

All of the preceding performance descriptions were based on measurements obtained within the turbomachine. An additional, essentially independent, and simple indicator of overall performance is provided by data which involve no measurements within the turbomachine, i.e., by the flow nozzle pressure drop, which determines the flow coefficient, and by the tunnel throttle position which was read from a mechanical counter.

The variation of flow coefficient with throttle setting at each R_T is given in figure 15. It can be seen that only a small difference in the throttle curve occurs between R_T of 150,000 and 20,000. The regions of rapid decrease in ϕ correspond to rapid reductions in turbomachine performance. (cf. figures 9, 10, 11) Below R_T of 20,000 the throttle characteristic begins to change significantly, as does the turbomachine performance. Below R_T of 12,000 the region of abrupt change is gradually eliminated and is almost non-existent at R_T of 2,000. This occurrence suggests an accompanying lack of sudden change in the turbomachine flow patterns. Later discussion will clarify this condition.

5:2 Blade Row Characteristics

When the viscous forces become a predominant factor in determining the flow process within an axial turbomachine, the flow details will become correspondingly more complex. Thickened boundary layers on blade surfaces will accentuate the non-steady character of the flow. Variations in pressure, velocity, and flow directions in radial, circumferential, and axial directions will make the flow pattern strongly three-dimensional. Mixing, blade boundary layer instability, corner flow, and secondary flow comprise some of the additional problems which assume greater importance. In the lowest R_T tests of the present investigation all of the above factors were prominent.

Although a detailed quantitative study of these effects could not be made, photographic and flow survey data did produce information

from which some of the important gross features of the complex flow patterns could be constructed, thereby providing some insight in regard to the nature of strong viscous flow effects in an axial turbomachine.

In the following, the observations for each blade row will be discussed separately.

5:2.1 Guide Vane Characteristics

The guide vanes had been designed to initiate a free-vortex flow with turning angles of about 19^{o} and 30^{o} at the tip and hub respectively (cf. figure 23, reference (26)). Except for the wall regions, the experimental values, obtained for an average guide vane Reynolds number ($R_{GV} \approx R_{\phi}$) of 80,000, were reasonably close to design.[26]

In the present study, a reduction in R_{GV} could be realized only with an accompanying increase in hub and casing wall boundary layer thicknesses upstream of the guide vanes. This condition meant, in turn, that secondary flow effects. (e.g. reference (35)) would change with Reynolds number. Furthermore, non-uniformity in Reynolds number would result along the guide vane span, and all of these effects would in turn modify the stage performance. This situation had to be accepted. On the other hand these features are properly a part of a practical installation which adds some importance to their occurrence.

5:2.1.1 Conditions at the Guide Vane Inlet

In order to examine the non-uniformity at the inlet, for two low values of R_{GV} radial surveys of total pressure were made at approximately one chord length upstream of the guide vanes and at one

circumferential position. The results, given in terms of the local-to-maximum velocity ratio, are shown in figures 16a and 16b for R_{GV} values of 630 and 1380 respectively. The boundary layer thicknesses, quite naturally large, are as follows:

R_{GV}	δ_{TIP}	δ_{HUB}
630	0.84"	0.47"
1380	0.58"	0.32"

On the basis of these measurements relatively large regions of rapid changes in turning are to be expected near the hub and tip at the guide vane exit, these regions diminishing in radial extent as R_{GV} increases. Correspondingly, underturned regions will occur over the major parts of the span.

The low pipe Reynolds numbers at which the data of figures 16a and 16b were obtained should produce laminar velocity profiles at both the hub and casing upstream of the guide vanes. With the boundary layer thickness defined as the point where $\frac{V}{V_{max}} = 0.99$, the boundary layer velocity profiles were determined. These are plotted in figures 16c and 16d. The Blasius profile[36] is also included, and its similarity to the data demonstrates that the profiles are laminar.

Surveys at the guide vane inlet were not made at higher Reynolds number. However, if the criterion, $R_P \geq 2 \times 10^5$,[28] is used to specify the beginning of turbulent boundary layers at the discharge of a

nozzle, then for all except the highest R_T (150, 000) test conditions used in the present study, the boundary layers entering the guide vanes should be laminar.

5:2.1.2 Turning Angle

In order to obtain information on the magnitude of the turning angle as it changes with R_{GV} , radial surveys were made directly behind the guide vanes, Station 2, in approximately the mid-pitch region. The angles so measured are expected to be sufficiently representative of circumferential averages so as to properly reflect the Reynolds number effect.

The results are given in figure 17 where the flow angle measured from the direction of the machine axis is plotted against radius-ratio for nine values of R_{GV} from 598 to 60, 000. The decrease in turning with reduced R_{GV} is evident over most of the span as is also the increase in width of the region of rapid change. Between these rapid change regions the spanwise variation of turning remains about the same for all test values of R_{GV} . In the end region near the tip the rate of turning angle change with radius is also much the same at all R_{GV} . Near the hub, however, the results reflect more than blade surface boundary layer and secondary flow causes. Although the guide vanes were situated over a stationary part of the hub (figure 2), the survey position was situated over a rotating part. Consequently, the angles measured near the rotating hub reflect the increased cross-flow produced by the hub rotation, and the changed boundary condition

which occurs between the stationary and rotating parts.

Some practical information in regard to the Reynolds number effect for the main part of the span can be obtained from the plot, figure 18, of the flow turning at the mid-radius ($\zeta = 0.80$) as a function of R_{GV}. For the range of R_{GV} between 80,000 and 10,000, the data indicate, very roughly, a decrease in turning of about 1^{o} for each 10,000 units reduction in R_{GV}. Below R_{GV} of 10,000 the data follow the relation

$$\theta_{GV} \propto (R_{GV})^{\frac{1}{10}}$$

In regard to the possibility of predicting the guide-vane turning angle curves at low R_{GV}, existing methods appear to be unsatisfactory. Although the curves have forms somewhat similar to those for high R_{GV},[37] (the reference data are based on circumferential averages while the data of figure 18 are for one circumferential position only) the computation is complicated by the thick boundary layer growth along the blade surfaces. Thus, calculations for the turning in the central-span part of the blade must include the blade-surface viscous effects. For the wall regions similar considerations are involved; for example, in the experiments at R_{GV} of 600 the Reynolds number based on the momentum thickness at the casing was about 50. Flow in this region, therefore, must be controlled by viscosity. One might expect, that the boundary layer analysis of Mager[12] would be appropriate for the wall regions, at least in cases where radial flow and turning in the main stream are not large.

Mager's results (ibid) were applied to the data for the lowest R_{GV} tests in order to obtain some indication of a theoretical value for the maximum deflection in the boundary layer at the casing. The assumption was made that

$$\frac{W}{U} \propto \xi$$

where W = Tangential velocity of main stream

U = Axial velocity of main stream

ξ = Axial coordinate measured from guide vane inlet

Then with the relation for the maximum deflection in the boundary layer

$$\beta_{b\ell} = \arctan\left[\frac{W}{U}\left(\frac{B}{0.332} - 1\right)\right] \quad \text{(Reference (12))}$$

and the value of B obtained from figure 3c (ibid) (for that figure m = 1, Ⓗ = 0.36), the value of $\beta_{b\ell}$ was found to be approximately 22 degrees. The experimental value obtained by extrapolating the experimental turning angles to the wall is approximately 20 degrees.*

The comparison is sufficiently close to at least indicate that the correct turning angle trends in the wall regions may be accounted for by Mager's boundary layer analysis.

5:2.1.3 Total Pressure Loss

The total pressure loss incurred by the fluid as it passes through the guide vanes at different values of R_{GV} is of course another important performance characteristic. In the present study detailed

---

* However, casing tufts (cf. fig. 23) show the deflections to be about 18° near the pressure surface and 38° near the suction surface.

surveys to determine the loss were limited to the lowest value of R_{GV} (R_{GV} = 600). For determination of the loss variation with Reynolds number, a different procedure was used. This will be presented below. For the survey tests the rotor was placed in the third stage and surveys were made at the first stage stator outlet position, Station 4. This downstream position was chosen in order to permit mixing to take place and thereby reduce the required number of circumferential surveys. Two additional features had to be accepted, however. First, an additional loss due to flow along the casing occurs, and second, rotational energy is added to the boundary layer by the rotating hub. These effects are not large and, moreover are compensating with regard to loss evaluation. They were not accounted for by any form of correction.

Radial surveys were made at five circumferential positions. In figure 19a are presented the radial variation of total pressure loss at two of the circumferential stations spaced a distance equivalent to about one half of the guide vane pitch. The large loss in the midspan region is a measure of the thick blade surface wakes. At the hub the negative values reflect the energy added by the rotating hub. The mass-weighted averages of the radial surveys are given in figure 19b. Although it appears that the larger losses occur near the casing, if the losses were computed on a streamtube basis, the casing region would exhibit smaller losses.

The average loss, referred to the mass-weighted average total pressure upstream of the guide vanes, was 36 $^{o}/o$ of the velocity

pressure based on the average axial velocity, i.e.,

$$\frac{(\Delta P_T)_{GV}}{\frac{1}{2} \rho u_t^2 \phi^2} = 0.36.$$

This is to be compared to the loss measured in reference (38) for similar guide vanes (but higher aspect ratio) at R_{GV} of about 80,000. In that case the loss coefficient over most of the span was about .02, with the average value being between .02 and .05.

In order to obtain information on the loss variation with Reynolds number, a simplified procedure was used. Application of the Bernoulli equation across the guide vanes at the casing gives as an approximation for the loss in this region

$$\frac{\Delta P_{T_t}}{\frac{1}{2} \rho u_t^2 \phi^2} \approx \left(1 - \frac{1}{\cos^2 \theta_b}\right) - \frac{\psi_{(2-1)}}{\phi^2}$$

where θ_b = Flow angle at guide vane exit near outer edge of casing boundary layer

$\psi_{(2-1)}$ = Change in casing static pressure coefficient across guide vane

ΔP_{T_t} = Total pressure loss across guide vanes at casing

Values of θ_b were obtained from figure 17, and corresponding $\psi_{(2-1)}$ values were obtained from experiments made at maximum flow rates at each Reynolds number.

The loss calculated in this manner is considerably larger than the average over the blade span. Nevertheless, the variation with R_{GV} is considered to be an indication of the average loss variation.

The experimental results are shown in figure 19c. Average loss values are included at both ends of the curve, and an estimated average loss variation between these end values has been drawn based on the form of the experimental curve. From these results it appears that the loss increase is gradual down to R_{GV} of about 10,000 below which the increase is rapid. It should be recognized, however, that the loss variation described in figure 19c is not confined to the guide vane profile losses alone, but rather includes the added effects due to casing and hub boundary layer changes coincident with Reynolds number changes.

It is interesting to note that in the above loss evaluation, the value, $R_{GV} = 10,000$, corresponds to R_T of about 20,000, which in figure 12 was seen to be the value of R_T for which the peak efficiency began to decrease rapidly.

5:2.1.4 Flow Reversal From Rotor to Guide Vanes

The casing static pressure change across the guide vanes provides an interesting approximate indication of the beginning of flow reversal from the rotor to the guide vanes. This effect can be deduced from figures 14a, 14b, and 14c.

In figure 20a experimental values of $\Psi_{(2-1)}$ are plotted as a function of ϕ for each R_T. Also included is a theoretical curve for

$\Psi_{(2-1)}$ based on vortex flow, no losses, and design turning at the tip. (This curve results simply from the Bernoulli equation for these conditions). In the range of negative $\Psi_{(2-1)}$ the difference between the theoretical and experimental curves is a measure of two things; namely, underturning in the flow outside of the casing boundary layer, and total pressure loss across the guide vanes, particularly in the casing region. Both of these problems have been discussed before. Here, however, it is to be noted that with or without losses (cf. p.45 for loss equation), the value of $\Psi_{(2-1)}$ should always be negative, unless a rotor influence, primarily as reversed flow, occurs. An example of such flow reversal is given by the tuft pictures in figure 20b. In figure 20b(1) the tufts near the rotor tip and along the casing at the guide vane exit show no reversal. In this case $\phi = 0.26$ and $\Psi_{(2-1)}$ is negative. In figure 20b(2) both the rotor tip and casing tufts give clear evidence of reversed flow. In this case $\phi = 0.15$ and $\Psi_{(2-1)}$ is positive.

A quantitative criterion which gives a fair approximation to the flow coefficient at which the flow reversal first begins can be obtained from the value of ϕ corresponding to a zero value of $\Psi_{(2-1)}$. For the present machine the variation of this ϕ, as determined from figure 20a, with R_T is presented in figure 20c. As an example, according to this criterion, the value of ϕ for initiation of flow reversal at R_T of 150,000 is about 0.28. Actual tuft observations gave a corresponding value of approximately 0.3.*

---

* This latter condition also corresponded to the onset of rotating stall as observed with tufts.

5:2.1.5 Flow Visualization

As a final aspect related to the guide vane characteristics, the photographic information obtained at various R_{GV} will be described. In the early part of the test program, i.e., the lowest Reynolds number phase, photographs were made at first with white tufts attached to the beryllium blades. The guide vane photographs taken in this way were unsatisfactory. Later, considerable improvement was effected by coating the blade surfaces with a thin layer of white paint and then using black tufts. As replacements for the unsatisfactory guide vane photos, sketches of tuft orientations, made during the tests, will be used. The results will be discussed in the sequence from low to high Reynolds numbers.

5:2.1.5.1 Results with Viscosity at 85 cps (Nominal Value)

Figure 21 shows a sketch of the pressure and suction surface tufts for $R_{GV} \approx 600$ and $\phi \approx 0.28$. A number of features are to be noted. First, permanent separation did not occur anywhere along the blade surface or in the corners at the blade ends. On the other hand, sufficiently close observation of the leading edge could not be made to ascertain the occurrence of a laminar bubble, although presumably such a bubble effect could exist. Along the front part of the blade, the flow is essentially chordwise on both surfaces except near the blade ends of the suction surface where the flow begins to move radially outward from the hub and radially inward from the tip. At the trailing-edge-half of the blade, along the suction surface the

radial motion increases at both ends. A region of no radial deviation exists at a distance of about 1/4 the span length measured from the hub.

One might have expected that radial movement of the boundary layer would increase with decreasing R_{GV}. It is well to recall, in this regard, that the tufts indicate some average direction of the boundary layer motion. Therefore, very close to the tip of the suction surface near the trailing edge stronger radial inward motions may occur. However, since motion from the hub also exists, there certainly must be a region or at least a line of no radial flow. A further factor which tends to lessen the radial flow follows from the fact that the radically reduced turning of the flow produces a smaller radial pressure gradient.

The three tufts closest to the tip at the trailing edge of the suction surface were observed to lie removed from the surface a distance of about 3/16", a condition which is a measure of a thick boundary layer and which, moreover, serves to indicate that the under-turning of the flow is caused to a large extent by thick surface boundary layers. The pressure surface flow is chordwise with some radial inflow near the trailing edge and close to the hub. The larger turning along the stationary hub is also indicated.

The flow along all of the surfaces and within the blade passage (this latter region was observed by tufts attached to thin rods) was extremely steady. The low turning described earlier is substantiated further by the rake tufts shown in the photo, figure 22. In this figure flow is from bottom to top and the rotor motion is from left to right.

The tuft rakes attached to the casing and located downstream between the guide vanes and rotor show the increased turning produced by the rotating hub. Tufts located at the trailing edge of the pressure surface show a deviation toward the suction surface, but at the same time they indicate smooth flow leaving the trailing edge region. (This, as might be expected, is quite in contrast to the stator and rotor results to be described later.)

The increased turning near the casing is shown in figure 23. In this case the compact stage configuration was used. In regard to the effect of the proximity of the rotor and guide vanes on the average turning through the guide vanes at the ϕ conditions of figures 22 and 23, measurements of flow angle made directly in front of the rotor and in the same position with the rotor moved one stage downstream revealed, for most of the radius, differences unimportant in terms of measurement accuracies.

Additional observations of the flow through the guide vanes were made at R_{GV} as low as 100, but under these conditions the flow coefficient was extremely low. Consequently, this information will be presented later in connection with a discussion of flow reversal and recirculation which occurs at low ϕ .

5:2.1.5.2 Results with Viscosity at 14 cps (Nominal Value)

The behavior of the tufts at R_{GV} of 600 and 1200 revealed no peculiarities or drastic motions. One might expect to find, therefore, as R_{GV} increases, a gradual thinning of the boundary layers, a

lessening of the radial flow, and finally increasing turning angles. The first and the last of these occur. The second, surprisingly enough, does not.

Evidence justifying the latter statement can be seen in figures 24a and 24b which show the suction surface tufts for R_{GV} of 3990 and ϕ of 0.323. The flow after about the rear 40 $^{o}/o$ of the blade and from the casing to a distance of perhaps 3/8" from the hub is strongly radial inward. The tufts which lie at the blade edge near the hub have very little radial outward motion. Associated with this are the tufts on the stationary hub; they do not move radically toward the suction surface. Although it can not be seen in the photos, the corner flow at the tip is separated. Consistent with this separation are the directions of the casing tufts shown at the left of figure 24b. They show that at the casing, part of the flow moves completely to the suction surface, a condition which is possible only if the corner separates thereby stopping the through flow. Part of the radially inflowing fluid is therefore originally low energy fluid from the casing.

The pressure surface flow, in contrast, is almost perfectly chordwise as can be seen in figure 25.

In order to examine the possibility of eliminating the tip corner flow separation with the aid of additional turbulence, a 5/16" diameter tubular barrier was placed circumferentially at the casing immediately upstream of the two guide vanes at the location of the window. Figure 26a shows that the separation remained. Still with the barrier, an increase in R_{GV} to 5480 (accomplished by raising ϕ to 0.443) caused

the radial inflow to become even more severe as shown in figure 26b.

One is led to the conclusion, therefore, that the increased radial flow at this value of R_{GV} must arise from an increase in turning and hence an increase in radial pressure gradient which becomes large enough to drive the boundary layer inward. Since at higher R_{GV} the radial inflow ceases, it appears that there exists a "critical" range of R_{GV} as far as the observed radial flow phenomena in the guide vanes are concerned. Although such a critical range of R_{GV} was not determined specifically in these tests, information given in the following section shows that the radial inflow was absent for values of R_{GV} of 16,000 and higher.

5:2.1.5.3 Results with Water

With water as the working fluid, the flow through the guide vanes in the higher ϕ range is smooth and without peculiarity. Figure 27a, taken at R_{GV} of about 16,000 and ϕ of about 0.45,* figure 27b, taken at R_{GV} of 49,500 and ϕ of 0.338, and figure 27c, taken at R_{GV} of 55,800 and ϕ of 0.381, show, as intended in the guide vane design, almost perfectly chordwise flow along the suction and pressure surfaces respectively. The hub and casing tufts between the guide vanes are also visible. For purposes of contrast with the results of the previous section, the casing tufts at the left of figure 27c show, consistent with the lack of radial inflow along the suction surface, no movement of casing flow completely to the suction surface.

---

* At this condition the rotative speed was about 40 rpm, so that accurate flow rate measurements could not be made.

At lower ϕ , behavior of the tufts changes, but this information will be reserved for a later section, since here the influence of R_{GV} is of primary interest.

5:2.1.6 Remarks on Applicability of Results

The Reynolds number effects described above are considered to be general for blading comparable to that used in this study. For other blading, quantitative differences are to be expected principally from factors associated with radial changes in chord length, design radial distribution of turning, and aspect ratio.

If the chord length is not constant from hub to tip, but the design is a free vortex, some differences in radial flow effects may occur. For example, if the chord is least at the tip, radial inflow from the tip region should affect a larger chordwise extent of the blading below the tip than was observed in the present design.

If the design radial distribution of turning differs from a free vortex, or if in any type of distribution the magnitude of the radial change in turning differs markedly from the present case, the results may not be generally applicable. For non-vortex-free flow, radial movement within the passage is inherent in the design, so that the radial motions caused by Reynolds number reduction will certainly encounter modifying influences. For the larger turning designs, a larger pressure gradient, compared to the present case, from hub to tip will occur, a condition which will provide a greater force for producing radial inflow from the tip. However, in this case an

alleviating feature also occurs, this being the larger acceleration through the blade row with corresponding thinner boundary layers.

Higher design turning will also lead to stronger boundary layer deflections at the casing and hub (cf. reference (20)) than were observed in the present experiments. Here again, it is worth recalling that the tufts do not necessarily give the flow deflections at the walls. On the other hand, even if fluid motions are different beneath the tufts, the quantity of fluid involved in this way is small.

In regard to aspect ratio, in the machine tested the guide vane aspect ratio was about 1.5, this being low relative to the values used for air compressor guide vanes. Consideration of the effect of higher aspect ratio on the flow near the hub and casing walls has been discussed in reference (7). It is explained (ibid) that if the aspect ratio is increased by a reduction of chord alone, because of increased curvature of the flow passing through the blade row, the secondary flow may increase. The increase will occur provided the increased curvature is not accompanied by a proportionate decrease in wall boundary layer thickness due to reduced chord length. Application of this reasoning to the present case of low Reynolds numbers leads to the observation that since the wall boundary layers are thick, the increased curvature effect should predominate. Thus one might expect stronger secondary flows than were obtained herein if the aspect ratio were increased by reduction of chord alone. An increase in span alone presumably would modify the radial extent of the overturned regions near the wall. Outside of the wall boundary layer regions, at low

Reynolds numbers the thick blade surface boundary layers would also exist for higher aspect ratio, so that the loss in this region should remain high and the turbulence source should still exist. In addition the underturning, insofar as it is caused by thick blade surface boundary layers, should also occur for higher aspect ratios.

5.2.1.7 Principal Effects on Rotor Performance

In regard to guide vane-rotor interaction, one can say that the guide vane characteristics at reduced Reynolds number have principally three effects on rotor performance. First, the reduced turning, over most of the blade span causes the rotor to operate, for a given average flow coefficient, at an effectively lower flow coefficient. This condition is a partial explanation of one of the differences between the present data and that of reference (23), namely, the variation of ϕ at η_{max} with R_T. Since no guide vanes were used in the configuration of reference (23), one should really compare the results of those tests with the variation of the effective flow coefficient in the present tests. Such a comparison will show somewhat larger reductions in ϕ at η_{max} for the present tests.

The second effect is produced by the secondary turning, within the guide vanes, of the hub and casing boundary layers. This turning reduces at the rotor inlet the otherwise high incidence angle caused by the low local flow coefficients.

A discussion of the third and most important effect, the formation of turbulence which suppresses rotor leading edge separation, will be deferred until the rotor characteristics are presented.

5:2.2 Rotor Characteristics

When fluid enters a rotating system, the boundary layers along the moving surfaces begin to approach the local rotative speed of these surfaces. Ordinarily in the case of an axial flow pump or compressor rotor the relative tangential velocity opposes the direction of rotor rotation, so that for small radial velocities the centrifugal force acting on part of the boundary layer fluid exceeds the radial pressure gradient. As a result, this part of the boundary layer moves radially outward. One expects, therefore, that as the Reynolds number is reduced and the boundary layers become thicker, more fluid will acquire radial motion.

On the other hand the chordwise motion of the blade surface boundary layer fluid can be interrupted by laminar and/or turbulent separation, particularly as the Reynolds number is decreased. These possibilities coupled with the likelihood of radial motions lead to the expectation of complex boundary layer behavior in a rotor at low Reynolds number.

A number of the important features of this behavior were observed in the present study. The most pronounced effects, of course, occurred at the lowest values of R_T, so that a major part of the following material will be concerned with information obtained at these R_T. The contrasting features of higher R_T operation will also be presented.

Wherever possible, quantitative flow survey data are correlated with photographs of tuft orientations, and where used, the paths followed by colored tracer fluid.

5:2.2.1 Flow Characteristics at R_T of 2000 and 4000 (Nominal Values)

The results of these experiments have been organized in terms of flow conditions associated with various parts of the rotor. The leading edge flow was of particular interest, since herein lay the expected link between the isolated airfoil (Part I) and turbomachine performance.

5:2.2.1.1 Flow Visualization

5:2.2.1.1.1 Leading Edge Flow

It is useful, first of all, to consider the flow conditions at the rotor inlet. The underturned fluid emerging from the guide vanes causes higher attack angles on the rotor blades compared to the condition of correct turning. The leading edge flow, of course, depends to a large extent on the inlet velocity diagram. In the present low Reynolds number experiments, because of the circumferentially and radially varying conditions at the guide vane exit, accurate velocity diagrams were difficult to form. Nevertheless, some indications of the attack angles were obtained from a diagram based on the mean flow coefficient and the guide vane turning angle measured at approximately the half-pitch position and at the mean radius. The approximate mean-radius velocity diagrams formed in this manner for R_T of 2,130 and 3,600 and for the corresponding maximum attainable ϕ (which also corresponded closely to maximum $\eta_{(5-2)}$, figure 11b) at each R_T are shown in figure 28.

The significance of these diagrams is made clearer in the following tabulation:

A. (Experimental results at low Reynolds numbers)

R_T	$\phi_{MEAS.}$	$\theta_{GV_{MEAS.}}$	α	i
2130	.281	11.6^o	25.5^o	15.3^o
3600	.348	12.2	20.5	10.3

B. (Same R_T and ϕ as in A. θ_{GV} assumed to be that obtained for $R_{GV} = 80,000$)

R_T	$\phi_{MEAS.}$	θ_{GV} at $R_{GV} = 80,000$	α	i
2130	.281	22.4^o	23^o	12.8^o
3600	.348	"	19.2	9

C. (Experimental results at high Reynolds number)

R_T	ϕ at $\eta_{(5-2)_{max}}$	θ_{GV} at $R_{GV} = 80,000$	α	i
146,000	.415	22.4^o	12.8^o	2.5^o

Comparison of A and B indicates that even though the turning produced by the guide vanes is about one-half the high Reynolds number value, the effect on α or i at the mean radius is relatively small. On the other hand, comparison of A and C shows the large increase in α caused by the reduction in ϕ. Certainly, based on the results of reference (6), the rotor in conditions A is in the region of high drag, and yet these are the conditions for maximum efficiency at the low R_T.

Thus it appears that the low values of R_T being considered here are accompanied by very high angles of attack for the rotor blade. Both of these factors are such as to make less likely the possibility of leading edge flow without complete separation. Yet in spite of this situation, tuft photos describing the leading edge flow show that except for the region within about 1/2" of the blade tip, the flow around the leading edge remains attached. Although later photos provide evidence of leading edge laminar bubbles, the photos to be described at this point do not show this condition, but it must certainly be true that such bubbles do exist.

Figures 29a through 29k are a series of photos of tufts located in various ways at or near the rotor blade leading edges. The photos were made with an expanded stage, i.e., with the guide vanes in the first stage, the rotor in the second stage, and the stator in the third stage. With regard to the rotor no basic differences in leading edge phenomena were observed with the rotor in either the first or second stage, although in the second stage position the angle of attack at the tip was slightly increased, while that at the hub was decreased.

Figure 29a* shows a group of 5 tufts on the blade between No. 2 and No. 3 which are actually attached near the leading edge of the pressure surface and which, therefore, pass completely around the

---

* Many features other than leading edge phenomena are to be seen in the photos; these will be described in later sections. Rotor rotation is from left to right in the photos. Flow is upward. The visible numbers are attached to the moving hub. The specified flow conditions are approximate, small variations from these values being due to room temperature changes leading to changes in viscosity.

leading edge. The flow conditions correspond to $\Phi = .282$, $R_T = 2230$. The two tufts closest to the tip have separated, the other three have not. A second picture of these same tufts having the same behavior is shown on the left blade of figure 29b. The tufts on the blade between No. 3 and No. 4 are a group which are attached close to the leading edge of the suction surface. Their behavior is the same as mentioned above. Figure 29c is a different view of these same tufts.

Figures 29d through 29f show the tufts described in the previous paragraph (observe the numbers at the hub) but with the flow conditions now given by $\Phi = 0.355$, $R_T = 3890$. Due primarily to the increased Φ, *the tip tufts are not as badly separated.* The other tufts appear unchanged from their orientations at the lower Φ and R_T.

The pressure surface attachment locations of the tufts shown in figures 29a and 29d are pictured in figure 29g. It is appropriate to note here that these tufts, while providing evidence of separation, or lack of it, around the leading edge of the suction surface, do not necessarily describe correctly the position of the stagnation points on the pressure surface. During the process of machine starting the attack angles are considerably higher than during steady state. At the initiation of starting, then, the tufts correctly reflect the location of the stagnation points. However, once the tufts become oriented around the leading edge, the shear forces are such as to sustain this orientation even though, as steady state is reached, the stagnation points move in the direction of the suction surface.

Groups of tufts used for different purposes but which nevertheless provide further evidence of the leading edge flow, are shown in figures 29h through 29j. Figures 29h and 29i are two views of tufts originating from a rod located near the leading edge of the pressure surface.

All of the tufts described above, except those closest to the tip, were quite steady in their orientation. The tip was less steady due to the complex, non-steady flow of the entire tip region from leading to trailing edge. Although more detailed discussion of this feature will follow later, figure 29k is nevertheless included here to indicate the flow reversal which occurs along the tip region and which extends at times nearly to the leading edge.

The foregoing results considered collectively with the isolated airfoil results of reference (45) and with the overall performance of the machine used in the present study compared to that of reference (23) (which contained no guide vanes) lead to the conclusion that the lack of completely separated leading edge flow is caused by turbulence originating primarily from the guide vane wakes and to non-steady flow associated with rotor blade passage through blade wakes.

Although no information regarding the character of the turbulence can be offered from the present experiments, the data of reference (39), wherein turbulence measurements were obtained in the wakes of guide vanes at high Reynolds numbers, offer a basis for judgement in the present situation. According to their results, (ibid) immediately

behind the guide vanes the fluctuation intensity outside of the wake regions was about 0.3 per cent, while within the wake the intensity was about 6 per cent. Thus, as in the present case, when the blade wakes are thick, (cf. figure 19a) the average fluctuation intensity may be on the order of 3 per cent or more. Values of this magnitude characterize turbulent flow in pipes[40] and are probably high enough to cause laminar reattachment.

In regard to the non-steady flow mentioned above, reference (39) shows that the fluctuation intensity increases five-fold as the outside-of-the-wake region reaches the rotor. Moreover, it is to be recalled (cf. reference (45)) that in the isolated airfoil tests, a vibrating airfoil, which produces an effect comparable to a non-steady flow of fluid, was found to be very effective in causing laminar reattachment on a thick Joukowsky airfoil at low Reynolds number.

The foregoing considerations certainly point to the importance of the flow emerging from the guide vanes in suppressing leading edge separation in the rotor.

5:2.2.1.1.2 Hub and Blade Corner* Flow

Two additional regions of importance which characterize the rotor flow lie first, in the vicinity of the rotating hub (hub flow) and second, in the corner between the suction surface and the hub (blade corner flow). The essential feature of the hub flow, at the higher ϕ , is the very strong motion of the fluid from the pressure toward the suction surface, while the eventual effect of such movement on the

---

* The corner fillet was formed by a radius of approximately $\frac{3}{64}$"

blade surface flow depends on the behavior of the corner flow.

a. Hub Flow

The characteristics of the hub flow are described in figures 30a through 30h. The photos include both the expanded and compact stage configurations. A reference frame for viewing the hub flow within the blade passage is provided by figures 30a and 30b which show, for the highest ϕ obtainable at R_T of 2230 and 3890, the direction of the hub flow upstream of the rotor. In figure 30a the appropriate tufts are numbered 7 (only partially visible), 8, and 9. The tufts slant from right to left in the direction of the relative flow. Figure 30b includes a fourth tuft numbered 11.

The movement toward the suction surface begins sharply at the rotor inlet as shown in figure 30c by the two tufts to the left of No. 1. The subsequent figures 30e through 30g show the hub tufts within the rotor passages of the complete compact stage (figure 30d), the expanded stator (figure 30e), and the expanded rotor and stator (figures 30f and 30g). For most of the rotor passage the tufts are approximately parallel, being directed from pressure toward suction surfaces.

The fluid near the pressure surface emerges from the rotor in approximately an axial direction (in the relative system) as shown, for example, by the tufts to the left of No. 4 and No. 12 in figure 30g. Within the fillet between the pressure surface and the hub, the flow follows the fillet as shown in figure 30i (observe the tuft to the right of lower No. 4) and in figure 30j (observe the tuft to the left of upper No. 2).

With the expanded stator the relative flow immediately downstream of the rotor varies considerably in direction. Yet within a

distance of about 1/2 chord length downstream, fair uniformity prevails. These conditions are shown in figure 30g by the six tufts above and to the right of No. 12. The large change in direction behind the trailing edge region is strikingly displayed by the crossed tufts, the one slanting in the general direction of left-to-right being radially above the other tuft.* However, these features are modified if the stator is placed in its normal stage position as shown in figure 30h by the five tufts located at the stator inlet.**

The most drastic motion of the hub boundary layer occurs near the suction surface. Most of the fluid in the lower part of the boundary layer passes completely to the suction surface and then, as will be shown shortly, moves radially to the blade tip region. The radial movement occurs even within the passage as shown, for example, in figure 30g by the tufts between upper No. 4 and No. 5. All of the radial movement of the hub boundary layer is in turn governed by the character

---

* This can be explained by the fact that the left-to-right tuft is immersed in a fluid of greater centrifugal force than the right-to-left tufts. The former, therefore, is more unstable (cf. p. 6) than the latter.

** The observed influence of the stator on the hub tufts was not to be expected. In fact, since the stator produces turning opposite to the rotor rotation, the stator influence, if any were to be anticipated, should be opposite to that which was observed, i.e., the hub tufts would be turned, in the relative system, more to the left in figures 30g or 30h. The reason for the observed result will be explained in the discussion of the stator performance (cf. 6:2.3.1.1).

of the blade corner flow. This situation will become clear in the following paragraphs.

At this point it is important to note that some of the qualitative features just described have been predicted analytically by A. Mager. Mention of this was made earlier. Mager's analysis[10] of the three-dimensional, laminar boundary layer flow over a plane provides a partial basis for understanding the deflection in the hub boundary layer between the rotor blades. In order to refer to quantitative values, the extension to Mager's work made by Hansen and Herzig[22] is more appropriate and will be used here. The following example is given to show a result provided by the theory.

Conditions:*

1. The free stream relative flow moves on the plane at an initial angle of 60 degrees from the axis.

2. The axial velocity is constant; the relative tangential velocity decreases linearly with the axial distance.

3. The relative free stream flow turns 10 degrees in an axial distance of 2".

With these conditions the following flow paths were determined from reference (22):

---

* Where possible the conditions have been chosen to be comparable to those in the present study.

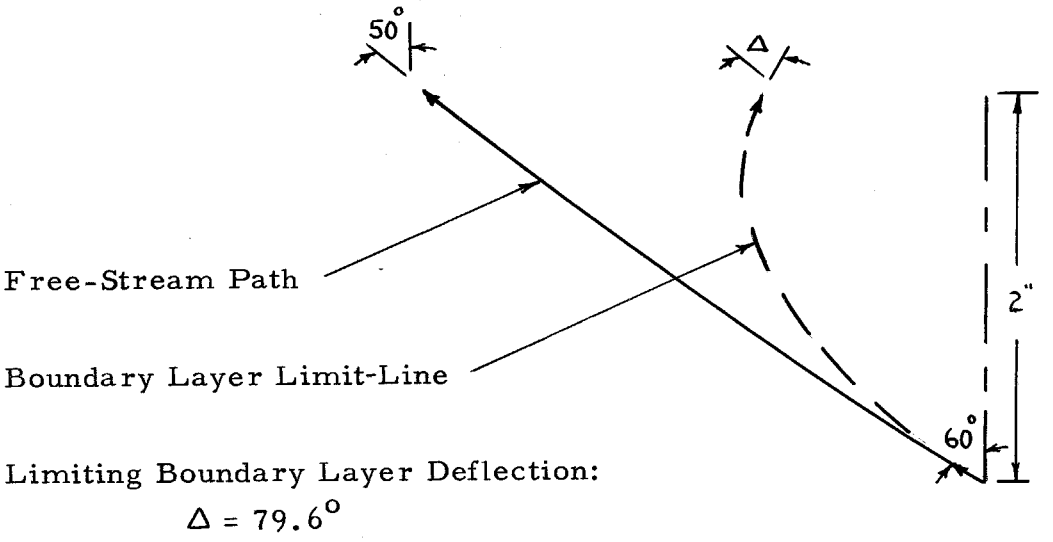

The theory thus gives a large limiting boundary layer deflection for the example chosen. However, the theory is necessarily specialized. For example, the boundary layer is laminar and has zero thickness at the inlet;* the total pressure in the direction of the plane leading edge varies in a specific manner. The possibility of radial and corner flows is not included; the corner flow, which has also been treated by Mager, will be seen shortly to be important. Mager's plane theory may be considered, therefore, as one step in the overall theoretical problem.

A further interesting product of Mager's work is worthy of mention here. This concerns the flow at the leading edge of a rotating hub.[12] In the present experiments, because of the low axial velocity

---

* Mager's small perturbation analysis[12] removes this restriction.

at the hub and the low guide vane turning, one expects to observe extremely high angles of attack on the rotor blade very near the hub. However the angles are actually much smaller than expected. This condition is borne out by the lack of separation at the rotor leading edge near the hub (cf. e.g., figure 39) and by the direction of the relative flow entering the rotor along the hub (cf. figure 43a(2)).

The physical explanation appears to be that as the flow crosses from the stationary to the rotating hub, the percentage change in the axial velocity close to the hub is very small, while at the same time the immediate growth in cross flow boundary layer produces a large percentage change in the cross flow velocity. The flow near the hub is thereby turned toward the axial direction, and the angle of attack is therefore reduced.

The theoretical solution to this problem for laminar boundary layers and for small cross flow velocities is given by Mager.[12] As an example to clarify the previous discussion, consider the condition of the flow at a distance of about 1/2" downstream of the front end of the rotating hub and about 0.10" radially out from the hub. Disregarding the guide vanes and assuming the measured conditions at the guide vane inlet exist at hub leading edge, one obtains from figure 2 (ibid), for the downstream position, a decrease in axial velocity of about 1-1/2 $^{o}/o$, and a decrease in relative tangential velocity of about 40 $^{o}/o$. For this case a velocity diagram would appear qualitatively as follows:

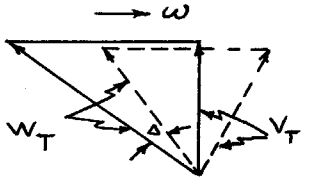

——— Conditions without cross-flow growth

---- Conditions with cross-flow growth

W_T Total relative velocity

V_T Total absolute velocity

$r\omega$ Rotation speed

Δ Reduction in angle of attack due to initial cross flow growth

In this connection it is also worth noting that if the flow at the hub of the rotor outlet passes onto a stationary hub, the flow relative to the stationary hub is also turned toward the axis. Thus for a shrouded stator the result would be a reduction in angle of attack at the hub end of the stator.

As a final remark regarding the hub leading edge flow, if the cross flow on the wall between the blades is strong, the turning effect at the wall may extend upstream and thereby reduce the angle of attack somewhat.

b. Blade Corner Flow

The flow in the corner formed by the suction surface and the hub begins to move radially immediately downstream of the leading edge. The hub boundary layer then moves in to the corner to maintain

continuity of flow. The radial motion increases as the flow progresses downstream, and finally at about 60 ^{o}/o chord the corner flow is completely separated, i.e., the flow is radially outward and no flow continues in the chordwise direction. These features are shown clearly in figures 31a and 31b. Downstream of the separation, flow in the fillet is in general radially outward and originates as the hub boundary layer. (Later photos will show that immediately at the trailing edge the fluid in the fillet originates from the pressure side of the blade.) Figure 31c shows a fillet tuft near the separation point in the compact stage configuration.

Further information regarding the blade corner flow arose from an experiment performed for the purpose of modifying the radial motion of the boundary layer. (This latter material will be described subsequently.) The results, appropriate here, are presented in figures 31d through 31h. A small lucite plate (figure 31g provides the clearest picture of the plate) was sealed at right angles against the suction surface with a gap of about 1/2" between the plate and the hub. The plate leading edge was situated downstream of the blade leading edge a distance of about 1/3 the blade chord length.

Two features of interest are to be noted. First, the flow in the corner between the shield and suction surface separates at about the same point as the flow, without the shield, in the actual blade corner. Second, with the shield in place the actual corner flow has no radial motion. Although this latter effect cannot be seen in the photos, an associated effect which can be seen is the changed hub flow. Figures

31e and 31h show the straightening experienced by the hub flow; movement to the suction surface no longer occurs. It appears, therefore, that the character of the hub flow is governed to a great extent by the blade corner flow.* If the corner flow does not separate, the hub flow passes through the rotor passage and remains confined to the hub. On the other hand a separated corner flow provides a path between the hub flow and the suction surface with subsequent movement of the hub flow radially outward along the blade.

The problem of laminar flow in a stationary corner subjected to crosswise and chordwise pressure gradients has been studied by A. Mager in reference (10). As an example, he solves for the flow in a hyperbolic, stationary, concave corner as depicted in the following sketch:

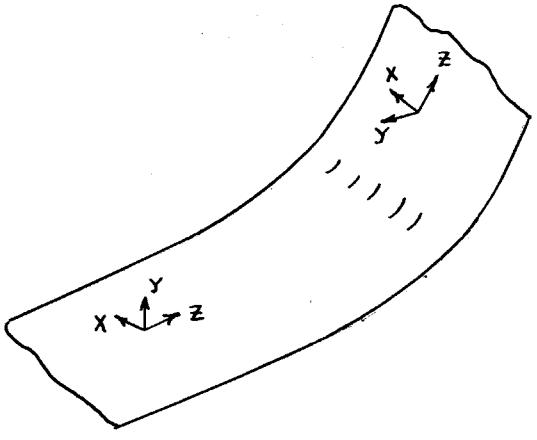

---

* With the shield another factor of importance is the probable change in chordwise pressure gradient produced by the shield.

The conditions of the problem are that

$$\frac{\partial P}{\partial y} = \frac{\partial P}{\partial x} = 0, \quad \text{and} \quad \frac{\partial P}{\partial z} \neq 0 \text{ (but small in magnitude).}$$

The velocity in the z direction is also small and varies linearly with x. The theoretical result predicts an accumulation of low momentum fluid in the corner as the flow progresses downstream. At the same time deflections in the z direction become very large.

In the present experiments, $\frac{\partial P}{\partial x}$ is positive, a condition which could lead to separation in the x direction and thereby increase the deflection in the z direction.

Mager's example thus provides theoretical emphasis to the observation that the corner flow must comprise an essential aspect, in fact an integral part, of the entire boundary layer cross flow process between blades.

5:2.2.1.1.3 Radial Flow and Separation Along the Rotor Blade Suction Surface

One of the prominent features which has appeared in several of the photos shown thus far, (eg., figures 29a, 29c, 29f, 29h), has been the strong radially outward motion of fluid along the suction surface. As a matter of fact this very feature constitutes one of the essential differences between low and higher Reynolds number performance of the rotor blades. Moreover, the radial flow is intimately connected to the separation of the fluid moving chordwise along the suction surface. Various aspects of the radial and separated flows are described in figures 32a through 32j.

In figure 32a tufts are shown (blade No. 2) attached at the leading edge and at about 60 °/o chord, the latter group being completely radial from hub to a region near the tip. The tuft nearest the tip is oriented in a direction which is essentially normal to the suction surface. Figures 32b (blade No. 1), 32c and 32d (blade No. 4), 32e (blade No. 1), 32f (blade No. 1), and 32g (blade No. 1), show that the radial motions are prominent from about the quarter-chord region completely to the trailing edge. The fluid which begins to move radially at about quarter chord is the boundary layer originating from the blade leading edge. At about 40 °/o chord, however, this fluid separates from the surface. Evidence of such separation is provided in figures 32h through 32j by the tufts attached to small rods and located close to the suction surface.

Downstream of the separation region, the fluid moving radially along the blade surface, having originated as hub boundary layer fluid, passes out toward the tip region from where a very non-steady motion then originates.* The directions taken by the fluid leaving the tip region vary almost 180°. For example, figure 32b shows a tip tuft oriented chordwise downstream, while in figure 32c a tip tuft is shown oriented chordwise upstream. The predominant direction, however, is into the blade passage and thence downstream.

---

* The possibility of constructing a continuous flow path from the hub, radially outward along the blade to the tip region, and then into the rotor passage was considered justification for interpreting the radial orientations of the tuft as being correct indications of the path followed by the fluid.

A more comprehensive picture of the radial motion on a single blade is given in the photos, figures 31d through 31h, which incorporate the plastic shield described earlier. In these cases, after separation of the chordwise flow occurs, fluid passes from the shield to the rotor blade and then moves radially outward along the suction surface. In these photos, tufts which were attached right at the trailing edge can be seen to be oriented radially outward along the edge.

The stage configuration did not change the radial motions along the suction surface in any material manner. This is borne out by comparison of figures 32b (expanded rotor and stator) and 32g (compact stage).

A further consideration regarding the radial motions is worthy of note. This involves the speculation as to what would happen to the flow over the rotor blade if the corner flow separation were prevented, say by suction or by special corner design as proposed by A. Mager. Two factors would then dominate the flow process, namely, the radial motion of the chordwise-moving boundary layer, and the possibility of chordwise separation of this same boundary layer. Both the radial motion and the chordwise separation would likely occur, the former ceasing at the onset of the later. Under such circumstances it seems possible that the corner separation would have to be accepted as being beneficial in that it makes possible the occupation of an otherwise separated region by fluid to which energy is added through the mechanism of centrifugal pumping.

Finally, one sees the order of complexity of the boundary layer behavior over the rotor blade suction surface. In this light a few conclusions can still be formulated in regard to the low R_T (at least as high as 4000) conditions being considered here.

a. Low Reynolds number tests on either two-dimensional or stationary three-dimensional cascades cannot produce all the important phenomena associated with rotor blade suction surface boundary layer flow.

b. A correct analytical description of the rotor boundary layer flow should include all of the following features:

(1) hub flow

(2) corner flow

(3) leading edge flow (laminar separation and reattachment)

(4) radial movement of the chordwise-moving boundary layer

(5) turbulent separation.

5:2.2.1.1.4 Flow Along the Rotor Blade Pressure Surface

For the most part the fluid flowing along the pressure surface experiences no radical motions. Exceptions occur at the tip where separation of the chordwise flow occurs, and at the trailing edge where the flow turns rapidly toward the suction surface. Examples of such behavior are given in figures 33a through 33e.

Figures 33a and 33b show the pressure surface tufts at the blade midchord region. Small radial components occur on the lower parts of the blade, but the prominent feature which is quite clear in the

photos occurs near the tip where the chordwise flow separates. Figures 33c and 33d provide further evidence of the tip region separation, this time near the trailing edge. In figure 33c the tip region tuft is separated, but because of the tuft length, the end follows the flow beyond the trailing edge and bends into the adjacent blade passage. The shorter tuft in figure 33d follows only the separated flow.* This separated condition was examined further by means of tufts attached at the very edge of the tip. Figure 33e shows that the fluid moves down from the tip. It appears, therefore, that the separation is caused by flow scraped by the rotor from the wall boundary layer. Approximately the top 1/4" tip region is apparently occupied by the scraped flow.

As shown in figure 33c the flow behind the trailing edge moves crosswise against the direction of rotor rotation. Such motion is compatible with the chordwise flow separation along the suction surface described previously. Although the flow around the trailing edge is unsteady, the direction counter to the rotor rotation prevails. Thus, for both the suction and pressure surfaces the flow leaving the trailing edge bears little relation to the surface tangents.

5:2.2.1.1.5 Rotor Tip Clearance Flow

An interesting aspect of the rotor tip clearance flow observed in the low R_T experiments indicated that all of the flow through the

---

* In figure 33d the tuft oriented in the direction of rotor rotation near the trailing edge and tip of blade No. 3 is attached to the casing and represents the direction of the clearance flow in the absolute system of coordinates.

clearance consists of wall boundary layer fluid. Figures 34a and 34b show a group of clearance tufts attached to the rotor blade. Very little axial motion is evident. The lack of flow from the pressure surface into the tip clearance is shown by the pressure surface tip-region tufts described earlier in figure 33e. These tufts show, it is to be recalled, that flow from the tip of the pressure surface moves in a radially inward direction which means, then, that none of the clearance flow originates along the blade surface.

5:2.2.1.1.6 Flow Within the Rotor Passage

The previous sections have been concerned primarily with the motions of boundary layer fluid over the surfaces which form the rotor passage. In the present section information will be presented regarding the flow through the main part of the rotor passage.

a. Remarks on Use of Rotating Rods

In order to examine such flow a group of .062" diameter rods, to which were attached tufts, were screwed into the rotor hub at various places within several rotor passages. The tufts were first attached so as to allow the free end to trail directly into the rod wake. Observations made with these tufts proved in some cases to be erroneous. The difficulty stemmed from a combination of several factors. To begin with, the rotating rods were operating at Reynolds numbers below 80. Below 50, according to reference (41), stationary vortices can exist behind a stationary cylinder. If now such vortices would tend to exist behind the rotating rods used in the present study, the vortices would acquire

the whirl velocity of the machine, and would become, as a consequence, unstable in the existing centrifugal force field. They would therefore move radially outward along the rod. Thus a short tuft located in the wake of such a rod would become oriented radially outward. Orientations of this nature, observed at first in many parts of the rotor passage, are exemplified in figure 35. Figure 35a (observe the exit rake in the uppermost passage) shows two radially oriented tufts in the pitchwise center of the blade passage. A similar picture on a rake closer to the suction surface is shown in figure 35b at the rotor inlet.

The difficulty was overcome by increasing the tuft length and attaching the tuft so that the free end was situated at the front of the rod. It this manner the tuft remained free of the wake immediately behind the rod and thereby was able to trail into the main stream beyond the rod.

b. Observations of Tufts

In order to provide some idea of the three-dimensional character of the flow, photos were made with a number of different geometrical views. Typical results are shown in figures 36a through 36f. Other photos, which describe the chordwise separation along the suction surface, are presented in figures 36h through 36j, these having been discussed previously.

Figures 36a and 36b show two views of three rakes located across the rotor inlet and six rakes located in the exit region. The inlet flow was observed to be reasonably smooth. The tufts near the tip show a strong deviation toward the pressure surface, a condition

caused by the tip leading edge separation, (cf. figure 33a). The exit tufts provide evidence of the strong gradients in flow directions near the hub and near the tip. The flow is turned in the direction of rotor rotation at the hub and in the opposite direction at the tip. The former effect has been discussed before. The latter effect, however, can be shown to stem from the chordwise separation along the suction surface. Figures 36c and 36d describe this tip effect more clearly. To be observed in these photos are three rakes located about midchord, one near the suction surface and two on the adjacent pressure-surface side. The suction surface rake clearly reflects the result of separation at the blade. The other two rakes, on the other hand, give some idea of the pitchwise extent of the separation effect, this being more than one half of the passage width.

Near the trailing edge the flow direction has a large component from pressure toward suction sides of the blade. The flow right at the trailing edge was described previously in connection with figures 33c and 33d.

Figures 36e and 36f show still different views of the rakes, and contain in addition a set of radially oriented tufts along the suction surface of one blade.

In general the rake observations, excluding the hub, tip, and blade surface regions, indicate that the flow within the rotor blade passage experiences no further unusual motions. The main complexity, therefore, appears to arise almost entirely from the boundary layer movements.

Of course one must bear in mind that the tufts are indicators of direction only. Within the rotor passage and particularly at the exit, because of the extensive boundary layer movements, there certainly exist large gradients in velocity and total pressure which can be expected, in turn, to cause measurement difficulties and to produce, eventually, large mixing losses. Information regarding the quantitative state of the fluid behind the rotor blades is presented in the following section.

5:2.2.1.2 Flow Surveys Downstream of Rotor

Radial surveys of flow angles, total pressures, and static pressures behind the rotor were made in several different ways. At R_T of 2000 and 4000 the surveys were carried out with the expanded stator configuration. Both Station 3 ($\sim$ 1/4 chord lengths downstream of the rotor) and Station 7 ($\sim$ 4-1/2 chord lengths downstream of the rotor) were used as survey positions for tests at R_T of 2000. Most of the surveys at R_T of 4000 were made at Station 7.

a. Remarks Concerning Measurements

A number of problems associated with the measurements warrant explanation. At Station 3 only one circumferential position was available for survey purposes. Therefore, because the thick guide vane wakes can be expected to persist to some extent through the rotor, the determination of accurate circumferential averages close behind the rotor is not to be expected. Furthermore, at these low Reynolds numbers the casing boundary layer may be circumferentially non-

uniform due, originally, to the pipe bend far upstream in the tunnel. Additional complications near the rotor exit are to be expected from large gradients in flow directions, velocities, and pressures arising from the boundary layer movements described in the previous sections.

At Station 7, on the other hand, the various non-uniformities will be reduced measurably, so that more reasonable circumferential averages can be expected from radial surveys obtained at a single circumferential position. The measurements, in other words, will reflect the mixing losses which undoubtedly occur between the rotor exit and Station 7. A few less desirable features will also characterize this data. First, the mixing process will lead to some radial redistribution in mass flow, velocities, and flow directions. Second, additional losses, not correctly chargeable to rotor performance, will take place in the casing boundary layer. Third, the flow near the rotating hub will experience changes which will modify the axial and cross-flow components of the boundary layer. All of these features will combine to produce a state of flow which will differ in many respects from that which would enter the stator row if it were placed in its proper single stage position. Care, therefore, must be used if the data at Station 7 are to be used to judge the effect of the rotor exit conditions on the stator performance.

In spite of these difficulties ample value is to be gained from all of the data. At R_T of 2000, for example, there is considerable corroboration to be found between the photographic studies and the rotor exit survey data. At this same value of R_T, the rotor exit

survey data are sufficiently similar to the downstream data and appear, moreover, to be related in certain ways to higher R_T results. Consequently, one is led to the opinion that many of the essential features of the flow leaving the rotor have been correctly determined.

b. Survey Results at $R_T = 2000$, $\Phi = 0.28$ (Nominal Values)

The results obtained from surveys at Stations 3 and 7 are presented in figures 37a through 37e. At Station 3 many of the measured flow characteristics can be shown to be consistent with the physical picture constructed earlier from the tuft studies.

Figure 37a gives the radial distribution of absolute flow angle measured with respect to the machine axis. Over most of the passage the fluid moves with a large tangential component in direction. The extreme change in angle with radius is confined, at the hub, between ζ of 0.64 and 0.60, whereas the entire upper half of the passage from 0.80 to 1.0 shows evidence of rapid change in angle with radius at the rotor exit. Of course, in the case of a rotor, relative rather than absolute flow angles are more indicative of occurrences in the rotor. Velocity diagrams, on the other hand, which are needed to determine the relative state of the fluid, are meaningful provided they can be related to conditions along streamlines or streamsurfaces. In the present case the hub and tip regions can be expected, from the tuft studies, to reflect the radical radial movement of the hub boundary layer. Velocity diagrams for these regions will lose their significance, therefore, since the quantity of fluid involved in the radial movement was not measured.

Some indication of the relative state of the fluid at the mean radius is obtained if the mean axial velocity, based on the mean flow coefficient obtained from the nozzle calibration, is assumed to prevail at this radius both in front of and behind the rotor. With the measured values of guide vane and rotor exit angles for the mean radius, a velocity diagram can be constructed. The result indicates a relative turning angle in the rotor of about 8^{o}. By comparison, extrapolation of the data given in reference (6) gives a corresponding value of 12^{o} which may be taken (disregarding the aspect ratio differences between the present machine and that of op. cit.) as the approximate high Reynolds number value for the blading under study. Thus, it is clear from the above estimate and the tuft studies, that the relative turning in the central region between the hub and tip, is reduced at R_T of 2000, a result which, in a general sense, was to be expected. The relatively large absolute angles in this region must therefore be attributed to the low average flow coefficient. Such an effect, of course, is also characteristic of high Reynolds number performance. For example, the data of reference (6) indicate that the absolute flow angle leaving the rotor at the mean radius changes from 38^{o} at ϕ of 0.5 to 59^{o} at ϕ of 0.28.

Figure 37a also describes the changes in absolute flow angle occurring between Stations 3 and 7. The largest change occurs near the tip where the flow is turned toward the axis. Such an effect would result from a larger growth in cross-flow boundary layer compared to the axial boundary layer between these two stations.

More meaningful information than is provided by the flow angles can be obtained from the measured pressures and calculated velocities at the rotor exit. Figure 37b gives the radial distribution of total pressure coefficients at Stations 3 and 7. For reasons mentioned earlier some question exists regarding the quantitative accuracy of the data at Station 3. In spite of this a number of evident features are considered to be correct. First, there is a very large peak near the hub and a lesser peak near the tip. Considered in the light of the tuft studies, these peaks must be related to the hub boundary layer behavior. When this fluid begins to move toward the suction surface, which it does at the rotor inlet (cf. figure 30c), a radially inward movement of fluid occurs downstream of the cross-flow. Since the cross-flow occurs through the entire axial extent of the rotor passage, a continuous flux of outer-region fluid takes place toward the hub. Consequently, a region of high energy input occurs near the hub, with an accompanying thinning of the axial boundary layer. Besides appearing in the total pressure data, the energy effect is also evident in the absolute tangential velocity distribution shown in figure 37e. The boundary layer effect, on the other hand, is indicated by comparison of the axial velocities near the hub as given in figure 37d with those at the guide vane inlet as given in figure 16a.

The peak region near the tip occurs in spite of the fact that the blade tip itself is separated (cf. figure 33e). The cause must again be the hub boundary layer which was shown to centrifuge radially outward from hub to tip along the suction surface (cf. figure 32). As in the hub

region case, the peak in total pressure occurs with a corresponding peak in tangential velocity, figure 37e. One expects, further, a large increase in axial boundary layer thickness near the tip; for, while the cross-flow and hub effects increase the whirl velocity, the axial velocity of the fluid leaving the hub and appearing at the tip retains its low value. This condition is quite evident in figure 57d.

A comparison of the total pressures at Stations 3 and 7, figure 37b, gives some evidence of the large mixing losses incurred downstream from the rotor. As expected, considerable uniformity prevails downstream.

Inspection of the static pressure distribution, figure 37c, at the rotor exit demonstrates one of the sources of measurement difficulty at this station. In the center of the passage the reversal in slope suggests the existence of radial velocities, a condition which could not be properly measured with the instrumentation used in this study. Near the hub and tip, however, these being the regions of greatest interest in the above discussions, the static pressure slope agrees with the centrifugal force term, $\frac{\rho V_\theta^2}{r}$, within 10 $^o/o$. The redistribution farther downstream is evident. At Station 7 the pressure slope agrees closely (less than 3 $^o/o$ difference) with the centrifugal force term.

Also included in figure 37c is the radial distribution of static pressure coefficient at the rotor inlet. If these data are compared to the values at Station 7, a further estimate, crude but probably indicative, of the relative turning in the rotor can be obtained by

applying the Bernoulli equation for the relative system. For the mean radius, such an estimate gives a relative turning of about 4^{o}, which is somewhat less than the value obtained from velocity diagrams (cf. p.58). This is a further indication of the reduced relative turning in the rotor.

The whirl velocity distribution downstream, figure 37e, is quite smooth and extrapolates correctly, moreover, to the known boundary value at the hub (ζ = 0.60). At Station 3 the hub cross-flow boundary layer is not distinct, whereas at Station 7 such a layer is distinct. A cross-flow boundary thickness of about 1/4" is indicated.

As a final remark, it is to be noted that figure 37b contains coefficients based on total pressures corrected for tube Reynolds number effect. The correction in ψ_T is fairly constant across the passage except near the casing. The actual correction to the total pressures, of course, is larger than appears in this data, since both terms in the numerator of ψ_T involve corrections, and these, in part, cancel each other. All velocities here and in subsequent data are based on corrected total pressures.

Survey data at R_T of 2000 were obtained at a number of ϕ values, the lowest value being .05. These contain some interesting characteristics which are described later. (cf. 5:3.2)

c. Survey Results at R_T = 4000, ϕ = 0.35 (Nominal Values)

Figures 38a and 38b contain the results of surveys made at Station 7 for R_T and ϕ nominally at 4000 and 0.35 respectively, the latter corresponding approximately to the maximum efficiency point.

It is to be recalled that the tuft studies at R_T of 2000 and 4000 indicated similar flow processes within the rotor. The casing and hub boundary layers, on the other hand, were measurably less at the higher R_T (and higher ϕ) (cf. figures 16a and 16b, and p. 58). Thus, one expects to find essentially the same flow patterns at Station 7 as were described in the previous pharagraphs with some modifications resulting from the thinner wall boundary layers. A further important feature, however, is the higher ϕ corresponding to maximum efficiency. At this condition, separation of the chordwise-moving fluid still occurs but with somewhat smaller wakes. The effects to be expected, therefore, when compared to R_T of 2000, are lower absolute flow angles, particularly in the tip region, more uniform axial velocities, and lower whirl velocities. Comparison of figures 37 and 38 shows that these conditions do, in fact, occur.

The drop-off in absolute flow angle close to the casing was not investigated. However, this effect also occurs in data obtained downstream of the stators. In these cases the flow angle near the casing was found to change circumferentially, the drop-off becoming essentially flat at a survey position removed from that in figure 38 by approximately one-half the blade pitch. Presumably, then, some type of secondary flow patterns persist at the downstream station and lead to the measurements as noted.

Comparison of the total pressure coefficients at Station 7 for both R_T (figure 37b and 38a) show approximately the same values in both cases. Higher values of ψ_T can be obtained, therefore, at

the higher R_T. This effect is consistent with the over-all performance data of figure 10b. From the latter figure, the indications are that a maximum ψ_T of 0.28 will occur at an average ϕ of 0.3.

5:2.2.2 Rotor Flow Characteristics at R_T of 12,000, 22,000, and ϕ Values Corresponding to $\psi_{T_{max}}$

The experiments at R_T of 2000 and 4000 provided a reasonable picture of many of the gross phenomena occurring within the rotor passage. The changes to be expected as R_T increased were at least partly clear. Since, with the exception of the tip region, the leading edge flow was attached at the lower R_T, (although laminar bubbles certainly existed) the higher Reynolds number effects should produce, primarily, changes in the hub boundary layer movement, in the corner flow, and in the radial flow along the suction surface. The boundary layers along all surfaces, i.e., the hub, casing, and rotor blades should become thinner, of course; the results at R_T of 4000 already had shown evidence of these conditions. Consequently, it was to be expected that $\psi_{T_{max}}$ would occur at higher ϕ as R_T increased. On the other hand, from the data of reference (6), $\psi_{T_{max}}$ for high R_T (200,000 - 300,000) occurs at ϕ of approximately 0.34. In the present case the corresponding ϕ value at R_T of 4000 was 0.30. Thus, the shift in ϕ would not be radical. (The measured shift has already been described in 5:1.4.)

Tuft studies of the rotor flow were made with improvement in clarity being realized by adding a thin coat of white paint to the blade

surfaces. The coating was approximately .002" thick, this being about 1-1/2 °/o of the blade thickness at the tip. The minor changes of the blade performance attributable to the additional thickness were considered unimportant for the present study.

All of the experiments at the higher R_T were made with the compact stage configuration only. A discussion of the tuft studies is presented in the next section. This is followed by the flow survey data.

5:2.2.2.1 Rotor Tuft Studies

The tuft experiments are summarized in figures 39 and 40.

a. Suction Surface Flow

Figures 39a and 40a show that the flow along the suction surface is primarily chordwise. Comparison of the figures 39a(1) to 39a(4) indicates that the flow is not perfectly steady at R_T of 12,000 and that occasional strong radial flows occur; but the complete separation of the chordwise-moving fluid is clearly absent. Additional pictures of the extent of the chordwise motion are given in figures 39c(3) and 40a(2) where two long tufts are shown extending chordwise from the leading edge. One of these tufts also appears on the right blade of figure 39c(1), and gives some idea of the thickness of the suction surface boundary layer near the tip at R_T of 12,000.

Earlier mention has been made of the occurrence of laminar bubbles at the leading edge. In figure 39a(4) the leading edge tufts are humped in a manner which strongly suggests the existence of bubbles.

b. Blade Corner and Hub Flow

The character of the blade corner and hub flow is described in

figures 39b and 40b. The contrast with lower R_T is very clear. The suction surface corner is not separated except near the trailing edge.*

Consistent with this state of the corner flow is the hub flow, which, though turned toward the suction surface, remains attached to the hub. The features of the hub flow are almost exactly as predicted by A. Mager in reference (7). The pressure surface corner flow experiences no turning toward the suction surface. The largest curvature of the hub flow occurs approximately in the mid-pitch region; the curvature decreases in the region near the suction surface. These features are very well described in figures 39b(1) and 40b(2). Although in the two photos, figures 39b(2) and 39b(3), evidence of non-steadiness appears, the general behavior is as described above.

Two additional features are to be noted: first, at the trailing edge the flow turns completely around the edge from pressure to suction surface. Second, the relative flow leaving the hub is inclined in the direction of rotation. This fact will explain, later, an interesting detail related to the cross-flow boundary layer at the hub.

c. Pressure Surface Flow

Pressure surface tufts are shown in figures 39c, 39d, 39e, 40c, and 40d. The flow is smooth and essentially chordwise over the entire surface. At the trailing edge the flow deviates toward the suction surface, but the deviation is less than at lower R_T, a condition which

---

* This separation is not shown due to omission of a tuft closer to the trailing edge. The separation was not steady and occasionally occurred farther upstream as shown in figures 39d and 40c(2).

reflects the absence of separation of the chordwise-moving flow along the suction surface.

d. Suction Surface Tip Region and Tip Clearance Flows

Figure 39d shows two features of the suction surface tip region flow. Along the right blade the leading edge flow is attached and separation occurs at about midchord. Along the left blade, separation occurs at the leading edge. The cause of this difference between blades is attributed to circumferential non-uniformity in rotor entrance conditions arising from the guide vane wakes. The left blade, presumably, is passing a guide vane wake. Figure 49c(2) shows a similar behavior of the leading edge region.

The tip clearance flow, in contrast to the condition at lower R_T, is characterized by flow from the pressure surface into the clearance as shown in figures 39e and 40d. However, very little radial extent of pressure surface appears to be affected by the flow into the clearance.

5:2.2.2.2 Flow Surveys at Rotor Exit, Station 3

The results of surveys made at flow rates corresponding approximately to $\psi_{T_{max}}$ are presented in figures 41 and 42.

a. Flow Angle and Total Head Coefficient

Both figures 41a and 42a show a sharp minimum in absolute flow angle near the tip. This minimum, moreover, corresponds closely to maxima in both the head coefficient and axial velocity (figures 41b and 42b). Since the hub boundary layer is no longer centrifuged to the blade tip, the large head rise near the tip must be attributed to the local effects in that region. A factor contributing to this effect is that

for thick casing boundary layers the total pressure in the boundary layer behind the rotor will be a maximum at some distance from the wall; since right at the wall the total pressure rise across the rotor is simply the static pressure rise, while at a small distance away from the wall, the same static pressure rise occurs and to this is added an increase in kinetic energy.

Near the hub the peak in total pressure is attributed to the high turning arising from the secondary flow in the boundary layer. As near the casing the peak is located away from the rotating hub, since the kinetic energy is greater a short distance from the rotating hub while the static pressure is essentially constant.

An additional feature of importance is to be noted. Even though the secondary turning in the hub boundary layer has been reduced (compared to the lower R_T results) and even though centrifugal pumping of this fluid out to the blade tip does not occur, the total pressures near the casing and hub are very high. Indeed, the magnitudes of the energy added to the hub and tip boundary layers are not really evident in a plot of ψ_T which is referred to a constant upstream pressure. If the addition of energy were computed on a streamtube basis, the peak in ψ_T at the tip would be larger than that shown in figures 41a and 42a. At the hub the peak would also increase, although to a much smaller extent than at the tip because the rotating hub adds some energy to the boundary layer before it enters the rotor.

b. Velocities

The axial velocity distribution indicates a radial displacement

of the main fluid outward toward the tip. Without this displacement, it is possible, as Mager points out in reference (7), that a growth in the axial boundary layer might be expected across the rotor tip.

The tangential velocity distributions, figures 41b and 42b, reveal a few features of general interest. Close to the hub the tangential velocity exceeds the velocity of the rotating hub. This condition was found to be characteristic of all the higher R_T data obtained in the present study as well as the data obtained in reference (5) (e.g. figure 75 and other unpublished data of that reference). Examination of the tuft pictures makes the reason clear. In figures 39b and 40b, almost all of the highly turned hub boundary layer passes out of the rotor along the hub. Very close to the hub the relative tangential velocity at the rotor exit is in the direction of rotor rotation, so that the absolute tangential velocity exceeds the hub velocity. This particular result, of course, is characteristic of the blade design used here and in reference (5). At R_T of 2000 two different results were obtained. With the expanded stator, the relative whirl direction at the hub exit, figure 30g, was opposed to the rotor rotation, while with the compact stage the relative whirl direction, figure 30h, was the same as the rotor rotation. (cf. footnote p. 64 and 6:2.3.1) In the former case, the absolute whirl velocity close to the hub (figure 37e) was less than the hub velocity. In the latter case, no quantitative data were recorded, but from the tuft pictures, it is clear that the absolute tangential velocity distribution would be the same as obtained at higher R_T, even though at the lower R_T much of

the hub boundary layer flows out to the blade tip. As R_T increases the width of the peak region decreases, while the magnitude of the peak remains essentially constant.

Near the tip a peak in the absolute tangential velocity also appears to be common to all R_T, as shown, for example, by figures 37e, 41b, and 42b in the present paper (also figures 46a and 46b which appear later) and by figure 75 in reference (5). Although the basis for a clear explanation of this effect does not exist in the data obtained in the present investigation, some plausible ideas can nevertheless be set forth. Factors to be considered are the tip clearance flow, the blade surface flow near the tip, the axial velocity and the flow angle distribution of the casing boundary layer emerging from the guide vanes, and the secondary turning of the casing boundary layer flow within the rotor. The tip clearance flow and blade surface flow near the tip affect the boundary layer closest to the wall. Both tend to reduce the relative turning hence the absolute tangential velocity at the rotor exit. Farther from the casing the condition of the inlet flow and the secondary flow are the more important factors. In reference (27) flow visualization data (figure 10 of that reference) near the rotor tip (the machine was the same as that used in the present study) indicate that as the casing is approached the relative flow is inclined more in the direction away from the rotor axis. The interpretation given by Raines is that the retarding drag on the flow by the case wall cancels the overturning cross flow and turns the flow toward the blade surface leading in the rotation. However, if the inlet flow is taken into account, another interpretation

which allows the possibility for increased relative turning (i.e. stronger secondary flow) closer to the casing is suggested. This interpretation is based simply on velocity diagrams for the boundary layer fluid near the tip. The following diagrams illustrate the point:

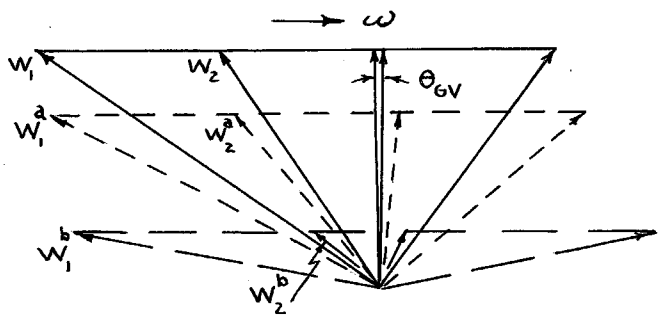

W_1 = Total relative velocity entering rotor at $\frac{y}{\delta} = 1$

W_1^a = Total relative velocity entering rotor at $\frac{y}{\delta} < 1$

W_1^b = Total relative velocity entering rotor at $\frac{y}{\delta} \ll 1$

W_2 = Total relative velocity leaving rotor at $\frac{y}{\delta} = 1$

W_2^a = Total relative velocity leaving rotor at $\frac{y}{\delta} < 1$

W_2^b = Total relative velocity leaving rotor at $\frac{y}{\delta} \ll 1$

Velocity diagrams are shown for three positions in the boundary layer. Changes in axial velocity through the rotor are omitted. Consistent with the known conditions at the rotor inlet, the axial velocity has been decreased and the angle θ_{GV} leaving the guide vanes has been increased as $\frac{y}{\delta}$ decreases. An examination of the three diagrams shows that the relative turning may increase as $\frac{y}{\delta}$ decreases; and yet the

direction of the relative velocity at the rotor outlet (or inlet) may be inclined more in the direction away from the rotor axis as $\frac{y}{\delta}$ decreases. The diagrams also show an increase in absolute tangential velocity at the rotor outlet for decreasing $\frac{y}{\delta}$. Considered with the reduced relative turning in the tip clearance region, the foregoing diagrams would then produce the observed peaks in the absolute tangential velocity distribution. If a decrease in axial velocity across the rotor were assumed to occur, with the relative turning remaining unchanged, the leaving absolute tangential velocity would be increased still further.

5:2.2.3 Rotor Flow Characteristics at R_T of 150,000 and ϕ Values Corresponding to η_{max} and $\psi_{T_{max}}$

It is to be recalled from the results discussed earlier that no radical changes in overall performance occurred above R_T of 20,000. A study of the rotor flow details at R_T of 150,000 revealed a further continuation of gradual changes accompanying thinner boundary layers along all surfaces. These details were studied by tufts over a wide range of average flow coefficients. Flow surveys, however, were limited to ϕ values corresponding approximately to η_{max} and $\psi_{T_{max}}$. The tufts revealed some of the interesting viscous effects accompanying a reduction in ϕ. These effects were observed at the $\psi_{T_{max}}$ condition as well as at lower ϕ.

In the present section the results at η_{max} and $\psi_{T_{max}}$ will be described. The tuft information obtained at higher and lower ϕ will be presented in a later section. (cf. 5:3)

5:2.2.3.1 Rotor Tuft Studies

a. Results at ϕ Corresponding Approximately to η_{max} ($\phi = 0.38$)*

The flow patterns along various parts of the rotor surface are shown in figure 43.** Along the suction surface (figure 43a(1) shows short tufts and figure 43a(2) shows long tufts) the flow is almost perfectly chordwise. A slight exception is revealed in the uppermost blade of figure 43a(1) where the flow near the bottom of the trailing edge shows evidence of radial flow. In addition the tip of the suction surface bore evidence of non-steady behavior as shown in figure 43c.*** In figures 43a(1) the blade corner flow is seen to be attached throughout the entire blade chord length, although small radial motions existed, and very near the trailing edge intermittent separation occurred (cf. hub near trailing edge in figures 43c(1), 43c(2), and 43c(3)).

In figure 43b the pressure surface flow is also seen to be chordwise except for the clearance flow, figure 43b(1), and the deviation toward the suction surface at the trailing edge, figure 43b(2).

The secondary flow along the hub is shown in figure 43c to be reduced (cf. figure 39b(1)) in the mid-pitch region, although the general movement from pressure toward suction surface is still evident. Figures 43c(1) and 43c(2) also provide further evidence of relatively smooth

---

* The value of ϕ at η_{max} is 0.41. (cf. figure 12)

** Stator tufts also are shown. These will be discussed later (cf. 5:2.3).

*** Some of the figures show places where the paint coating has loosened. The flow was not affected by this in any significant way.

corner flow.

At this point it is desirable to interpret the tuft pictures in the light of the flow visualization data of reference (27). For convenience, the data from reference (27)* are reproduced in figure 43d. Comparison of figures 43c and 43d(1) indicates that stronger secondary flows were observed with the injected fluid than are indicated by the tufts. Both data, however, are considered to be correct. The differences are attributed to the fact that the data of reference (27) were obtained with an expanded stator. This meant that a greater length of rotating hub existed upstream of the rotor in that case. Consequently, because of the hub length and the hub rotation the boundary layer would be thicker. For the expanded stage,** in comparison to the compact stage, a given pitchwise pressure gradient would then be expected to turn this flow more in the direction of rotor rotation. Aside from this discrepancy, however, figure 43d(2) indicates a rapid decrease in the secondary flow as $\frac{y}{\delta}$ increases; while figures 43d(3) and 43d(4) show, as in the present data, reduced secondary and radial flow as ϕ increases.

---

* These photos were made available for publication here by Dr. A. Acosta.

** At low R_T the tuft behavior in the rotor was essentially the same for both the expanded and compact stage.

b. Results at ϕ Corresponding to $\Psi_{T_{max}}$ ($\phi = 0.33$, $\Psi_{T_{max}} = 0.41$)

Several changes in boundary layer flow patterns within the rotor were observed when ϕ was reduced from 0.38 to 0.33.* The flow is described in figure 44.

In figures 44a(1) and 44a(2) the flow near the trailing edge of the suction surface is seen to be radial over most of the blade height. The blade corner flow near the trailing edge was observed to separate intermittently; e.g., the corner flow is attached in figure 44a(1) and separated in figure 44c(1).

At the trailing edge of the pressure surface, figure 44b(1), evidence of separation of the chordwise-moving fluid along the suction surface appears in the increased deviation of the lower three tufts.

Consistent with the separated corner flow and radial flow, the secondary turning at the hub is increased (compare figures 43c(1) and 44c(1)).

5:2.2.3.2 Flow Surveys at Rotor Exit, Station 3

The results of the flow surveys made at the rotor exit are presented in figures 45 and 46. Since most of the flow details related to the hub and tip regions have been discussed previously, only a few additional remarks will be made here.

In the mid blade-height region the irregularities in total and static pressures which occurred at lower R_T no longer exist. This

---

* The changes probably occurred at $\phi > 0.33$.

condition reflects reductions in blade-wake width and in circumferential and radial mixing. The addition of energy to the hub and casing boundary layers is still quite large. The peak in absolute tangential velocity near the tip increases as ϕ decreases, and is accompanied by an increase in axial boundary layer thickness. The radial extent of the overturned regions near the hub and tip increases as ϕ decreases, the increase at the tip being more marked. This effect is due, for the most part, to increased casing and hub axial boundary layer thicknesses and to stronger secondary turning in the boundary layers. The later condition arises from increased blade loading and hence increased blade-to-blade pressure gradients.

One final feature is to be noted. Comparison of the total pressure distribution obtained in the higher aspect ratio machine of reference (6) at $\phi = 0.394$ (figure 32 of op. cit.) with the present data given in figure 46a shows a larger energy addition near the hub in the present case. However, the integrated average stage performances compare very closely at this ϕ, and no attempt was made to reconcile the differences in the detailed radial distributions.*

5:2.3 Stator Characteristics

The Reynolds number effects exhibited by the stator blades were similar in many respects to those observed in the rotor blades. For example, at low Reynolds number the leading edge flow remains

---

* It is to be recalled that significant aspect ratio effects on single stage performance are in evidence in the data of reference (23).

attached over most of the blade height. In the same case flow over the suction surface is characterized by radial inflow of the boundary layer accompanied by separation of the chordwise-moving fluid. Behavior of the flow in the corner of the stator between the suction surface and the casing resembles that which occurs at the hub of the rotor, while along the pressure surface the flow is quite similar to the rotor, even in regard to clearance and scraping flows. A number of important differences occur, however, and these are most pronounced at the lower Reynolds number.

In the present section the observed characteristics of the flow within and downstream of the stator blades are described. As in the case of the rotor, most of the discussion is concerned with observations made at the lower Reynolds numbers, for it is here, of course, that the predominant viscous effects manifest themselves. The flow vizualization data obtained with tufts and with colored fluid injection are discussed and are followed, for each R_T condition, by an examination of the flow survey data obtained far downstream of the stator row. In order to establish a basis for connecting the stator and rotor performance, the stator discussion will be classified by R_T. Most of the observations were made with the compact stage configuration which placed the stator over the rotating hub. A few observations will be presented at the low values of R_T for the condition where the stator was situated over a stationary part of the hub. The viscous effects were found to be very different in the two cases.

5:2.3.1 Flow Visualization at R_T = 2000, ϕ = .28

If the data of reference (6), which give conditions entering the stator, are extrapolated to ϕ of 0.28, the results indicate that the incidence angles would be about 10^o at the hub, 15^o at the mean radius, and 17^o at the tip. Therefore, in the present situation the stator might be expected to be completely stalled. Again in the light of the high R_T data, at ϕ of 0.28 the stage is in a rotating stall condition.(42) From these data, it would seem rather futile to study the stators at such low ϕ. However, examination of the performance data presented herein shows that the actual situation differs in several important ways from the extrapolated condition.

First, because of the low relative turning in the rotor, the stator incidence angles for a large part of the blade height do not exceed by much the optimum values for minimum loss given in figure 67 of reference (6). The average incidence angles based on the measured flow angles at the rotor exit are tabulated below.

Incidence Angles for Stator

$\phi = 0.28$ $R_T = 2000$

ζ	Incidence Angle, i
.606	19.8^o
.613	11.0
.62	6.2
.66	2.6
.70	2.3
.75	2.3
.80	2.1
.85	4.4
.90	12.9
.92	21.7
.95	30.3
.98	36.9
.99	40.2

The experimental values of incidence for minimum loss as given in reference (6) are between -4^o and $+2^o$. Thus in the present case one expects to find the hub and tip regions separated, but the blade elements between ζ of .62 and .90 are in a somewhat reasonable incidence range. It is of interest to note that the mean radius incidence listed in the above table would be obtained at high R_T[38] at a ϕ of about 0.43. Hence, in the present case the central part of the blade is in a sense operating at an effectively higher ϕ .

Second, the maximum efficiency point at R_T of 2000 occurs at ϕ

of approximately 0.28, the corresponding ϕ in reference (6) and in the present experiments at R_T of 146,000 (figure 10b) being approximately 0.41. It is perhaps significant that this latter value of ϕ also produces the measured incidence angle at the mean radius (v. s.).

Third, periodic disturbances, if they existed at all, were not sufficiently strong to modify in any visible way the flow pattern through any blade row.

Thus, in spite of the low ϕ , the flow conditions entering the stator are probably characteristic of a practical low R_T operating condition. Moreover, the information to be obtained at such a condition should be indicative of some of the strong viscous effects in a stator blade row.

5:2.3.1.1 Tuft Studies

Photographs of tufts attached to the stator suction and pressure surface, to the casing and hub, and to a rod connected to the casing at the stator exit are presented in figure 47.

a. Suction Surface Flow

The suction surface tufts, figure 47a, though not very clear in the photo, indicate the following flow pattern along the blade surface:

1. The flow is separated at the leading edge near the casing and very close to the hub. Based on the incidence angles listed above, this result is to be expected.

2. For the rest of the blade the leading edge flow is attached.

3. The chordwise-moving fluid separates at about 40 - 50 $^{o}/_{o}$

chord, except near the hub where the flow moves radially inward.

4. Behind the separation the flow is radially inward.

5. The flow reaching the hub end of the blade moves tangentially toward the pressure surface.

Many of the foregoing features can be recognized as having been characteristic of the previously described rotor performance.

Thus, in the stator the radial inflow, just as the radial outflow in the rotor, is caused by the radial motion of the blade surface boundary layer coupled with separation in the corner flow which, for the rotor, is at the hub and for the stator at the casing.

The tuft orientations near the hub are shown more clearly in figure 47b. Although the flow conditions differ in this case from that of figure 47a, the observed tuft orientations near the hub were essentially the same. The path followed by the fluid after leaving the blade near the hub will be clarified in the discussion of results obtained with fluid injection. (cf. 5:2.3.1.2)

b. Pressure Surface Flow

The tuft orientations in figure 47c indicate the following flow pattern over the pressure surface:

1. The flow is apparently attached everywhere.

2. Gradual radial inflow begins near the leading edge at the casing and extends the full chord length.

3. A very small radial outflow occurs from the hub end of the blade.

4. The flow leaving the trailing edge deviates strongly toward

the suction surface.

Condition 4, of course, reflects the separation of the chordwise-moving fluid on the suction surface.

Condition 3 reflects the scraping effect from the hub boundary layer. However, the extent of the blade height subjected to this effect appears small. Analogous to the rotor, none of the clearance flow in the stators comes from the pressure surface.

Condition 2 implies that the casing boundary layer is diverted to both the pressure and suction surface.

Condition 1 reflects the occurrence of positive incidence angles for the entire blade height.
However, the fluid injection studies will show that a separation actually occurs along the pressure surface near the hub.

c. Casing Boundary Layer Flow

The directions taken by various parts of the casing boundary layer are indicated in figures 47a, 47b, and 47c. A number of features are to be noted:

1. The secondary motion is fan-like, the flow in the mid-pitch region being essentially axial, while near the blades the flow deviates toward the suction surface on one side and toward the pressure surface on the other, the former deviation being greatest.

2. As in the case of the rotor hub, the flow in the blade corners at the casing controls the secondary motion. The suction surface corner separates, and fluid moves from the casing onto the suction surface and then radially inward to the hub. The pressure surface

corner is not separated, so that flow from the casing does not extend radially inward very far. The occurrence of radially inward flow on the pressure surface is noted as being contrary to the radially outward motion which would be expected from the results of reference (7).

3. A concentrated vortex forms near the casing immediately behind the trailing edge. This was observed with longer tufts than those shown in figure 47. However, the beginning of the vortex formation is indicated at the right side of figure 47c.

4. By extrapolation from these observations, it is clear that downstream of the stator, part of the casing boundary layer will be found near the hub.

d. Hub Boundary Layer Flow

Because of the rotating hub and the small blade clearance, (.005") the use of tufts to describe the movement of the hub boundary layer was not feasible. The observations described above, however, indicated that the incoming hub boundary layer (cf. footnote p.64) must experience some interaction with the blade suction surface boundary layer as well as with the casing boundary layer since these were observed to move onto the hub. This complicated situation will be clarified in the subsequent discussion of the fluid injection tests.

Outside of the hub boundary layer and in the main part of the fluid passage, the flow (cf. rake of tufts at stator exit, figures 47a and 47b) exhibited no radical behavior.

5:2.3.1.2 Colored Fluid Injection Studies

The foregoing discussion pointed to the inadequacy of tufts for description of the hub boundary layer flow. In addition it was desirable to verify the tuft description of the rather complex suction surface boundary layer movement. Because many aspects of this motion were similar to that observed in the rotor, verification of the correctness of the stator tuft orientations would also tend to substantiate the validity of the rotor blade suction surface tuft orientations. As a consequence of these considerations the flow within the stator passage was examined with colored fluid injected through a small tube placed at various points in the passage. The results will be seen to verify the tuft pictures.

Earlier mention has been made of the difference in specific gravity of the injected colored water and the tunnel fluid. Enough evidence exists to show that the specific gravity effect was not of major importance. For example, figure 48a shows the flow paths of injected fluids with specific gravities of 1.2 (the value of the tunnel fluid) and 1.0. The lighter fluid has a somewhat more extensive radial movement along the blade but the general behavior is the same as the heavier fluid. Far downstream, however, the movement of the lighter fluid toward the hub is in part attributed to the density effect, although the fluid is in the wake region which, as shown by Kofskey[20] can be expected to move radially inward.

a. Suction Surface Flow Near Leading Edge and Near Casing

The suction surface flow near the leading edge is indicated in figures 48b(1) and 48b(2). The positions of fluid injection are listed in Table III. The photos show that over the central part of the blade span the flow is attached around the leading edge and that separation occurs near mid chord. The separated fluid moves into the passage and thence downstream.

At this point it is useful to amplify the foregoing result which was also observed with the tufts. In reference (6) surface static pressures were measured chordwise at the mean radius of the stator with a full stage configuration. The resulting velocity distributions for positive incidence are very close to the single roof-top profile used by Kármán.[43] In reference (45) Kármán's laminar separation criterion for such profiles was observed to be valid. If this criterion is applied to the data of reference (6), in particular to figure 60 (ibid), there is obtained the interesting result that for an incidence angle of about 2.2° (cf. table on p. 102 for $\zeta = 0.80$) separation should occur at about 45 ^{o}/o chord. This is approximately the same result as was indicated in figures 47a(1) and 48b(1). Thus, it appears from this comparison that laminar separation has occurred at the point predicted by high Reynolds number data at the same incidence.* Reasoning further, one might expect, based on the rotor

---

* The flow coefficients at high and low Reynolds number differ, however, for the same incidence.

leading edge flow, a reattachment. The fact that this does not occur would seem to stem from the condition that in the stator the separated region is followed immediately by strong radial inflow from the casing, whereas in the rotor the laminar separation must occur very near the leading edge while the radial outflow occurs near midchord.

Further examination of the fluid injection shows that close to the casing, figures 48b(3) and 48b(4), the flow is badly separated. Some of the separated fluid moves radially inward along the blade while most of it separates out into the passage.

Near the trailing edge and close to the casing, the flow, figure 48b(5), is very distorted. An initial reversal upstream occurs followed by strong radially inward flow. The fluid at the top of the photo is on the hub.

b. Regions of Complete Radially Inward Flow Along Suction Surface

The radially-inward flow indicated previously by the tufts is shown very clearly in figure 48c. Fluid over the final 40 $^{o}/_{o}$ of the chord has essentially no chordwise motion and travels into the hub as shown in figure 48c(1). Close to the hub and near the leading edge, the flow, figure 48c(3) is diagonally along the suction surface toward the hub.

Figure 48c(2) is a top view with the injection as in figure 48c(1), and shows clearly that the fluid leaving the suction surface at the hub flows over to the pressure surface. Actually, the flow path from the suction surface is more complex and will be described more fully in figure 48d. However, it is to be noted that in figure 48c(3) the injected fluid exhibits a depth effect, i.e., the flow direction varies from that of

the rotor rotation to that essentially the same as the tangent to the suction surface at the point where the fluid moves onto the hub. Of course, the direction of rotor rotation is followed by the fluid closest to the wall. This latter condition was emphasized further by lowering R_T thereby lowering the through-flow velocities. The result, figure 48c(4), shows the predominant tangential flow. Also to be noted in the flow is a further depth effect. The clearance flow is shown in the passage on the right, the remainder of the fluid having scraped onto the pressure surface.

c. Flow Along Hub and Along Hub End of Pressure Surface

A description of the flow along various parts of the hub within the stator passage is given in figure 48d. The cross-flow from the suction to the pressure surface begins at about 10 or 15 $^{o}/_{o}$ chord, figure 48d(3), and extends to 70 or 80 $^{o}/_{o}$ chord, figure 48d(1). As indicated in the previous paragraph, the hub flow direction varies with depth in the boundary layer. In the outermost part of the layer, the colored fluid mixes with the through flow and is not easily observed.

The flow which moves across the passage consists of clearance flow,* which moves into the next passage, (a good example of this is given in figure 48a(2)) and flow which scrapes onto the adjacent pressure surface, as shown in figures 48d(1), 48d(2), and 48d(3). The radial movement of the scraped flow outward along the pressure surface is small (except at lower R_T; cf. figure 48a). Clearly, from continuity

---

* The stator clearance was approximately .005".

considerations alone, all of the scraped flow cannot move chordwise. Separation must therefore occur. Figure 48d(3) shows this condition both with colored fluid and with a tuft located at the leading edge very close to the hub. The separation at lower R_T is more extensive; an example of this is presented in figure 48d(4) in order to emphasize the separation condition.

The previous photos demonstrate that a part of the hub boundary layer within the stator blade passage originates from the blade suction surface and, moreover, from the casing. It is of interest, therefore, to examine the path followed by the hub boundary layer entering from the rotor.

The flow pattern formed by fluid injected at the hub upstream of the stator is indicated in figure 48d(5). The dispersal is extensive. Part of the fluid moves tangentially in the direction of rotor rotation. Part of the fluid moves through the stator passage and must experience a radial displacement in order to pass over the fluid moving into the passage from the suction surface. Finally, a part reaches the pressure surface near the leading edge and then separates quickly. This separation was indicated by the tuft in figure 48d(3). Because of the wide dispersal, a deep coloring of fluid could not be obtained except at lower R_T, two examples of which are given in figures 48d(6) and 48d(7). The latter figure gives a fairly clear picture of the leading edge separation.

The reason for the stator influence (cf. footnote p.64) on the hub boundary layer emerging from the rotor hub is now clear. The

cross flow within the stator is not part of the incoming boundary layer, and it effectively forces the incoming boundary layer to turn in the direction of rotor rotation.

Finally, it is to be noted from the tufts of figure 30h that at the stator exit the fluid emerging close to the hub has experienced sufficient turning so that the relative tangential velocity is opposite to that of the inlet hub flow.

d. Flow Within and Outside of Hub Boundary Layer

Descriptions of the flow patterns within and outside of the hub boundary layer are given in figure 48e. Figures 48e(1), 48e(2), and 48e(3) show the flow near the pressure surface within the bottom .06" of the hub boundary layer (the dimensions are very approximate). The radial extent of the scraped flow on the pressure surface is about 1/4". The small amount of clearance flow appears in the left passages of figures 48e(1) and 48e(2).

At a distance of about 1/4" from the hub very little cross flow is observable, figure 48e(4). Still farther from the hub, the flow, figures 48e(5) and 48e(6), moves in a general downstream direction. Thus, it appears that all of the cross flow is confined to within about 1/4" of the hub.

5:2.3.2 Flow Surveys Downstream of Stator; $R_T = 2000$, $\Phi = 0.28$; $R_T = 4000$, $\Phi = 0.35$

Radial surveys of the flow downstream of the stator were made at Station 7 a distance of about 3-1/2 chord lengths from the stator

trailing edge. This procedure served two purposes. First, it reduced the number of surveys needed for a reasonable circumferential average. Second, comparison of the data obtained in this way with rotor data obtained at the same position gives a fair estimate of the stator loss. Mixing losses as well as hub and casing effects which occur between the stator exit and Station 7 are partially canceled when the average total head coefficient for the stator (obtained with the compact stage) is subtracted from the same coefficient for the rotor (obtained with the stator expanded). Of course, many of the details of the flow pattern at the stator exit are not observable in the downstream data. In this respect the data are not adequate.

The data which follow comprise radial surveys made at two circumferential positions a distance of about one-half blade pitch apart. Some of the data are compared to the rotor data taken at the same station with the stator expanded.

5.2.3.2.1 Results for $R_T = 2000$, $\phi = 0.28$

a. Circumferential Comparisons

The characteristics of the flow are given in figure 49. There is evidence of some circumferential non-uniformities, particularly in the flow angles near the tip. This result has been noted before (cf. P.86). No attempt was made to study these detailed differences. It seems reasonable, however, that the average state of the fluid is described by the average of the data at the two circumferential positions.

b. Flow Angles

Comparison of the stator and rotor flow angles, figure 49a, gives some indication of the average turning through the stator. For example, at the mean radius, where the stator incidence angle was about 2^{o} (cf. p.102), the indicated turning is 14^{o}. At the same incidence at high Reynolds number, the turning is about 23^{o} (cf. figures 42 and 45, reference (38)). The large reduction in turning prevails over the entire blade height. It is interesting to note that in the data of reference (38) (figures 42 and 45, ibid), the turning angle near the casing is about 32^{o} for all incidences greater than 15^{o}. In the present case at the casing where the incidence was about 40^{o}, the indicated turning is about 30^{o}.

The indicated underturning for the main part of the fluid, in spite of low incidence angles, is, of course, understandable in view of the observations made from the flow visualization data. Very near the hub and casing the curves for the rotor and stator represent different fluid elements due to the radical boundary layer movements in the stator. Elsewhere, of course, radial displacements are probably involved, but these were not evaluated in the present study.

c. Total and Static Head Coefficients

Figures 49b and 49c give the total and static head coefficients respectively downstream of the stator. In figure 49b several features are to be noted in the total head characteristics.

1. The maximum loss region exists at ζ of about 0.63, i.e., at a distance of about 1/4" from the hub. This distance corresponds

to the approximate boundary between the cross-flow and through-flow parts of the hub boundary layer inside the stator (cf. p. 112 and figure 48e(4)). Large shear and mixing losses in this region are to be expected.

2. The peak head coefficient region near the center of the annulus is common to both the rotor and stator curves. This is the region of minimum loss in all three blade rows.

3. In spite of the strong separation near the casing end of the stator blades, the total head distribution downstream does not show evidence of this. Three reasons can be cited. First, the total head, figure 37b, near the casing at the rotor exit had a peak which would tend to compensate for the stator separation loss. Second, part of the casing boundary layer is removed in the stators by the action of fluid movement from the casing onto the blade surfaces, primarily onto the suction surface. Third, downstream of the stator the inherent instability of the casing boundary layer (cf. p. 6) causes the displacement of fluid particles to lower radii.

The static head coefficients have been included, figure 49c, in order to show the relative reactions in the rotor and stator. The data give for these reactions at the mean radius:

Rotor Reaction	Stator Reaction
$\frac{\psi_{S_R} - \psi_{S_{GV}}}{\psi_{S_S} - \psi_{S_{GV}}}$	$\frac{\psi_{S_S} - \psi_{S_R}}{\psi_{S_S} - \psi_{S_{GV}}}$
0.8	0.2

This result, which is common to the entire blade span, shows that the major part of the reaction occurs in the rotor.

d. Velocities

The axial and absolute tangential velocity distributions are presented in figures 49d and 49e respectively. The axial velocities indicate a concentration of mass flow in the region of $\zeta = 0.74$. This result would appear to stem from the movement of casing and stator suction surface boundary layers to the hub. The fluid with higher axial velocity would then be displaced outward. The data also indicate a considerable reduction in axial boundary layer thickness at the casing and an opposite increase at the hub across the stator. The latter effect is consistent with the stator boundary layer movements described previously. The former, however, appears attributable, possibly, to three causes; namely, first, the removal of part of the casing boundary layer in the stator; second, the thinning effect caused by the secondary flow in the casing boundary layer within the stator; and third, the mass transport associated with the inherent instability of the casing boundary layer and with rotational flow downstream of the stator. That the second effect, which is discussed in reference (7), occurs is not certain, since the tufts, figure 47a, do not describe a simple secondary flow pattern at the casing. (cf. p.105) Moreover, the reduction in thickness of the axial boundary layer will be shown to exist at higher Reynolds numbers where again the secondary flow in the casing boundary layer appears small. These considerations, in

addition to others to be presented in connection with the highest Reynolds number data, give the greatest weight to the mass transport effect. One might expect, therefore, that close to the stator exit the reduction in axial boundary layer thickness would be less evident than farther downstream. Furthermore, the downstream effect would be most pronounced at off-design conditions. In this connection the data of reference (38) show no off-design boundary layer thickness reduction in data obtained close to the stator. Thus in a multistage machine the thickness reduction might be unobserved close behind the stator, and yet the effect might still exist and be a factor in producing an essentially constant casing axial boundary layer thickness throughout the machine. The latter condition is to be found in the results of reference (6).

The absolute tangential velocity distribution shows that behind the stator the fluid has approximately constant angular momentum between ζ of 0.66 and 0.86. The cross flow boundary layer thickness at the case has increased across the stator and remained unchanged at the hub.

5:2.3.2.2 Results for $R_T = 4000$, $\Phi = 0.35$

The data for this test condition are presented in figure 50. The average results for the two circumferential positions are generally the same as for the lower R_T tests, although somewhat greater circumferential non-uniformity in the data appears in the present case. Rotor exit surveys and flow visualization in the stator were omitted for these tests. However, since both the guide vane and rotor flow processes

were found to be qualitatively the same at R_T of 2000 and 4000, it seems reasonable that the same situation applies to the stator.

The relative rotor and stator reactions at the mean radius for the present case are 0.83 and 0.17 respectively. These are essentially the same as at the lower R_T.

5:2.3.3 Flow Visualization at R_T of 12,000, $\Phi = 0.33$

The results of flow visualization tests with tufts are presented in figure 51. The following features are to be noted:

1. The leading edge flow, figures 51a, 51b, and 51c, is attached over the entire observable blade height, even though in the last 1/4" near the casing the incidence angle increases from 12 to 30°, while near the hub the incidence angle is about 15°.

2. The suction surface flow near the tip, figures 51a and 51c, separates about mid chord. Behind this point the corner flow is separated.

3. The chordwise-moving fluid along the suction surface, figures 51a, 51b, and 51c, separates between 60 and 80 °/o chord. Behind this region the flow is unsteady and fluctuates from a direction almost normal to the blade to a radially-inward direction.

4. At the hub end of the suction surface the flow, figures 51a, 51b, and 51c, is reversed from the trailing edge. Flows from the leading and trailing edges meet at about 40 °/o chord where the subsequent flow direction fluctuates from a radially outward direction to one nearly normal to the blade surface. The reversal is closely related to the pressure rise across the blade row at the hub. Data to

be presented later (cf. p.134) show the reversal to be absent at both higher and lower values of ϕ .

5. The large cross flow from suction to pressure surface which occurred at lower R_T is absent.

6. The pressure surface flow, figures 51d and 51e, is smooth and generally chordwise. At the hub end of the blade, flow moves from the pressure surface into the blade clearance. (The same effect was observed at the rotor tip, (cf. p.90).) This condition implies essentially no scraping flow, at least none which moves radially outward along the blade surface.

At the trailing edge the flow bends sharply around the edge to the suction surface, a condition which reflects the separation along the suction surface.

7. Over most of the blade passage within the blade row, strong secondary flow does not occur within the casing boundary layer.* Near the suction surface, flow moves from the casing to the blade corner where the chordwise flow has separated (v.s.).

5:2.3.4 Flow Surveys Downstream of Stator; R_T = 12,000, ϕ = 0.33; R_T = 21,000, ϕ = 0.33

Although the tuft studies showed evidence of separation in the stators at R_T of 12,000, the flow surveys downstream of the stator

---

* Again it must be emphasized that the tufts may not reflect the motion at the wall. However, since the tufts are submerged deep in the boundary layer, the amount of fluid which may possibly experience greater deflection must be small.

produced results which are very similar to those obtained in reference (38) at high R_T. The experimental data at ϕ of 0.33 are presented in figures 52a and 52b. Comparisons* with op. cit. are also included to show that at R_T of 12,000 the flow pattern behind the stator over most of the blade height is already comparable to high R_T flow conditions.

Similar results are shown in figure 53 for R_T of 21,000. Thus it appears that regardless of the flow details in each blade row, high Reynolds number flow patterns provide a reasonable estimate of the conditions behind the entire stage at R_T values as low as 12,000. It seems possible that this situation might prevail in subsequent stages.

A few details of the flow patterns in figures 52 and 53 are to be noted. First the axial boundary layer thickness at the casing is thin, a condition observed and discussed in connection with the lower R_T results (cf. p. 116). Second, the rotor and stator reactions at the mean radius are about 0.62 and 0.38 respectively for both 12,000 and 21,000 R_T . This division is comparable to higher R_T performance and is a further indication of the similarity in flow patterns cited above.

5:2.3.5 Flow Visualization at R_T of 150,000, ϕ = 0.33, 0.39

The results at these conditions can be found in the following figures presented in connection with previous discussions:

---

* High R_T results from the present investigation are also included. These curves correspond to the data of figure 54.

ϕ	Figure	Part of Stator Passage to be Seen in Figure
0.33	27a	Pressure surface and casing
"	44a(2)	"
"	44a(3)	"
"	44c(1)	"
"	44b(1)	Suction surface and casing
"	44b(2)	"
"	44c(1)	"
"	44c(2)	"
0.39	27b	"
"	43a(2)	"
"	43b(1)	"
"	43b(2)	"
"	43c(1)	"
"	43c(2)	"
"	43c(3)	"
"	43a(1)	Pressure surface and casing

At ϕ of 0.39 the flow is chordwise over both blade surfaces. The casing and clearance flows are essentially the same as described in the previous section.

At ϕ of 0.33 the higher incidence angles cause separation in the corner flow at the casing. Radial inflow occurs near the trailing edge. There is also evidence of random motion near the hub of the suction surface. Elsewhere the flow is the same as at higher ϕ .

5:2.3.6 Flow Surveys Downstream of Stator; R_T = 150,000; ϕ = 0.33, 0.39

Downstream surveys were made at flow rates corresponding

approximately to $\psi_{T_{max}}$ ($\phi \sim 0.33$) and η_{max} ($\phi \sim 0.39$). The first condition was used in order to have a common operating point for most of the Reynolds number range. In regard to the second condition, since flow separation near the casing end of the stator was still in evidence at the lower ϕ (v. s.), it was desirable to examine the flow in the absence of such separation.

The results are presented in figures 54 and 55. Some comparisons with the data of reference (38) are included; these indicate, as in the case of the rotor, more uniform conditions near the hub in the present data. While this effect probably involves the relative influence of hub and casing boundary layers in machines which differ only in blade aspect ratio, and also influences associated with measuring near and far downstream of the blade row, no study of the problem was undertaken in the present investigation.

Comparison of the flow angles for ϕ of 0.33 and 0.39 shows a difference near the casing. The rise at ϕ of 0.33 is apparently characteristic of low ϕ operation at high Reynolds number (cf. op. cit.). Examination of the rotor exit data and the stator tuft photos indicates that there are three contributing factors which are characteristic of low ϕ operation; namely, higher flow angles leaving the rotor, separation at the casing end of the stator, and an absence of strong secondary flow at the casing end of the stator.

Comparison of the axial velocity distributions at the two values of ϕ shows that the axial boundary layer thickness downstream of the stator is smallest for the lower ϕ even though the opposite

situation exists at the rotor exit. The cause is attributed to the instability of the casing boundary layer coupled with increased rotational mixing at lower ϕ . Near the hub the largest axial boundary thickness exists at the lower ϕ , an effect which would stem from a more rapid increase in cross-flow boundary layer thickness compared to the growth in axial boundary layer thickness. This difference in growth would increase with a reduction in ϕ due to the increase in flow path length between the stator exit and downstream stations. As the cross-flow boundary layer grows, it would tend to turn the outer fluid more in the direction of rotor rotation, thereby reducing the axial velocity.

Finally, it is to be noted that the rotor and stator reactions at the mean radius are approximately 0.62 and 0.38, which are the same as at R_T of 12,000 (cf. p.120).

5:2.3.7 Stator Total Pressure Loss

In order to obtain some indication of the variation in stator total pressure loss with Reynolds number the mass-weighted average total pressure drop across the stator was calculated from the experimental data. The loss, as a fraction of the rotor and stage total heads, is given in figure 56a as a function of R_T. In figure 56b the loss is referred to the mean-radius dynamic head at the rotor outlet and is plotted against R_ϕ . In figure 56c R_S is used. All of the curves show that the loss rises rather rapidly below R_T of 20,000 (or R_ϕ of 7000). The rise should be somewhat steeper than appears in the figures since the loss at R_T of 12,000 and 21,000 includes rotor mixing losses whereas the low R_T data do not include this effect. The loss is seen

to increase from about 7-1/2 °/o of the stage output at R_T of 150,000 (R_ϕ = 60,000, R_S = 85,000) to about 25 °/o at R_T of 2000 (R_ϕ = 560, R_S = 850).

It is interesting that at the ends of the curves, the loss variation is about the same for both high and low Reynolds numbers. This occurs even though at the high end the loss variation is associated mostly with changing blade-surface boundary layer thicknesses, while at the low end the complex boundary layer movements within the stator passages are involved.

5:2.3.8 Some Observations with Stator Located Over Stationary Hub

Theoretical treatments of secondary flows in stators[35] usually consider the hub to be stationary. In practical applications stationary hubs are found in the outlet stator rows of multistage machines as well as in every stage in cases where the stators are shrouded. It is useful, therefore, to examine the stator flow characteristics with the stators located over a stationary part of the hub.

In the present investigation a cursory examination of this condition was made at the lower R_T with the stator located in the blade row immediately following the end of the rotating hub. Since the viewing window did not extend over the blade row, only parts of the blade passages could be seen.

A sketch resulting from visual observations of tufts is presented in figure 57a. Some similarities and contrasts with the results for the rotating hub are to be noted. These are listed in the following:

Similarities

1. The leading edge flow is attached over most of the blade height. Along the suction surface, separation occurs near the casing and at the very hub end of the blade.

2. Near midchord the chordwise-moving fluid separates.

Contrasts

1. The hub boundary layer moves radially outward along the suction surface downstream of midchord.

2. Near the trailing edge end of the passage the radial motion of the hub boundary layer occurs even in the mid-pitch region.

3. Elsewhere along the hub within the passage, strong secondary motions from the pressure to the suction surface are absent.

4. Near the midspan part of the trailing edge of the suction surface the flow reverses and is very unsteady.

The radial outward movement of the suction surface boundary layer in a three-dimensional stationary stator cascade was observed in reference (2). There also occurred (ibid) an inward flow from the casing. Presumably, then, in the present situation the corner flow at the casing is separated. Consequently, as in the guide vanes, the boundary layers move radially inward and outward and meet in the upper half of the blade span.

An indication of the effect of the stationary hub on the flow angle at the stator exit is provided by the data of figure 57b. The measurements were made directly behind the stator at one circumferential position, and thus they may differ considerably from

the average state. Nevertheless they provide indications of major differences, particularly near the blade ends. (cf. figures 49a and 50a)

A total pressure survey indicated large losses across the lower half of the blade, a result which is consistent with the flow patterns described by the tufts.

Observations were not made at higher Reynolds numbers. In reference (2), however, no radical effects in cascade performance were observed at Reynolds numbers (based on the inlet velocity at the mean radius) down to 50,000. In the present case this would correspond to R_ϕ of approximately 30,000 which indicates a "critical" range possibly comparable to the rotating hub configuration.

5:3 Additional Observations

A number of additional observations were made at various Reynolds numbers and flow rates. Some of the information which appeared to be sufficiently interesting to warrant it being reported, is described in the present section.

5:3.1 Casing and Hub Boundary Layer Profiles Behind Rotor and Stator

A clear description of the casing and hub boundary layer profiles could not be derived from the present experiments. Aside from the instrumentation, which was not designed for accurate boundary layer probing, distortions in the velocity profiles, particularly at the lower R_T, made difficult the separation of the boundary layer regions from

the remainder of the fluid. A number of criteria may be used to fix this division. For example, in reference (7), the outer extent of the boundary layer was fixed at the point where the absolute flow angle began to change rapidly. Total pressure and velocity profiles may also be used for this purpose. In the present case the use of velocity profiles for establishing the division provided the least randomness in results.

In figure 58 are plotted a number of sets of axial and cross-flow boundary layer data, the curves having been omitted. The Blasius laminar profile and the turbulent 1/7 power law are included for comparision. The data show no specific form of profile, although the distributions conform more nearly to a turbulent than to a laminar boundary layer. The data between the laminar and turbulent curves approximate the form of a stagnation point profile.[36]

In reference (7) the casing boundary layers in turbulent flow were studied from the point of view of the momentum integral equations developed in reference (44). It would seem that a similar approach might be applicable at lower Reynolds numbers in cases where radial movements of blade surface and hub boundary layers are not important, and where distortions in the velocity profiles are not excessive.

A comparison of one set of data obtained in the present study is made with data given in reference (7). For purposes of clarifying the comparison, a few remarks are necessary. In Mager's theoretical development[44] the casing boundary layer velocities are divided into two components, one u in the direction of the flow at the outer edge

of the boundary layer, the other w at right angles to the first. The boundary layer profiles are described by two parameters; namely,

$$G\left(\frac{y}{\delta}\right) = \frac{u}{v}$$

and

$$g\left(\frac{y}{\delta}\right) = \frac{w}{u}\,\frac{l}{\epsilon}$$

where ϵ is the maximum deflection in the boundary layer. In the reference (7), the functions G and g are given at the rotor exit of a single stage compressor for the case of a 1/8" spoiler located upstream. Data with the spoiler were considered to provide the better basis for comparison with the present data which were obtained at lower R_T.

The comparisons of a set of G and g from reference (7) with those from the present study are shown in figure 59. The correspondence is reasonably close. This single comparison, of course, does not justify any definite conclusion. For lower R_T the importance of the blade surface boundary layers increases, and even though radial flows be absent, a modification of the wall boundary layers might be expected due to interaction with thick blade boundary layers. This effect would probably have to be included.

5:3.2 Absolute Flow Angles and Total Head Coefficients at Rotor Exit for Flow Coefficients Approaching Shut-Off; R_T = 2000, 4000

The absolute flow angles at the rotor exit for R_T of 3900 and ϕ values between 0.36 and .05 are shown in figure 60. The variation

with ϕ is seen to be rather systematic in spite of the increasing complexity of the flow. A part of the complexity for the case of the expanded stator can be explained as follows: as ϕ decreases an increasing percentage of the flow entering the rotor recirculates back along the casing to the guide vanes. Thus the flow leaving the rotor is considerably less than the flow entering the rotor, and as a consequence the axial velocity decreases across the rotor, the magnitude of the decrease becoming greater as ϕ decreases. This is the essential reason for the increase in the level of the absolute flow angle data. The centrifugal pumping action of the rotor also increases as ϕ decreases, and the drop in flow angle near the casing suggests a concentration of flow leaving the rotor in this region.

The centrifugal action of the rotor probably accounts for the form of the measured total head distributions, (figure 61) at the rotor exit. The peak near the hub, which is attributed to secondary flow in the hub boundary layer, decreases slightly as ϕ decreases, while at the same time the peak near the tip increases. It is believed that this effect provides the relatively large heads at complete shut-off in axial flow machines.

5:3.3 Flow Visualization Near Shut-Off; $R_T = 2000$

Several interesting flow patterns as described by tufts were observed at near shut-off conditions ($\phi \sim 0.05$). Examples for three stage-configurations are given in figure 62. In viewing the photos, one should remember that tufts attached to stationary surfaces are

oriented in the direction of the absolute flow, while tufts attached to moving surfaces are oriented in the direction of the relative flow.

a. Expanded Stator

Figure 62a is shown for purposes of reference. Here the stator is expanded and ϕ is 0.15. Flow near the rotor tip is reversed and moves upstream (down in the photo) to the guide vanes, then radially inward along the guide vane suction surface and back into the rotor. Downstream the flow directions are given as follows:

1. Tufts immediately to the left of numbers are attached to the rotating hub. The axial velocity is seen to be directed downstream and the relative tangential velocity is opposite to the rotor rotation. The spiral motion near the hub tightens as the flow proceeds downstream which implies a more rapid growth in axial compared to the relative cross-flow boundary layer thickness.

2. Downstream of the rotor and at the left of the photo, tufts attached to the casing (cf. figure 62b(1)), show the absolute flow to be directed downstream in an unwinding spiral motion. Thus in contrast to the condition near the hub, the cross-flow boundary layer grows more rapdily than the axial boundary layer.

3. Two rakes are visible; one to the left and above No. 7, the other to the left and below No. 14. These describe the warped shape of the absolute stream surface.

As ϕ is reduced further, flow reversal begins far downstream along the hub. At ϕ of 0.05 the flow pattern is as shown in the photos of figure 62b. Figure 62c is an estimated model of the recirculating

flow. (cf. infra.) The casing tufts in figure 62b(1) show that the flow moves downstream along the casing. As deduced from the hub tufts between No. 16 and No. 10, the axial velocity near the hub is seen to be directed upstream until a region between No. 10 and No. 9 is reached (region c in figure 62c) where the axial velocity reverses direction. Within the main part of the annulus there exist two regions of flow (see rake near No. 14 in figures 62b(1) and 62b(2)) which are characterized by opposing axial velocities. Between these two regions, therefore, must exist a layer of fluid which rotates in the direction of the rotor but in which the magnitude of the axial velocity decreases to zero. The outlet rake near No. 7, figure 62b(3) shows a flow reversal near the tip of the rotor blade. This condition is also to be noted in the measured flow angles given in figure 60 for $\phi = .05$, since flow angles greater than 90° imply a reversal in axial velocity.

It appears possible to represent the flow pattern by the vortex system sketched in figure 62c . The assumption is made that the vortices are stabilized by the action of the blade rows in a manner somewhat analogous to the case of a two-dimensional cylinder to which is attached a trailing vortex pair. The reversed flow pattern within the rotor is not axially symmetric, while the pattern downstream, as far as was observed, appeared axially symmetric. (The region within the stators could not be seen.)

b. Expanded Rotor and Stator

When the rotor is placed in the second stage position, (i.e. near the region c (figure 62c) of zero axial velocity at the hub) the

downstream reversal of flow along the hub extends into the rotor passage as shown in figure 62d(1). The flow reversal near the tip at the rotor exit is no longer observable. The flow patterns upstream and downstream of the rotor now appear symmetrical, (figures 62d(1) and 62d(3)) with the layer of diminishing axial velocity occurring in both regions. Within the rotor passage, the hub fluid from upstream and downstream (figures 62d(1) and 62d(2)) meet in the chordwise center of the passage and flow to the suction surface to be pumped radially out to the tip and thence in part upstream to the guide vanes and in part downstream.

c. Compact Stage

Placement of the stator in its normal single stage position, figure 62e, causes the flow within the rotor to be quite similar to the expanded stator configuration. In the stator the flow, figure 62e(1), now reverses along the suction surface, the fluid originating from the casing. The reversed stator flow does not appear to extend into the rotor.

The far-downstream flow was not traced in detail, although reversal along the hub still is evident in the photos. Two hub tufts are shown in figure 62e(2) to the left of No. 8. Upstream the flow appears as in the case of the expanded stator.

It thus appears that the closeness of either the guide vane or stator changes markedly the pumping process in the rotor near shutoff. In addition the axial extent of the upstream and downstream reversed flow patterns is modified by the stage configuration.

5:3.4 Flow Visualization at Low and High ϕ ; R_T = 12,000 - 150,000

Most of the results within the earlier parts of the paper were concerned with flow conditions near $\psi_{T_{max}}$ and η_{max}, these being the conditions for which Reynolds number comparisons could be made. It is important of course to examine the flow patterns at both lower and higher flow rates. Observations made under these conditions are included in the present section.

5:3.4.1 Results at R_T = 12,000, ϕ = 0.15

a. Guide Vane

In figures 63a and 63b the leading edge flow near the casing is seen to be separated. The reversed flow along the casing moves to the suction surface and then radially inward. The radial flow appears to separate as it nears the chordwise moving fluid along the lower parts of the blade. The pressure surface flow is smooth.

b. Rotor

Flow along the rotor surfaces is shown in figures 63a, 63c, and 63d. The flow reversal near the tip of the suction surface is seen to originate from clearance flow and from the rear part of the suction surface.

The radial flow along the suction surface is confined to the rear part of the blade. In fact near the hub the flow fluctuates from a radial to a chordwise direction as shown in figure 63a. This condition implies that although the stage pressure rise is low, the angular momentum of the fluid within the rotor is large enough to produce a

radial pressure gradient sufficiently strong to suppress radial motion of the surface boundary layer.

The secondary flow along the hub between blades, figure 63c, does not appear strong, and radial motion onto the suction surface is confined to the trailing-edge corner.

c. Stator

The stator flow, figures 63a, 63b, 63c, and 63f, is separated at the leading edge of the casing end of the blade span. The combination of radial inflow, reversal, and chordwise separation is indicated in figure 63e. At the hub end of the blade the flow near the trailing edge is no longer reversed as at the $\psi_{T_{max}}$ condition (cf. figure 51). This reflects the reduced static pressure rise across the stator. At the casing there is a predominant movement of boundary layer onto the suction surface.

5:3.4.2 Results at R_T = 12,000, 35,000; ϕ = 0.45

Flow conditions at high ϕ are described in figure 64. The radial flow in the guide vanes has been described earlier (cf. p.51). An interesting similarity, figure 64b, is to be observed on the rotor suction surface. A strong radial outward flow of the boundary layer occurs. In this case the cause is attributed to the reduced radial pressure gradient associated with high ϕ operation.

In the stator the radial inflow occurs with a tendency to chordwise motion as shown by comparison of figure 64a and 64c.

All of the strong radial flow at high ϕ in each of the blade rows is absent at R_T of 35,000. At this condition the guide vane flow was

presented earlier in figure 27a. In figure 64d chordwise flow in the rotor is indicated by the chordwise orientation of the trailing edge tufts attached to the left rotor blade. The smooth stator flow is also evident.

Thus, with regard to the radial flow on the suction surfaces, there must exist a "critical" relation between Reynolds number and turning angle for each blade row. For a specific stage design the "critical" Reynolds number is related to R_T and ϕ . In the present case at ϕ of 0.45, the "critical" value of R_T is between 12,000 and 35,000 for all three blade rows.

5:3.4.3 Results at $R_T = 150,000$; $\phi = 0.30, 0.27$

A number of details observed at these conditions are considered to be of general interest for high Reynolds number operation of axial turbomachines.

In figure 65a the blade-row flow patterns are shown for ϕ of 0.30. Two features are to be noted. First, the flow over the entire rear part of the rotor suction surface is radial, and the chordwise flow is separated. This condition was partly in evidence at ϕ of 0.33 (cf. figure 44a(3)). In references (5), (6), and (38), experiments established that "stall" incidence for a blade element in a three-dimensional cascade was lower than in a two-dimensional cascade. It is believed that the explanation for this difference lies in the fact that three dimensional cascades experience radial flow of the hub and suction surface boundary layers which in turn cause the separation of the chordwise flow at lower incidence. "Stall" in a three-dimensional

cascade is therefore a three-dimensional boundary layer flow process, and its prediction must include considerations of the hub corner flow and the radial movement of the suction surface boundary layer.

The second feature as described in figure 65a(2) is the flow separation at the corner and casing end of the stator suction surface. This condition along with the rotor flow noted above is "steady" (i.e. only random fluctuations occur), and immediately precedes the onset of rotating stall in the stage configuration tested. A detailed examination of rotating stall was not attempted. However, it is interesting to observe the photos in figure 62b which were taken with rotating stall present.

In figure 65b(1) the rotor flow is seen to be the same as in the previous photos. The stator flow is also the same in figure 65b(2); the stall region has not yet entered these passages. The right rotor blade also shows two long chordwise tufts which demonstrate the extent of the "steady" chordwise separation.

Comparison of the guide vane casing tufts in figure 65b(3) and 65b(4) shows the large flow direction change in figure 65b(3) as the stall region moves by. Also to be seen in figure 65b(3) is the improved chordwise flow on the suction surface of the stator blade. The stator casing-tufts at the left of the photo (cf. figure 65b(4)) indicate the reduced incidence which has served to "unstall" the stator suction surface.

5:3.4.4 Results at R_T = 150,000; ϕ = 0.49

Two photos at this condition are presented in figure 66 in order to describe a contrast with lower R_T flow. The flow over all surfaces within the stage is seen in figures 66a and 66b to be almost perfectly chordwise. At R_T of 12,000 and ϕ of 0.45, it is to be recalled that radial flow existed along the suction surface in each blade row, (cf. figures 64a, 64b, 64c). Such flow did not exist at R_T of 35,000 (cf. figure 64d). Thus the present observation is further proof that no strong radial flows exist at high ϕ above R_T of 35,000.

VI. SUMMARY OF RESULTS

The experimental results obtained with a single stage, axial flow turbomachine operated with incompressible fluid in a low Reynolds number range are summarized in part as follows:

1. No critical changes in overall performance occurred at R_T values down to 20,000. Below R_T of 20,000, the performance deteriorated more rapidly. However, even at R_T of 2000, the peak efficiency was still about 29 °/o. A quantitative indication of the Reynolds number influence on efficiency is given by the following output-to-loss ratios at peak efficiency:

$$\frac{\eta}{1-\eta} \propto R_T^{0.18} \qquad 150,000 > R_T > 20,000$$

$$\frac{\eta}{1-\eta} \propto R_T^{0.65} \qquad R_T < 20,000$$

The more rapid deterioration in performance is associated with radial movements of boundary layer fluid which cause separation of the chordwise-moving fluid. The flow in the corner formed by the blade suction surface and the casing or hub is an important element in the radial flow process.

For the guide vanes the corner flow at the casing was separated at R_{GV} of 12000. Above 35,000 and below 4,000 this corner separation did not occur.

For the rotor the corner at the rotating hub was separated near midchord at R_T = 4000 for all flow rates. At higher R_T the separation occurred closer to the trailing edge and depended, moreover,

on the flow rate.

For the stator the corner flow at the casing was separated for R_T below 20,000.

2. The performance of each blade row was characterized by the following Reynolds number effects:

a. Guide vane performance

(1) A gradual reduction in turning occurred over the main part of the span. The reduction at the mean radius was about 1 degree for each 10,000 units reduction in R_{GV}. Below R_{GV} of 10,000 the turning varied approximately as $(R_{GV})^{\frac{1}{10}}$.

(2) The average total pressure loss across the guide vanes varied gradually between R_{GV} of 80,000 and 10,000. Below 10,000 the loss increased sharply. At R_{GV} of 600 the loss was approximately 36 $^{o}/o$ of the average dynamic head at the guide vane inlet. This loss included the combined effects of blade surface and wall boundary layers.

(3) For a given average flow coefficient the reduced turning by the guide vanes increases the incidence angles on the rotor blades. In this respect, however, turning due to the strong secondary flow in the wall boundary layers compensates for the low axial velocities in the wall boundary layers and thereby tends to lower the incidence angles at the hub and tip of the rotor.

(4) The thick boundary layers emerging from the guide vanes appear to provide an important source of turbulence which aids in preventing separation of the leading edge flow over the rotor blades.

b. Rotor performance

(1) In the high flow coefficient range at each R_T down to 2,000, the leading edge flow, except near the tip, remained attached.

(2) The rotor output remained high even at very low R_T. The flow patterns, however, became increasingly more distorted. These distorted flow patterns are a source of large mixing losses.

(3) At low R_T the rotor behaves in part as a centrifugal pump. Part of the hub boundary layer flows to the suction surface and then radially outward to the casing. This radial movement of boundary layers causes the chordwise moving fluid to separate, thereby adding to the rotor loss.

(4) For $R_T > 12,000$ the secondary flow in the hub boundary layer is markedly reduced. A main element in this reduction is the delay of corner flow separation until the flow reaches a point near the trailing edge.

(5) At high R_T radial flow of the boundary layer along the suction surface occurs only at low ϕ and is confined to the trailing edge region.

c. Stator performance

(1) In the high flow coefficient range at each R_T down to 2,000, the leading edge flow, except near the casing and hub, remained attached.

(2) Below R_T of 20,000 the casing end of the stator was separated at all values of ϕ, and the suction surface boundary layer

moved radially inward. At R_T of 2,000, this fluid flows completely across the passage along the hub to the pressure surface where it is scraped and then forced downstream.

(3) For $R_T > 12,000$ the scraping flow at the hub end affects only a very small radial extent of the blade.

(4) The radial flow of the boundary layer, when the hub is stationary, differs markedly from that which occurs when the hub is rotating.

(5) The total pressure loss across the stator in the high ϕ range increases gradually with a decrease in R_T down to 20,000. Below 4,000 the rate of increase again becomes gradual. At R_T of 2,000 the stator loss is about 25 °/o of the stage output; at R_T of 150,000 the loss is about 8 °/o.

VII. CONCLUDING REMARKS

The findings reported herein were obtained in a single stage, free-vortex machine with an incompressible working fluid. For non-free-vortex designs, radial flow in the main stream is inherent in the design. In the present investigation the flow patterns were studied at flow rates for which radial flows also occurred in the main stream. The results suggest that the radial flows usually present in the main stream of an axial flow turbomachine should not in themselves introduce any radical changes in Reynolds number effects.

In the absence of compressibility effects, the importance of Reynolds number is expected to be greatest for the inlet stage of a multistage machine. It is anticipated, therefore, that if additional stages were added to the single stage studied herein, the flow patterns observed for the latter would be repeated in subsequent stages. In addition the critical Reynolds number range should remain essentially the same.

Where compressibility effects, particularly in the nature of shocks within blade passages, are involved, the results reported herein are not likely to be applicable. One important difference can be cited. In the present study, radial flow of blade surface boundary layers in the region of design flow rate was found to be relatively unimportant at Reynolds numbers R_T as low as 20,000. However, the presence of shocks may cause this radial flow to be significant regardless of the magnitude of Reynolds number. Other factors, such as laminar bubble behavior, may also be influenced by the presence of

shocks. Moreover, even though the relative Mach number entering a blade row be held fixed while the Reynolds number is reduced, the shock patterns within the blade passages are likely to change, since the effective blade shape is changed by increased boundary layer growth. Thus, low Reynolds number effects at high Mach numbers may actually modify the compressibility effects. As a general observation, it would seem that for high Mach numbers, a reduction in Reynolds number should produce important changes in performance at Reynolds numbers higher than those reported herein. The problem, however, certainly requires special attention.

As a final remark, it should be noted that in cases of higher blade loadings than were used in the present machine, more severe Reynolds number effects are to be anticipated. For example, a laminar bubble which may reattach on a low-cambered blade at a given Reynolds number and turbulence level, may not reattach for a higher cambered blade at these same flow conditions.

REFERENCES

1. Blight, F. G., and Howard, W.: Tests on Four Aerofoil Cascades: Part II, Boundary Layer Characteristics, Aeronautical Research Laboratories (Australia) E 75, (July 1952)

2. Thurston, S., and Brunk, E.: Performance of a Cascade in an Annular Vortex-Generating Tunnel Over Range of Reynolds Numbers, NACA RM E51G30 (September 1951)

3. Ruden, P.: Investigation of Single Stage Axial Fans, NACA TM No. 1062 (April 1944)

4. Weske, John R.: An Investigation of the Aerodynamic Characteristics of a Rotating Axial-Flow Blade Grid, NACA TN No. 1128 (February 1947)

5. Rannie, W. D., Sabersky, Rolf H., and Bowen, John T.: Theoretical and Experimental Investigations of Axial Flow Compressors, Summary Report, California Institute of Technology, Mechanical Engineering Laboratory (January 1949)

6. Rannie, W. D., Sabersky, Rolf H., and Bowen, John T.: Theoretical and Experimental Investigations of Axial Flow Compressors, Part 2, California Institute of Technology, Mechanical Engineering Laboratory (July 1949)

7. Mager, Artur, Mahoney, John J., and Budinger, Ray E.: Discussion of Boundary-Layer Characteristics Near the Casing of an Axial-Flow Compressor, NACA TR 1085 (1952)

8. Fogarty, Laurence Eugene: The Laminar Boundary Layer on a Rotating Blade, Journal of the Aeronautical Sciences, Vol. 18, No. 4, pp. 247-252 (April 1951)

9. Graham, M. E.: Calculation of Laminar Boundary Layer Flow on Rotating Blades, Cornell U., AF 33(038)-21406 (September 1954)

10. Mager, Artur: Laminar Boundary Layer Problems Associated with Flow Through Turbomachines, Doctoral Thesis, California Institute of Technology, (1953)

11. Mager, Artur: Three Dimensional Laminar Boundary Layer with Small Cross-flow, Journal of the Aeronautical Sciences, Vol. 21, No. 12, pp. 835-845 (December 1954)

12. Mager, Artur: Thick Laminar Boundary Layer Under Sudden Lateral Perturbation, Sonderdruck Aus 50 Jahre Grenzschichtforschung , Festschrift, (Verlag Frier, Vieweg and Sohn, Braunschweig) (March 1954)

REFERENCES (Cont'd)

13. Smith, W. E.: Some Examples of Laminar Boundary Layer Flow on Rotating Blades, M. Aero. Thesis, Cornell University, Ithaca, N.Y. (1952)

14. Goldstein, Arthur W.: Analysis of the Performance of a Jet Engine from Characteristics of the Components, I - Aerodynamic and Matching Characteristics of the Turbine Component Determined with Cold Air, NACA TN No. 1459 (October 1947)

15. Kofskey, Milton G., Rohlik, Harold E., and Monroe, Daniel E.: Experimental Investigation of Flow in an Annular Cascade of Turbine Nozzle Blades of Constant Discharge Angle, NACA RM E52A09 (March 1952)

16. Hansen, A. G., Costello, G. R., and Herzig, H. Z.: Effect of Geometry on Secondary Flows in Blade Rows, NACA RM E52H26 (October 1952)

17. Hansen, A. G., Herzig, H. Z., and Costello, G. R.: Smoke Studies of Secondary Flows in Bends, Tandem Cascades, and High-turning Configurations, NACA RM E52L24a (March 1953)

18. Rohlik, Harold E., Allen, Hubert W., and Herzig, Howard Z.: Study of Secondary-flow Patterns in an Annular Cascade of Turbine Nozzle Blades with Vortex Design, NACA TN 2909 (February 1953)

19. Hansen, A. G., Herzig, H. Z., and Costello, G. R.: A Visualization Study of Secondary Flows in Cascades, NACA TN 2947 (May 1953)

20. Kofskey, Milton G., Allen, Hubert W., and Herzig, Howard Z.: Comparison of Secondary Flows and Boundary-Layer Accumulations in Several Turbine Nozzles, NACA TN 2989 (August 1953)

21. Kofskey, Milton G., and Allen, Hubert W.: Smoke Study of Nozzle Secondary Flows in a Low Speed Turbine, NACA TN 3260 (November 1954)

22. Hansen, Arthur G., and Herzig, Howard Z.: Cross Flows in Laminar Incompressible Boundary Layers, NACA TN 3651 (February 1956)

23. The Influence of Physical Dimensions (Such as Hub:Tip Ratio,

REFERENCES (Cont'd)

Clearance, Blade Shape) and Flow Conditions (Such as Reynolds Number and Mach Number) on Compressor Characteristics, Buships 338, Volume 3 (May 1946)

24. Sohn, Robert L.: An Analysis of the Performance of an Axial-Flow Compressor at Low Reynolds Number, Journal of the Aeronautical Sciences, Vol. 23, No. 8, pp. 741-746 (August 1956)

25. Ippen, A. T.: Influence of Viscosity on Centrifugal Pump Performance, Trans. ASME, Vol. 68, pp. 823-848 (1946)

26. Fuller, T. W., and Acosta, A. J.: Report on Design and Construction of the Axial Flow Pump Test Facility, Department of the Navy, Bureau of Ordnance, Contract NORD 9612, Report No. E-12.1.3 (June 1953)

27. Rains, Dean A.: Tip Clearance Flows in Axial Flow Compressors and Pumps, California Institute of Technology, Hydrodynamics and Mechanical Engineering Laboratories, Navy Contracts N6-ori-102, Task Order IV and NOrd 9612, Report No. 5 (June 1954)

28. Rivas, Miguel A. Jr., and Shapiro, Ascher H.: On the Theory of Discharge Coefficients for Rounded-entrance Flowmeters and Venturis, ASME Paper No. 54-A-98, Preprint of Paper Presented to ASME (November 1954)

29. Physical Measurements in Gas Dynamics and Combustion, Volume IX, High Speed Aerodynamics and Jet Propulsion, Princeton University Press, Princeton, New Jersey, pp. 111-122 (1954)

30. Hurd, C. W., Chesky, K. P., and Shapiro A. H.: Influence of Viscous Effects on Impact Tubes, Journal of Applied Mechanics, Vol. 20, No. 2, pp. 253-256 (June 1953)

31. Sinclair, Archibald R., and Robins, A. Warner: A Method for the Determination of the Time Lag in Pressure Measuring Systems Incorporating Capillaries, NACA TN 2793 (September 1953)

32. Macmillan, F. A.: Viscous Effects on Pitot Tubes at Low Speeds, Journal of the Royal Aeronautical Society, Vol. 58, pp. 570-572 (August 1954)

33. Schlichting, H: The Laminar Boundary Layer on a Spinning Body of Revolution in Axial Flow (Translated by A. H. Lange), U.S. Naval Ordnance Laboratory, Navord Report 4195 (December 1955)

REFERENCES (Cont'd)

34. Davis, Hunt, Kottas, Harry, and Moody, A.M.G.: The Influence of Reynolds Number on the Performance of Turbomachinery, ASME Trans., Vol. 73, pp. 499-509 (1951)

35. Loos, Henk, G.: Analysis of Secondary Flow in the Stator of an Axial Turbomachine, Office of Scientific Research, ARDC, Tech. Rept. No. 3 (September 1953)

36. Schlichting, H.: Lecture Series "Boundary Layer Theory" Part I - Laminar Flows, NACA TM No. 1217 (April 1949)

37. Lieblein, Seymour, and Ackley, Richard H.: Secondary Flows in Annular Cascades and Effects on Flow in Inlet Guide Vanes, NACA RM E51G27 (August 1951)

38. Alsworth, Charles C., and Iura, Toru: Theoretical and Experimental Investigations of Axial Flow Compressors, Part 3, Progress Report on Loss Measurements in Vortex Blading, California Institute of Technology, Mechanical Engineering Laboratory, (July 1951)

39. Yeh, Hsuan, Croner, Harry M., and Andrews, Donald E.: Preliminary Measurements of Nonsteady Velocities in a Single Stage Axial-flow Compressor, Johns Hopkins University, Institute for Cooperative Research, Report I-25 (May 1955)

40. Laufer, John: Investigation of Turbulent Flow in a Two-dimensional Channel, NACA TN 2123 (July 1950)

41. Goldstein, S. (ed): Modern Developments in Fluid Mechanics, Vol. II, Clarendon Press (Oxford) (1950)

42. Iura, T., and Rannie, W. D.: Observations of Propagating Stall in Axial Flow Compressors, California Institute of Technology, Mechanical Engineering Laboratory, Report No. 4 (April 1953)

43. Karman, Th. von and Millikan, Clark B.: A Theoretical Investigation of the Maximum Lift Coefficient, Journal of Applied Mechanics, Vol. 2, No. 1, pp. A-21 - A-27 (March 1935)

44. Mager, Artur: Generalization of Boundary-Layer Momentum-Integral Equations to Three-dimensional Flows Including Those of Rotating System, NACA TR 1067 (1952)

45. Neustein, Joseph: Experiments at Low Reynolds Numbers, Part I: Isolated Airfoils, Part II: Axial Flow Turbomachine, California Institute of Technology, Hydrodynamics and Mechanical Engineering Laboratory, (March 1957)

TABLE I

BLADE DESIGN DATA (REFERENCE (5))

ξ	s/c	γ_1	γ_2	θ	γ'	t_m/c	i
			ROTOR				
.600	.870	$51^\circ 12'$	$86^\circ 49'$	$46^\circ 40'$	$74^\circ 48'$	0.12	0°
.700	1.015	$42^\circ 24'$	$65^\circ 17'$	$31^\circ 0'$	$57^\circ 54'$	0.11	"
.800	1.160	$36^\circ 2'$	$50^\circ 40'$	$20^\circ 19'$	$46^\circ 12'$	0.10	"
.900	1.305	$31^\circ 21'$	$41^\circ 3'$	$13^\circ 47'$	$38^\circ 15'$	0.09	"
1.000	1.450	$27^\circ 45'$	$34^\circ 29'$	$9^\circ 48'$	$32^\circ 36'$	0.08	"
			STATOR				
.600	.966	$38^\circ 3'$	$61^\circ 46'$	$31^\circ 53'$	$54^\circ 0'$	.10	0°
.700	1.031	$42^\circ 24'$	$65^\circ 17'$	$31^\circ 6'$	$57^\circ 57'$	.10	"
.800	1.088	$46^\circ 13'$	$68^\circ 4'$	$29^\circ 59'$	$61^\circ 12'$	.10	"
.900	1.136	$49^\circ 34'$	$70^\circ 18'$	$28^\circ 41'$	$63^\circ 55'$	.10	"
1.000	1.179	$52^\circ 31'$	$72^\circ 8'$	$27^\circ 20'$	$66^\circ 11'$	.10	"
			GUIDE VANES				
.600	.746	90°	$61^\circ 28'$	$36^\circ 48'$	$105^\circ 00'$	.08	0°
.700	.874	"	$64^\circ 16'$	$34^\circ 00'$	$102^\circ 54'$	"	"
.800	.999	"	$66^\circ 18'$	$32^\circ 03'$	$101^\circ 24'$	"	"
.900	1.124	"	$68^\circ 46'$	$29^\circ 18'$	$100^\circ 12'$	"	"
1.000	1.248	"	$71^\circ 21'$	$26^\circ 18'$	$99^\circ 6'$	"	"

DEFINITIONS FOR TABLE I

ξ	Radius Ratio	θ	Camber Angle
s/c	$\frac{\text{Blade Spacing}}{\text{Chord}}$	γ'	Blade Stagger Angle
γ_1	Air Inlet Angle	t_m	Maximum Thickness
γ_2	Air Outlet Angle	i	Incidence Angle

TABLE I (Cont'd)

DESCRIPTION OF ANGLES

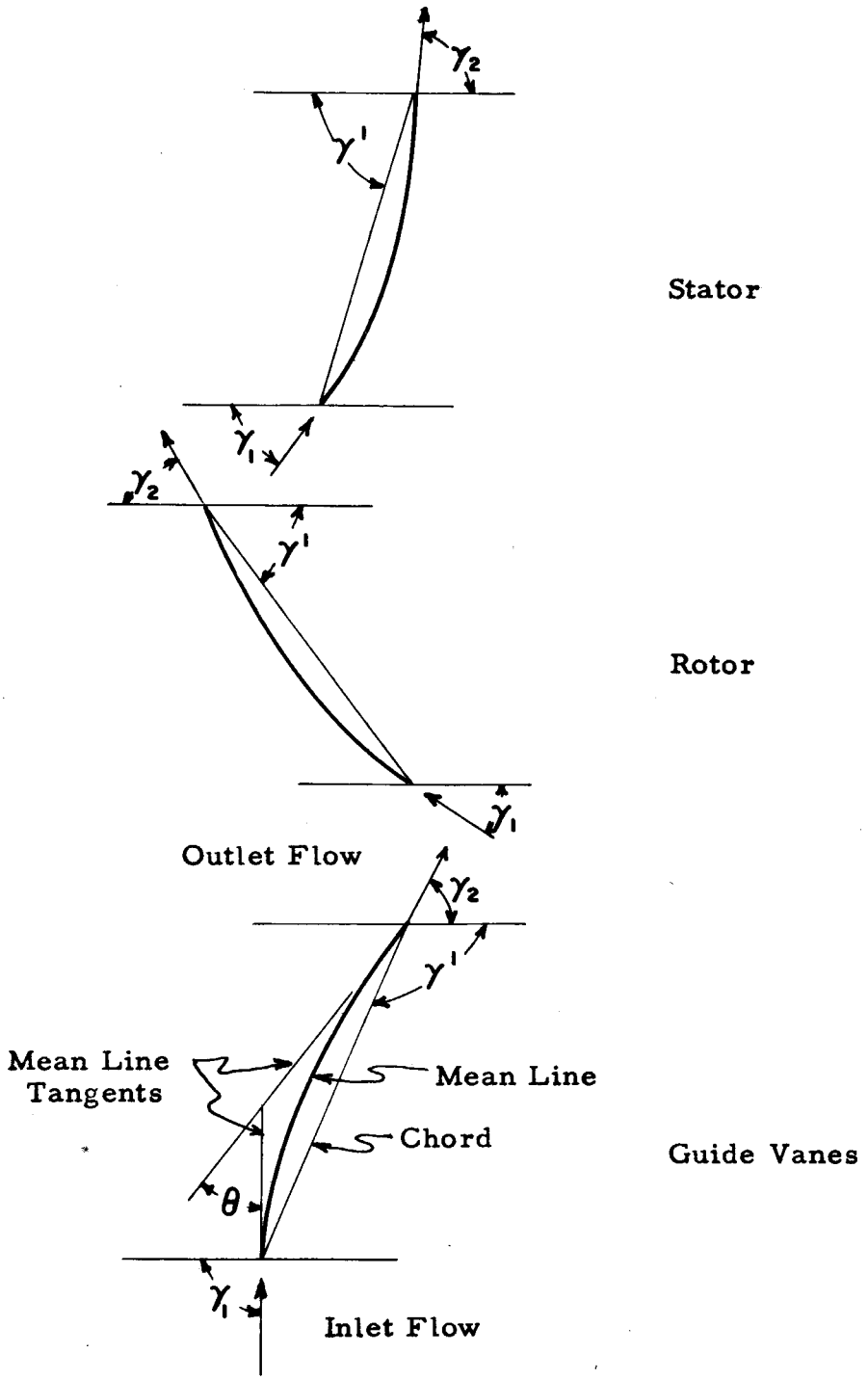

TABLE II

COMPARISON OF FLOW RATE MEASUREMENTS

R_T (Nominal)	ϕ_N	ϕ_{RE}	ϕ_{SD}	ϕ_{RD}	ϕ_{GI}	ϕ_{GD}
2,000	0.285	0.333	0.312 [a] 0.320 [a]	0.308	0.291	0.306
4,000	0.355		0.381 [a] 0.387 [a]	0.384	0.348	
12,500	0.322	0.359	0.356			
21,500	0.327	0.359	0.364			
150,000	0.333 0.388	0.336 0.398	0.361 0.399			

Definitions:

ϕ_N	Nozzle calibration
ϕ_{RE}	Radial survey at rotor exit, Sta. 3
ϕ_{SD}	Radial survey downstream of stator, Sta. 7
$\}^a$	Radial survey downstream of stator, two circumferential positions $\sim\frac{1}{2}$ pitch apart
ϕ_{GI}	Radial survey upstream of guide vanes
ϕ_{GD}	Radial surveys at 5 circumferential stations downstream of guide vanes

TABLE III

APPROXIMATE LOCATIONS FOR FLUID INJECTION

Figure	Injection Location
48a(1)	At hub near pressure surface; 50% chord
48a(2)	At hub near pressure surface; 50% chord
48b(1)	Upstream of leading edge and on pressure surface side of blade; 1/3 blade span measured from case
48b(2)	Against suction surface; 5% chord; mid blade height
48b(3)	1/4" from case; 1/4" from suction surface; 30% chord
48b(4)	3/8" from case; 1/4" from suction surface; 50% chord
48b(5)	Trailing edge; 1/8" from case; 1/8" from suction surface
48c(1)	Against suction surface; 4/10 of blade height measured from case; 60% chord
48c(2)	Same as 48c(1)
48c(3)	Against suction surface; 3/8" from hub; 20% chord
48c(4)	Against suction surface; 1" from hub; 20% chord
48d(1)	Against hub; 1/8" from suction surface; 60% chord
48d(2)	Against hub; 1/32" from suction surface; 15% chord
48d(3)	Same as 48d(2)
48d(4)	At leading edge; $\frac{1}{2}$" from hub
48d(5)	Against hub; $\frac{1}{2}$" upstream of leading edge on suction surface side of blade passage
48d(6)	Same as 48d(5)
48d(7)	Same as 48d(5)
48e(1)	Against hub; near pressure surface; 60% chord

TABLE III Cont'd.

Figure	Injection Location
48e(2)	.02" from hub; 60%o chord
48e(3)	.06" from hub; 60%o chord
48e(4)	1/4" from hub; mid pitch region; 50%o chord
48e(5)	$\frac{1}{2}$" from hub; $\frac{1}{2}$" from suction surface; passage inlet
48e(6)	Mid blade span; 3/4" from suction surface; 30%o chord

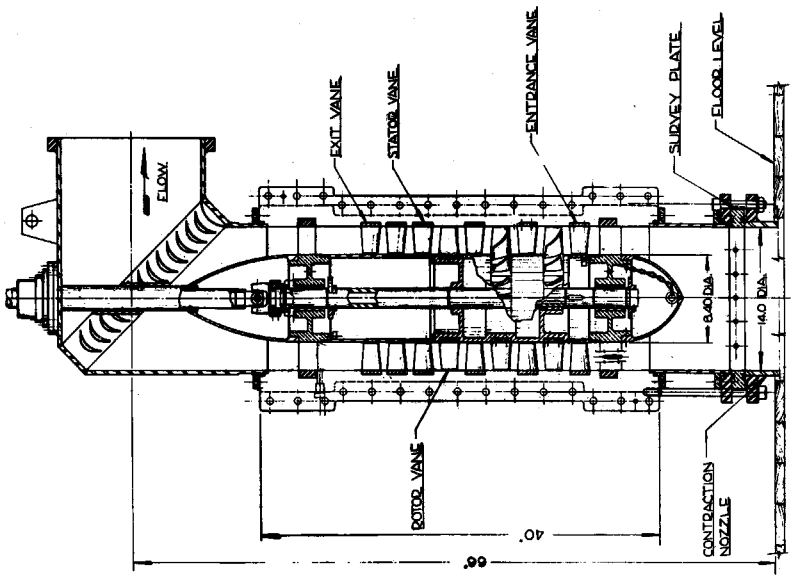

FIG. 2. ASSEMBLY OF TEST UNIT (3 STAGES SHOWN; ONLY ONE STAGE WAS USED.)

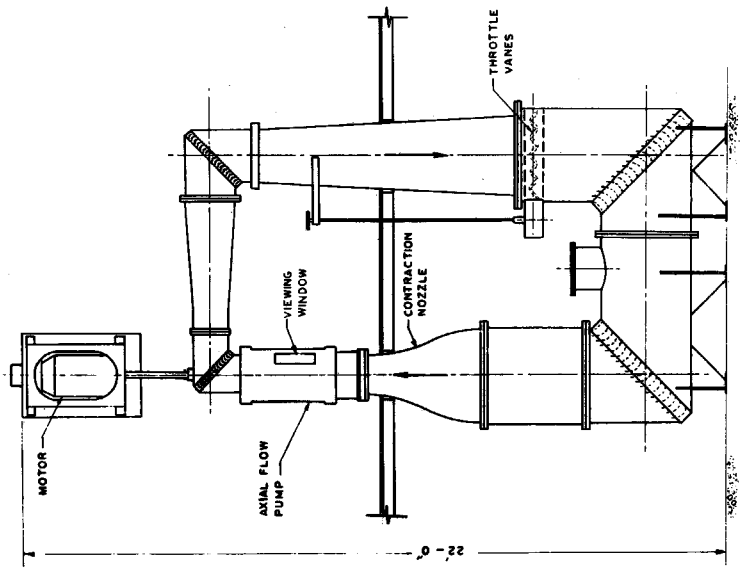

FIG. 1. SCHEMATIC DIAGRAM OF PUMPING CIRCUIT AND INSTALLATION

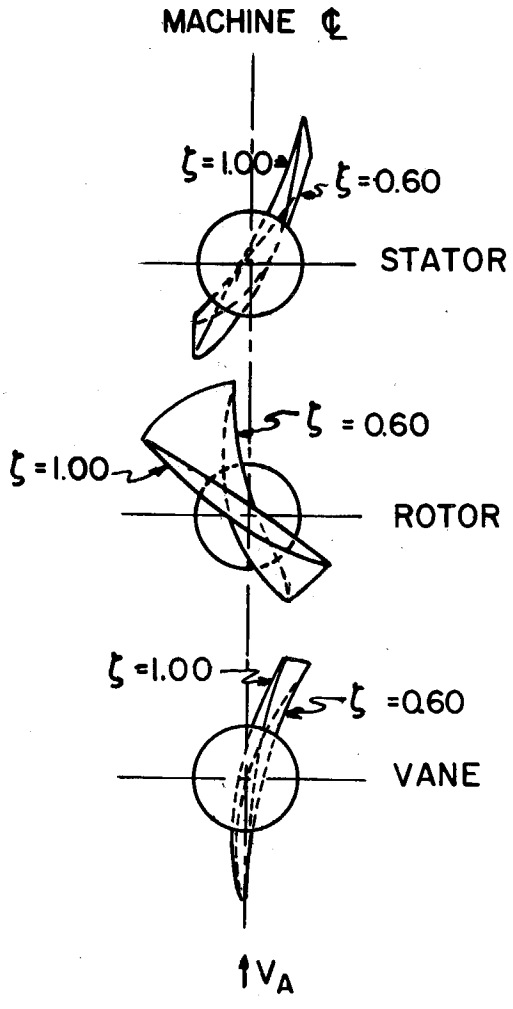

FREE VORTEX BLADING

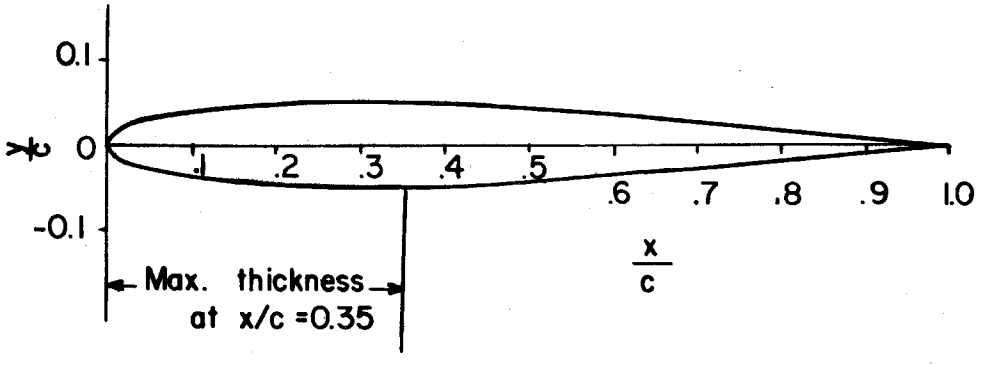

BASIC PROFILE THICKNESS DISTRIBUTION

FIG. 3. FREE VORTEX BLADING GEOMETRY

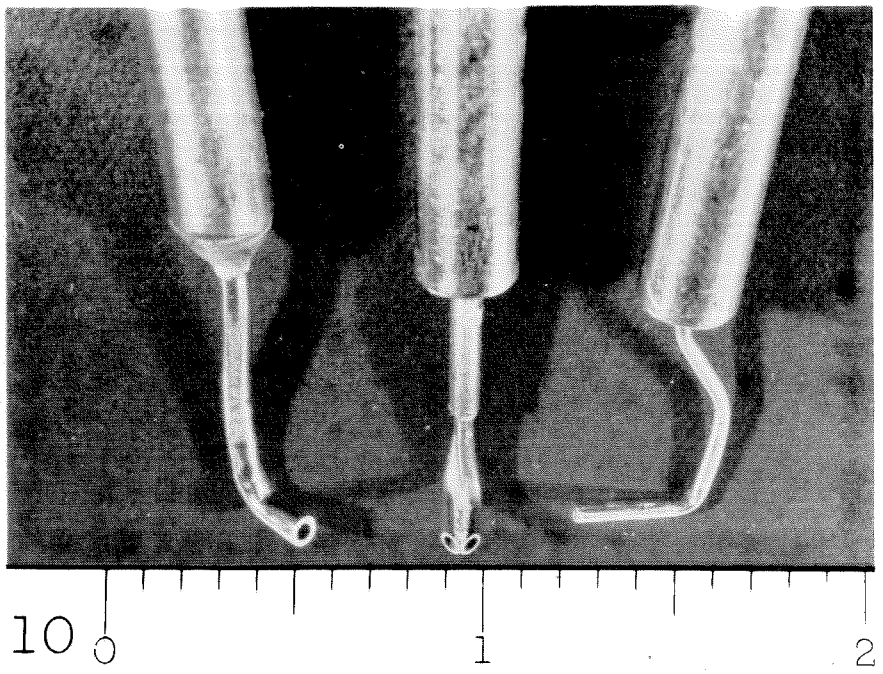

FIG. 4. FLOW MEASURING INSTRUMENTS

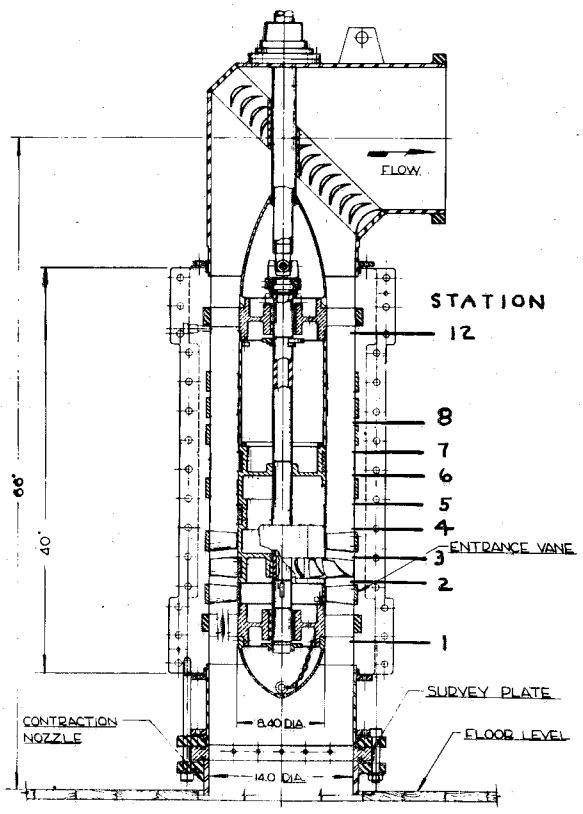

FIG. 5. MEASURING STATIONS AND STATIC PRESSURE LOCATIONS ALONG CASING; BLADES SHOWN ARE IN CS CONFIGURATION

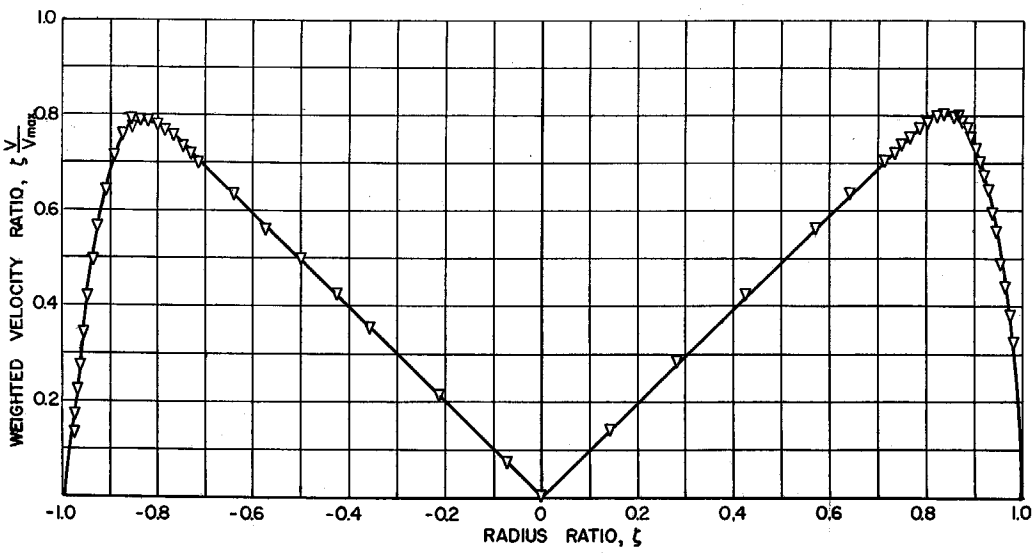

FIG. 6. VELOCITY DISTRIBUTION AT NOZZLE DISCHARGE; R_p = 2685

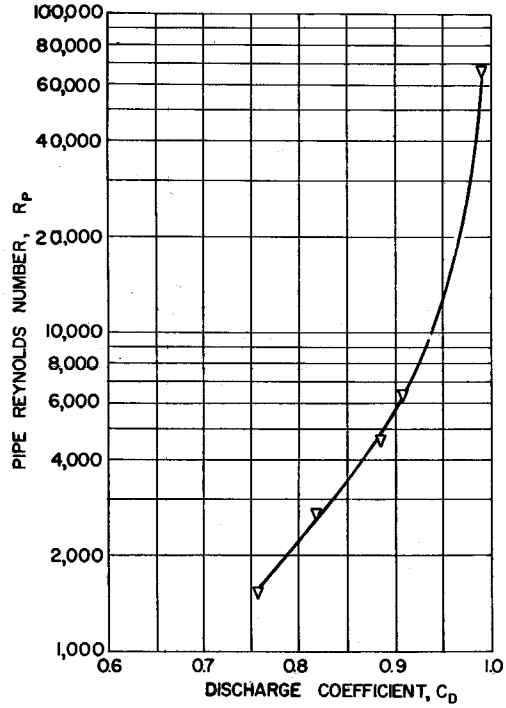

FIG. 7. NOZZLE DISCHARGE COEFFICIENT VARIATION WITH PIPE REYNOLDS NUMBER

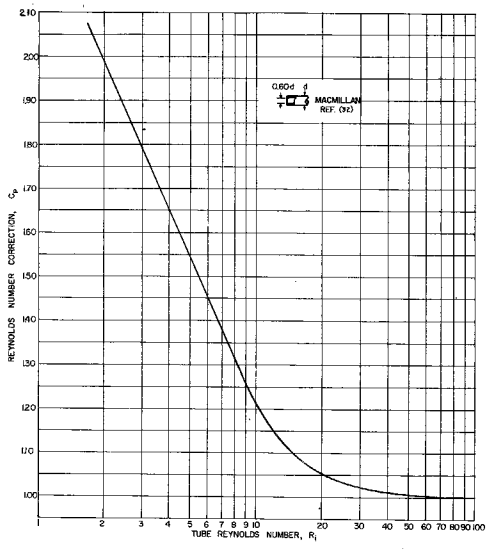

FIG. 8. TOTAL PRESSURE TUBE REYNOLDS NUMBER CORRECTION

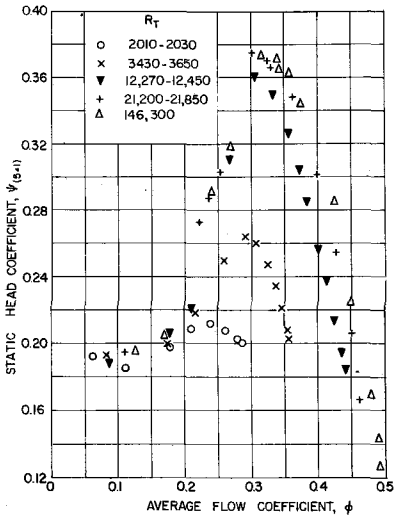

FIG. 9. HEAD COEFFICIENT VARIATION WITH AVERAGE FLOW COEFFICIENT; CS; R_T = 2000-146,000

a. $\psi_{(5-1)}$

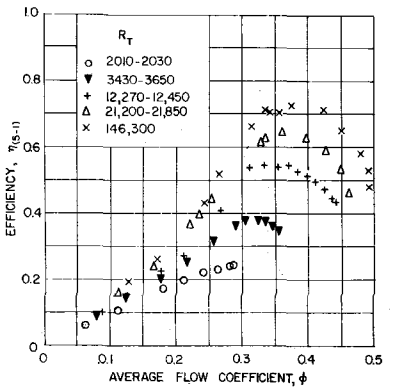

FIG. 10. EFFICIENCY VARIATION WITH AVERAGE FLOW COEFFICIENT; CS; R_T = 2000-146,000

a. $\eta_{(5-1)}$

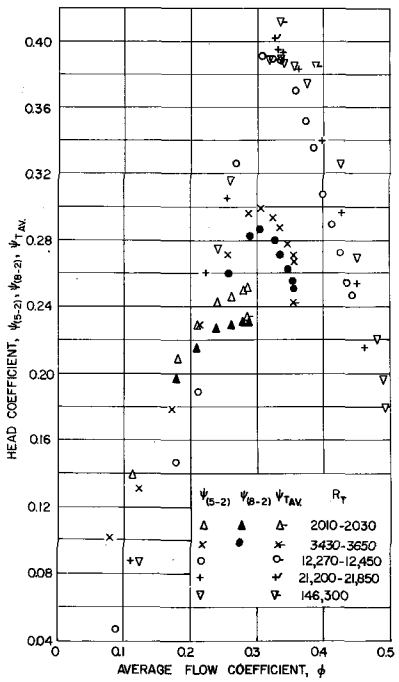

FIG. 9. (CONT'D)

b. $\psi_{(5-2)}$, $\psi_{(8-2)}$, $\psi_{T_{av.}}$

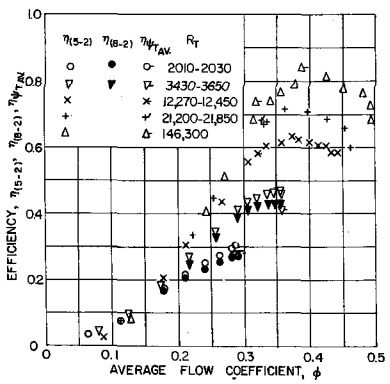

FIG. 10 (CONT'D)

b. $\eta_{(5-2)}$, $\eta_{(8-2)}$, $\eta_{\psi_{T_{av.}}}$

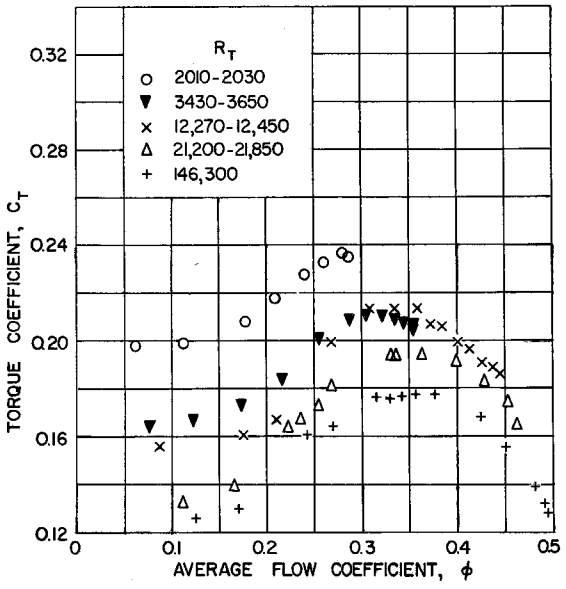

FIG. 11. TORQUE COEFFICIENT VARIATION WITH AVERAGE FLOW COEFFICIENT; CS; R_T = 2000-146,000

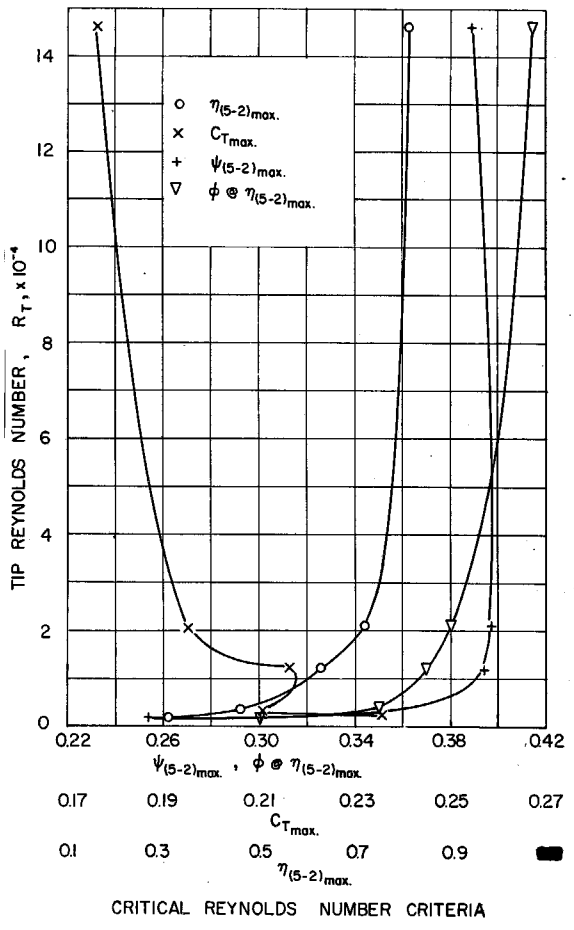

FIG. 12. CRITICAL REYNOLDS NUMBER CRITERIA; CS

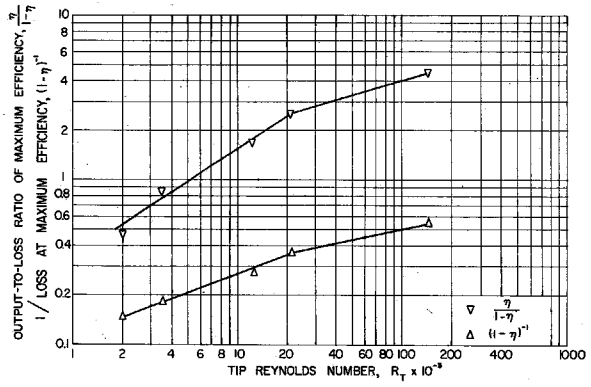

FIG. 13. VARIATION OF LOSS AND OUTPUT-TO-LOSS RATIO AT MAXIMUM EFFICIENCY, WITH REYNOLDS NUMBER; CS

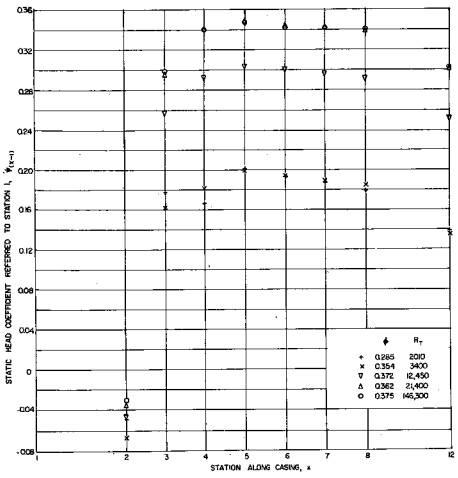

a. ϕ Corresponding to η_{max}

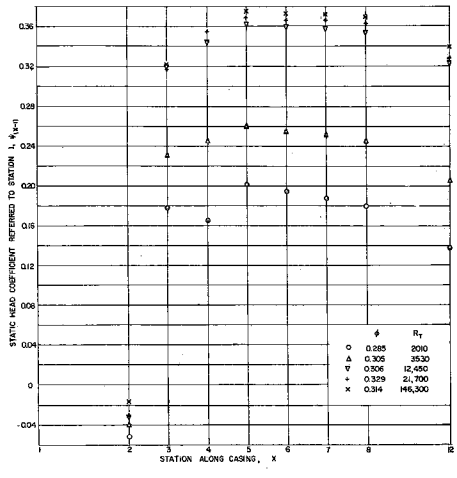

b. ϕ Corresponding to $\psi_{T_{max}}$

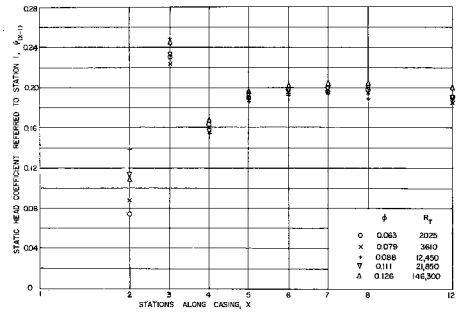

c. Minimum Attainable ϕ

FIG. 14. CASING STATIC PRESSURE VARIATIONS WITH ϕ AND R_T; CS; R_T = 2000-150,000

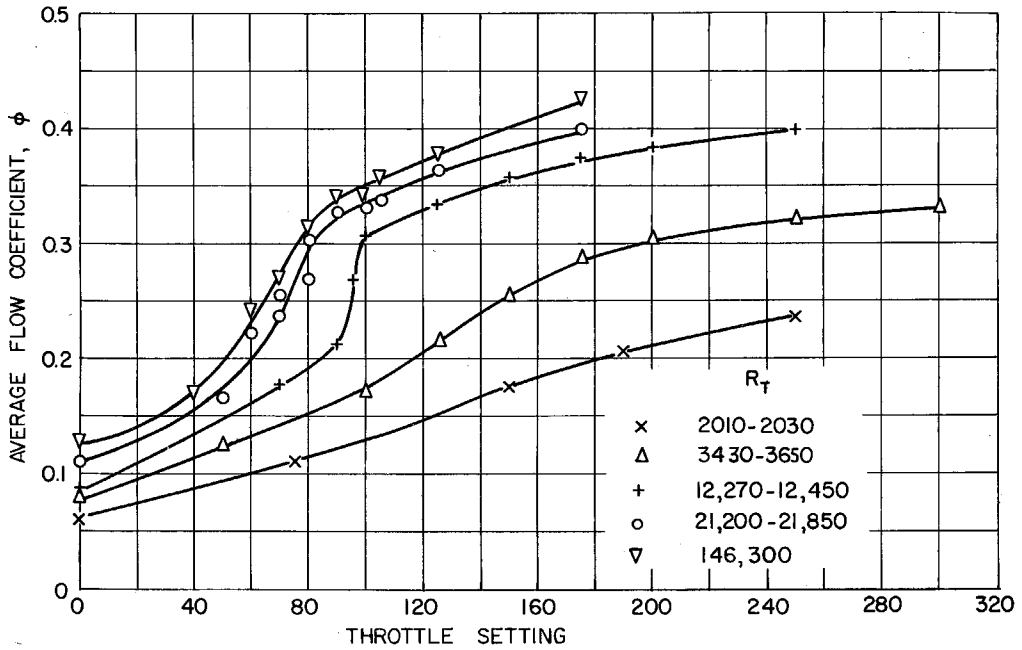

FIG. 15. THROTTLE SETTING DEPENDENCE ON R_T

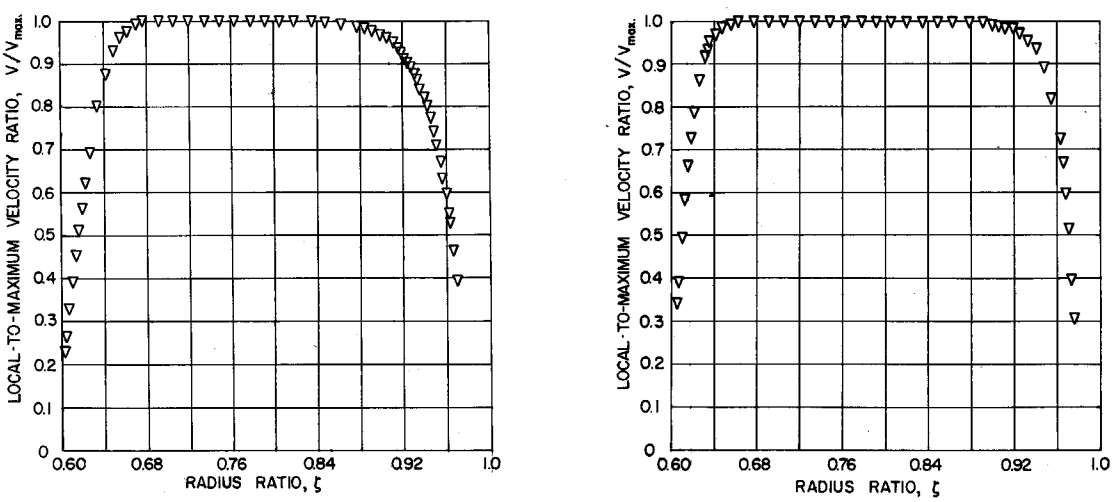

a. $R_{GV} = 630$

b. $R_{GV} = 1380$

FIG. 16. VELOCITY DISTRIBUTION UPSTREAM OF GUIDE VANES

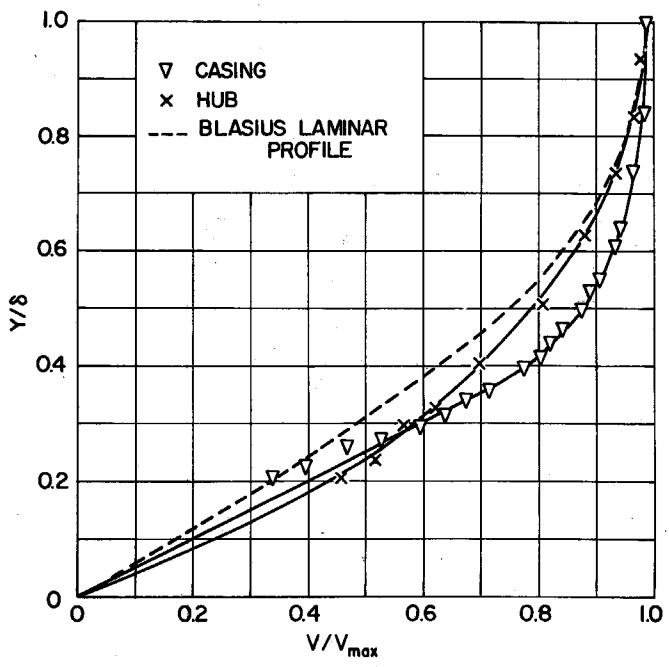

FIG. 16c. CASING AND HUB BOUNDARY LAYER PROFILES; STATION 1; R_{GV} = 630

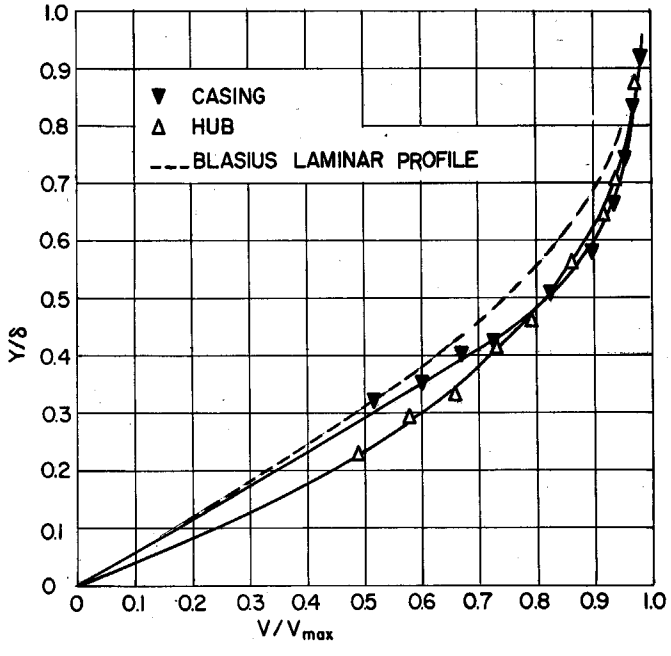

FIG. 16d. CASING AND HUB BOUNDARY LAYER PROFILES; STATION 1; R_{GV} = 1380

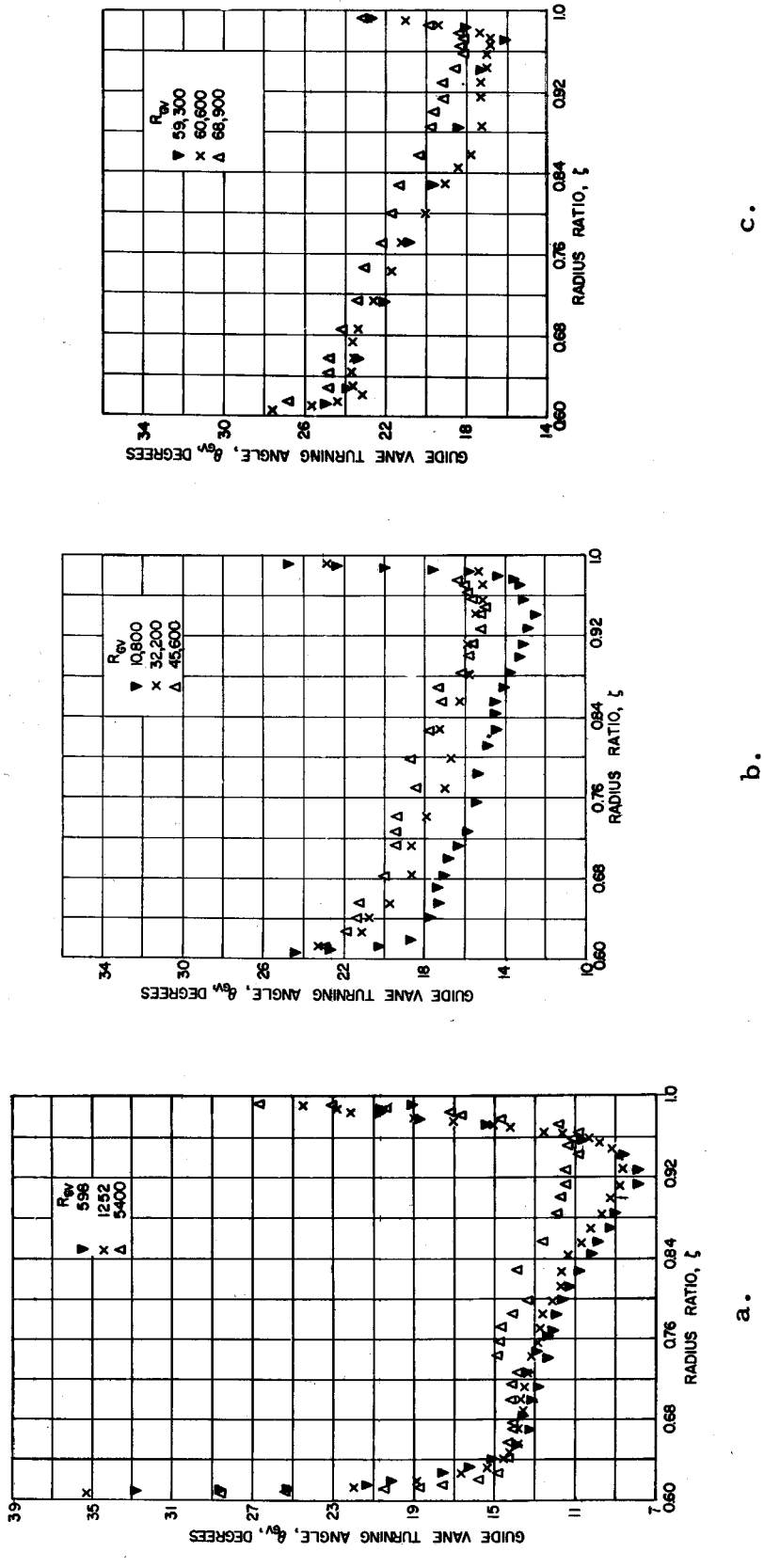

FIG. 17. RADIAL VARIATION OF FLOW ANGLES AT GUIDE VANE EXIT; APPROXIMATELY MID-PITCH REGION; R_{GV} = 600-69,000

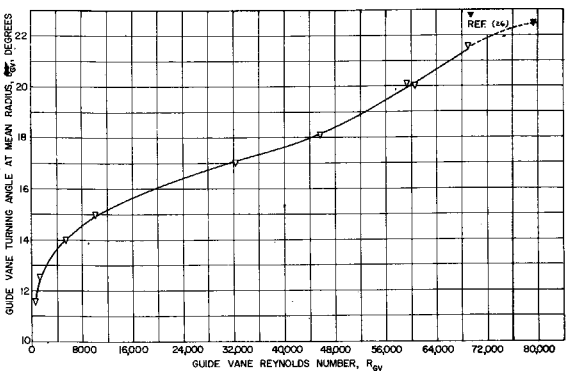

FIG. 18. INFLUENCE OF R_{GV} ON FLOW ANGLE AT MEAN RADIUS; GUIDE VANE EXIT

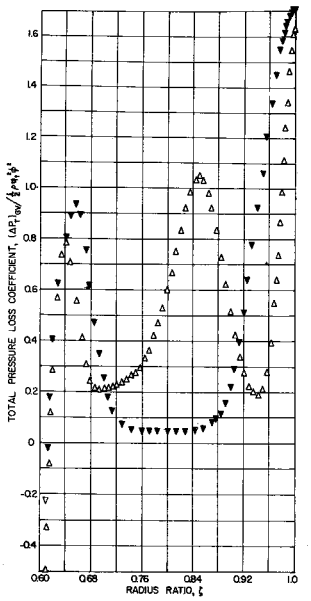

FIG. 19a. RADIAL DISTRIBUTION OF GUIDE VANE TOTAL PRESSURE LOSS UNCORRECTED FOR NOZZLE LOSS; R_{GV} = 600

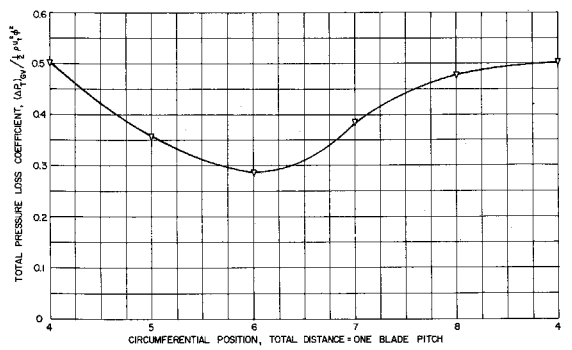

FIG. 19b. CIRCUMFERENTIAL VARIATION OF RADIALLY AVERAGED GUIDE VANE TOTAL PRESSURE LOSS CORRECTED FOR NOZZLE LOSS; R_{GV} = 600

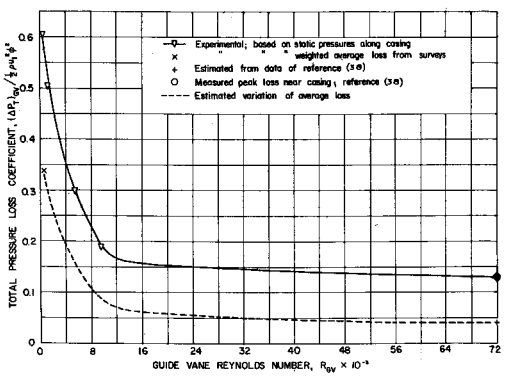

FIG. 19c. GUIDE VANE TOTAL PRESSURE LOSS VARIATION WITH R_{GV}

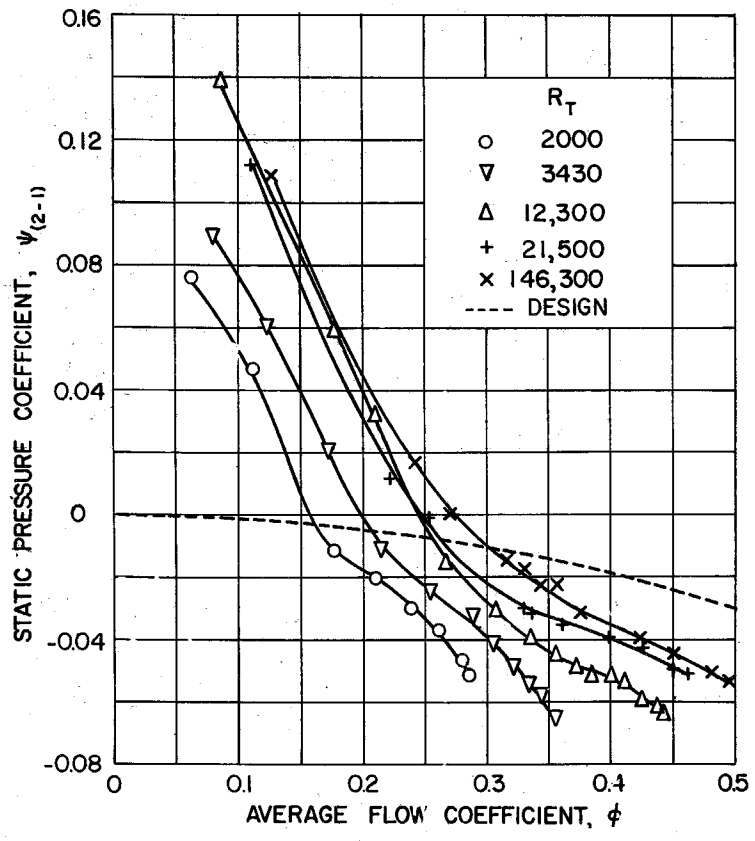

FIG. 20a. CASING STATIC PRESSURE COEFFICIENT CHANGE ACROSS GUIDE VANES AS FUNCTION OF ϕ; CS; R_T = 2000-150, 000

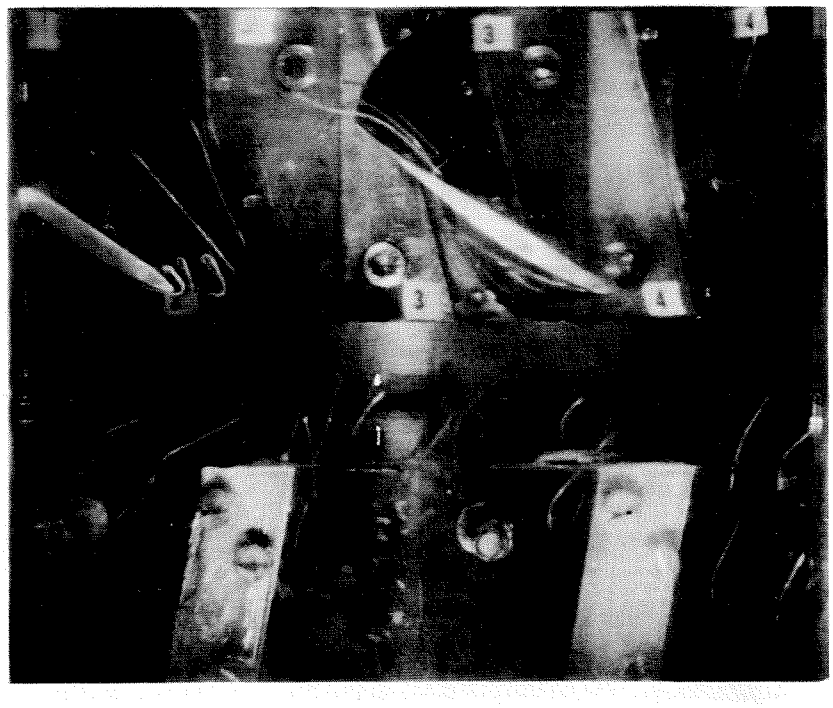

(1) ϕ = 0.26 (No Reversal)

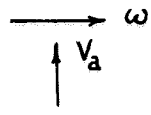

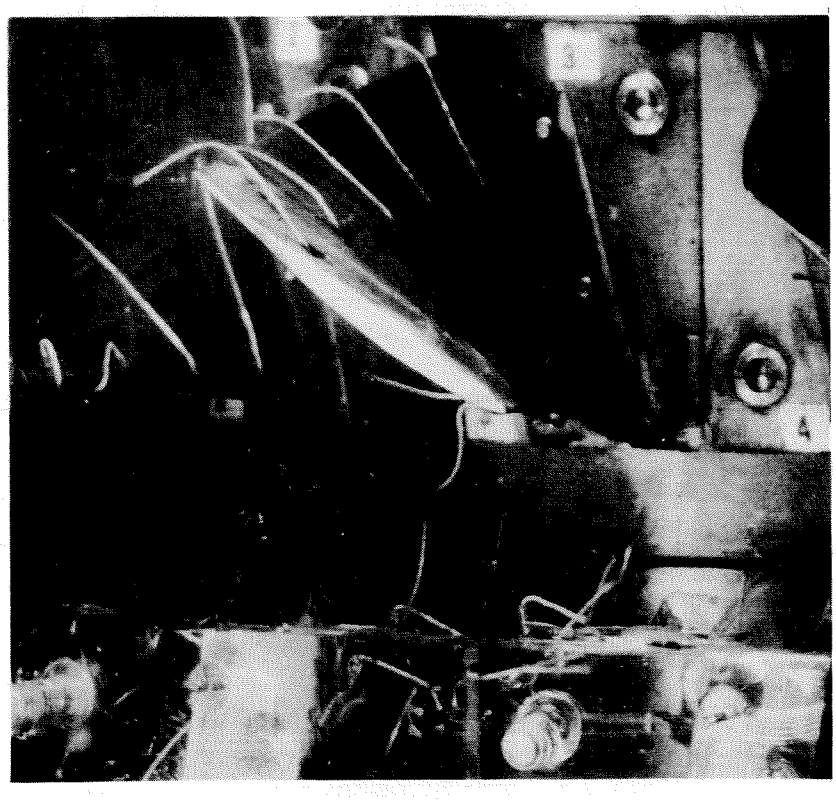

(2) ϕ = 0.15 (Flow Reversed)

FIG. 20b. FLOW REVERSAL FROM ROTOR TO GUIDE VANES ALONG CASING; ES; R_T = 2000

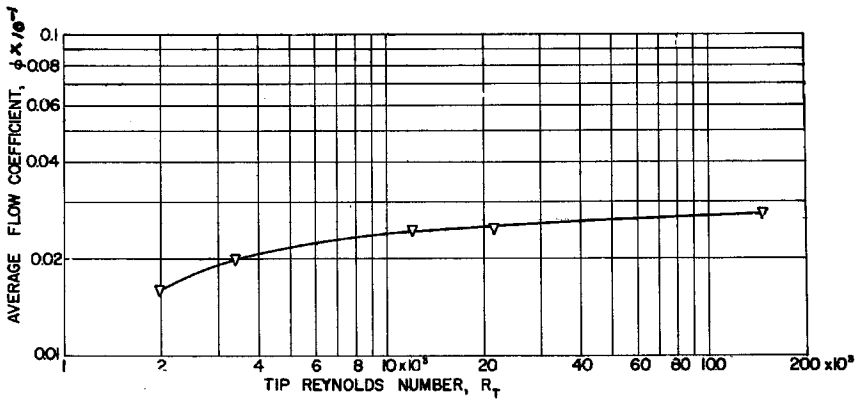

FIG. 20c. AVERAGE FLOW COEFFICIENT FOR ZERO CASING STATIC PRESSURE CHANGE ACROSS GUIDE VANES; CS; R_T = 2000-150,000

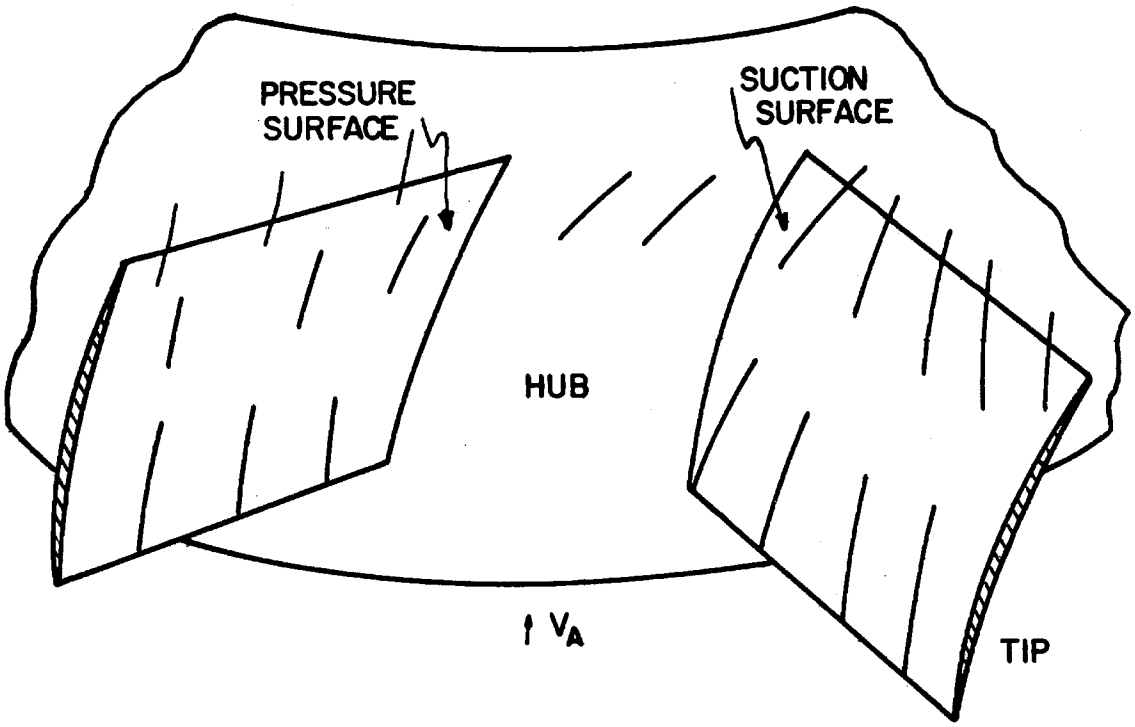

FIG. 21. SKETCH OF GUIDE VANE TUFTS; ES; R_{GV} = 600, ϕ = 0.28

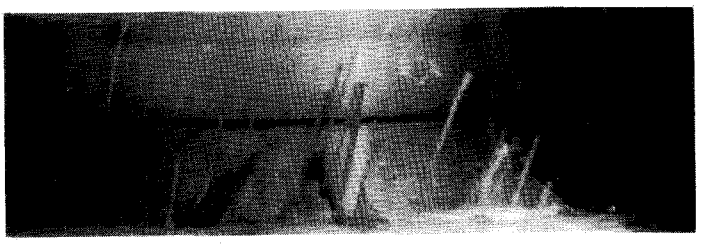

FIG. 22. GUIDE VANE EXIT TUFTS, R_{GV} = 600; ϕ = 0.28

FIG. 23. GUIDE VANE EXIT; TUFTS AT CASING; R_{GV}= 573; ϕ = 0.29

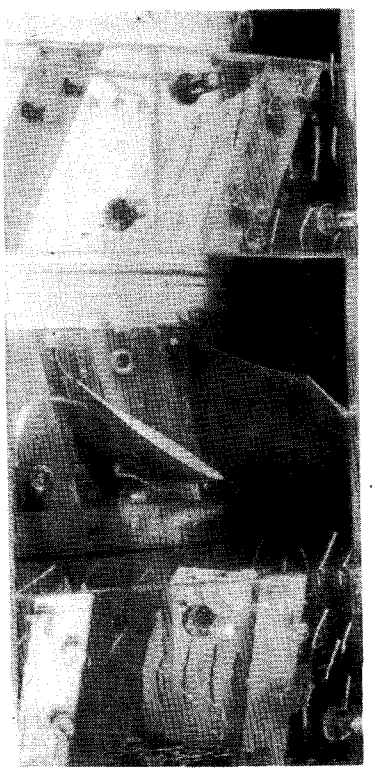

a

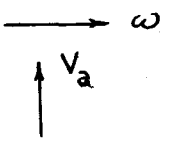

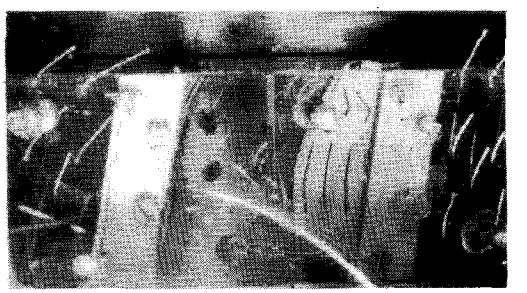

b

FIG. 24. GUIDE VANE SUCTION SURFACE; R_{GV} = 3990; ϕ = 0.323

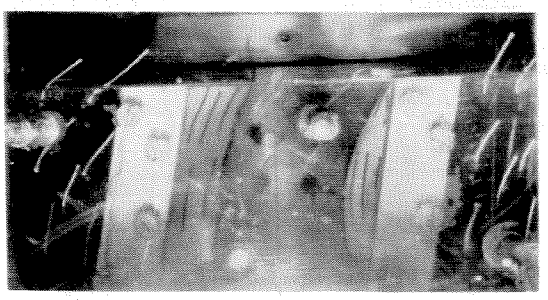

FIG. 25. GUIDE VANE PRESSURE SURFACE; R_{GV} = 3990; ϕ = 0.323

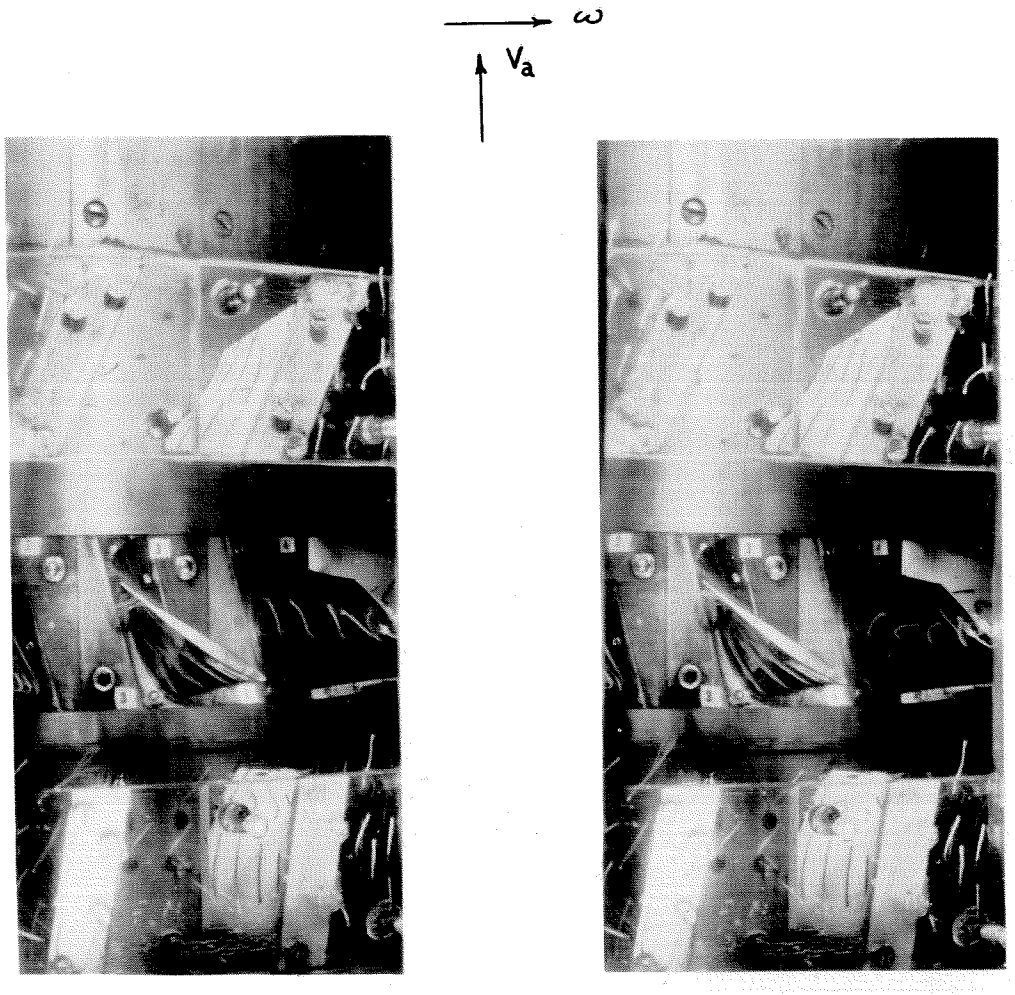

a. R_{GV} = 3990; ϕ = 0.323

b. R_{GV} = 5480; ϕ = 0.443

FIG. 26. GUIDE VANE SUCTION SURFACE; 5/16" DIA. BARRIER ACROSS INLET AT CASING

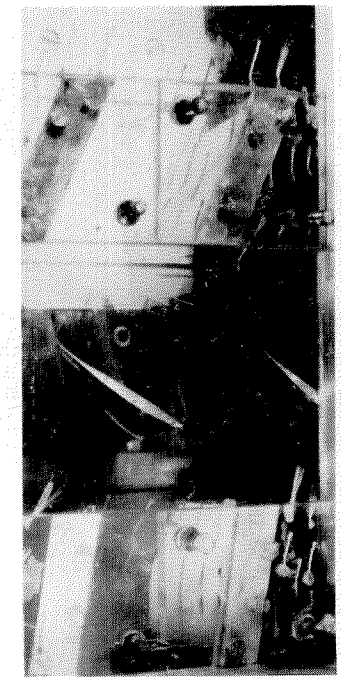

Suction Surface;
R_{GV} 16,000; $\phi \sim 0.45$

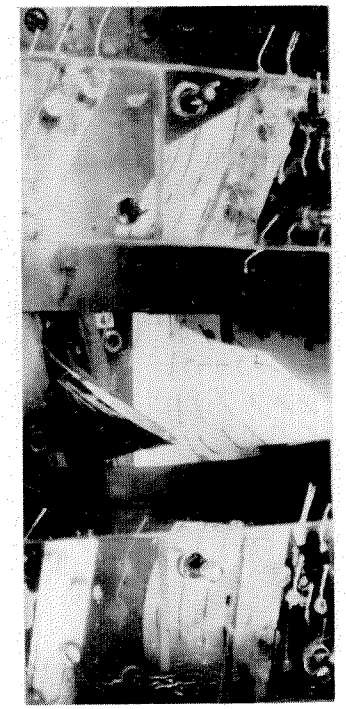

Suction Surface;
R_{GV} = 49,500; ϕ = 0.338

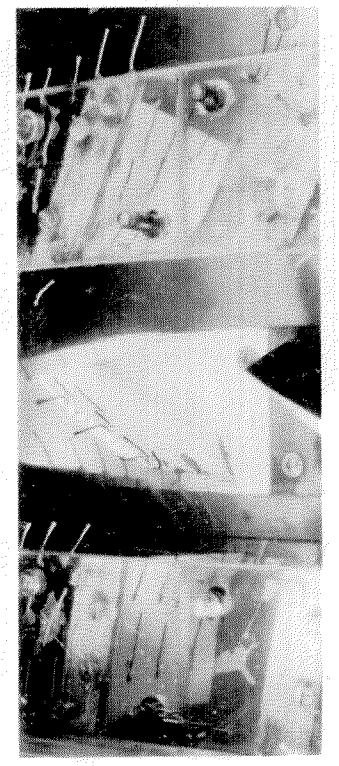

Pressure Surface;
R_{GV} = 55,800; ϕ = 0.381

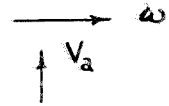

FIG. 27. GUIDE VANE

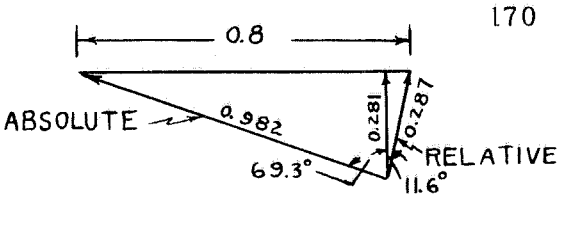

$R_T = 2130$; $\phi = 0.281$

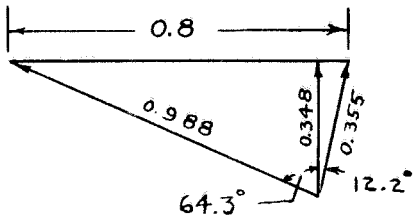

$R_T = 3600$; $\phi = 0.348$

FIG. 28. APPROXIMATE VELOCITY DIAGRAMS AT ROTOR INLET; $\zeta = 0.80$; CS

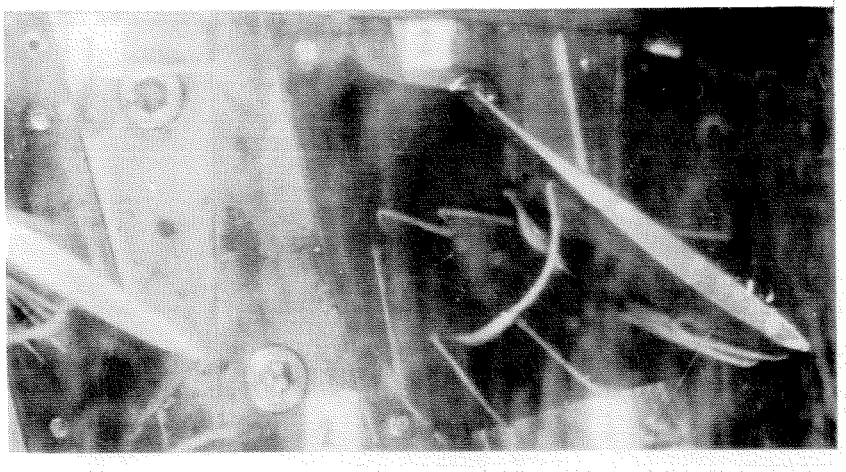

ω

V_a

a. $R_T = 2230$; $\phi = 0.282$

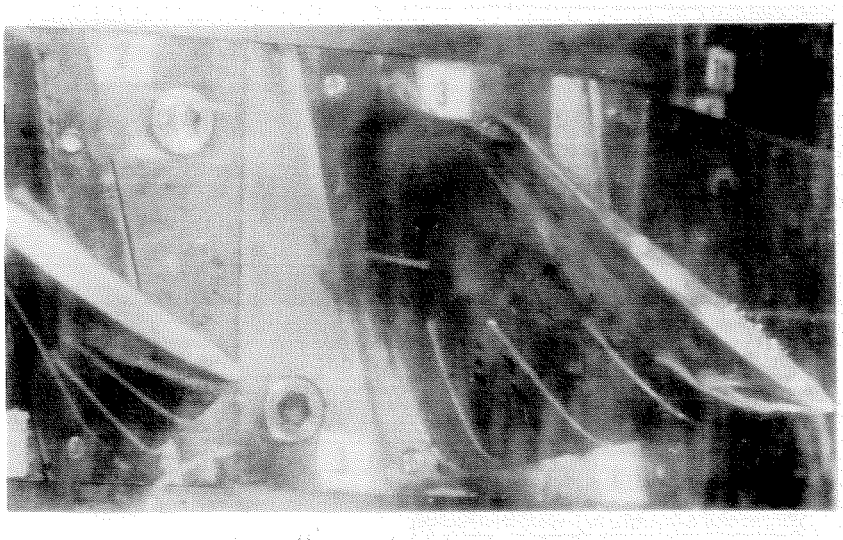

b. $R_T = 2230$; $\phi = 0.282$

FIG. 29. ROTOR LEADING EDGE FLOW; ERS

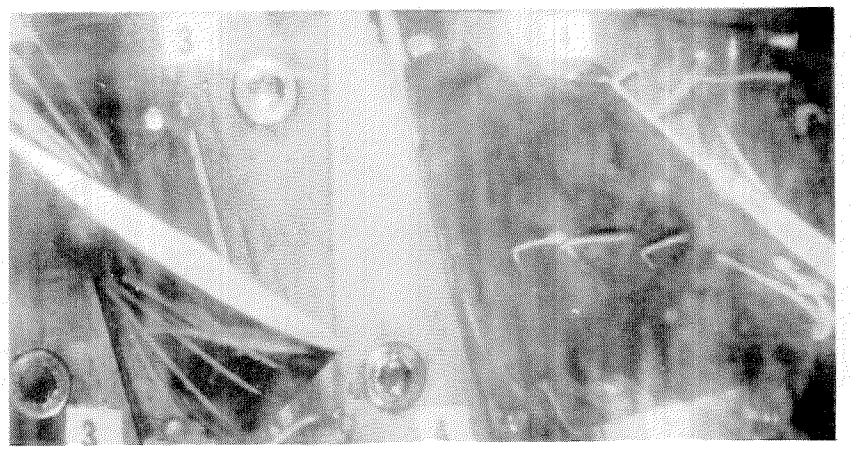

c. R_T = 2230; ϕ = 0.282

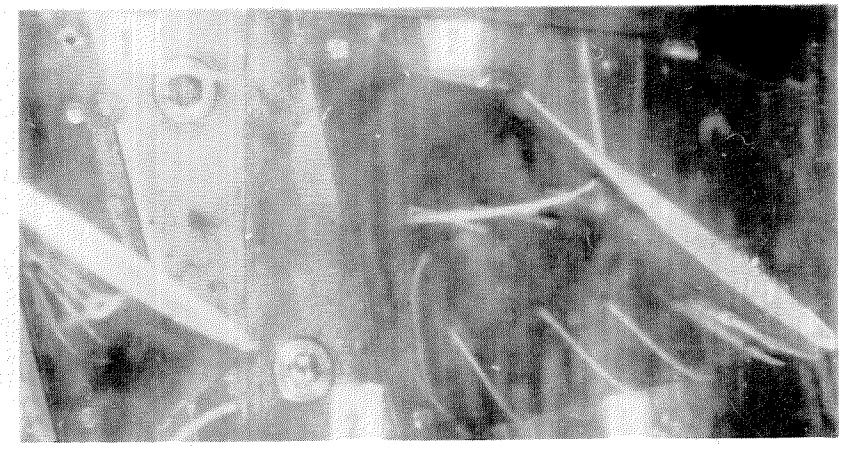

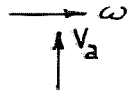

d. R_T = 3890; ϕ = 0.355

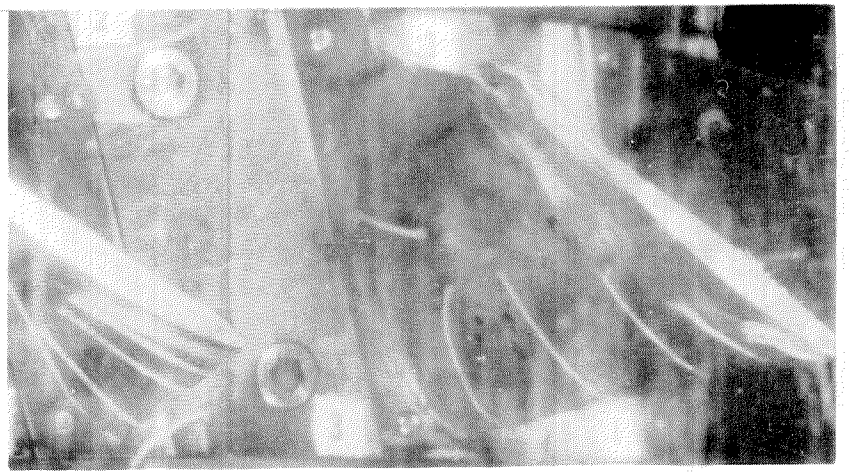

e. R_T = 3890; ϕ = 0.355

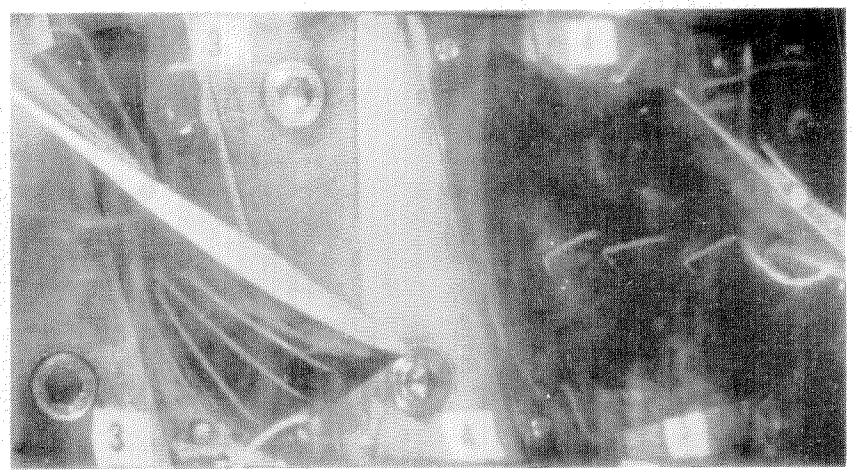

f. R_T = 3890; ϕ = 0.355

FIG. 29 (CONT'D)

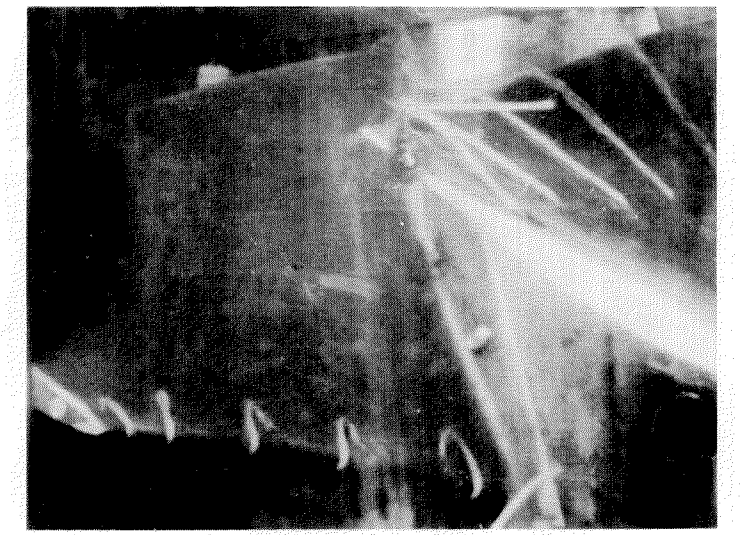

g. $R_T = 3890$; $\phi = 0.355$

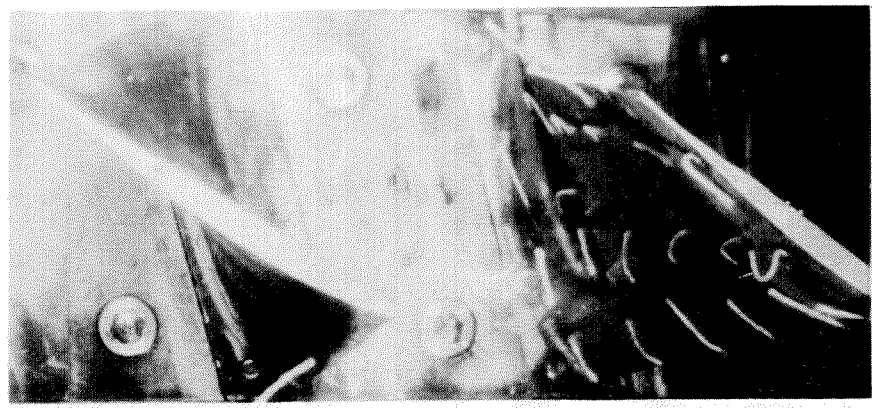

h. $R_T = 2230$; $\phi = 0.282$

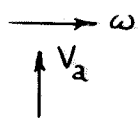

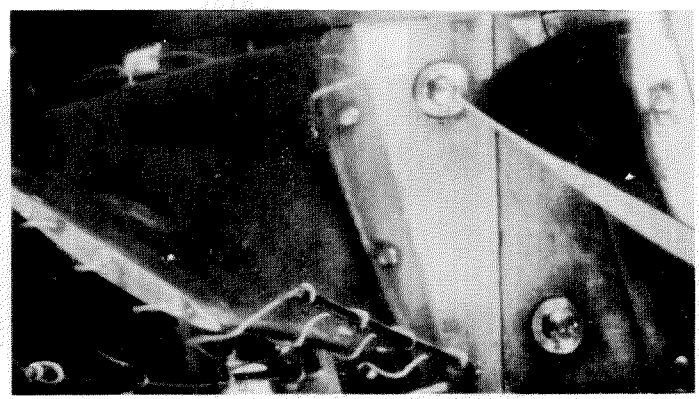

i. $R_T = 2230$; $\phi = 0.282$

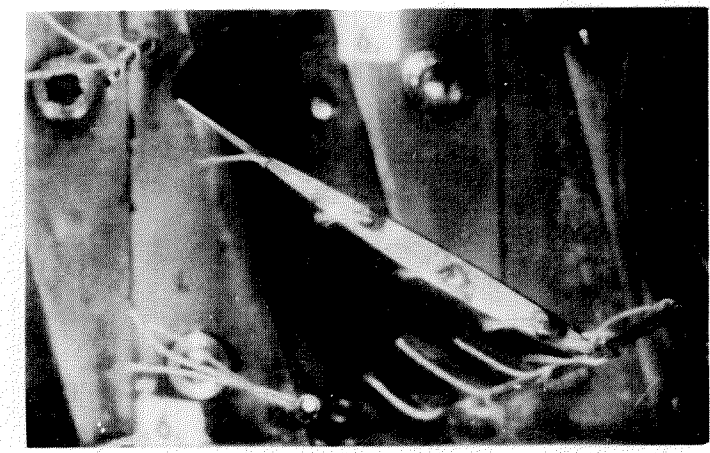

j. $R_T = 2230$; $\phi = 0.282$

FIG. 29 (CONT'D)

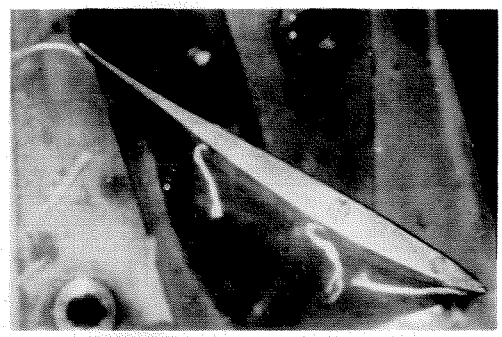

k. Rotor Leading Edge and Tip Region Flow; ERS; $R_T = 2230$; $\phi = 0.282$

FIG. 29 (CONCLUDED)

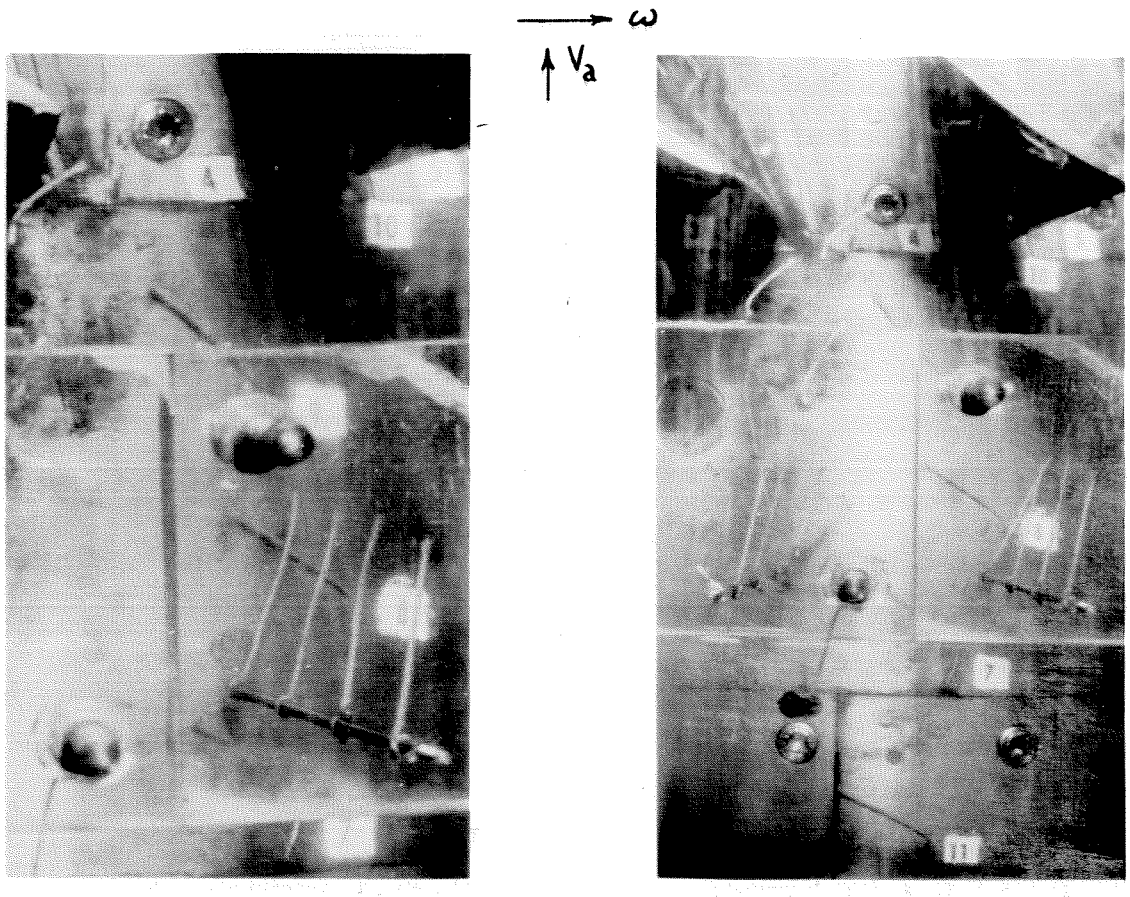

a. Upstream of Rotor; ERS; $R_T = 3890$; $\phi = 0.355$

b. Upstream of Rotor; ERS; $R_T = 2230$; $\phi = 0.282$

FIG. 30. HUB FLOW

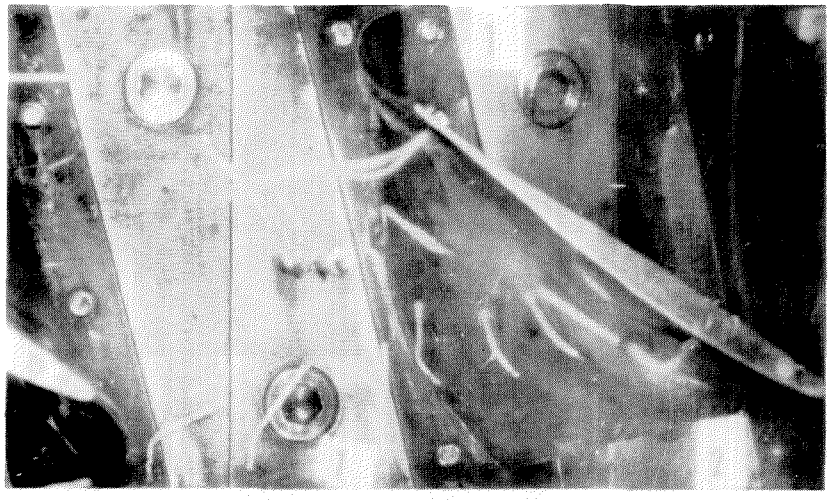

c. Rotor Inlet; ERS; R_T = 2230; ϕ = 0.282

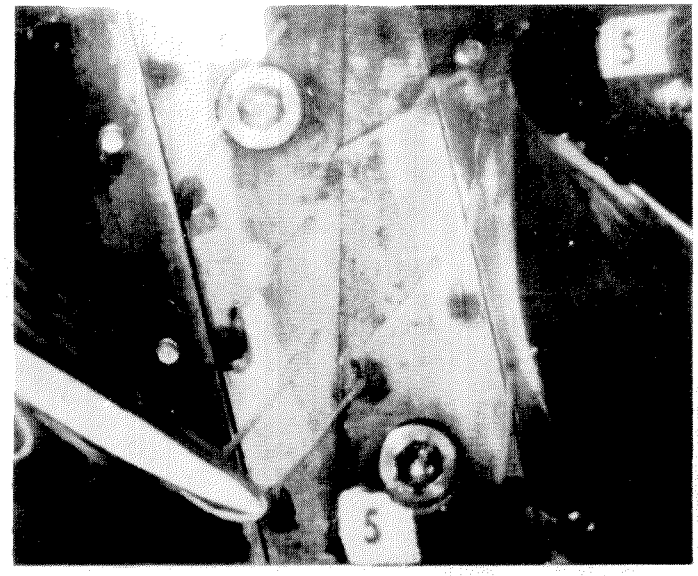

d. Within Rotor Passage; CS; R_T = 2010; ϕ = 0.285

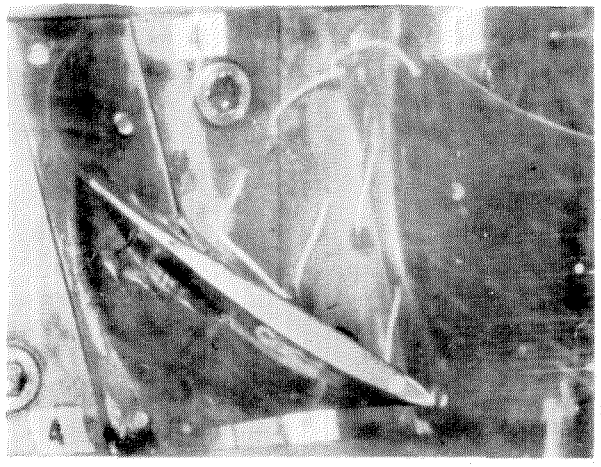

e. Within Rotor Passage; ES; R_T = 2030; ϕ = 0.26

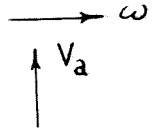

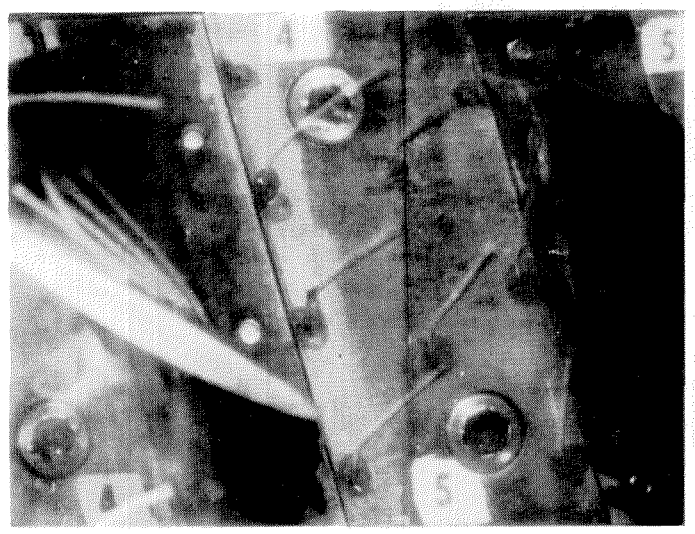

f. Within Rotor Passage; ERS; R_T = 2030; ϕ = 0.282

FIG. 30 (CONT'D)

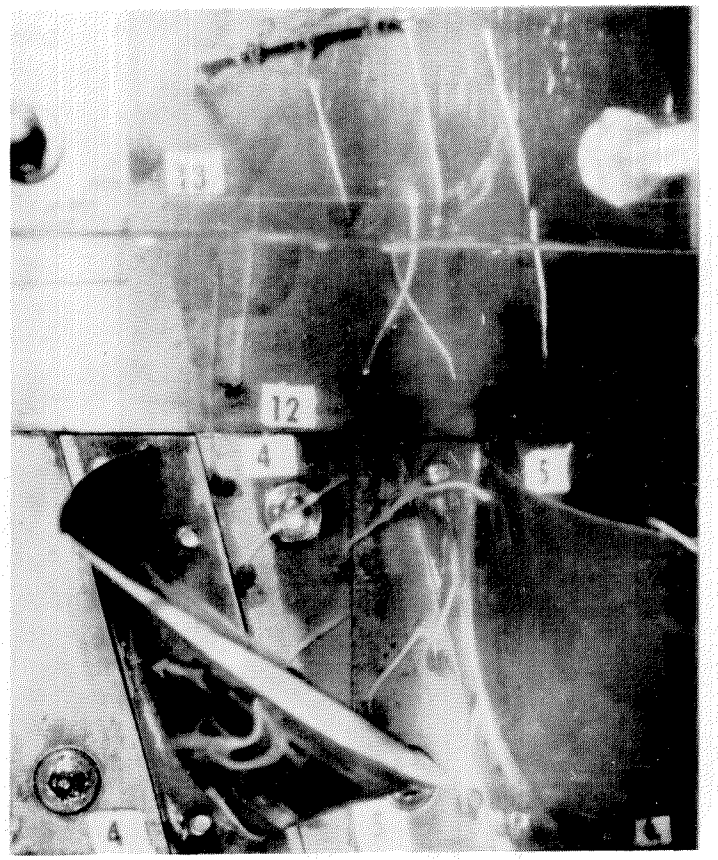

g. Within Rotor Passage and Downstream of Rotor; ERS; R_T = 2280; ϕ = 0.291

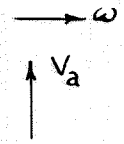

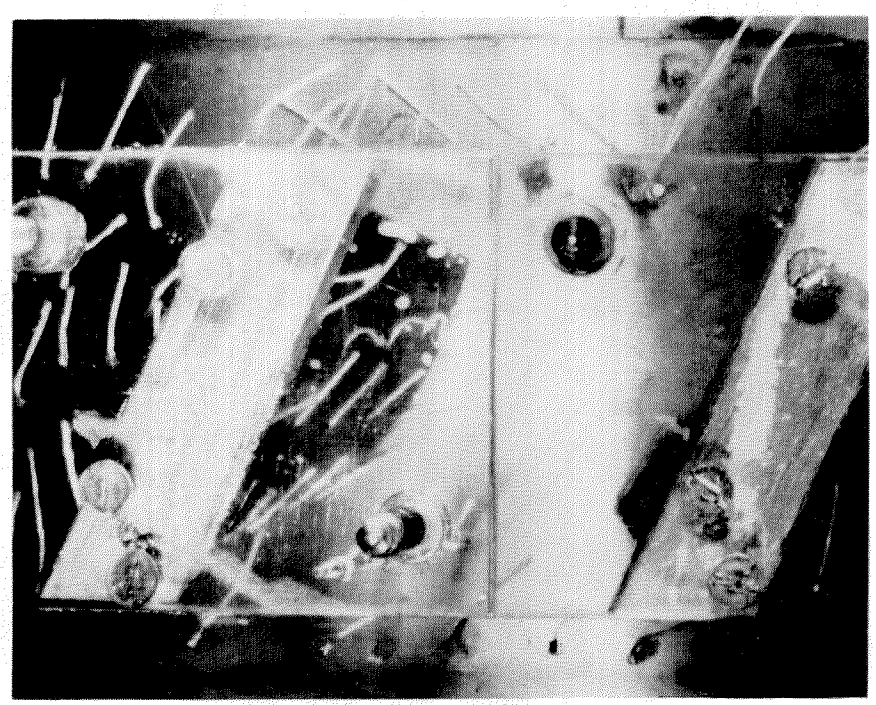

h. Downstream of Rotor (or Stator Inlet; Blades Shown are Stators); CS; R_T = 2010; ϕ = 0.285

FIG. 30 (CONT'D)

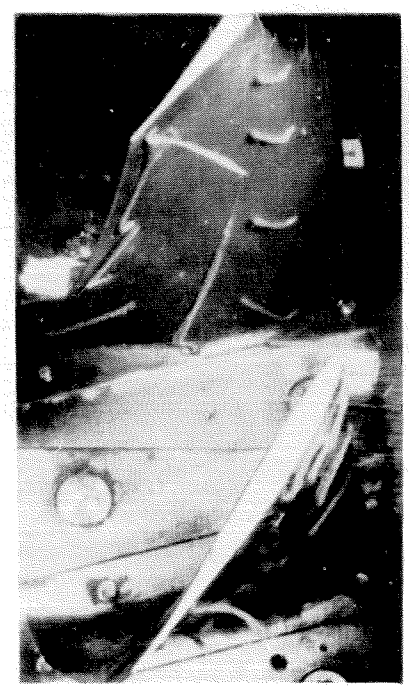

c. CS; R_T = 2010; ϕ = 0.285

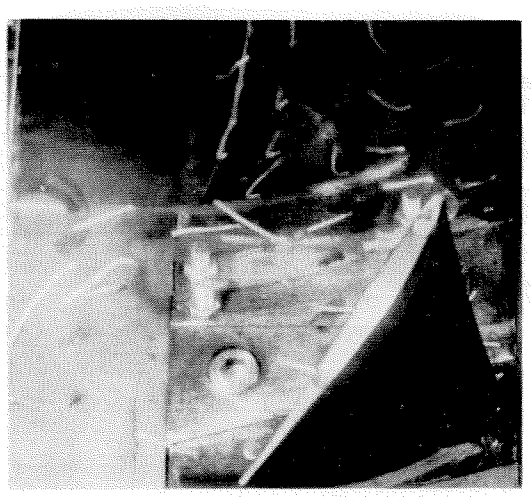

d. Effect of Circumferential Shield; ERS; R_T = 2230; ϕ = 0.282

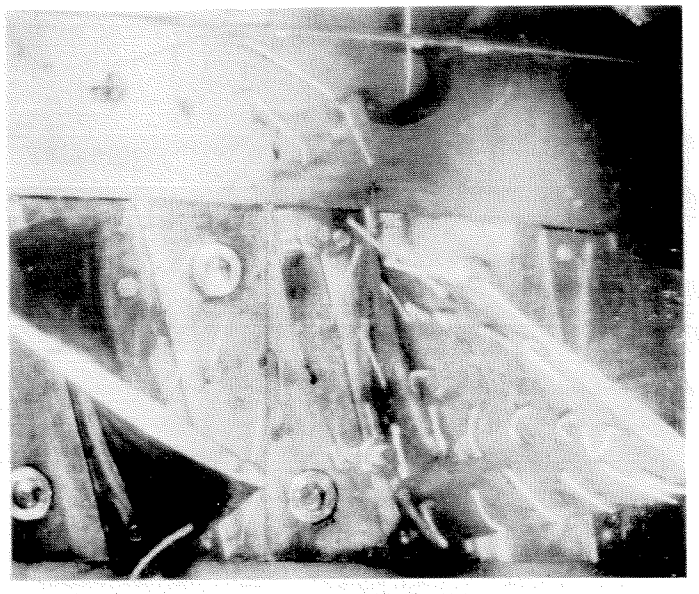

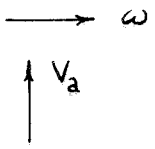

e. Corner and Hub Flow; Effect of Circumferential Shield; ERS; R_T = 2230; ϕ = 0.282

FIG. 31 (CONT'D)

f. Effect of Circumferential Shield; ERS; R_T = 2230; ϕ = 0.282

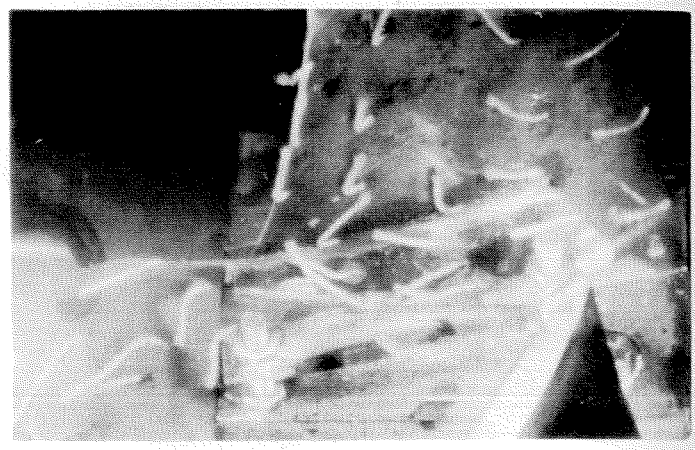

g. Effect of Circumferential Shield; ERS; R_T = 2230; ϕ = 0.282

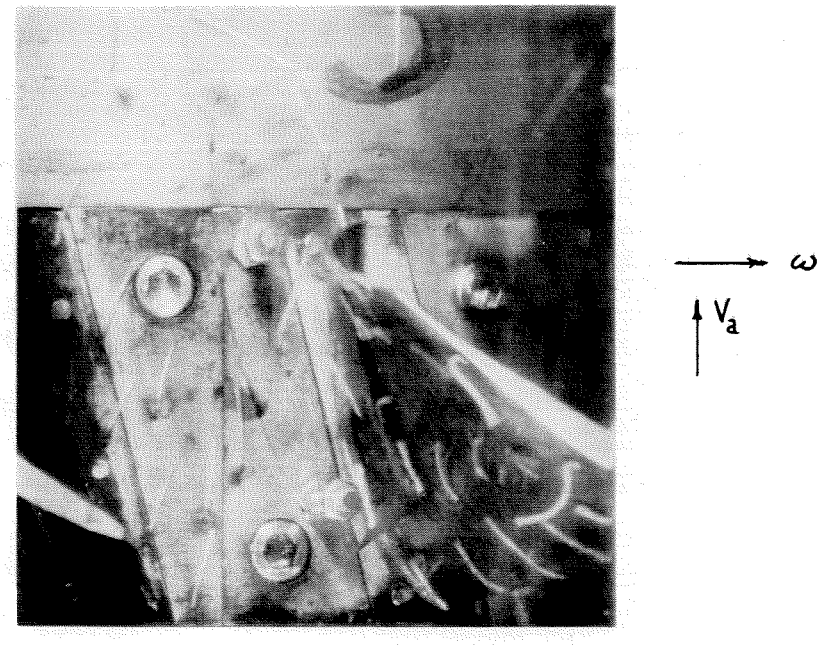

h. Corner and Hub Flow; Effect of Circumferential Shield; ERS; R_T = 2230; ϕ = 0.282

FIG. 31 (CONCLUDED)

a. ERS; R_T = 3890; ϕ = 0.355

b. ERS; R_T = 3890; ϕ = 0.355

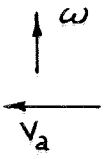

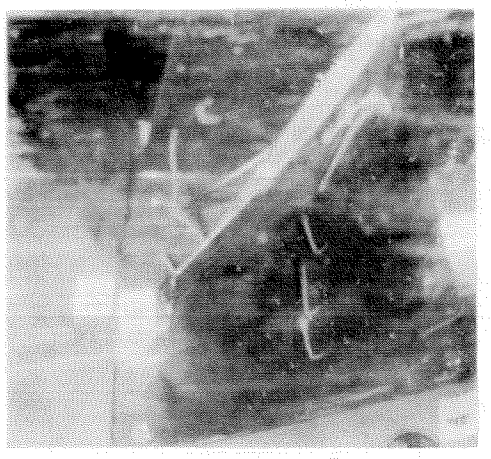

c. ERS; R_T = 2230; ϕ = 0.282

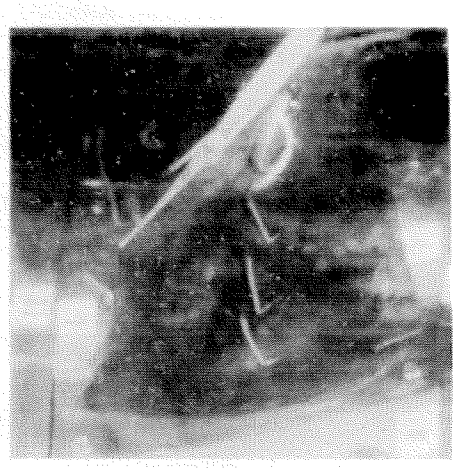

d. ERS; R_T = 3890; ϕ = 0.355

FIG. 32. RADIAL FLOW ALONG ROTOR BLADE SUCTION SURFACE

e. ERS; R_T = 3890; ϕ = 0.355

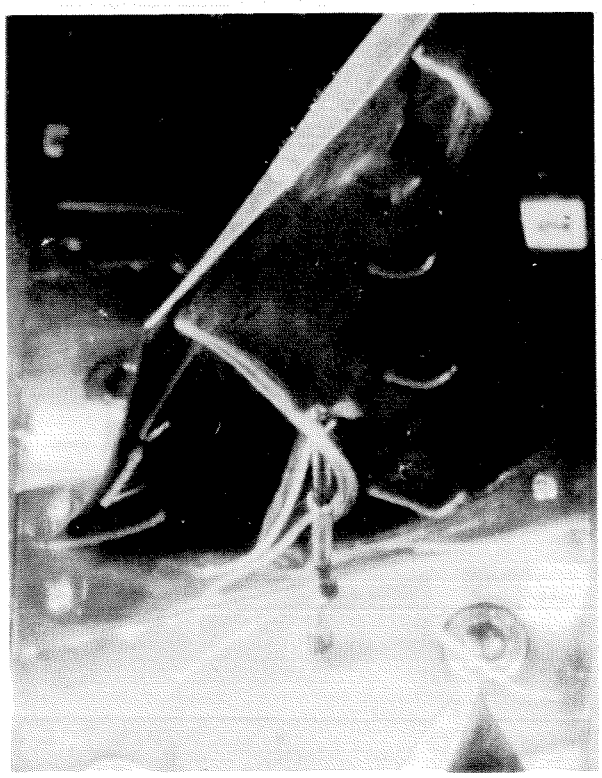

f. ERS; R_T = 2230; ϕ = 0.28

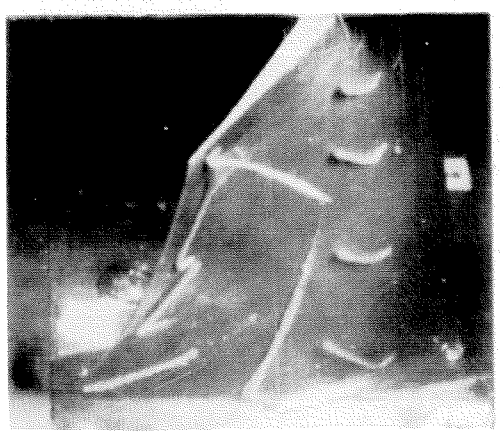

g. CS; R_T = 2045; ϕ = 0.28

FIG. 32. (CONT'D)

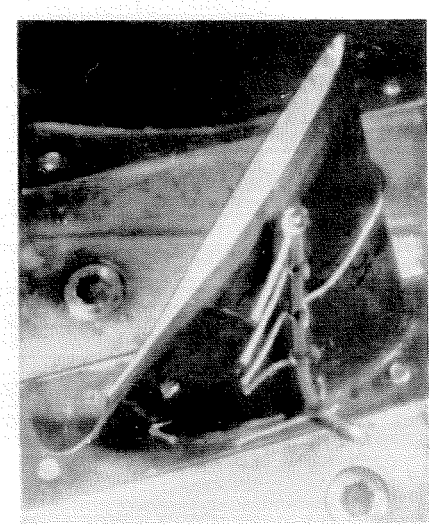

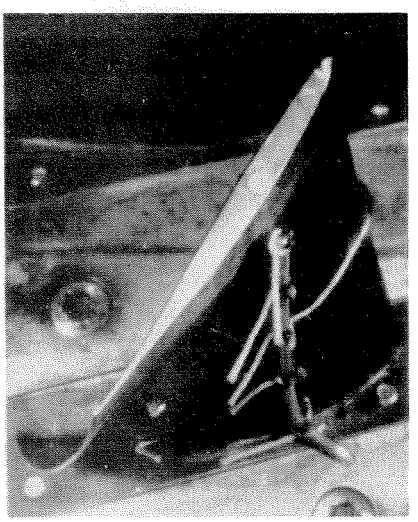

h; i; Separation of Chordwise Moving Fluid From Suction Surface; ERS: $R_T = 2230$; $\phi = 0.28$

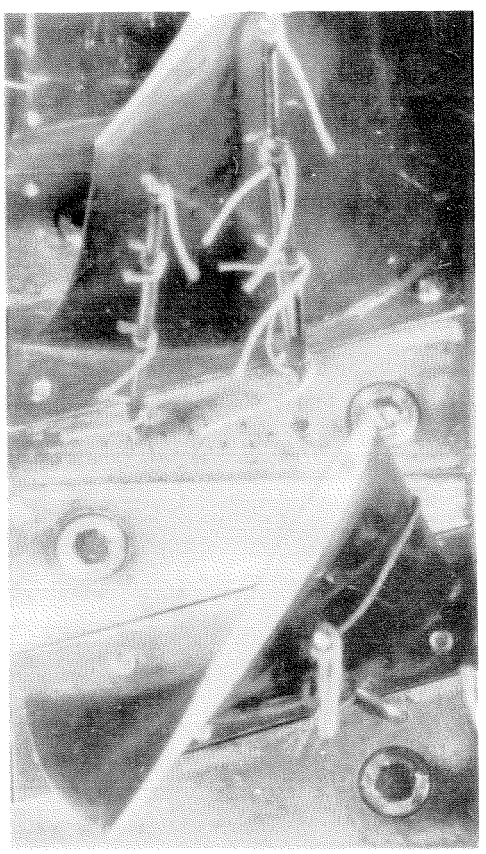

j. Flow Directions Near Suction Surface; ERS; $R_T = 2280$; $\phi = 0.28$

FIG. 32 (CONCLUDED)

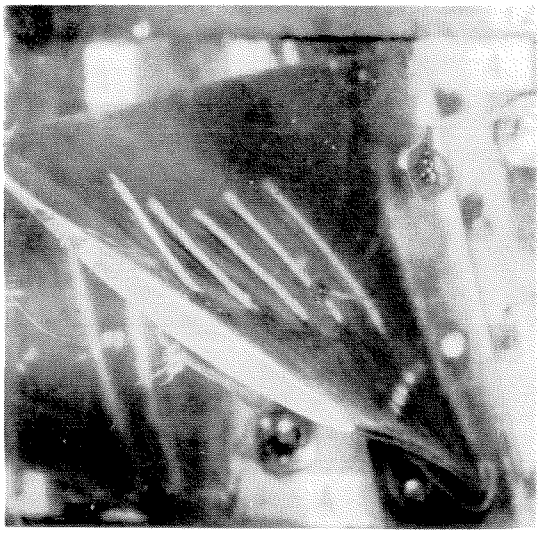

a. Midchord Region; ERS;
R_T = 2230; ϕ = 0.28

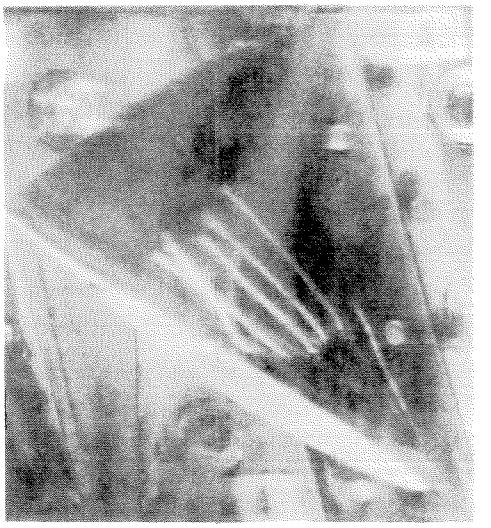

b. Midchord Region, ES;
R_T = 2030; ϕ = 0.26

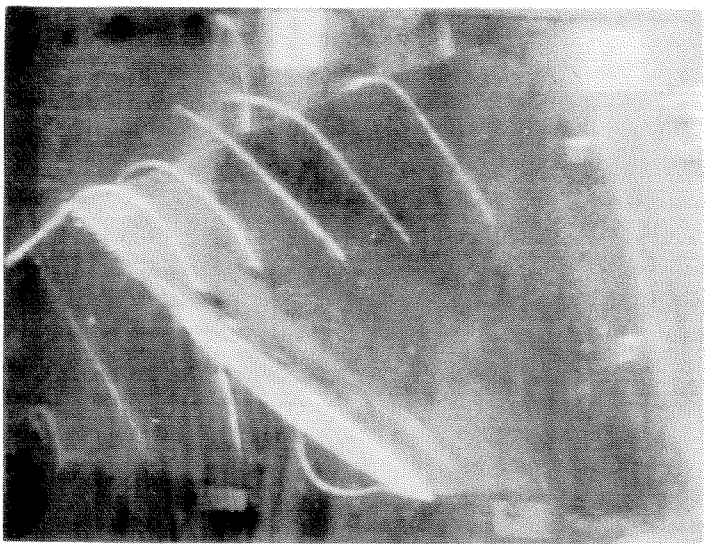

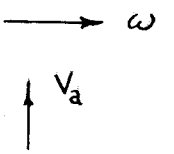

c. Trailing Edge Region; ES;
R_T = 2030; ϕ = 0.26

FIG. 33. ROTOR BLADE PRESSURE SURFACE

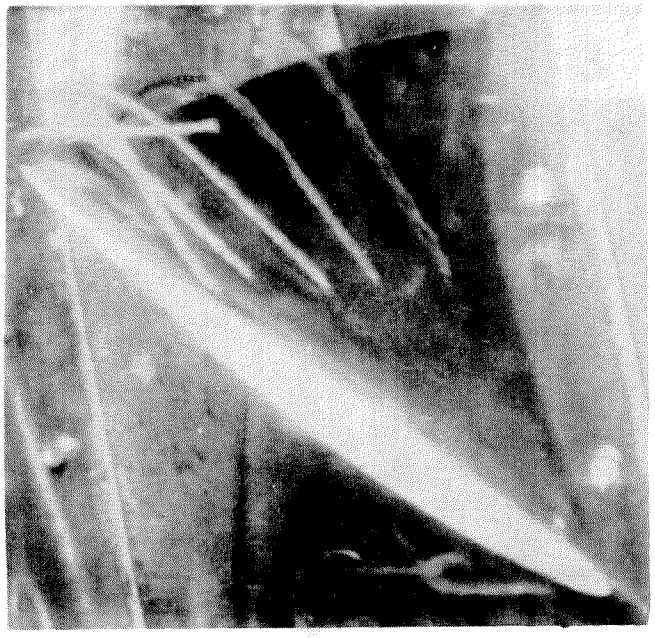

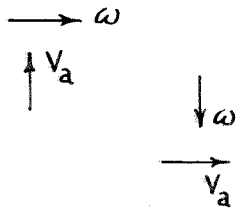

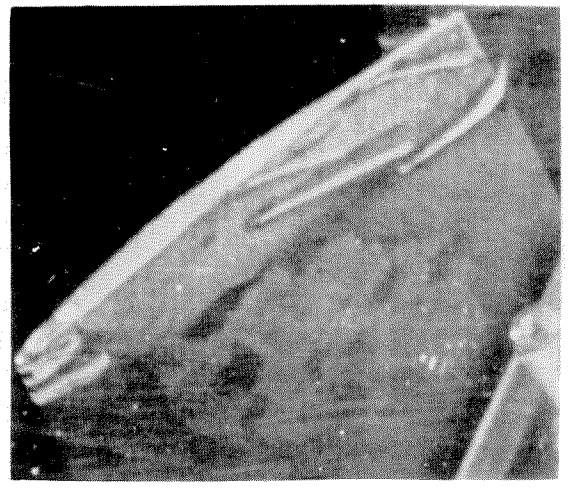

e. Tip Region; CS;
R_T = 2010; ϕ = 0.29

d. Trailing Edge Region; ERS;
R_T = 2230; ϕ = 0.28

FIG. 33 (CONCLUDED)

a

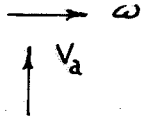

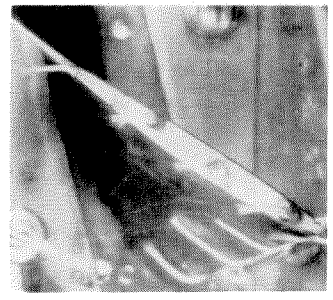

b

FIG. 34. ROTOR TIP CLEARANCE FLOW; ERS;
R_T = 2230; ϕ = 0.28

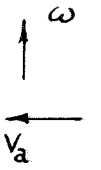

a. Rotor Exit

b. Rotor Inlet

FIG. 35. RAKE TUFTS SHOWING ROD WAKE EFFECT; ERS; R_T = 2280; ϕ = 0.28

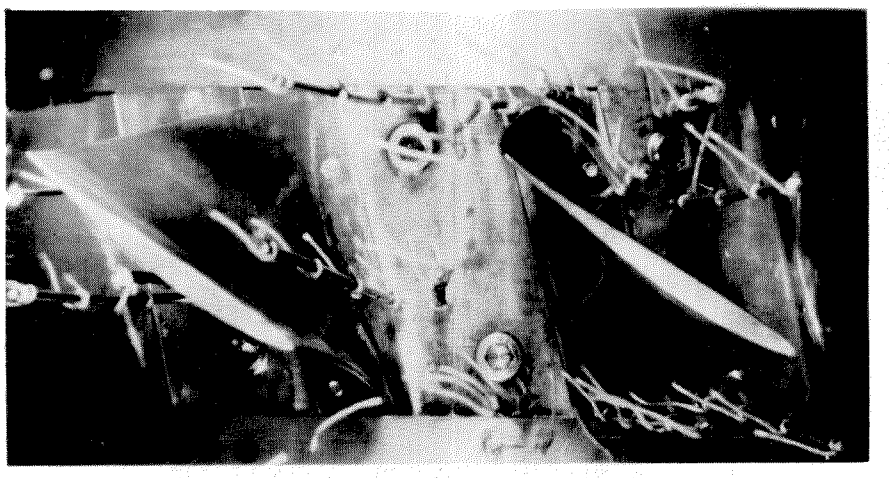

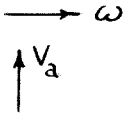

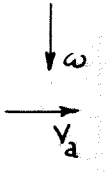

a

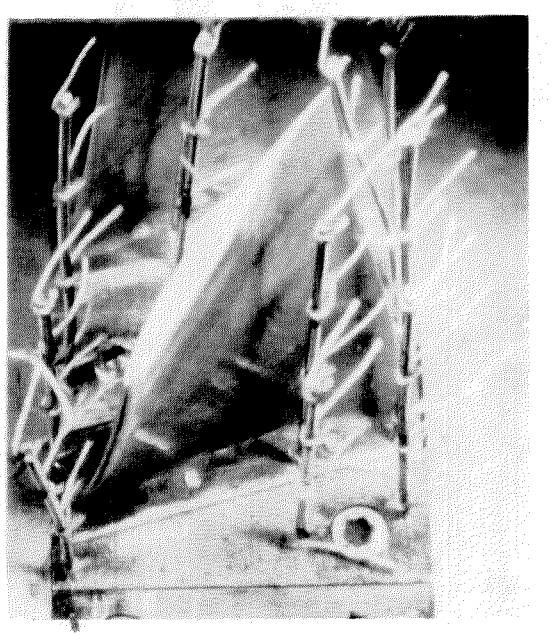

b

FIG. 36. FLOW DIRECTIONS WITHIN ROTOR PASSAGE; ERS; R_T = 2280; ϕ = 0.28

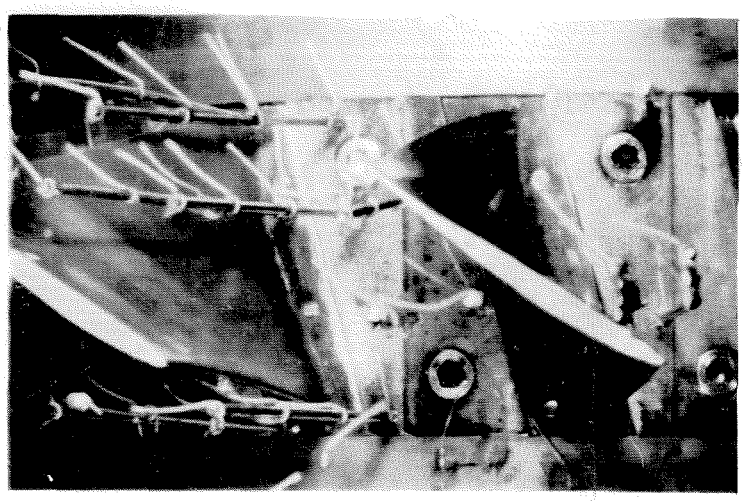

c

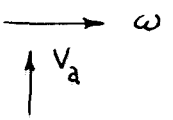

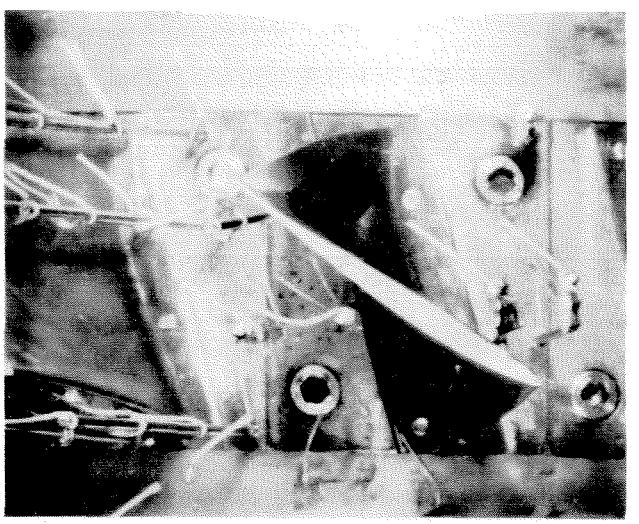

d

FIG. 36 (CONT'D)

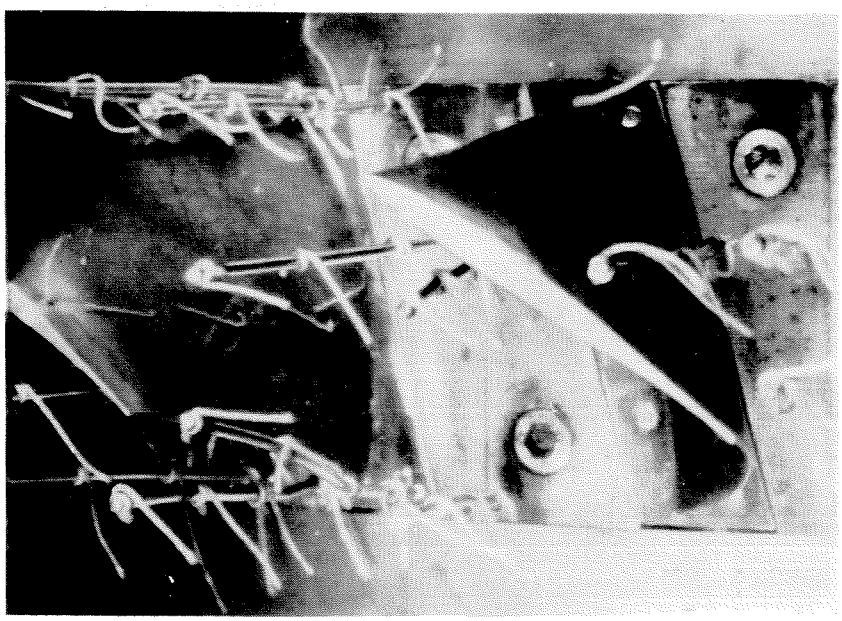

FIG. 36 (CONCLUDED)

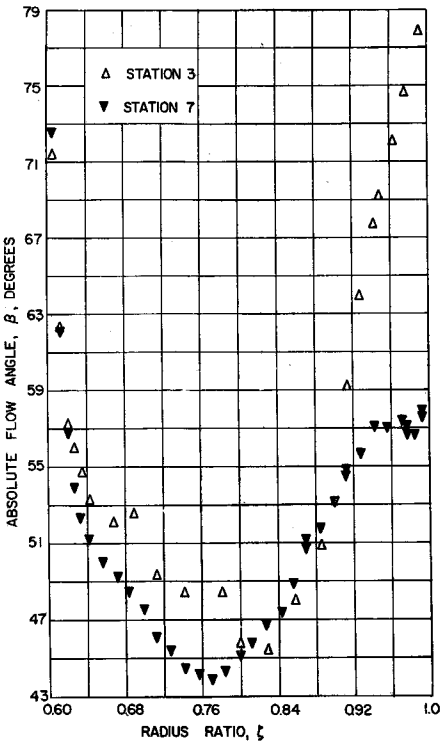

a. Flow Angles

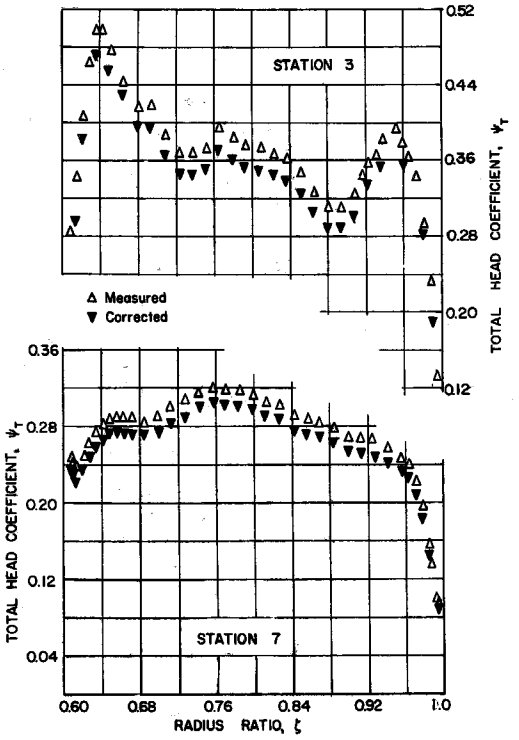

b. Total Head Coefficients

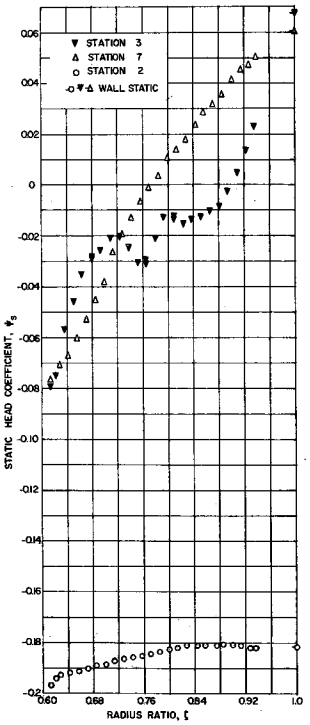

c. Static Head Coefficients

FIG. 37. FLOW SURVEYS DOWNSTREAM OF ROTOR; ES; R_T = 1986-2045; ϕ = 0.282-0.289

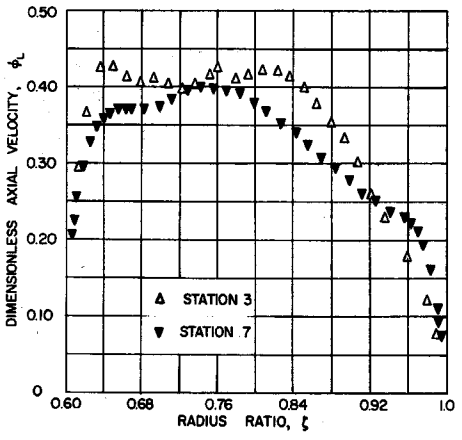

d. Axial Velocity

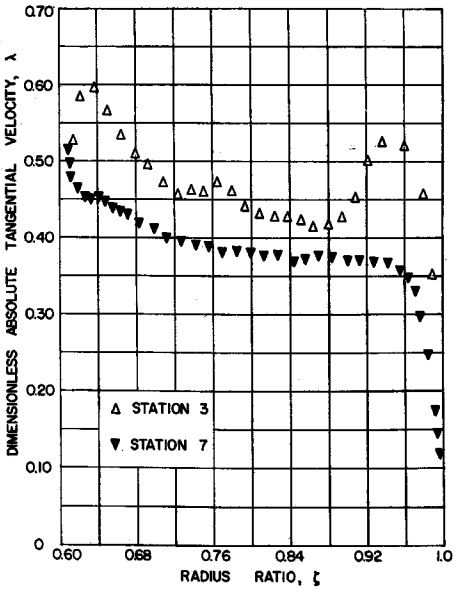

e. Absolute Tangential Velocity

FIG. 37. (CONCLUDED)

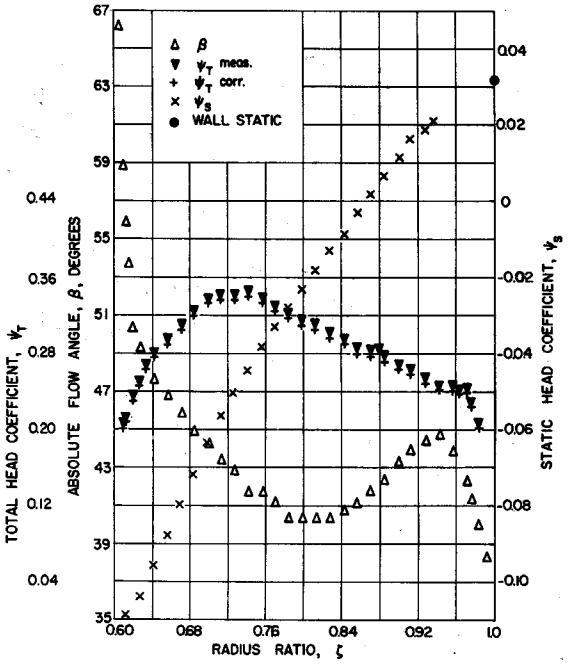

a. Flow Angles; Head Coefficients

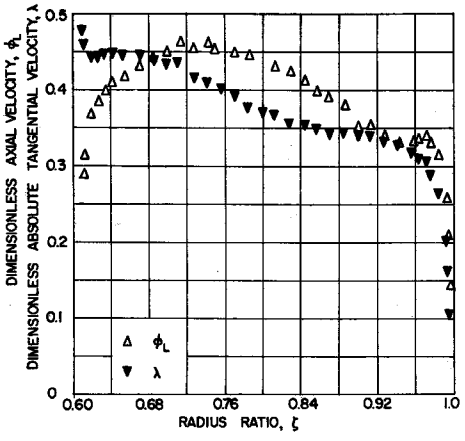

b. Velocities

FIG. 38. FLOW SURVEYS DOWNSTREAM OF ROTOR: STATION 7; ES; R_T = 3400-3510; ϕ = 0.358-0.360

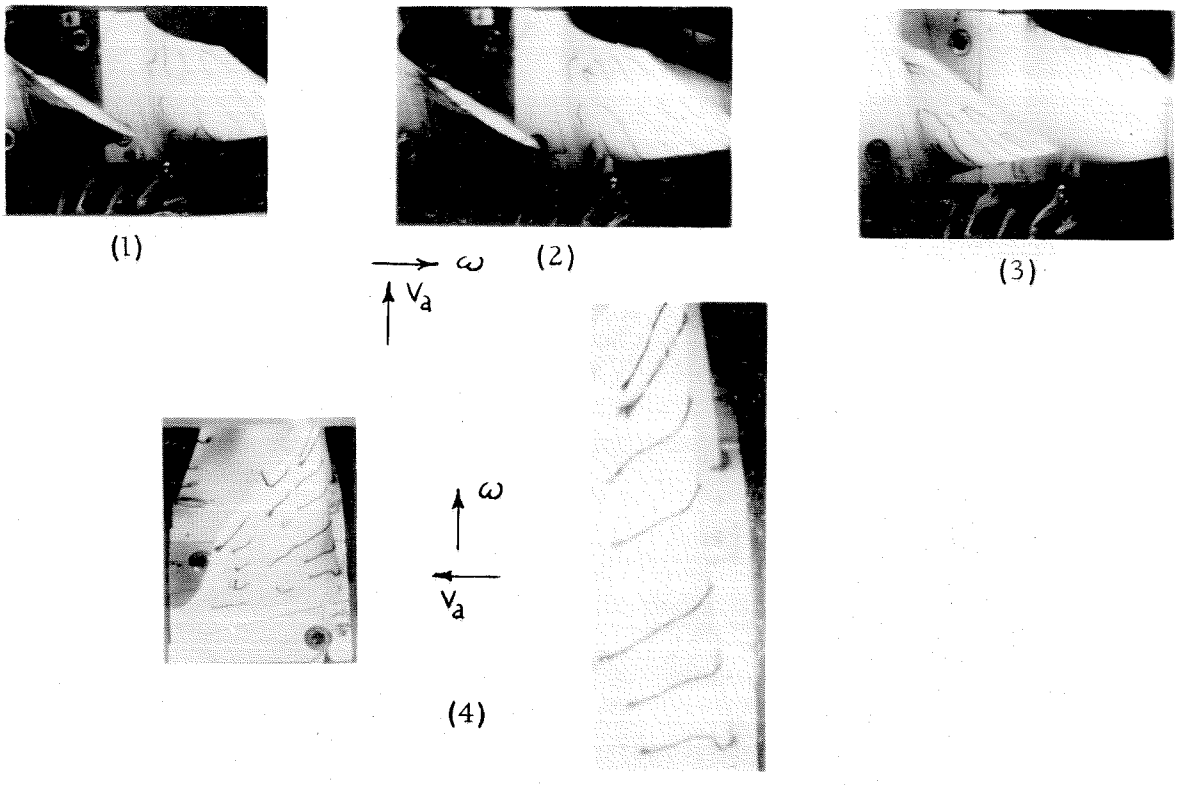

FIG. 39a. ROTOR BLADE SUCTION SURFACE; CS; R_T= 12, 500; ϕ = 0.325

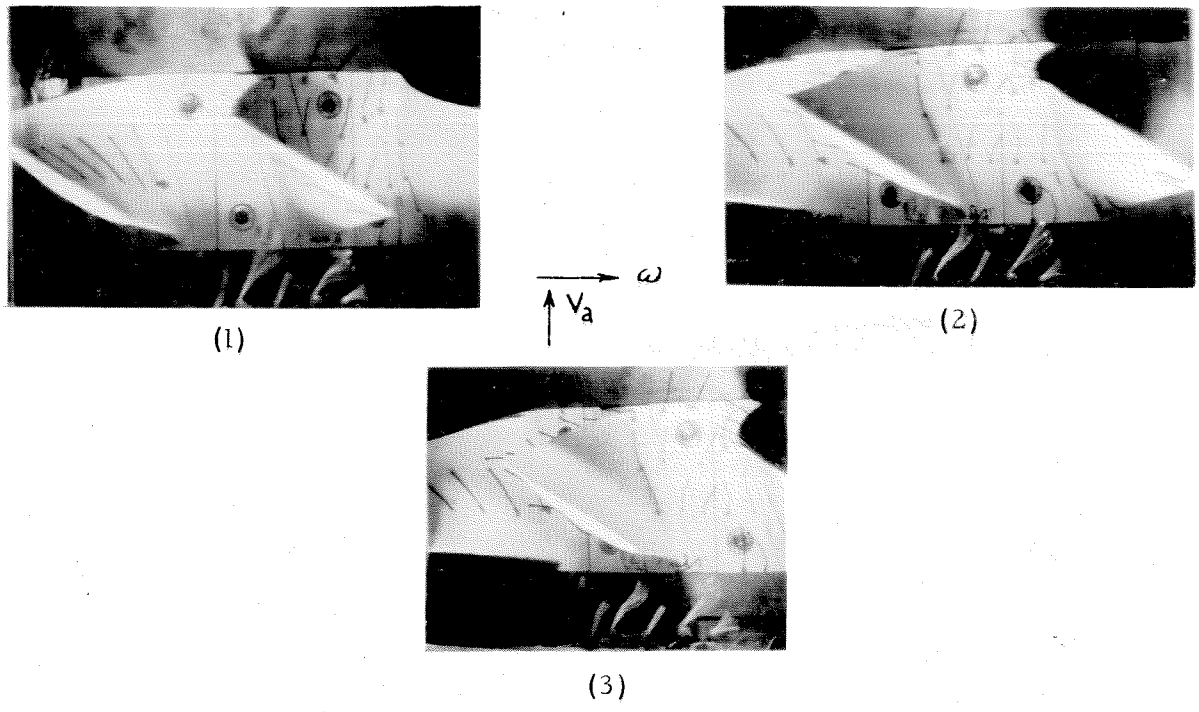

FIG. 39b. ROTOR HUB; CS; R_T = 12, 500; ϕ = 0.325

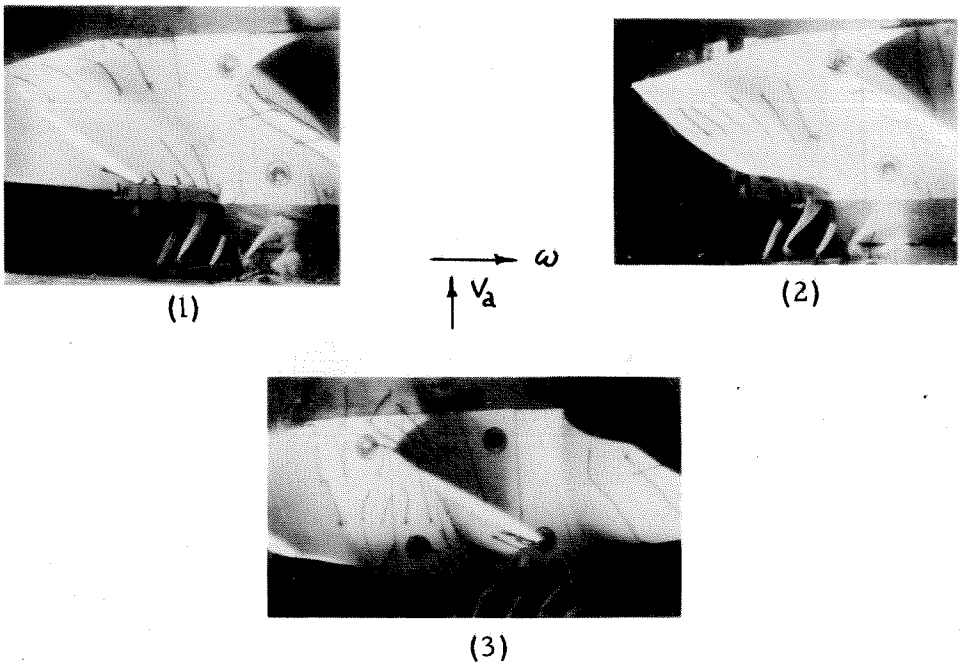

FIG. 39c. ROTOR BLADE PRESSURE SURFACE; CS; R_T = 12,500; ϕ = 0.325

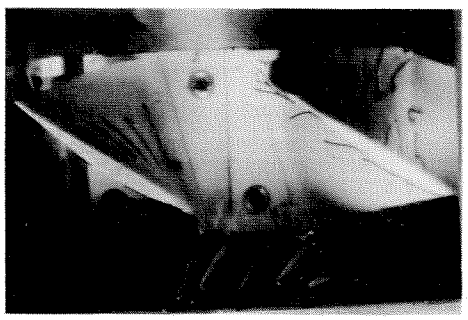

FIG. 39d. ROTOR BLADE SUCTION SURFACE NEAR TIP; CS; R_T = 12,500; ϕ = 0.325

FIG. 39e. ROTOR BLADE PRESSURE SURFACE NEAR TIP; TIP CLEARANCE FLOW; CS; R_T = 12,500; ϕ = 0.325

(1)

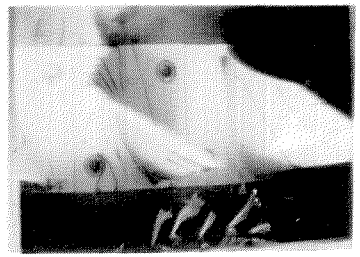

(2)

a. Suction Surface

(1)

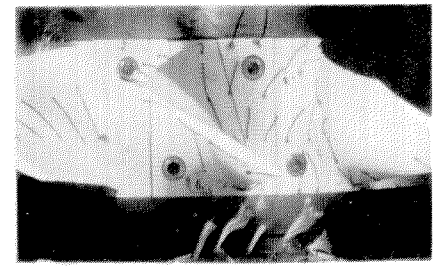

(2)

b. Rotor Hub

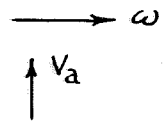

(1)

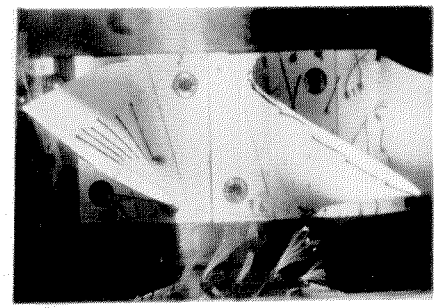

(2)

c. Pressure Surface and Suction Surface Near Tip

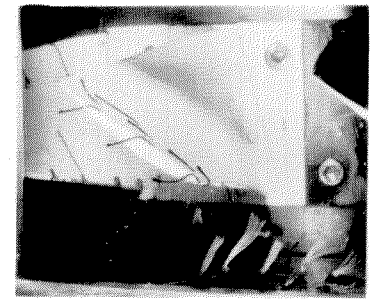

d. Pressure Surface Near Tip; Tip Clearance Flow

FIG. 40. ROTOR TUFTS; CS; R_T = 21,000; ϕ = 0.327

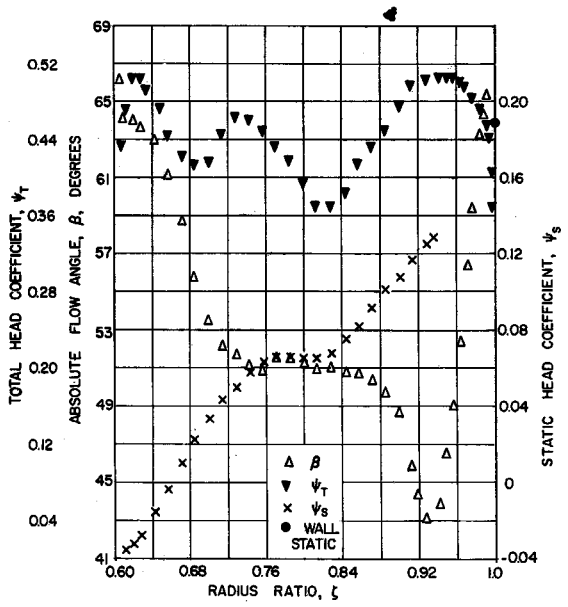

a. Flow Angles and Head Coefficients

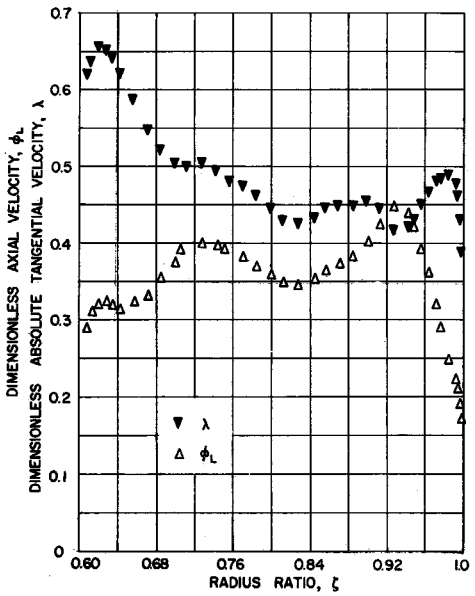

b. Velocities

FIG. 41. FLOW SURVEYS AT ROTOR EXIT; STATION 3; CS; R_T = 12, 290-12, 800; ϕ = 0.319-0.322

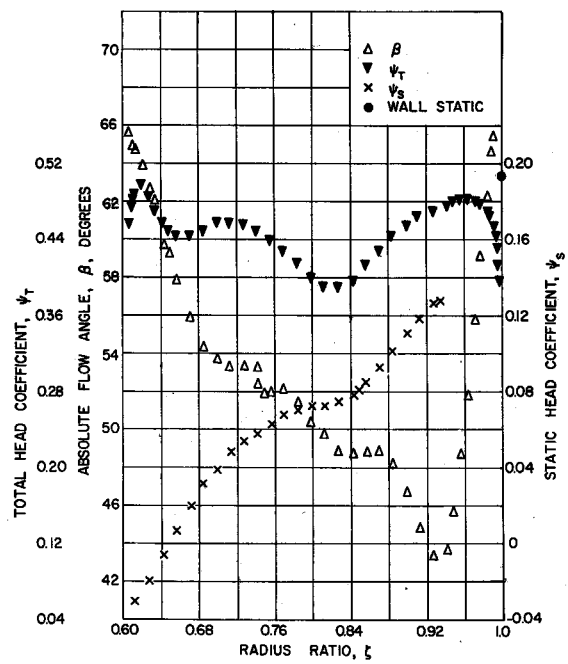

a. Flow Angles and Head Coefficients

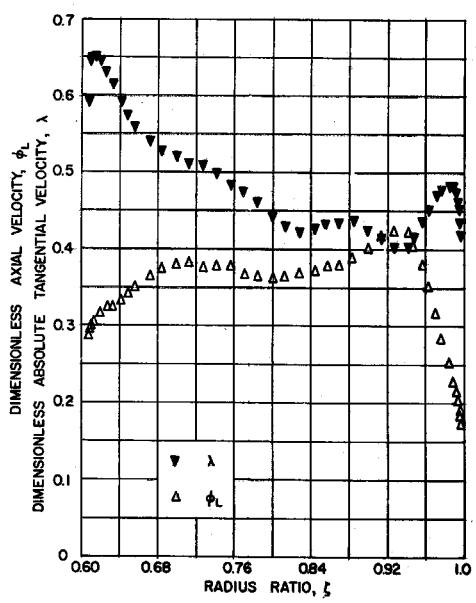

b. Velocities

FIG. 42. FLOW SURVEYS AT ROTOR EXIT; STATION 3; CS; R_T = 20, 200-21, 450; ϕ = 0.327

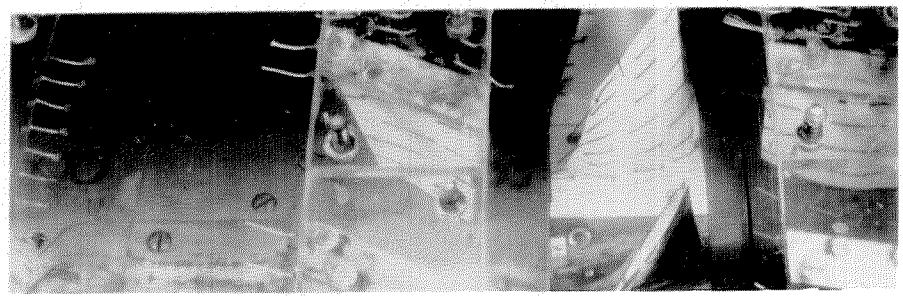

(1)

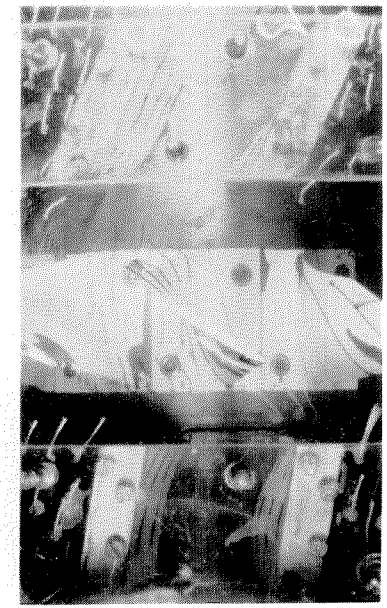

(2)

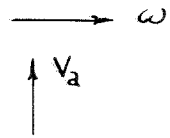

a. Suction Surface; CS; R_T = 152, 000; ϕ = 0.38

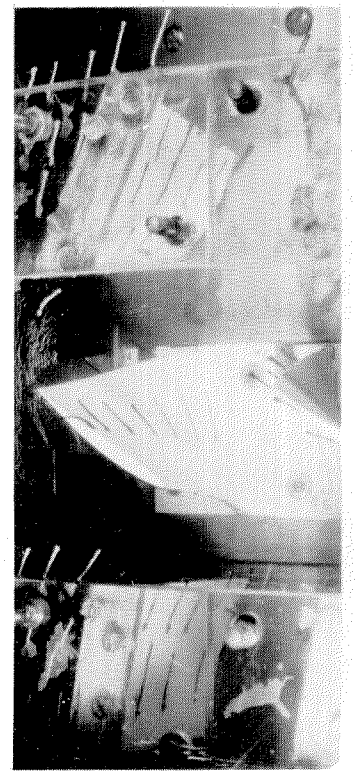

(1)

(2)

b. Pressure Surface; CS; R_T = 152, 000; ϕ = 0.38

FIG. 43. ROTOR TUFTS

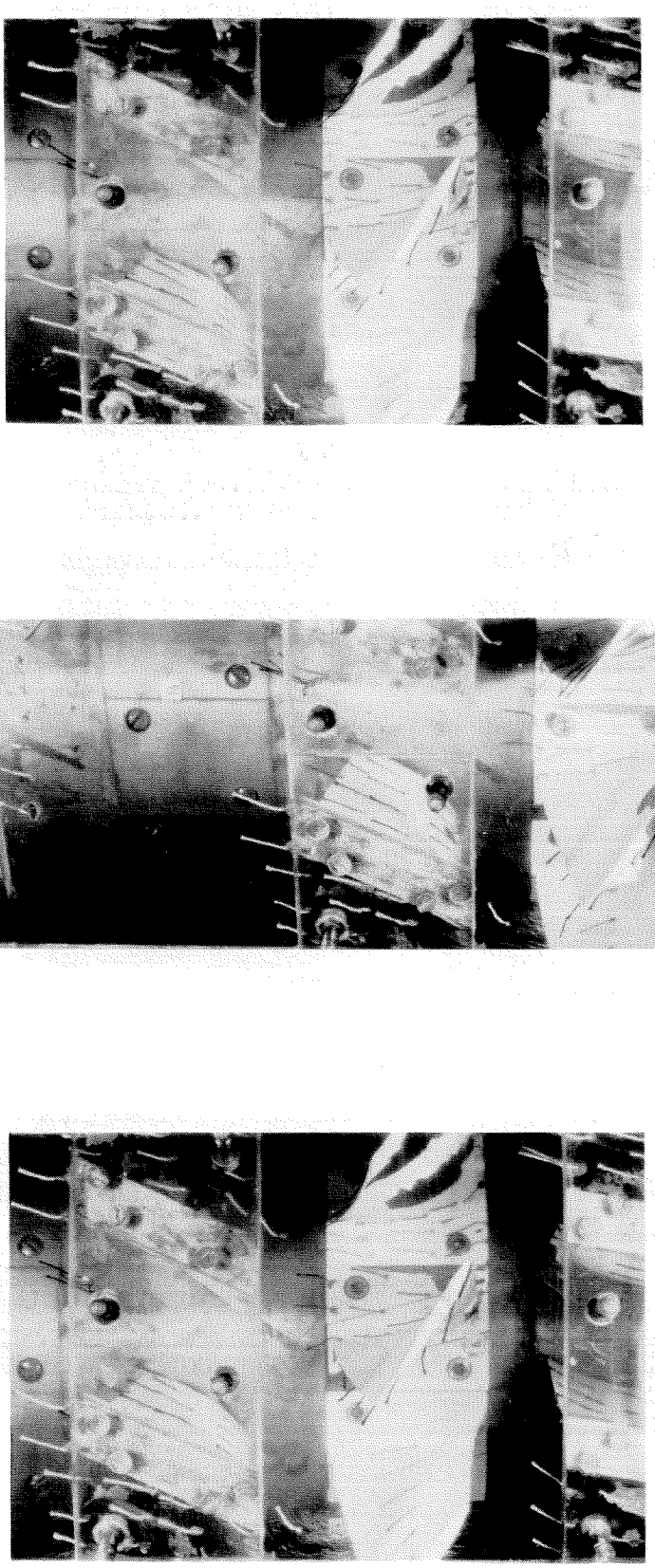

c. Rotor Hub; CS; R_T = 152, 000; ϕ = 0.38

FIG. 43. (CONT'D)

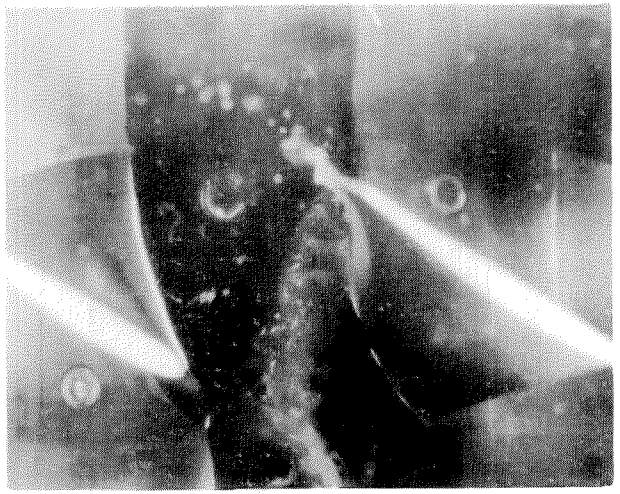

(1) $\phi = 0.41$; $\frac{y}{\delta} = 0.08$

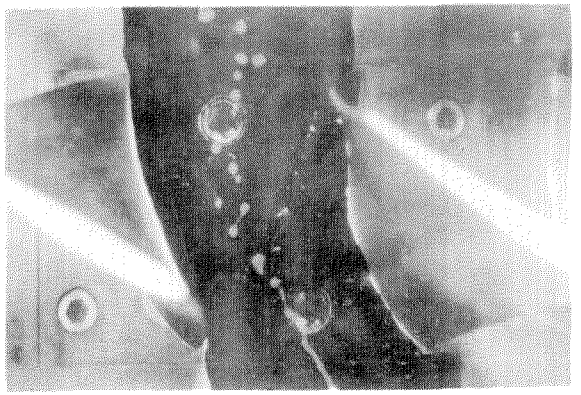

(2) $\phi = 0.45$; $\frac{y}{\delta} = 0.18$

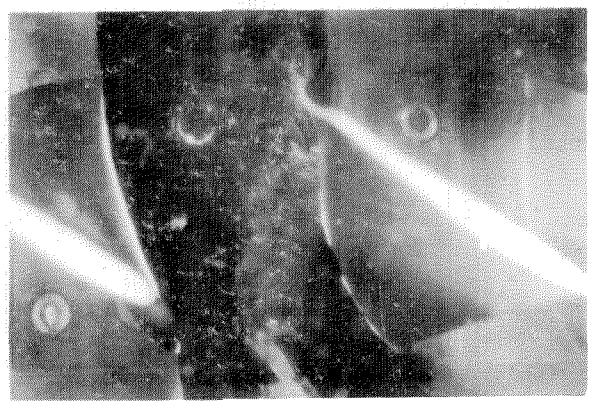

(3) $\phi = 0.45$; $\frac{y}{\delta} = 0.08$

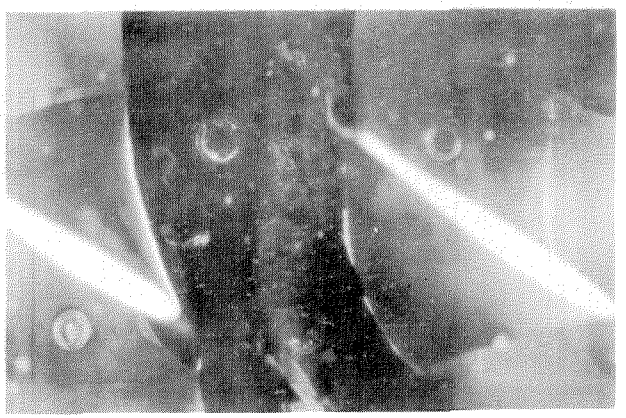

(4) $\phi = 0.53$; $\frac{y}{\delta} = 0.08$

ω

V_a

d. Rotor Hub; Fluid Injection; ERS (Photos from Ref. (27), cf. p (97))

FIG. 43. (CONCLUDED)

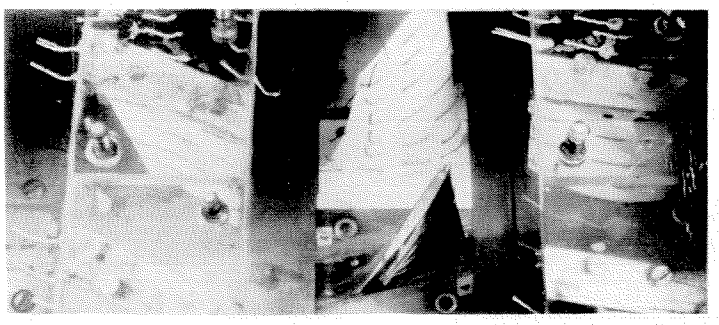

(1)

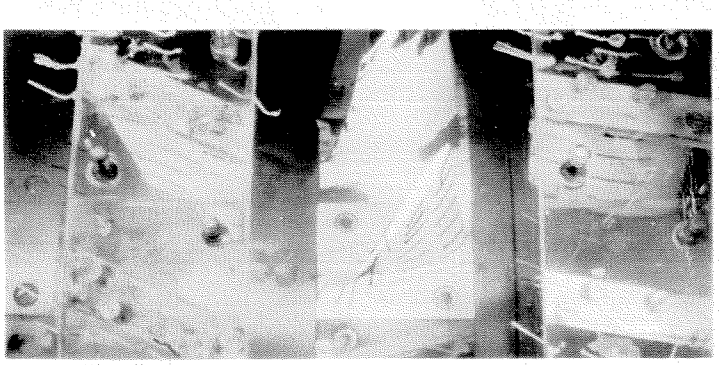

(2)

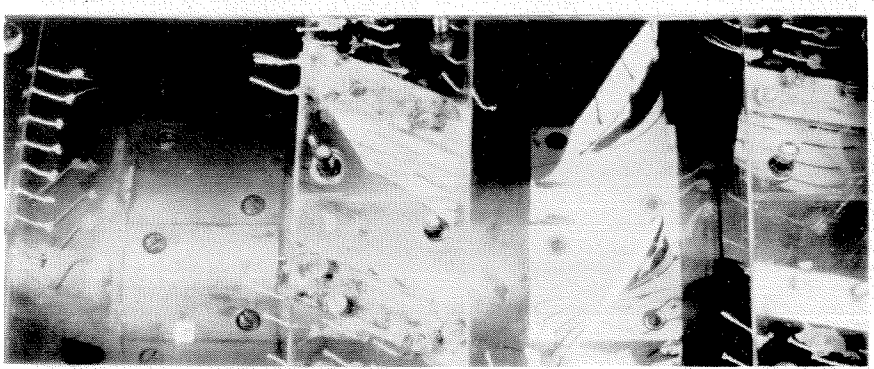

(3)

a. Suction Surface

FIG. 44. ROTOR TUFTS; CS; R_T = 152,000; ϕ = 0.33

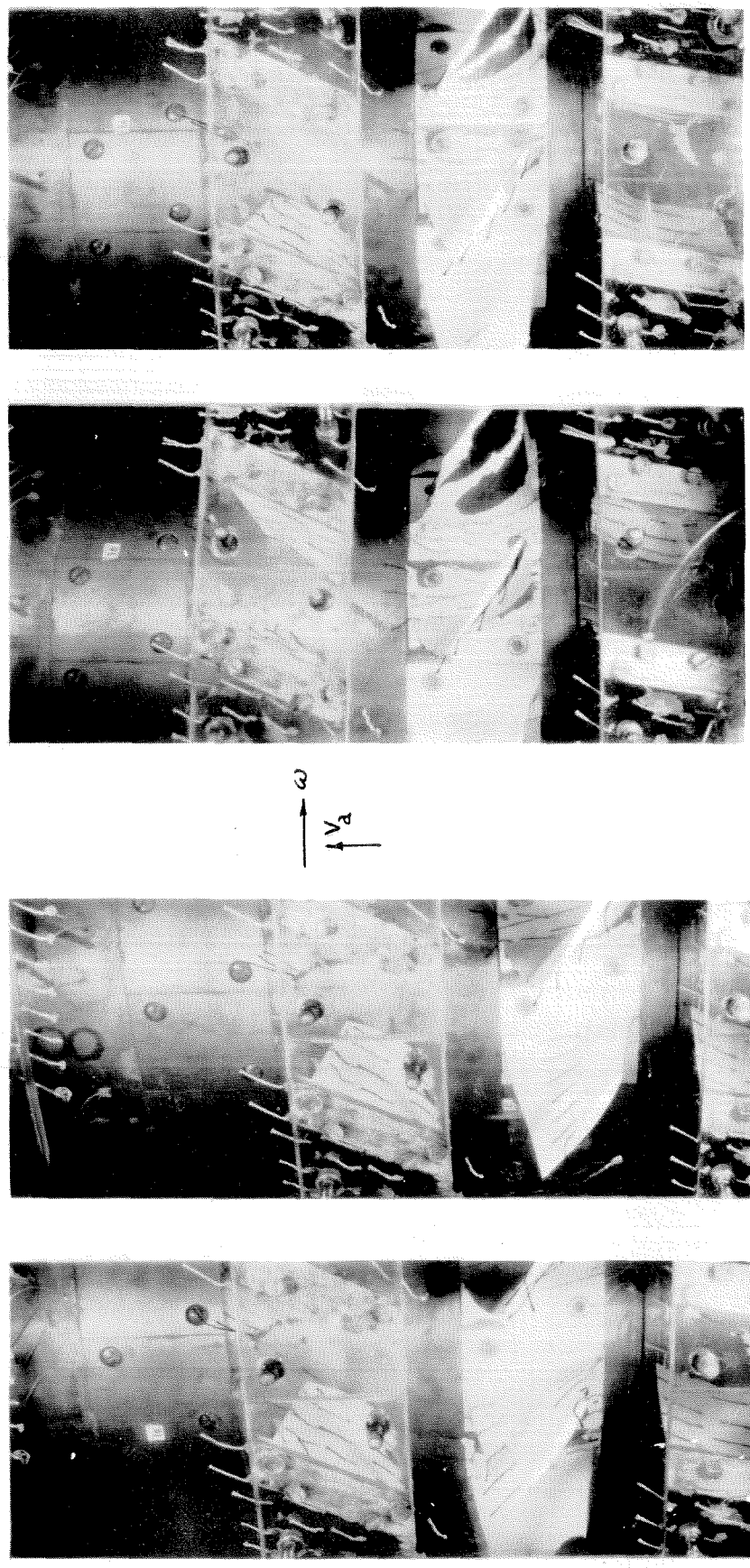

(1) (2) (1) (2)

b. Pressure Surface c. Rotor Hub

FIG. 44 (CONCLUDED)

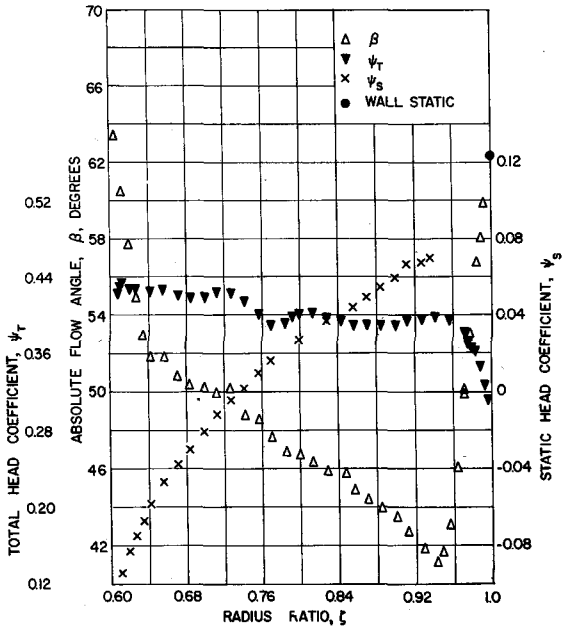

a. Flow Angles and Head Coefficients

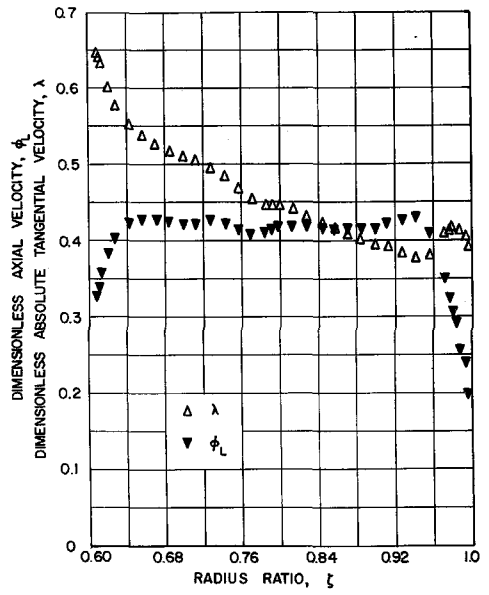

b. Velocities

FIG. 45. FLOW SURVEYS AT ROTOR EXIT; STATION 3; CS; R_T = 151,400-156,500; ϕ = 0.39

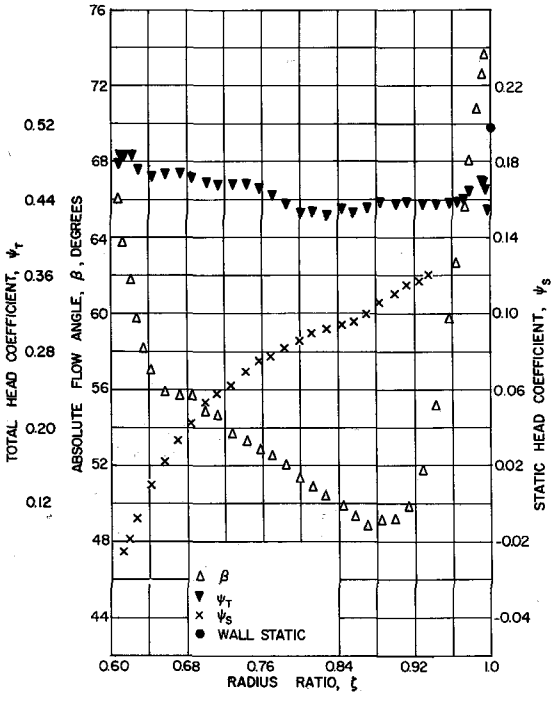

a. Suction Surface

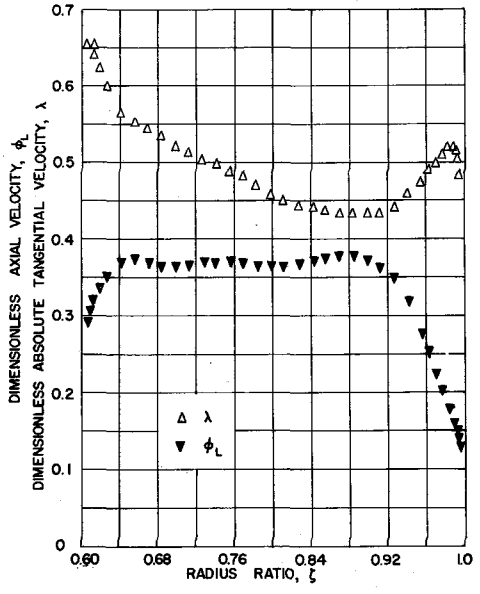

b. Suction Surface Near Hub $R_T \sim 250$; $\phi \sim 0.2$

FIG. 46. FLOW SURVEYS AT ROTOR EXIT; STATION 3; CS; R_T = 152,200-156,500; ϕ = 0.34

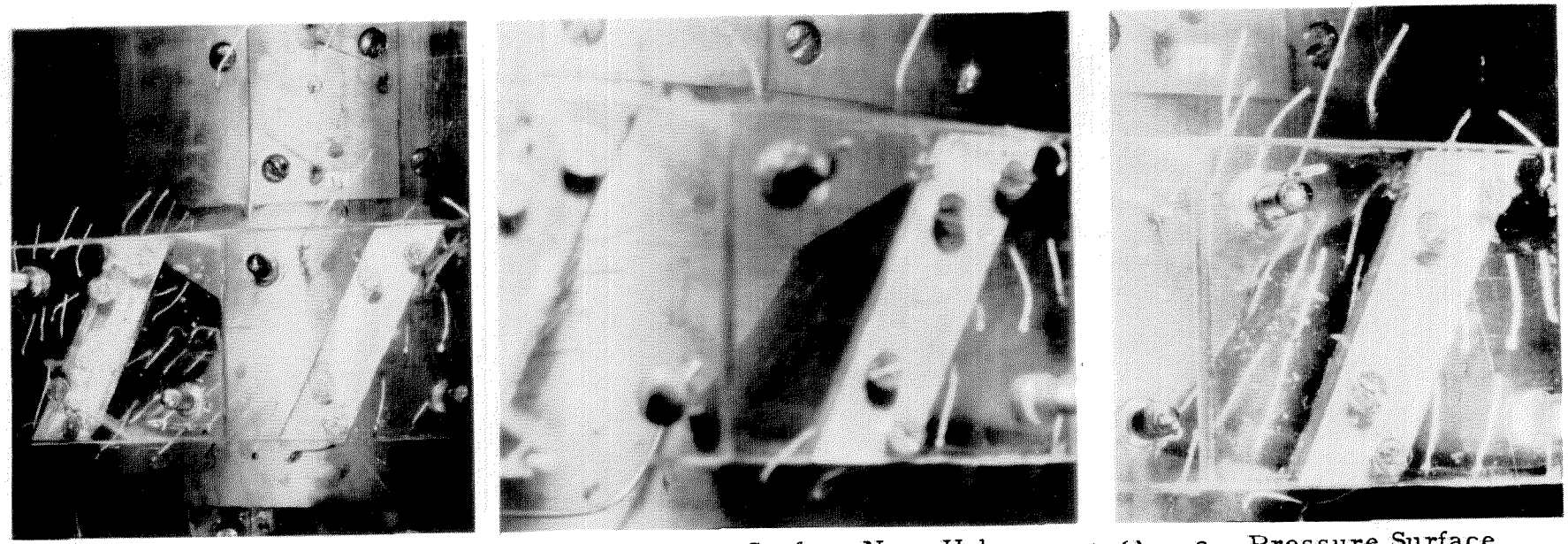

a. Suction Surface → ω, ↑ V_a

b. Suction Surface Near Hub $R_T \sim 250$; $\phi \sim 0.2$ → ω, ↑ V_a

c. Pressure Surface

FIG. 47. TUFT IN STATOR; CS; $R_T = 2000$; $\phi = 0.28$ (Except in b)

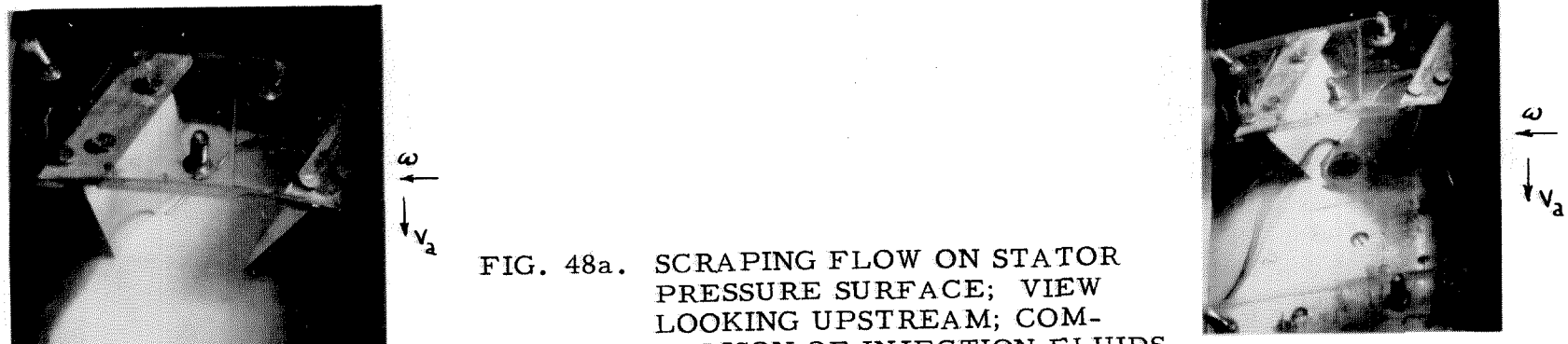

(1) (Glycerine-Water) + $KMnO_4$; Sp. Gr. = 1.2

ω ←, ↓ V_a

FIG. 48a. SCRAPING FLOW ON STATOR PRESSURE SURFACE; VIEW LOOKING UPSTREAM; COMPARISON OF INJECTION FLUIDS WITH DIFFERENT SPECIFIC GRAVITIES; CS; $R_T \sim 500$

(2) (Water + $KMnO_4$); Sp. Gr. = 1.0

ω ←, ↓ V_a

(1)

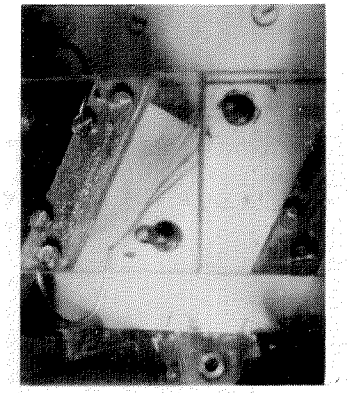

(2)

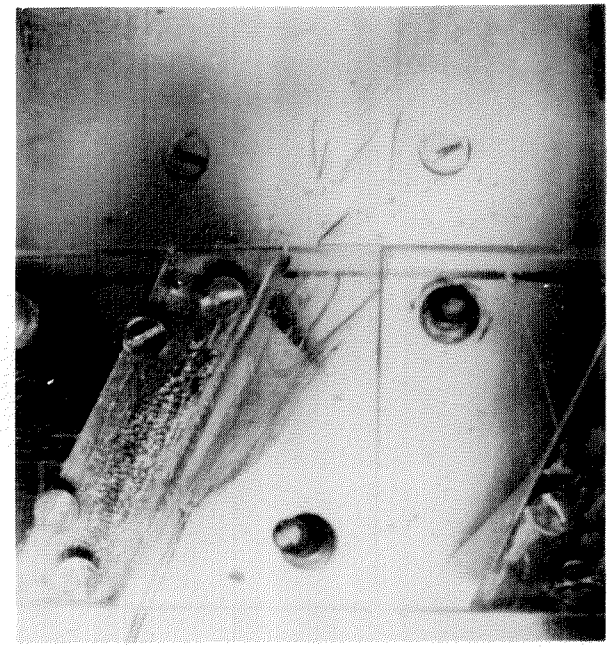

(3)

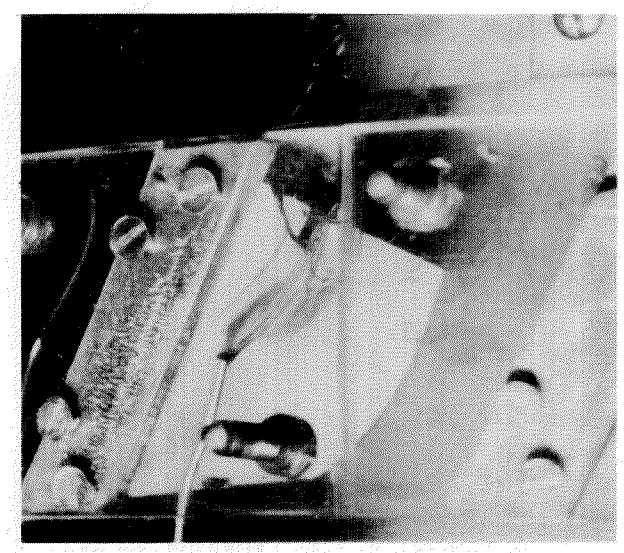

(4)

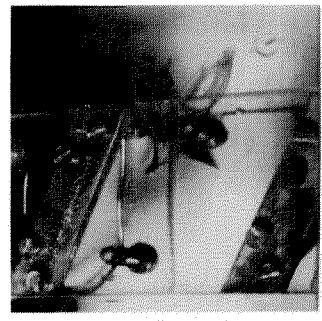

(5)

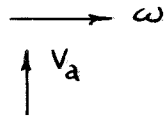

FIG. 48b. STATOR SUCTION SURFACE; FLUID INJECTION NEAR LEADING EDGE AND NEAR CASING; R_T = 2000; ϕ = 0.28

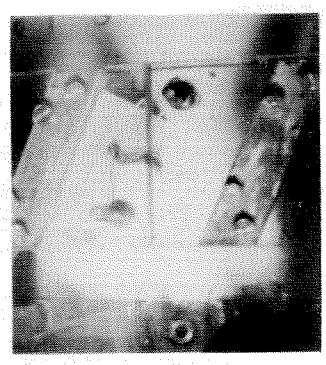

(1)

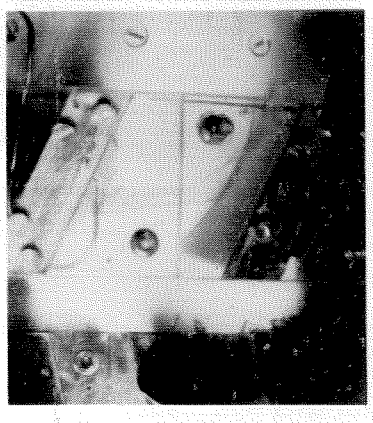

(2)

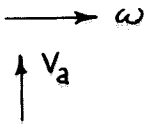

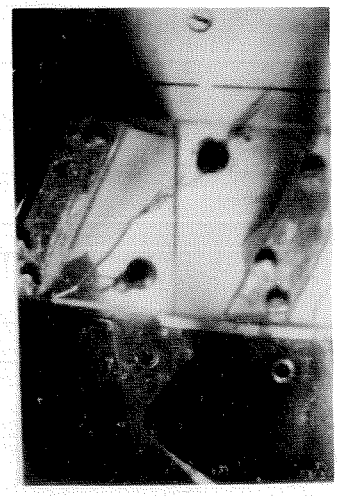

(3)

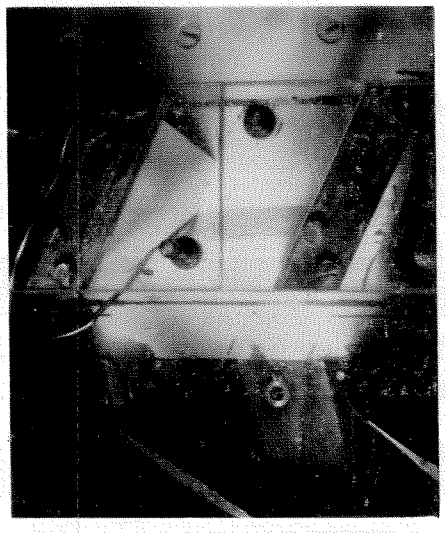

(4)
$R_T \sim 500$

FIG. 48c. STATOR SUCTION SURFACE; REGIONS OF COMPLETE RADIALLY INWARD FLOW; $\phi = 0.28$; $R_T = 2000$ (EXCEPT IN (4))

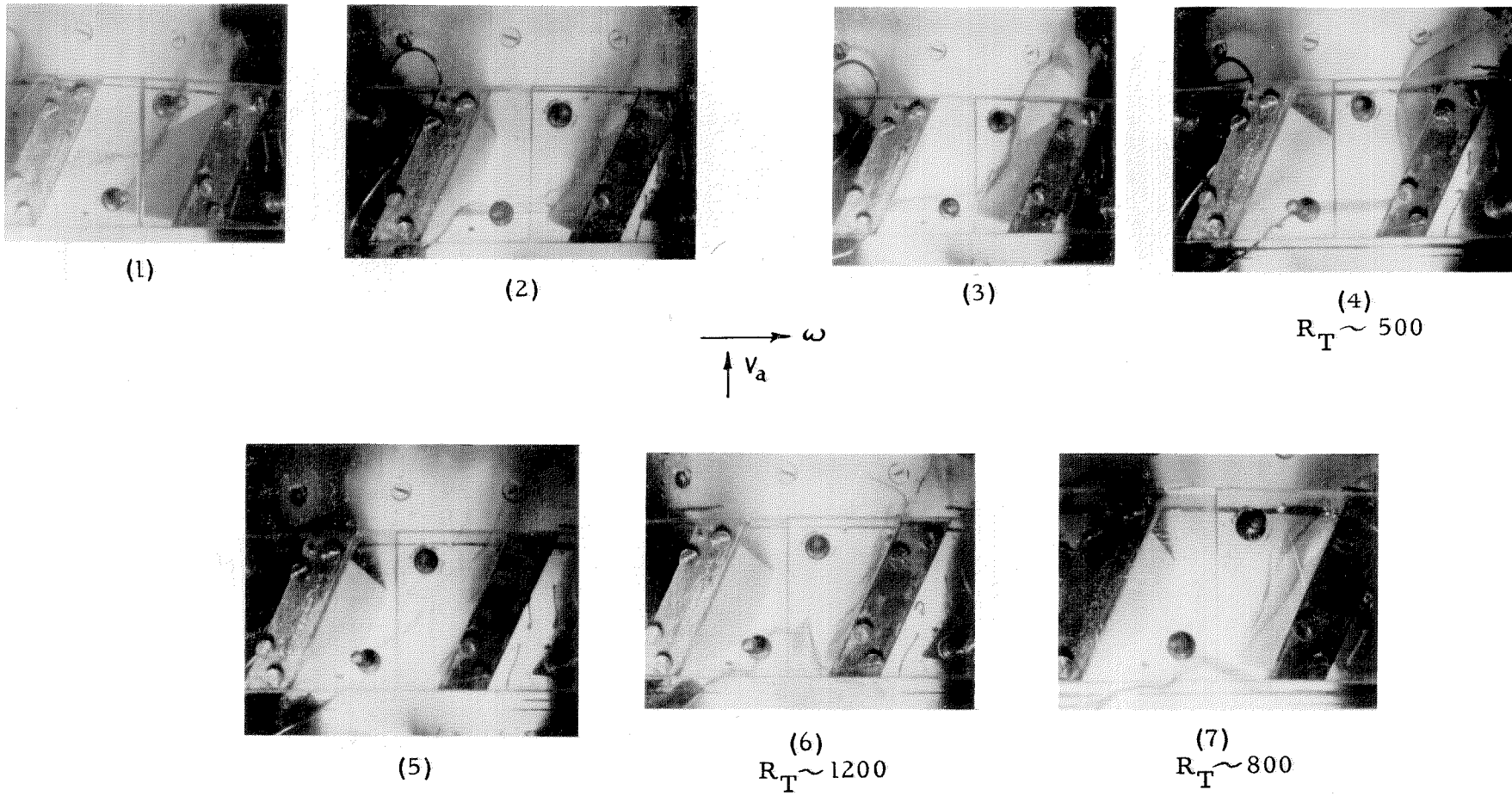

FIG. 48d. STATOR PASSAGE; FLOW ALONG HUB AND ALONG HUB END OF PRESSURE SURFACE; $\phi = 0.28$; $R_T = 2000$ (EXCEPT AS NOTED)

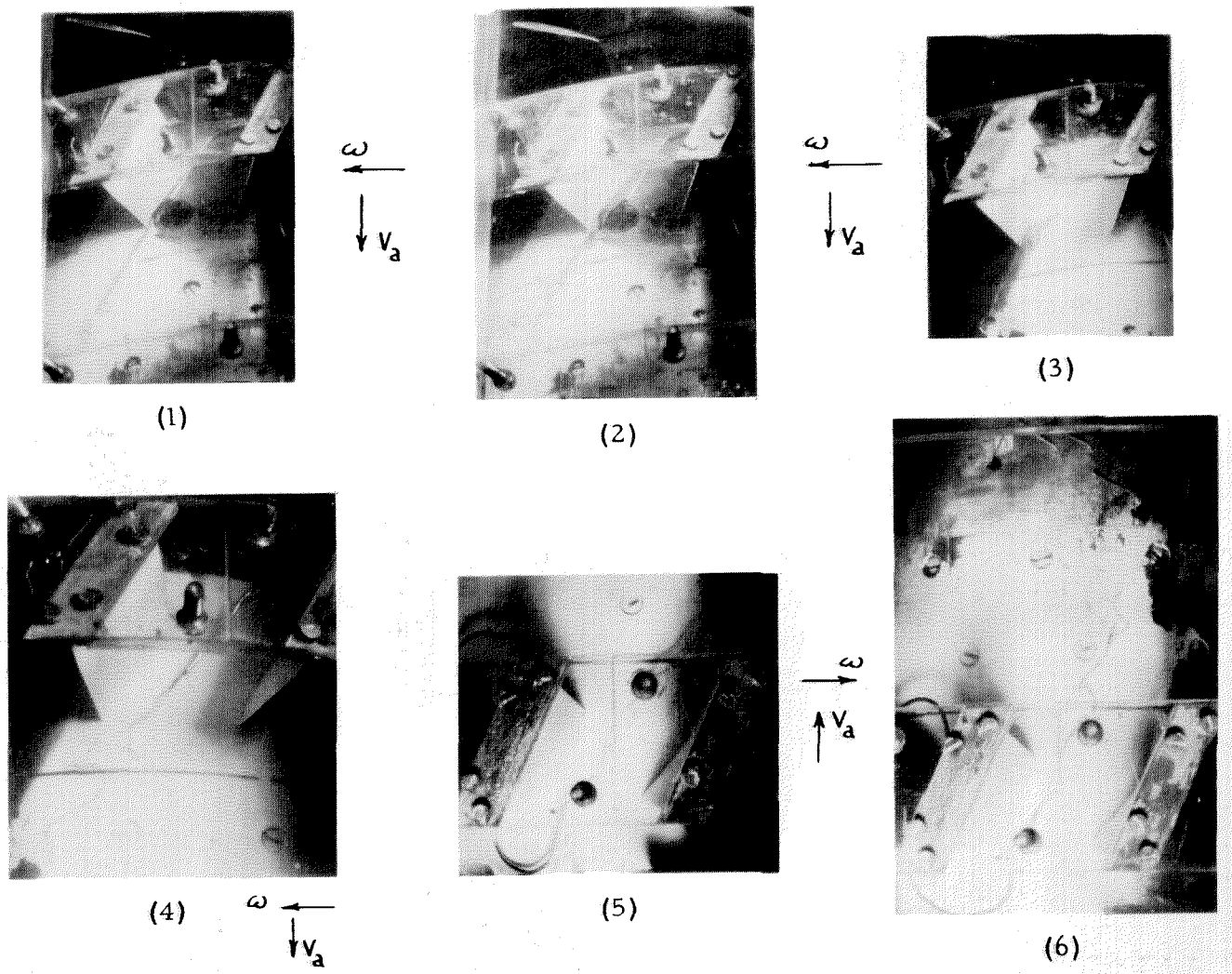

FIG. 48e. STATOR PASSAGE; FLOW AT VARIOUS DISTANCES FROM HUB; (CF. TABLE III); CS; R_T= 2000; ϕ = 0.28

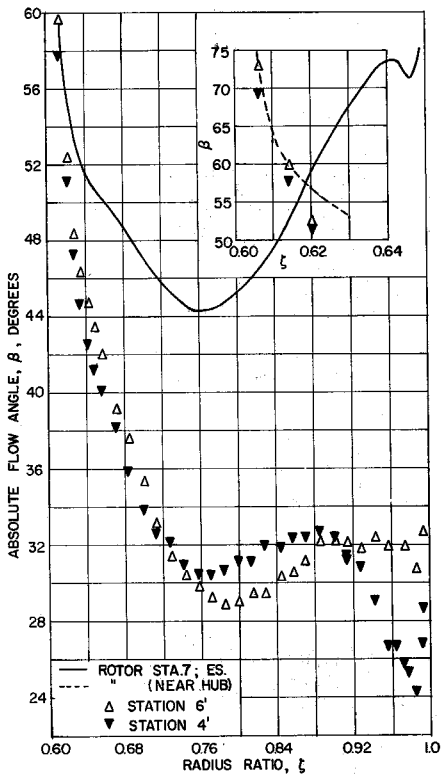

a. Flow Angles

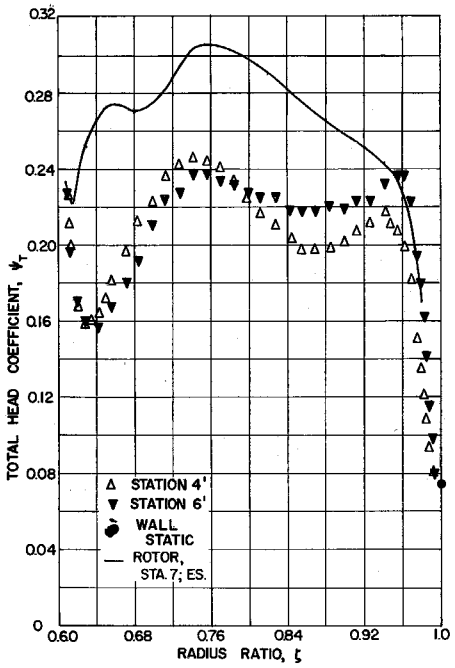

b. Total Head Coefficients

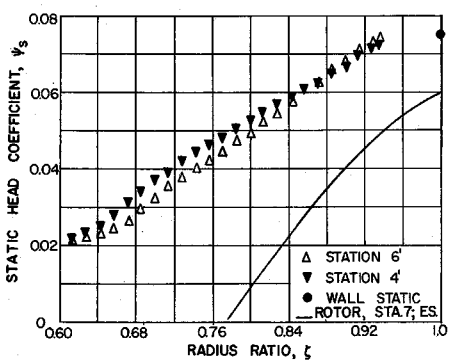

c. Static Head Coefficients

FIG. 49. FLOW SURVEYS DOWNSTREAM OF STATOR; STATION 7; CS; R_T = 1986-2045; ϕ = 0.282 - 0.289

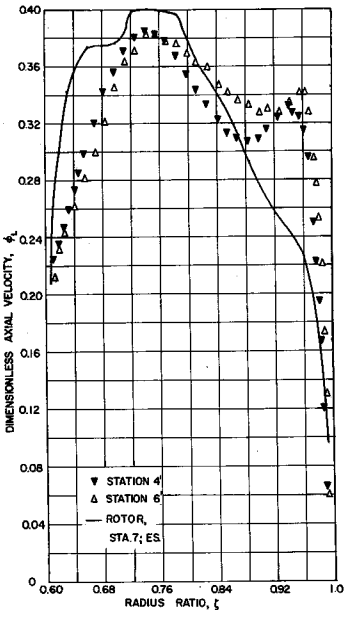

d. Axial Velocity

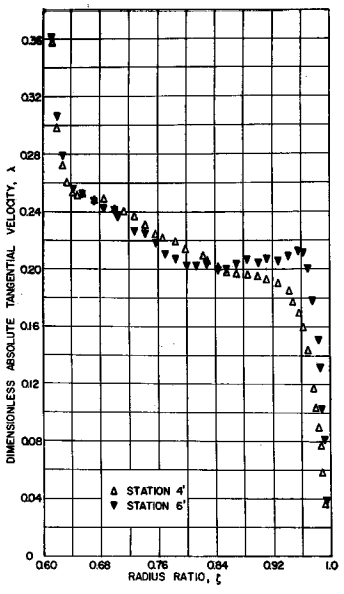

e. Absolute Tangential Velocity

FIG. 49 (CONCLUDED)

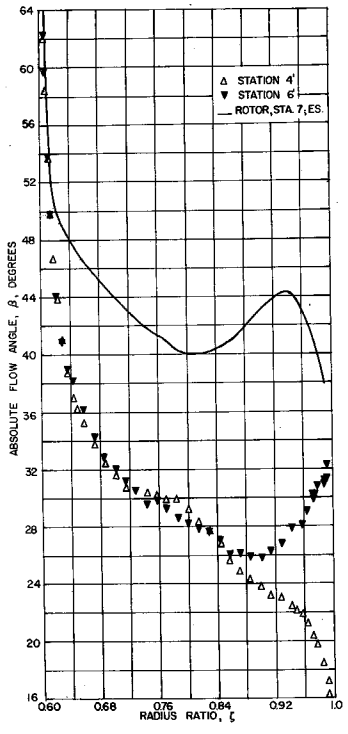

a. Flow Angles

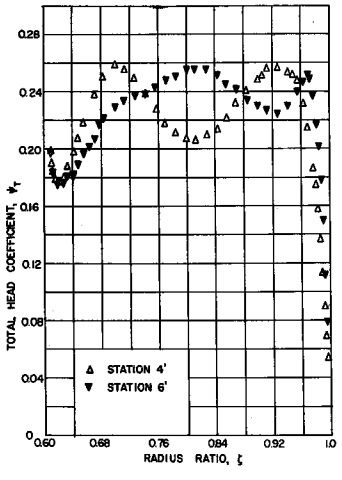

b. Total Head Coefficients

FIG. 50. FLOW SURVEYS DOWNSTREAM OF STATOR; STATION 7; CS; R_T = 3400 - 3510; ϕ = 0.358 - 0.360

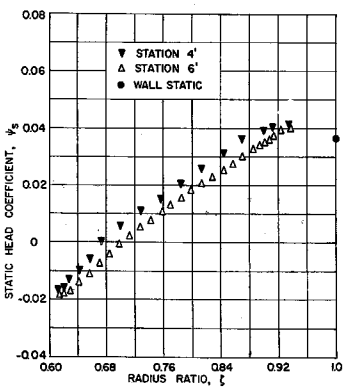

c. Static Head Coefficients

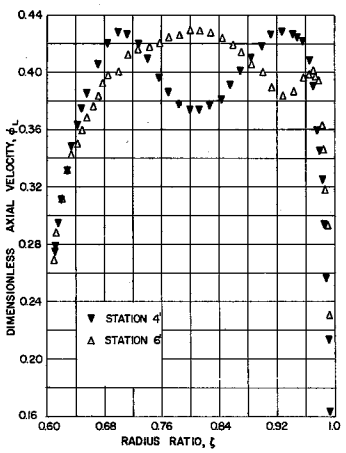

d. Axial Velocity

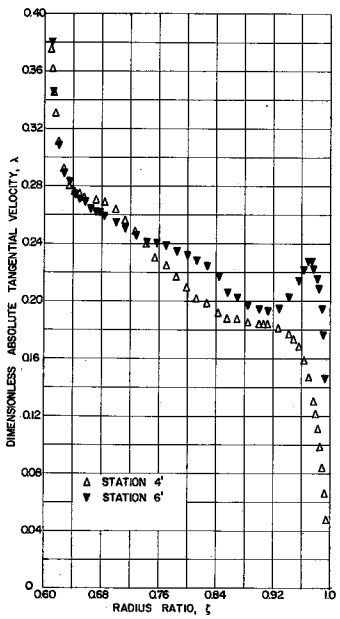

e. Absolute Tangential Velocity

FIG. 50. (CONCLUDED)

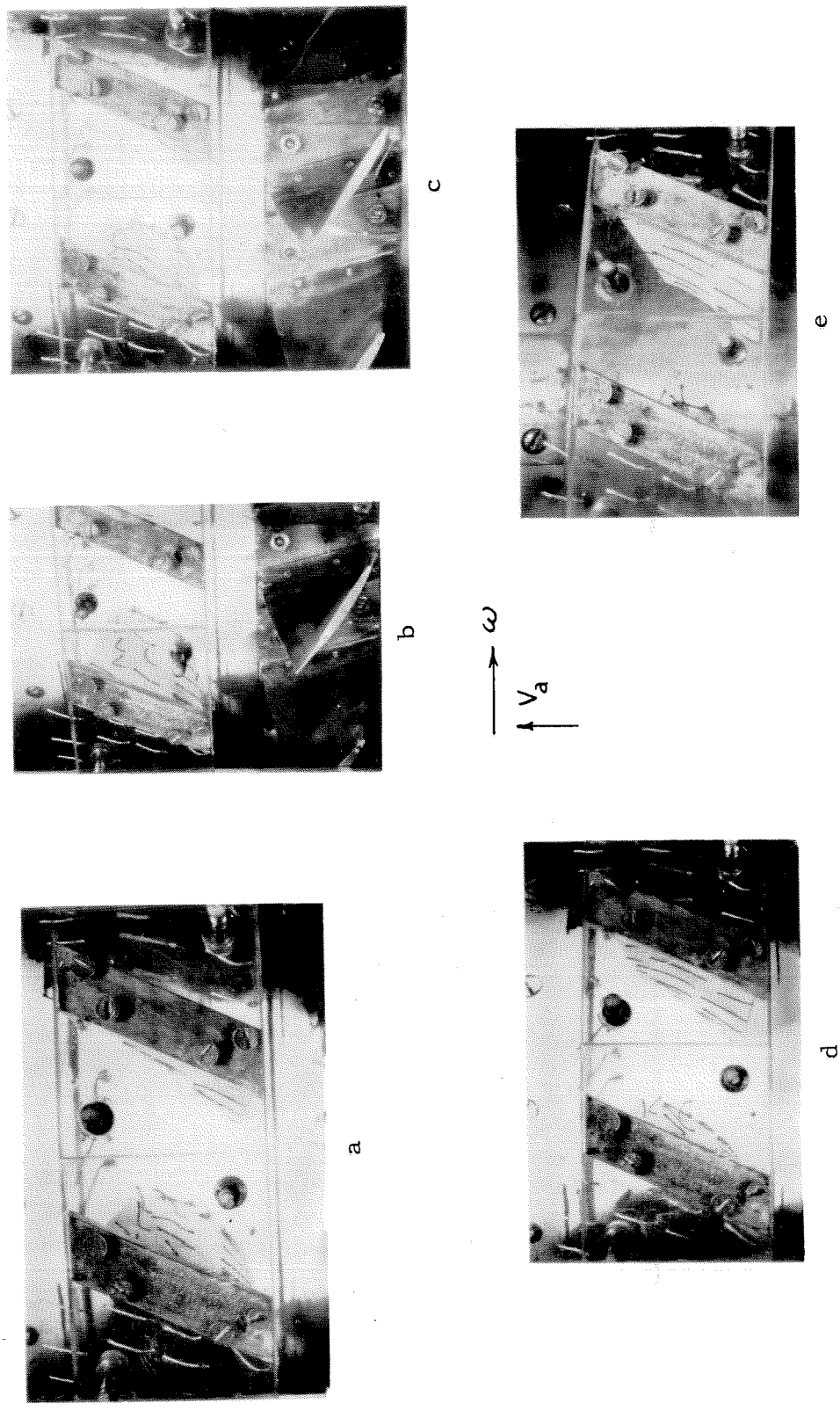

FIG. 51. TUFTS IN STATOR; CS; $R_T = 12,500$; $\phi = 0.325$

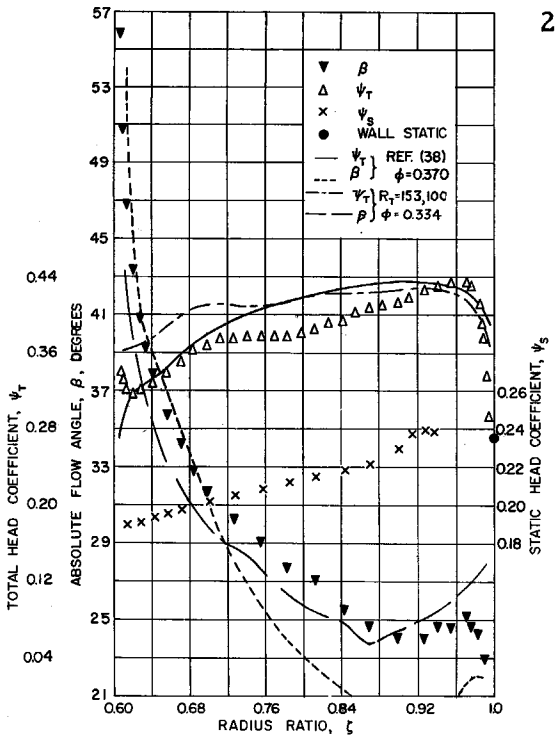

a. Flow Angles and Head Coefficients

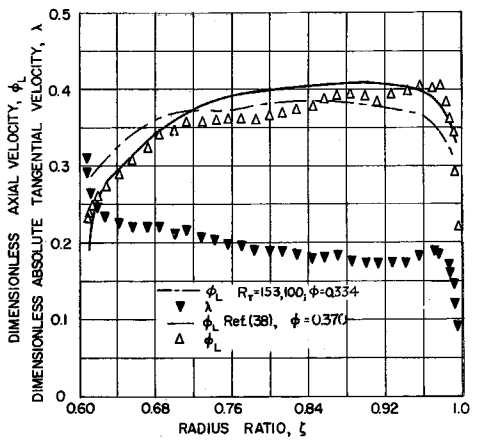

b. Velocities

FIG. 52. FLOW SURVEYS DOWNSTREAM OF STATOR; STATION 7; CS; R_T = 12,800; ϕ = 0.319 - 0.322

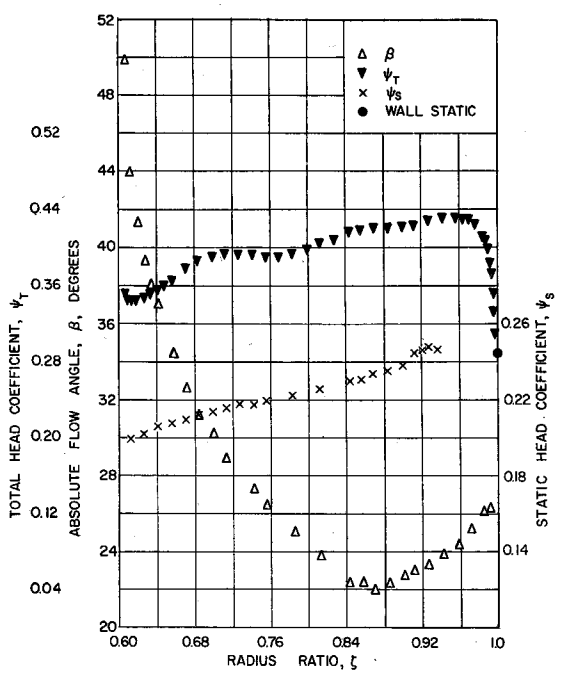

a. Flow Angles and Head Coefficients

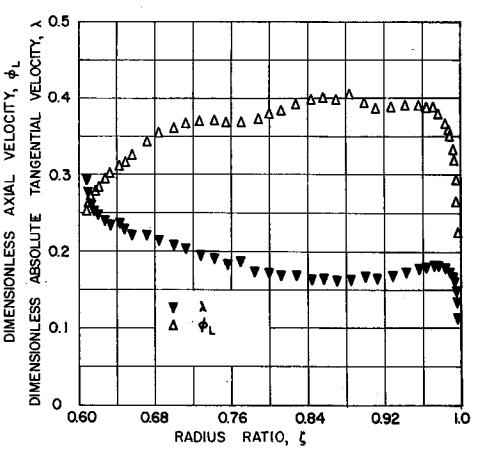

b. Velocities

FIG. 53. FLOW SURVEYS DOWNSTREAM OF STATOR; STATION 7; CS; R_T = 20,200 - 21,450; ϕ = 0.327

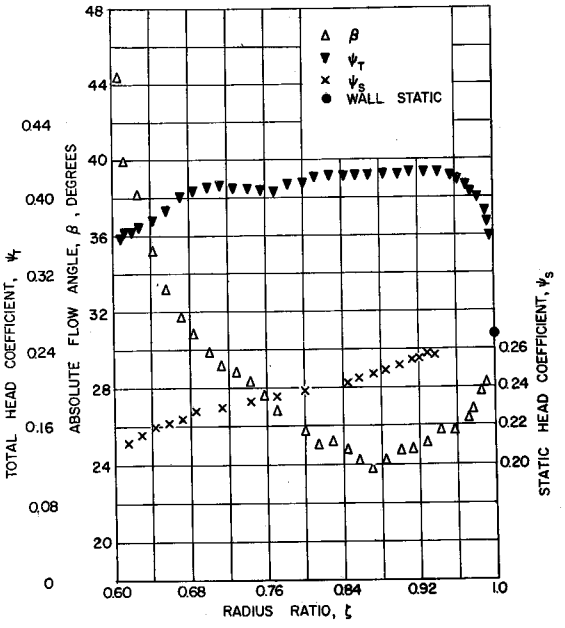

a. Flow Angles and Head Coefficients

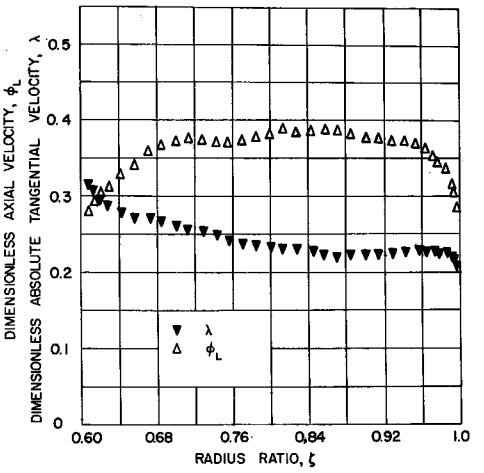

b. Velocities

FIG. 54. FLOW SURVEYS DOWNSTREAM OF STATOR; STATION 7; CS; R_T = 150,400 - 156,600; ϕ = 0.333 - 0.335

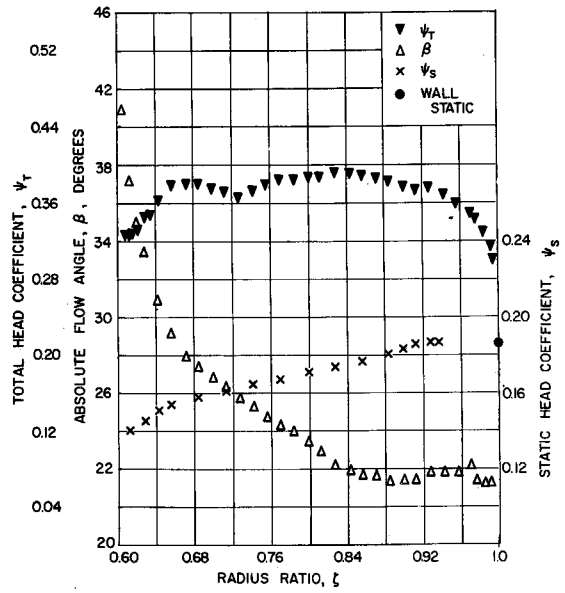

a. Flow Angles and Head Coefficients

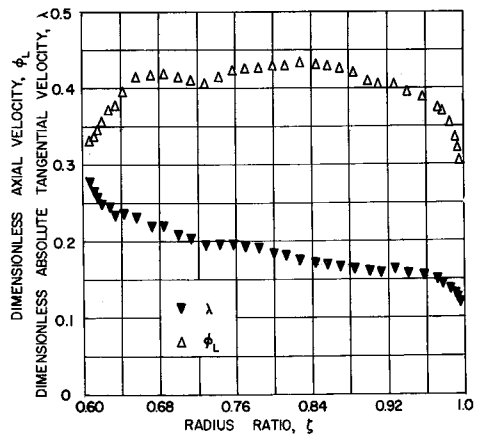

b. Velocities

FIG. 55. FLOW SURVEYS DOWNSTREAM OF STATOR; STATION 7; CS; R_T = 150,400 - 156,600: ϕ = 0.383 - 0.391

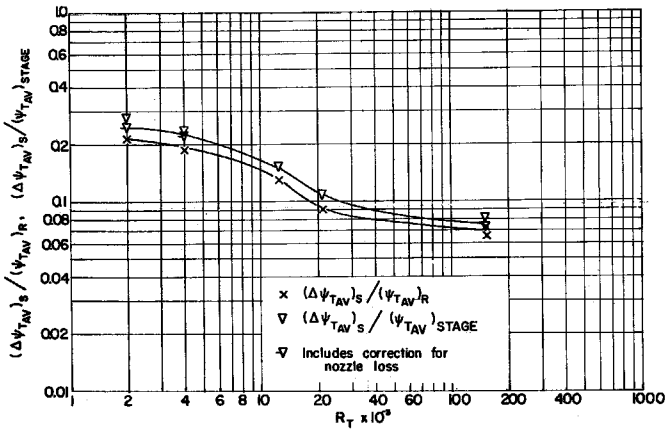

a. Loss as Fraction of Rotor and Stage Total Head Coefficients; Variation with R_T

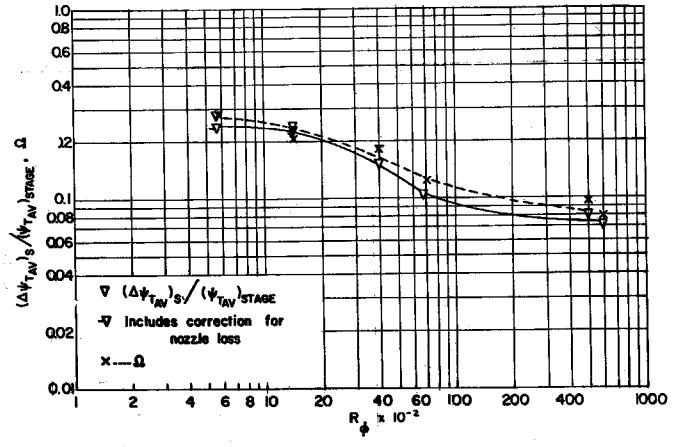

b. Loss as Fraction of Stage Total Head Coefficient and Stator Inlet Dynamic Head at $\xi = 0.80$; Variation with R_ϕ

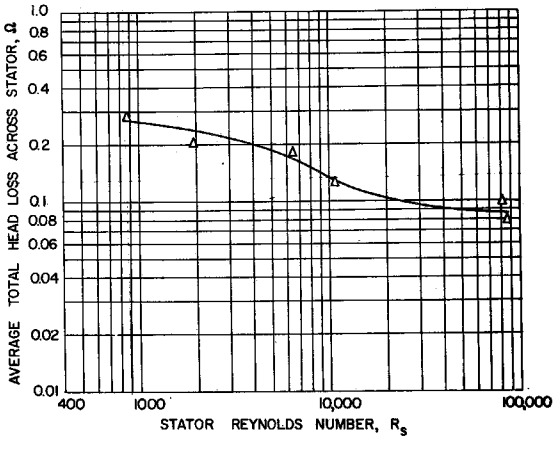

c. Loss as Fraction of Stator Inlet Dynamic Head at $\xi = 0.80$; Variation with R_S

FIG. 56. VARIATION OF STATOR AVERAGE TOTAL HEAD LOSS WITH REYNOLDS NUMBER

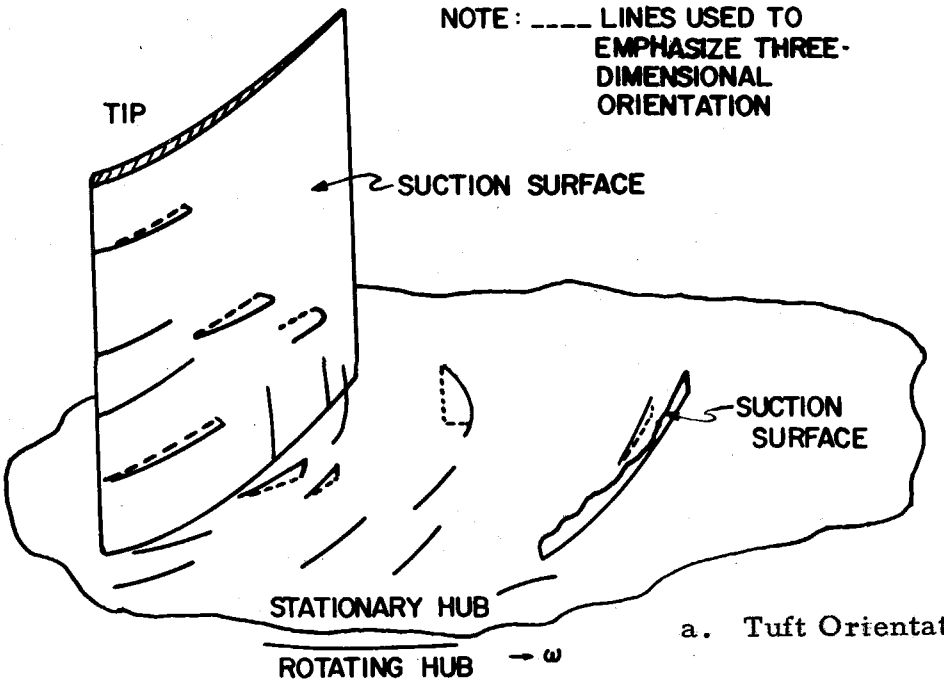

a. Tuft Orientations

FIG. 57a. OBSERVED TUFT ORIENTATIONS WITH STATOR LOCATED OVER STATIONARY HUB: ERS: $R_T = 2000$; $\phi = 0.28$.

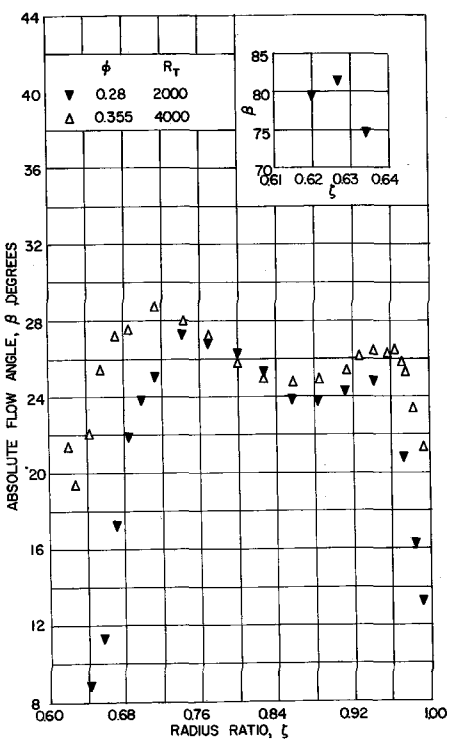

b. Absolute Flow Angles at Stator Exit; Station 8; One Circumferential Position

FIG. 57. OBSERVATIONS WITH STATOR LOCATED OVER STATIONARY HUB; ERS

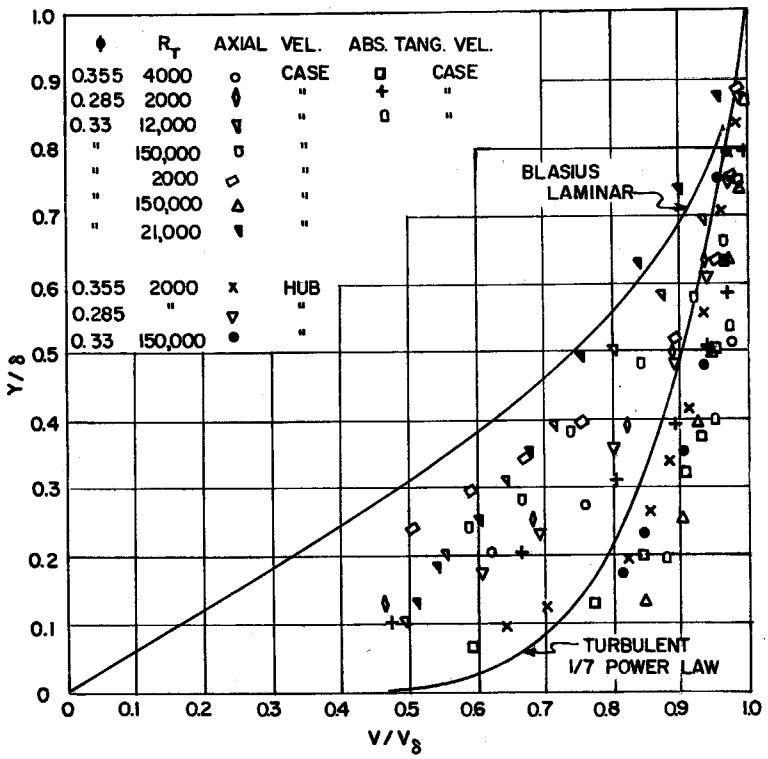

FIG. 58. CASING AND HUB BOUNDARY LAYER PROFILES BEHIND ROTOR AND STATOR AT VARIOUS REYNOLDS NUMBERS

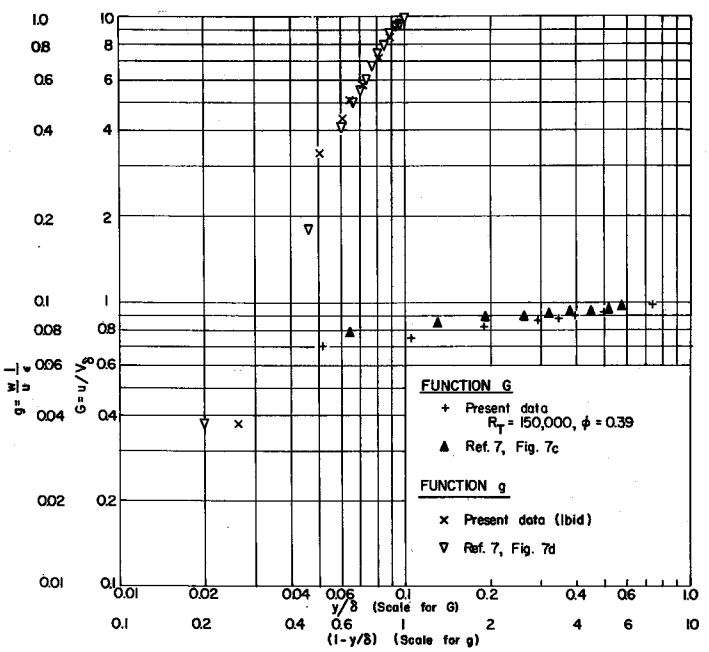

FIG. 59. COMPARISON OF CASING BOUNDARY LAYER FUNCTIONS AT ROTOR EXIT; DATA FROM PRESENT EXPERIMENTS AND FROM REF. (7)

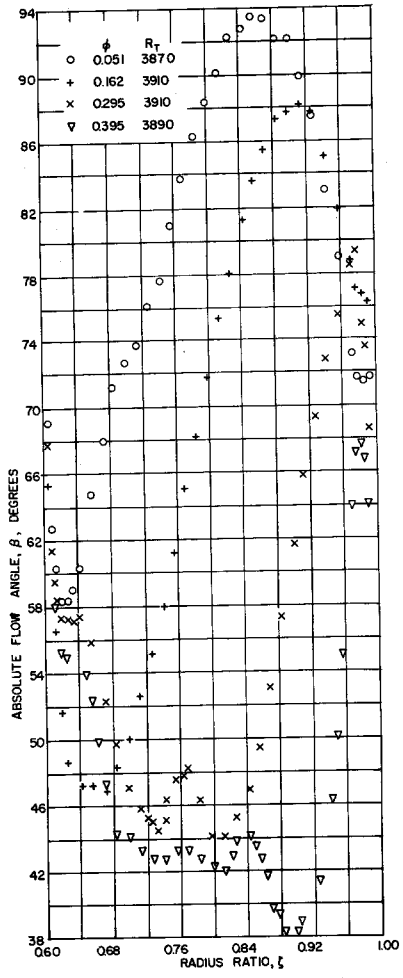

FIG. 60. FLOW ANGLES AT ROTOR EXIT FOR FLOW COEFFICIENTS APPROACHING SHUT-OFF; STATION 3; ES; R_T = 3900; ϕ = 0.36 - 0.05

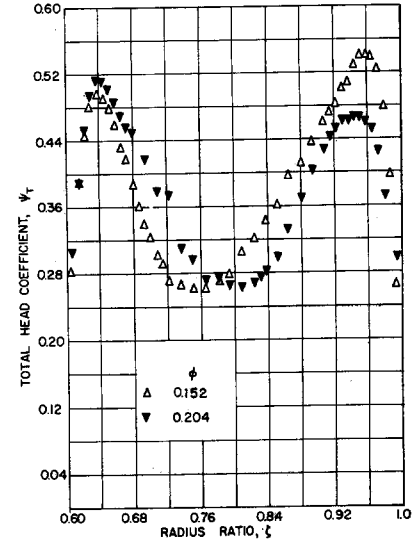

FIG. 61. TOTAL HEAD COEFFICIENTS AT ROTOR EXIT FOR FLOW COEFFICIENTS APPROACHING SHUT-OFF; STATION 3; ES; R_T = 2200; ϕ = 0.2 AND 0.15

a. ES; ϕ = 0.15
Hub and Rake Tufts

(1)
Casing and Rake
Tufts

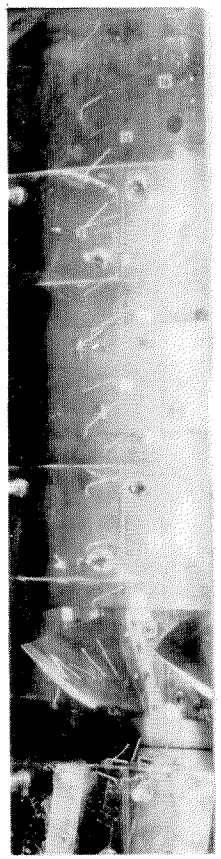

(2)
Casing, Hub, and
Rake Tufts

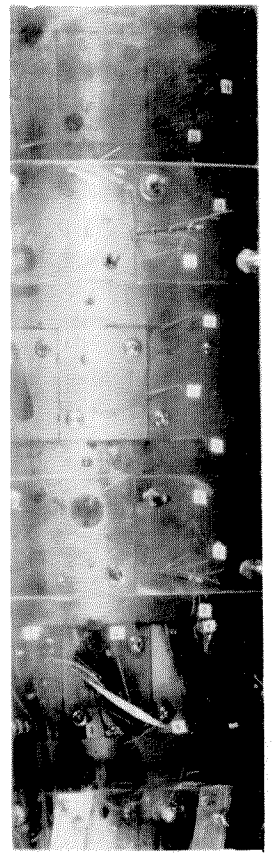

(3)
Hub and Rake
Tufts

b. ES

FIG. 62. FLOW VISUALIZATION AT APPROXIMATELY SHUT-OFF CONDITIONS; R_T = 2000; ϕ = 0.05 (EXCEPT IN a)

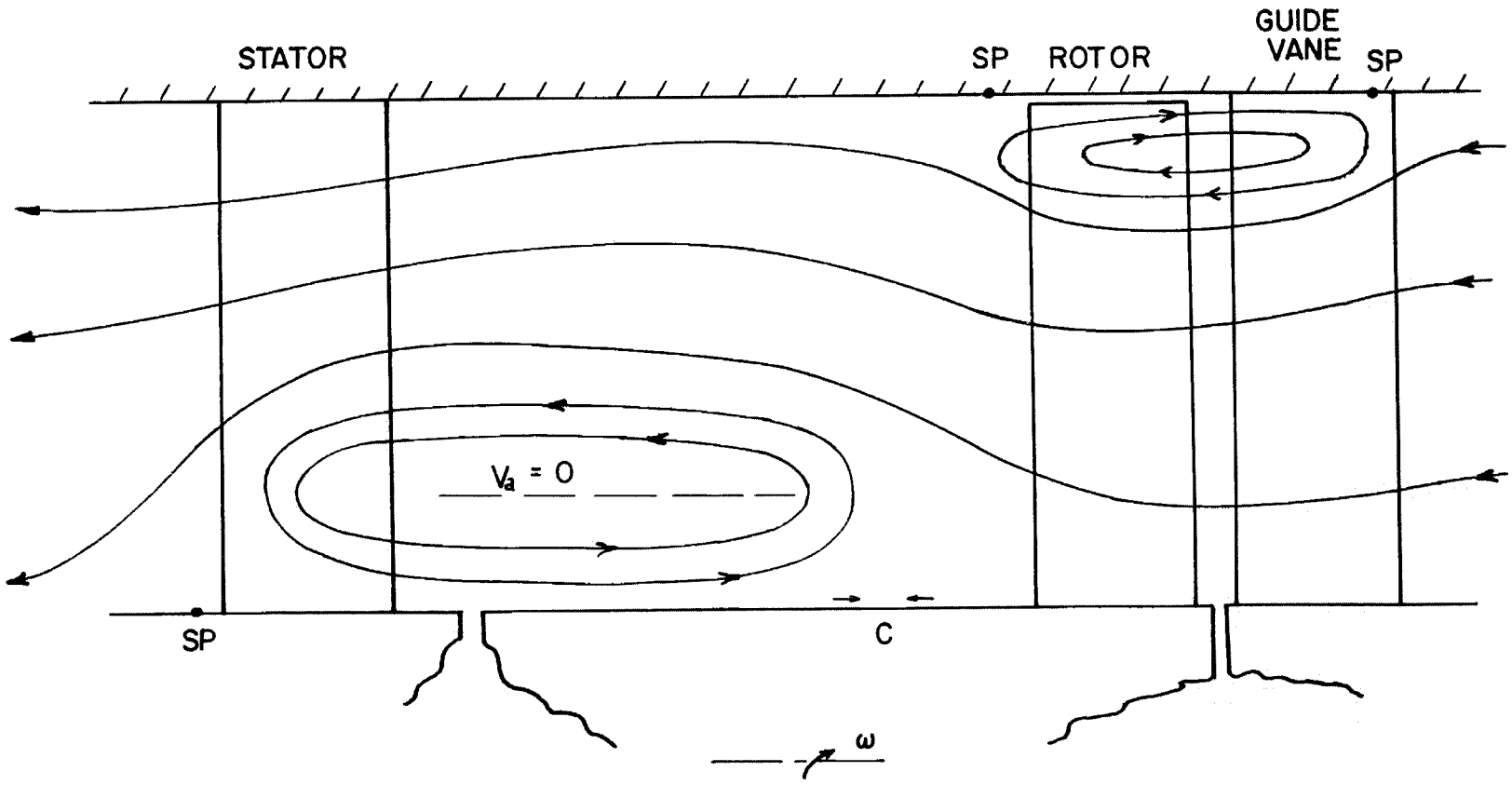

c. Estimated Model of Recirculating Meridian Flow Pattern; ES

FIG. 62 (CONT'D)

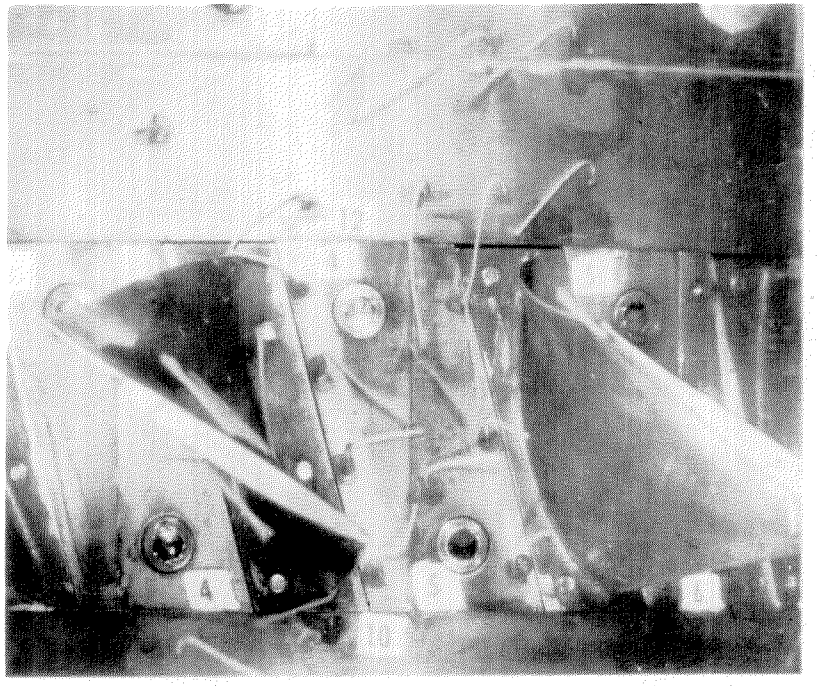

(1) Hub Tufts Within Rotor Passage

(2) Rotor Blade Suction Surface

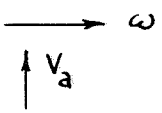

d. ERS

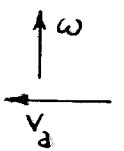

FIG. 62 (CONT'D)

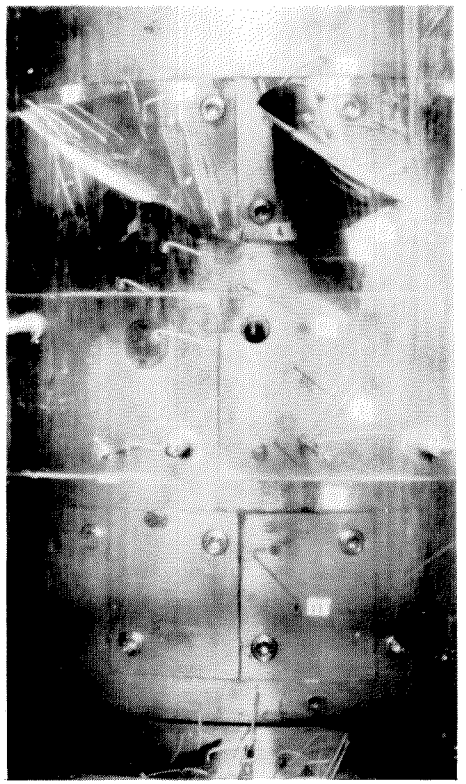

(3) Hub, Casing, and Rake Tufts Upstream of Rotor

d. (Concluded)

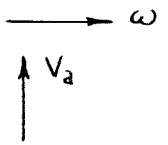

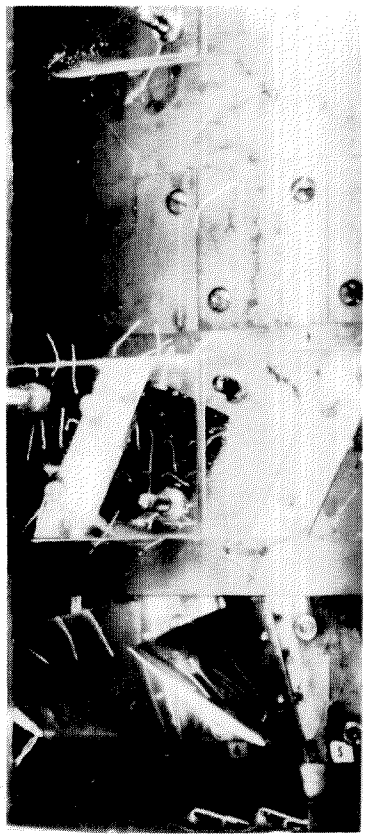

(1)

(2)

e. CS

FIG. 62. (CONCLUDED)

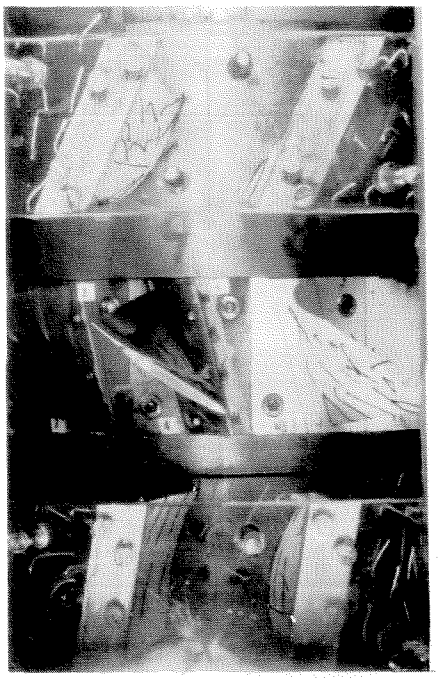

a. Stage

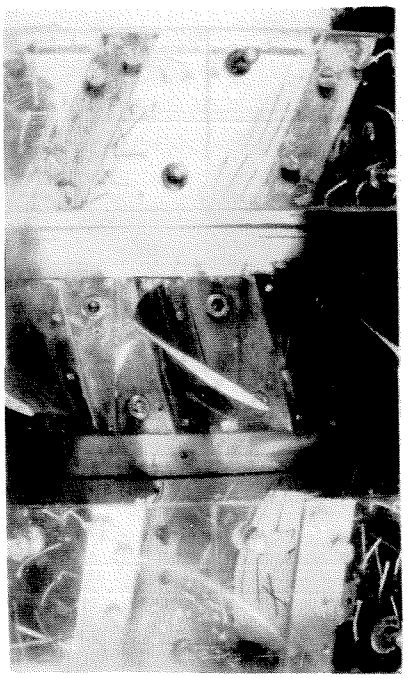

b. Stage

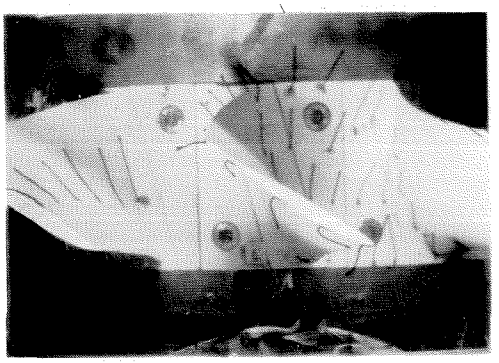

c. Rotor

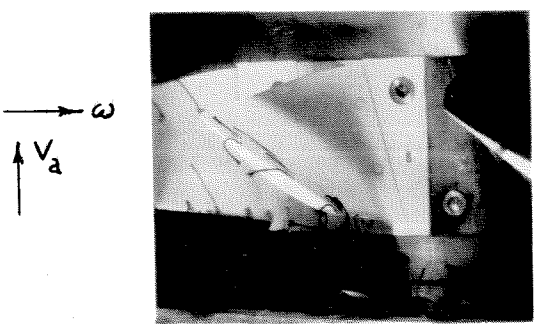

d. Rotor

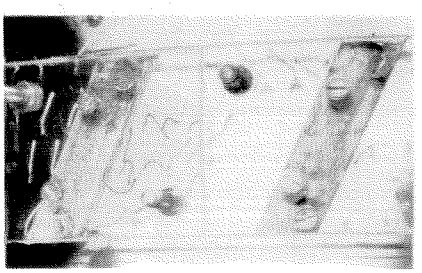

e. Stator

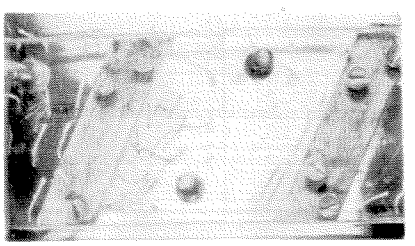

f. Stator

FIG. 63. FLOW VISUALIZATION AT LOW ϕ; CS; R_T= 12,000; ϕ = 0.15

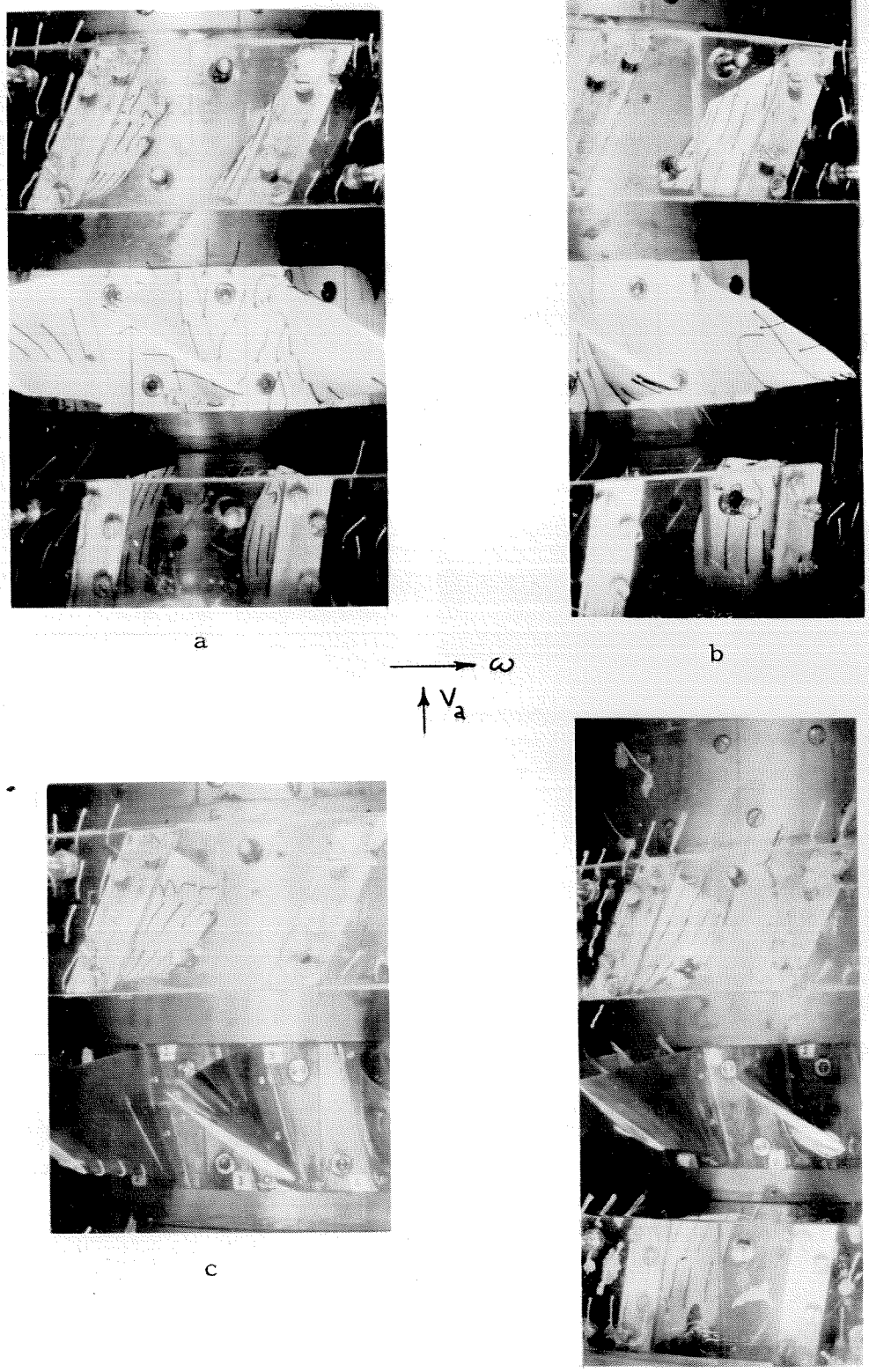

FIG. 64. FLOW VISUALIZATION AT HIGH ϕ; CS; R_T = 12,000 (EXCEPT IN d); ϕ = 0.45

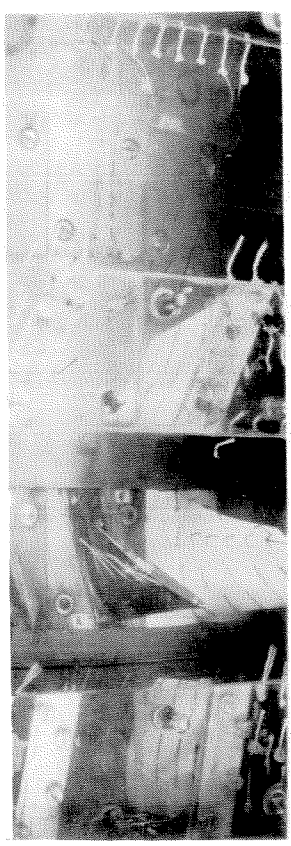

(1)

a. $\phi = 0.30$

(2)

(2)

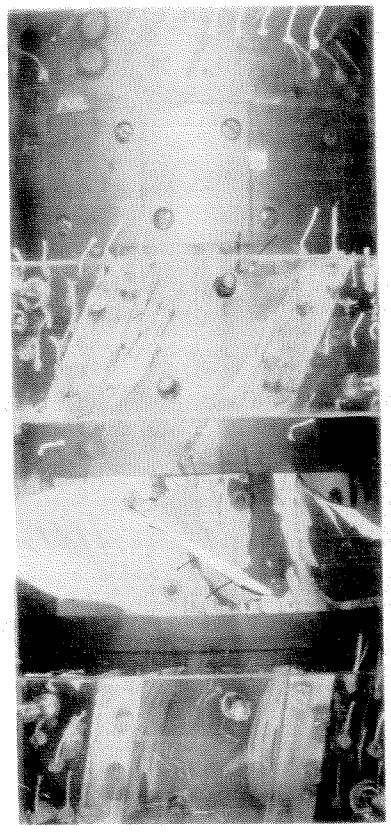

(3)

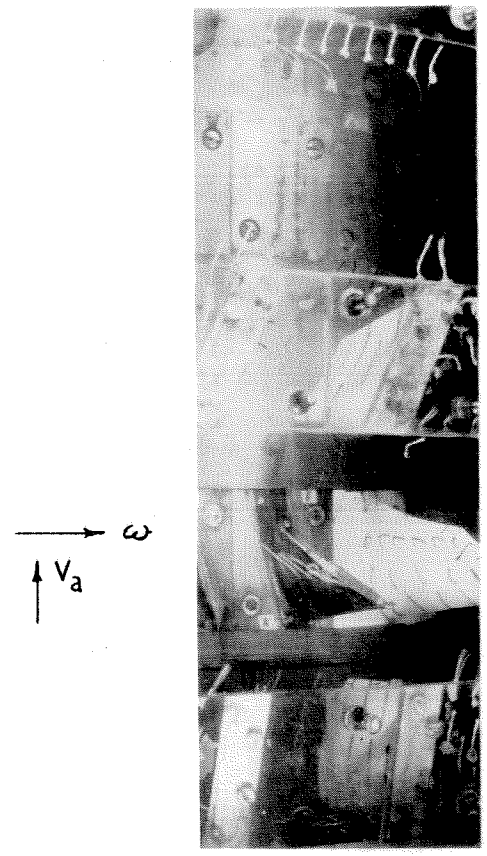

(1)

b. $\phi = 0.27$

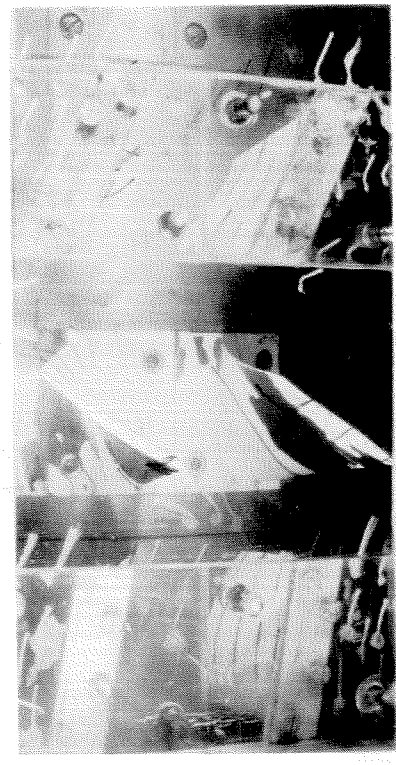

(4)

b. $\phi = 0.27$

FIG. 65. FLOW VISUALIZATION AT LOW ϕ; CS; $R_T = 150,000$

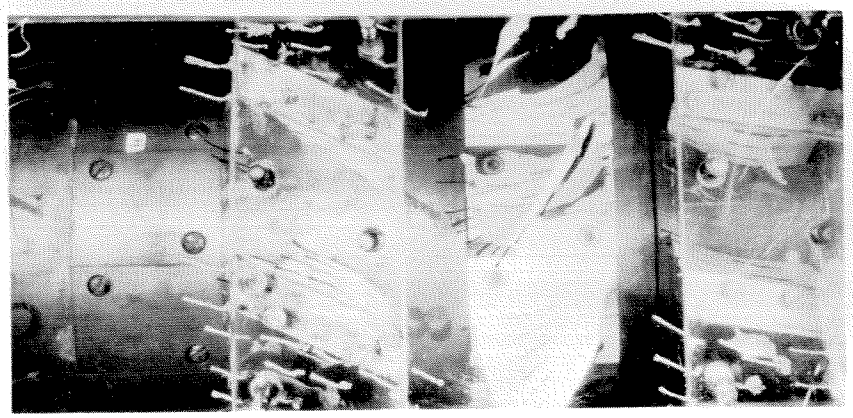

b

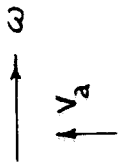

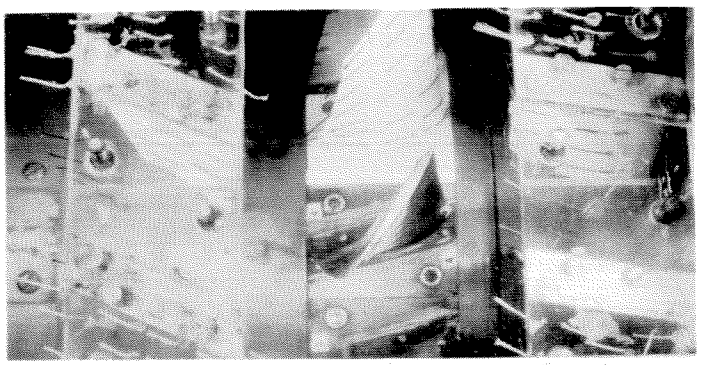

a

FIG. 66. FLOW VISUALIZATION AT HIGH ϕ; CS;
$R_T = 150,000$; $\phi = 0.49$